A MATHEMATICAL MODEL FOR THE THERMAL REGENERATION OF SPENT ACTIVATED CARBON

BY

JOHANNES PETRUS WILLEM VAN DER WESTHUYSEN

A THESIS SUBMITTED IN PARTIAL FULFILMENT OF THE REQUIREMENTS FOR THE DEGREE OF MASTER OF ENGINEERING AT THE UNIVERSITY OF STELLENBOSCH

Supervisors:
Prof. J.S.J. van Deventer
Mr. L. Lorenzen

Stellenbosch
December 1992

DECLARATION

I declare that this thesis is my own original work, except where specifically acknowledged in the text. Neither the present thesis nor any part thereof, has been submitted previously at any other university.

J.P.W. VAN DER WESTHUYSEN

31 DECEMBER 1992

Ek dra hierdie tesis op aan my moeder vir haar onvoorwaardelike ondersteuning, vir haar oneindige liefde, dat sy in haar kinders glo, en dat sy my elke my elke aand aan haar God offer.

ABSTRACT

It is essential to have a mathematical model available for predicting and evaluating the performance of the regeneration of spent activated carbon in a rotary kiln. Real regeneration systems are, however extremely complex in nature. This thesis describes an approach to the modelling of the regeneration of spent activated carbon in a rotary kiln.

A simulation model was developed to describe the energy transfer and the reaction kinetics in a rotary kiln. In this model, the kiln is divided into a number of axial length increments. The mass loss due to the heat transfer and reaction kinetics is calculated in each increment. The total mass loss is then the sum of the individual mass losses along the length of the kiln.

Samples of spent activated carbon were regenerated at different temperatures and the mass loss was recorded. The Freundlich-isotherm was used to correlate equilibrium adsorption data for the adsorption of gold cyanide on the regenerated carbon. The Freundlich A parameter was used to quantify the capacity of the regenerated carbon. The relationship between the mass loss during regeneration and the Freundlich A parameter was investigated. A maximum capacity was observed. The mass loss was used to evaluate rotary kiln performance.

A simulation analysis was performed to investigated the influence of the operating conditions, the rotary kiln design parameters and the properties of the activated carbon on the capacity of the regenerated carbon. The influence of the capacity on the CIP circuit was further investigated and satisfactory agreement was obtained between the simulation results and experience within the industry. The wall temperature inside the kiln and the composition of the freeboard gas is critical to the performance of the kiln. Inefficient regeneration resulted in a loss of gold in the effluent of the CIP circuit and low gold loadings were also obtained.

SAMEVATTING

Dit is noodsaaklik om 'n wiskundige model beskikbaar te hê vir die voorspelling en evaluering van die doeltreffendheid van die regenerasie van bevuilde koolstof in 'n draai-oond. Werklike regenerasie is egter baie kompleks. Hierdie tesis beskryf 'n benadering tot die modellering van die regenerasie van bevuilde koolstof in 'n draai-oond.

'n Simulasie model is ontwikkel om die energie oordragte en die reaksie kinetika in die oond te beskryf. In hierdie model word die oond in 'n aantal aksiale lengte inkremente verdeel. Die massaverlies as gevolg van die hitte oordrag en die reaksiekinetika word dan in elke inkrement bereken en oor die oond gesommeer om die totale massaverlies te bereken.

Monsters bevuilde geaktiveerde koolstof is teen verskillende temperature geregenereer. Die massa verlies is by elke temperatuur bepaal. Die Freundlich adsorpsie-isoterm is vir elke monster met sy spesifieke massa verlies eksperimenteel bepaal. Goudsianied oplossings is hiervoor gebruik. Die Freundlich A veranderlike is as maatstaf van die kapasiteit van die geregenereede koolstof gebruik. Die verband tussen die A parameter en die massaverlies gedurende regenerasie is bepaal. Daar is bevind dat die kapasiteit 'n maksimum waarde bereik. Die massaverlies is vervolgens gebruik om die doeltreffendheid van die oond te evalueer.

'n Volledige simulasie analise is gedoen. Die invloed van veranderinge in die bedryfskondsies, ontwerpsveranderlikes en einskappe van die geaktiveerde koolstof op die kapasiteit van die koolstof is ondersoek. Vervolgens is die invloed van die kapasiteit van die geregenereerde koolstof op die koolstof-in-flodder aanleg ondersoek. Die resultate korreleer goed met dit wat op die aanleg ondervind word. Die wandtemperatuur en die samestelling van die gas is as kritiese parameters itentifiseer. Swak regenerasie verlaag die goud lading op die koolstof en verhoog die konsentrasie in die uitvloei.

ACKNOWLEDGEMENTS

The work discribed in this thesis was carried out in the Department of Chemical and Metallurgical Engineering at the University of Stellenbosch between June 1991 and December 1992.

I wish to thank the following persons.

My supervisors, Prof. J.S.J. van Deventer and Mr. L. Lorezen, for their encouragement and guidance throughout this work. I appreciate their friendship.

Prof. J.S.J. van Deventer for contributing financially to this research from his FRD grant.

Leonie Strydom and the workshop staff of the Department of Chemical and Metallurgical Engineering at the University of Stellenbosch for their assistance when I needed it.

Sarel Rautenbach for making the silica crucibles at very short notice.

My mother and Toni for their invaluable assistance in proof reading the manuscript.

The women in my life, my mother and three sisters for their friendship and understanding throughout this project and to Toni for her love and complete tolerance during the many nights and week-ends devoted to this thesis instead of to her.

Finally, in humble acknowledgment, I thank my God for giving me the inspiration, perseverance and the tolerance and not just during those early morning hours when everything went wrong but also in the joy of the greatest present He gave man - Life...

CONTENTS

		Page
ABSTRACT		I
SAMEVATTING		II
ACKNOWLEDGEMENTS		III
CONTENTS		IV
LIST OF FIGURES		VII
LIST OF TABLES		XI
LIST OF SYMBOLS		XII
CHAPTER 1	INTRODUCTION	1
1.1	The carbon-in-pulp (CIP) circuit	2
1.2	The need for carbon regeneration	6
1.3	Carbon regeneration	6
1.4	Objectives of this study	8
CHAPTER 2	LITERATURE REVIEW	
2.1	Physical and chemical properties of activated carbon	11
2.2	Activated carbon foulants and their classification	14
2.3	Kinetics of steam regeneration	[illegible]
2.4	Mass transfer during thermal regeneration	21
2.5	Activated carbon regeneration	22
2.6	Catalysts for gasification	24
2.7	Parameters to evaluate regeneration	25
2.8	Heat transfer in a rotary kiln	28
2.9	Significance of the literature review	31

CONTENTS

CHAPTER 3		EXPERIMENTAL PROCEDURES	33
	3.1	Experimental materials	33
	3.2	Experimental apparatus	34
	3.3	Experimental procedures	36
	3.3.1	Drying kinetics	36
	3.3.2	Mass loss of spent sample	36
	3.3.3	Batch adsorption experiments	37
	3.3.4	Adsorption of materials on fresh activated carbon	37
	3.3.5	Experimental procedure for determining the mass loss during decomposition and pyrolysis as a function of the temperature	38
	3.4	Analytical methods	38
CHAPTER 4		ROTARY KILN SIMULATION MODEL	39
	4.1	Introduction	39
	4.2	Conceptual representation	41
	4.3	Heat transfer to the solids	42
	4.3.1	Radiation	43
	4.3.2	Convection	47
	4.3.3	Conduction	48
	4.3.4	Heat transfer in the solids bed	49
	4.3.5	Calculation of the temperature distribution in the solids bed	49
	4.4	Heat transfer to the kiln wall	51
	4.5	Heat transfer to the gas	52
	4.6	Kinetics during steam regeneration	54
	4.6.1	Water evaporation	55
	4.6.2	Other freeboard gases	55
	4.6.2.1	Calculation of the gas composition	59
	4.6.2.2	Heat of reaction	61

	4.7	Mass loss of the carbon	62
CHAPTER 5		COMPUTATIONAL PROCEDURES	69
	5.1	Introduction	69
	5.2	Hard-and software requirements	69
	5.3	Computational procedure	70
	5.3.1	Menu for kiln design, operating and carbon parameters	71
	5.3.2	Temperature profiles and the mass loss	72
	5.3.3	Calculation of the equilibrium gas temperature and composition	75
	5.4	Relationship between the capacity of regenerated carbon and the calculated mass loss	75
	5.4.1	Results	77
CHAPTER 6		DETERMINATION OF THE PARAMETERS REQUIRED FOR THE SIMULATION OF A ROTARY KILN	81
	6.1	Emissivity, absorptivity and transmissivity of the gas	81
	6.1.2	Models for calculating gas emissivity, absorptivity and transmissivity	82
	6.2	The effective thermal conductivity of GAC	84
	6.3	The kinetics of drying	87
	6.3.1	Results	88
	6.4	Determination of the parameters of equation 4-46	94
CHAPTER 7		SIMULATION	96
	7.1	Sensitivity analysis	96
	7.1.1	Thermal conductivity, specific heat capacity and the bulk solids density	97
	7.1.2	Emissivity of the solids	103
	7.2	Design parameters	104

7.3	Operating conditions	106
7.3.1	Rotation speed	107
7.3.2	Freeboard gas composition	108
7.3.3	Temperature of the kiln wall	111
7.3.3.1	Temperature profile	111
7.3.3.2	Drying and heating of the solids	112
7.3.4	Mass flow of solids	112
7.4	Carbon parameters	113
7.5	Influence of the Freundlich A parameter on the CIP circuit	114
7.5.1	CIP simulator	115
7.5.2	Results	115
CHAPTER 8	CONCLUSIONS AND SIGINFICANCE	119
REFERENCES		122
APPENDIX A	THE FINITE DIFFERENCE HEAT EQUATION	135
APPENDIX B	EQUILIBRIUM BOUDOUARD CONSTANT	142
APPENDIX C	CALCULATION OF GAS PROPERTIES	147
APPENDIX D	EXPERIMENTAL DATA	155
APPENDIX E	GRAPH	159
APPENDIX F	FLOW DIAGRAMS	160
APPENDIX G	SIMULATION PROGRAM	169

LIST OF FIGURES

Figure		Page
1.1	Schematic process flow diagram for a typical CIP circuit.	3
2.1	The pore volume distribution of typical activated carbons.	13
2.2	The activity of GAC vs regeneration conditions.	23
2.3	Infra-red thermal regeneration of eluted carbon.	26
3.1	Schematic diagram of the experimental setup.	35
4.1	Conceptual representation of the k^{th} length increment.	41
4.2	Heat transfer paths in the rotary kiln.	42
4.3	Schematic diagram of the cross-section of a rotary kiln showing the path of radiant energy leaving the solid surface.	44
4.4	Definition of Φ_L and the fill height.	47
4.5	Schematic diagram of the cross-section of a rotary kiln showing the path of radiant energy emitted from the freeboard gas.	52
4.6	Correlation between the calculated and experimental mass loss.	65
5.1	Flow diagram of the main program.	70
5.2	Flow diagram of the menu for kiln design, operating and carbon parameters.	71
5.3	Flow diagram of the main calculation procedure.	73
5.4	Equilibrium adsorption curves for the regenerated mine sample.	78
5.5	The relationship betweem the Freundlich A parameter and the mass loss.	79
6.1	The effective thermal conductivity of GAC.	86
6.2	TGA curve for carbon loaded with 21.02 weight per cent moisture.	89
6.3	TGA curve for carbon loaded with 30.23 weight per cent moisture.	89
6.4	TGA curve for carbon loaded with 40.06 weight per cent moisture.	90

6.5	TGA curve for carbon loaded with 50.57 weight per cent moisture.	90
6.6	Diagram for obtaining x = E/RT from (x).	91
6.7	TGA curve for carbon loaded with 150mg/g phenol.	95
7.1	Sensitivity of the mass loss to changes in the values of the physical properties.	98
7.2	Sensitivity of the mass loss to changes in the physical properies of the carbon.	100
7.3	Influence of the temperature on the mass loss sensitivity.	101
7.4	Sensitivity of the mass loss to a combination of changes to the physical parameters of the carbon.	101
7.5	The influence of the emissivity of the solids and the kiln wall on the mass loss.	104
7.6	Influence of the mass loss to changes in the kiln length at constant temperature.	105
7.7	Sensitivity of the mass loss to changes in the reflectiviy of the kiln wall.	106
7.8	Influence of the speed of rotation on the mass loss at different temperatures.	107
7.9	Calculation of the freeboard gas composition.	108
7.10	Influence of the moisture content of the carbon on the mass loss.	109
7.11	Temperature profile of the solids and kiln wall.	112
7.12	Influence of the mass flow rate.	113
7.13	Influence of the Freundlich A parameter on the equilibrium gold loading on the regenerated carbon in the CIP cascade	117
7.14	Influence of the Freundlich A parameter on the equilibrium loading concentration of gold in the solution of the CIP cascade	117
B.1	The Boudouard equilibrium constant.	146
F.1	Flow diagram for procedure "MainInPut".	160

F.2 Flow diagram for the calculation of the gas properties. 163
F.3 Flow diagram for procedure "Calc." 164
F.4 Flow diagram for calculating the gas properties. 165
F.5 Flow diagram for the calculation of the heat transfer rate to the solids. 165
F.6 Heat transfer rate to the gas. 166
F.7 Flow diagram for calculating the solids temperature. 166
F.8 Flow diagram for calculating the gas temperature. 168
F.9 Flow diagram for procedure "React." 168

LIST OF TABLES

Table		Page
5.1	Experimental mass loss data.	77
5.2	The calculated Freundlich parameters.	77
6.1	Activation energies and the frequency factors.	93
6.2	Parameters for equation 4-46.	95
7.1	Parameters used for the base simulation run.	97
7.2	X-axis legend.	102
7.3	Initial gas composition.	106
7.4	Comparison of wall temperature profiles.	112
7.5	Mass loss for different foulants.	114
7.6	Values for the operating parameters in the simulation runs.	116

LIST OF SYMBOLS

A	Area	[m^2]
	also parameter in eq. 2-12 to 2-14	[g/kg]
A_g	Representative area of the gas	[m^2]
A_s	Area of the solids bed	[m^2]
A_w	Area of the wall	[m^2]
b	Self-broadening coefficient	[1]
B	Parameter in eq. 2-14	[1]
c	Speed of light ($2.998*10^8$)	[m/s]
C	Concentration	[ppm]
C_5	Constant	[1]
Cp	Specific heat capasity	[kJ/kg.K]
d	Line spacing	[1/m]
D	Kiln Diameter	[m]
e_{bw}	Spectral blackbody radiosity	[$W/m^2.m^{-1}$]
E	Emissive power	[W/m^2]
E_d	Activation energy of the drying reaction	[J/mol]
E_{dp}	Activation energy of decomposition and pyrolysis	[J/mol]
f	Fractional function	[1]
F_{sw}	View factor of the solids to the wall	[1]
F_{ws}	View factor of the wall to the solids	[1]
F_{ww}	View factor of the wall to the wall	[1]
g	Gaunt factor	[1]
G_g	Gas mass flux	[$kg/m^2.s$]
G_f	Gibbs free energy of formation	[kcal/mol]
h	Planck's constant ($6.625*10^{-34}$)	[J.s/molecule]
h	Convective heat transfer coefficient,	[W/m.K]
ΔH_r	Standard heat of reaction, $-\Delta H^\circ > 0$ for an exothermic reaction	[kJ/mol]

i_b	Spectral radiant intensity	$[W/m^2.m^{-1}]$
k	k^{th} length increment	[1]
k	Boltzmann's constant ($1.38*10^{-23}$)	[J/K.molecule]
k_1	Rate constant for steam-carbon reaction	[kg/kg.s.Pa]
K_1	Reaction rate constant Eq 2-10	$[Pa^{-1}.s^{-1}]$
k_2	Parameter in rate Eq. 2-8	$[Pa^{-1}]$
K_2	Reaction rate constant Eq 2-10	$[Pa^{-1}]$
k_3	Parameter in rate Eq. 2-8	$[Pa^{-1}]$
k_d	Frequency factor	$[s^{-1}]$
k_d^*	Freguency factor	$[s^{-1}]$
K_p	Equilibrium constant	[1]
L	Length	[m]
L_m	Mean beam length	[1/m]
m	Nodal position	
	on the x-axis	[1]
m'	Heating rate	[K/s]
m_s	Mass flow of wet carbon	[kg/kg]
M	Mass loss	[kg/kg]
n	Pressure broadening exponent, Eq (C-8) or	[1]
	also nodal position on the y-axis	[1]
	also parameter in eq. 2--13 and 3-42	
	also number of moles	[mol]
p	Constant	[1]
P	Pressure	[atm],$[kN/m^2]$
p	Partial pressure Eq. 2-8, 2-10	[Pa]
P_a	Partial pressure of gas species	[Pa]
P_e	Equivalent broadening pressure	[1]
Pr	Prandtl number	[1]
q	Equilibrium loading	[g/kg]
Q	Heat flow	[W]
Q_g	Heat flow to the gas	[W]

Q_s	Heat flow to the solids	[W]
Q_w	Heat flow to the wall	[W]
r	Reaction rate	[s^{-1}]
R_0	Universal gas constant	[kJ/kmol.K]
R	Reaction rate	[kg/kg.s]
Rd	Drying rate	[kg/kg.s]
Re	Reynold's number	[1]
s	Empirical exponent	[1]
t	Time	[s]
t_{Hk}	k^{th} band-head optical depth	[1]
Δt	Time increment	[s]
T	Temperature	[K]
T^p	Temperature at new time	[K]
u	Partition energy	[1]
v	Empirical rate constant	[1/s]
w	Moisture content	[kg/kg]
x_a	Fraction of the absorbing gas species	[1]
x	Constant	[1]
Δx	Length increment	[m]
y	Constant	[1]
Δy	Length increment	[m]
z	Constant	[1]

Greek Symbols

α_k	Integrated intensity of the k^{th} band	[m^2/kg.m]
α	Absorptivity, thermal diffusivity	[1]
$\acute{\alpha}_g$	Absorptivity of real gas for own radiation	
β_k	Line-width to spacing parameter of the k^{th} band for its own radiation	[1]
δ	Vibrational quantum number differences	[1]

ϵ	Emissivity	[1]
n	line width to spacing parameter for an arbitary P_e	[1]
λ	Wavelength	[cm], [m]
ν	Vibrational quantum number	[1]
π	pi	[1]
ρ	Reflectivity	[1]
ϱ	Density	[kg/m^3]
σ	Stefan-Boltzman constant ($5.67*10^{-8}$)	[W/m^2.K^4]
τ_{gk}	Gas transmissivity of the kth band	[1]
Φ	Upper-state band overlap parameter	[1]
Ψ	Upper-state band intensity parameter	[1]
ω_{bk}	Bandwidth parameter for the kth band	[m^{-1}]
ω^*_{ak}	Band width adsorptance of the adsorbing species in the kth band	[1]
$\Delta\omega_k$	kth Band width	[m^{-1}]
ω_{uk}	Upper limit of the kthspectral block	[m^{-1}]
ω_{lk}	Lower limit of the kth spectral block	[m^{-1}]

Subscripts

a	absorbing species
Au	gold
b	band
C	carbon
C*	carbon reacitng
cd	conduction
CO	carbon monoxide
CO_2	carbon doxide
cv	convection
dp	decomposition and pyrolysis

e	equilibrium
g	gas
H	head of band
H_2	hydrogen
H_2O	water
k	k^{th} band or block index, also k^{th} length increment
l	lower limit
rad	radiation
s	solids
u	upper limit
w	wall
0	reference value

Sub-Subscripts

g→s	Gas to solids
g→w	Gas to wall
k	k^{th} length increment

CHAPTER 1

INTRODUCTION

The discovery of the adsorptive property of charcoal[1] from solutions can be traced back as far as 1785 when J. T. Lowitz observed that several dissolved organic substances were precipitated on charcoal[1]. Metallurgical interest in activated carbon, however, was initiated almost 100 years later in 1880 when W.N. Davis patented a process in which wood charcoal was used for the recovery of gold from chlorinated leach liquors[2]. Although W.D. Johnson patented the use of wood charcoal as a precipitant for gold from cyanide solutions in 1894[3], it was never extensively used for the recovery of gold from cyanide leach liquors. The following two factors probably retarded the development of an economical carbon adsorption process. The carbon possessed very low loading capacities and no suitable procedure for the elution of gold from the loaded carbon was known. This meant that the gold had to be recovered by smelting after burning of the carbon.

The availability of granules of hard activated carbon, developed during the Second World War, made it possible to use the activated carbon, now known as granular activated carbon (GAC), directly in the cyanided pulp. Accordingly, the costly filtration step is avoided. This approach was first employed in an experimental program at the Getchell Mine in Nevada[3]. Acting on request from this mine, J.B. Zadra developed a technique to elute the gold from the loaded carbon using sodium sulphide/sodium hydroxide mixtures. The gold was then recovered from the eluate by electrolysis[3]. In 1952 Zadra[4] proposed a hot hydroxide/sodium cyanide stripping technique. This

---

1. Activated charcoal, granular activated carbon and activated carbon are used synonymously in this thesis.

technique was effective in stripping both gold and silver.

The discovery of an appropriate elution process made the use of activated carbon as a adsorbent for gold from cyanide solutions very attractive. By 1961 a flowsheet for the so-called carbon-in-pulp (CIP) process had been developed[3]. This process was first applied at Cripple Creek, Colorado in 1961[5]. By 1973 the process had also been introduced at the Homestake Mine in South Dakota for the treatment of 2050 tons/day cyanide slime[6]. This operation changed the image of the CIP process from an experimental process into an economically viable process for the treatment of high tonnage slimes.

Today, the CIP process enjoys widespread acceptance as an economically viable and effective method for precious metal recovery. The CIP process is extensively used at South African mines for the recovery of gold. Menne[7] predicted that CIP circuits with a total capacity of 4.7 million tons per month would be operational in South Africa by the end of 1985.

1.1 THE CARBON-IN-PULP (CIP) CIRCUIT

Figure 1.1 shows a schematic process flow diagram for a typical CIP circuit.

Ore containing between 3 and 12 g/ton of gold is usually ground in a system of ball or autogenous mills operating in closed circuit with sizing devices such as hydrocyclones. The properly sized overflow from the hydrocyclones must be dewatered prior to leaching. Thickeners increase the pulp density to between 45 and 50% solids.

In each leach tank lime, sodium cyanide and air are added and mixed into the pulp. According to Finkelstein[8] most of the gold dissolves according to the reaction:

$$2Au + 4CN^- + O_2 + 2H_2O \leftrightarrow 2Au(CN)_2^- + H_2O_2 + 2OH^-$$

and a small but significant proportion dissolves via the Elsner reaction:

$$4Au + 8CN^- + O_2 + 2H_2O \leftrightarrow 4Au(CN)_2^- + 4OH^-$$

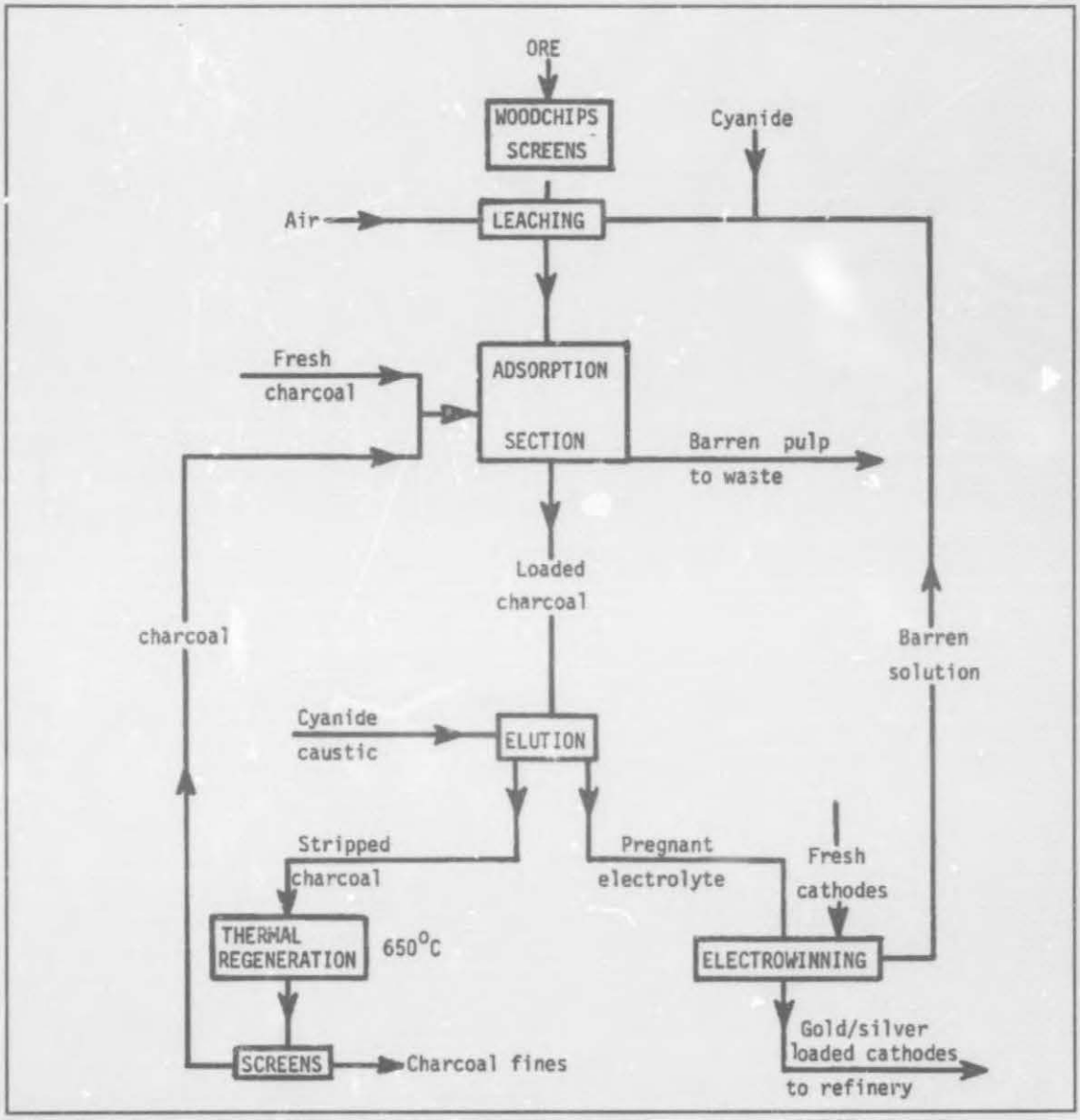

Figure 1.1: A schematic process flow diagram for a typical CIP circuit.

The decomposition of cyanide by acid constituents in the ore is minimized by using sufficient lime as an alkali to maintain the pH between 9 and 11. Iron sulphide minerals, copper minerals and other foreign constituents usually inhibit the rate of cyanidation by reacting with one or more of the primary reagents such as cyanide, the hydroxyl ion and oxygen.

Before entering the CIP adsorption section the pulp is pre-screened at 0,6 mm to remove any large particles or wood chips that might possibly block the 0,84 mm interstage screens that retain the charcoal in each adsorption stage[3,9-11]. Some CIP plants now use two stages of fine screening [11,12]. The pulp flows by gravity through a series of stirred tanks countercurrent to the movement of activated charcoal until the barren pulp is discharged from the last stage. Effective charcoal-pulp separation between stages is essential to maintain the countercurrent mode of operation.

The North American CIP plants have generally employed external vibrating screens for the interstage separation of charcoal from pulp. Most South African plants have, however, installed stationary air-cleaned screens in the periphery of the adsorption tanks with equalized pulp pressures across the screen. This technique reduces mechanical failures of the screens and minimizes charcoal abrasion. Mechanical agitation in the tanks has generally proved superior to air agitation[8,12]. Draught-tube circulators fitted with slitted skirts are generally preferred to designs incorporating baffled tanks with unshrouded impellers[7,12].

Pulp flows continuously through the system, whereas charcoal is usually moved countercurrent to the flow of pulp on an intermittent basis. The frequency of movement is dependent upon gold throughput and plant operating strategy. Air lifts are most commonly used to move charcoal and pulp countercurrent to the pulp flow, which means that a fraction of the pulp is backmixed. At some plants[10,13] slurry pumps are utilized to move charcoal and pulp countercurrent to the gravitational flow of pulp in a continuous fashion.

Loaded charcoal from the last adsorption stage is conveyed to a stripping vessel, where the gold and silver are stripped from the charcoal into a concentrated pregnant solution. Three techniques of stripping, all of which use a caustic cyanide solution to dissolve the gold and silver as $Au(CN)_2^-$ and $Ag(CN)_2^-$ ions, have been developed. These include:

- the Zadra method[4,13,14], which operates at atmospheric pressure and 90°C, exhibits slow kinetics which not only necessitate large stripping plants but also result in a significant lock-up of gold values in the plant;

- the AARL method[16,17] which involves pre-treatment of loaded charcoal with a strong cyanide solution, followed by elution with water at 110°C and 50 to 100 kPa in a pressure vessel. Total cycle time, including an acid wash to remove calcium carbonate on the charcoal, is 9 hours. Most large South African plants use this method of elution[15];

- in the alcohol stripping method[9,13,18], a caustic cyanide solution containing about 20 volume per cent ethanol, is used at 80°C and atmospheric pressure, reducing stripping cycle time to five or six hours. Major disadvantages include high fire risk and higher operating costs due to alcohol loss by volatilization.

Gold is recovered from the pregnant stripping solution by either electro-winning or zinc cementation. The steel wool cathodes from the elctrolytic process or gold slime from sementation can be smelted with suitable fluxes to yield Doré bullion, which is sold to a refinery.

Compared with the conventional Merrill-Crowe process[13], the CIP process offers a number of advantages. Savings in capital and operating costs of up to 50% and 33% respectively can be achieved by using CIP[12]. This is possible because a solid-liquid separation step is not required. Ores that are difficult to treat by conventional methods owing to poor settling or filtration characteristics, such as clayey ores[20], can be more

readily treated by the CIP process. Gold recovery from very dilute solutions is more efficient when the CIP process[12] is used.

1.2 THE NEED FOR CARBON REGENERATION

During the adsorption cycle in the CIP circuit, apart from the aurocyanide complex, several organic and inorganic species are also adsorbed on the carbon. These species occupy some of the active sites in the carbon. They can also block access for the aurocyanide complex into the pores of the carbon. Not all of these species are stripped from the carbon during elution or acid washing prior to re-entry into the circuit. Thus, the capacity (also called activity) for adsorption of the aurocyanide complex of the recycled carbon would be less than that of new (virgin) carbon.

Reduced activity can lead to gold losses in the tails of the CIP circuit and a lower tonnage throughput[21]. Since maintaining a high activity on the carbon is critical for the satisfactory recovery of gold, virgin carbon has to be added to the CIP circuit to maintain the rate and extent of aurocyanide adsorption onto the carbon. The high cost of virgin carbon necessitates the regeneration of spent (used) carbon to restore the activity to that of virgin carbon before re-entry into the CIP circuit.

1.3 CARBON REGENERATION

Several methods, such as thermal regeneration, chemical regeneration, biological regeneration, and solvent extraction have been proposed for the regeneration of spent activated carbons[22]. Chemical, biological and extractive methods are not suitable when the adsorbed organic materials are unknown[22]. Therefore these methods are not used in the gold recovery industry.

Thermal regeneration is performed in flow type reactors such as the multiple hearth furnace, the rotary kiln and the fluidized bed furnace. It involves heating of the spent carbon to between 650°C and 850°C for up to 30 minutes in a steam atmosphere[22]. The reactivated charcoal is screened at 0,84 mm (20 mesh) to remove the fines before being recycled to the adsorption circuit. In South Africa the rotary kiln is the most widely used furnace for the thermal regeneration of activated carbon.

The rotary kiln consists of a cylinder, rotated on suitable bearings and usually slightly inclined to the horizontal. The length of the cylinder usually ranges from 4 to more than 10 times its diameter, which may vary from less than 0.3 to more than 3 m. Solids fed into one end of the cylinder progress through it by virtue of rotation and/or internal flights and/or the slope of the cylinder. The solids are discharged as the product at the other end. Gases flowing through the cylinder may retard or increase the rate of solids flow, depending upon whether gas flow is countercurrent or co-current with the solids flow. Rotary kilns can be classified as direct or indirect. The terms refer to the method of heat transfer, that is direct when heat is added to the solids by direct exchange between the burning fuel and the solids, and indirect when the heating medium is separated from physical contact with the solids by a metal wall or tube.

A wide variety of rotary kilns are available for the regeneration of spent activated carbon. The development of a mathematical model for the thermal regeneration of activated carbon depends on the construction and the operating conditions[2] of the kiln itself. Therefore it is not possible to cater for all the possible rotary kiln configurations. The subject of this study is a rotary kiln operating at Freegold South's New Gold Plant at Anglo American Corporation of South Africa's President Brand Gold Mine in the Orange Free State, Republic of South Africa. The configuration of this kiln is summarized as follows:

---

2. The construction and operating conditions of a rotary kiln are referred to as the configuration of the kiln.

- The kiln is of the indirect type with electrical elements as an external heat source. There are three sections of electrical elements along the length of the kiln. Accordingly, it is possible to select different temperatures for each section.
- An internal spiral scroll transports the solids through the kiln. This means that the kiln is not inclined to the horizontal.
- There is no flow of external gas through the kiln.
- The kiln is open to the atmosphere at both ends.

Spent carbon from the CIP circuit is stored in a hopper from where it is fed to the rotary kiln. The regeneration of the spent carbon can be regarded as a four-stage process[22], comprising the drying of the wet carbon, the vaporization of the volatile adsorbates, the pyrolysis of the non-volatile adsorbates and the oxidation of the pyrolysed adsorbates. The time and temperature of regeneration are critical to the success of the process, since it will determine whether the activity of the spent carbon has been fully restored or not.

1.4 OBJECTIVES OF THIS STUDY

Throughout the world and especially in South Africa, the 1980's will be remembered for the soaring profitability of the gold mining companies. This was a result of the very high gold price during those years. Unfortunately, the situation changed dramatically. The gold price dropped by more than 60 per cent and accordingly, profit margins fell to such low values that gold mining companies considered the closure of some of their mines. This situation also arose from the consistent lack of productivity, so typical of mining operations and gold recovery during the eighties. Today, mines throughout the world are forced to cut their production costs in order to survive.

Since the gold recovery system, including the CIP circuit, is fairly well established, only small modifications to the equipment and techniques can be madec to improve performance. However, significant improvement can be attained by effective process

control. This implies that conditions for the regeneration of the spent carbon should be manipulated in such a way that the activity on the carbon is regained completely with regard to adsorption.

It is therefore essential to have a model available for predicting and assessing regeneration in a rotary kiln. It should be able to predict the optimum regeneration conditions (also referred to as variables) so as to maintain the highest possible activity of the carbon. Such a model can be used in combination with econometric models to optimize plant operation and reduce operating costs.

A fundamental model should be able to use experimental data to predict the behaviour under various kiln operating conditions. Thermogravimetric analysis (TGA) is an easy and effective method of studying the behaviour of activated carbon during heating and will formed the basis of the model development.

The main purpose of this study was to develop and verify a fundamental mathematical model to predict the capacity of regenerated carbon under different operating conditions. The specific objectives were:

- to develop a model for the heat transfer, drying and kinetics in a rotary kiln in order to predict the mass loss of the regenerated carbon;

- to use the developed mathematical model for writing a computer program in order to predict the temperature profiles through the kiln and hence the mass loss of the spent activated carbon;

- to relate the mass loss of the regenerated carbon to its adsorrption capacity by means of batch adsorption tests;

- to identify the sensitivity of the mass loss to changes in the physical constants of the activated carbon;

- to investigate the sensitivity of the mass loss (and hence the adsorption capacity) of the regenerated carbon to changes in design parameters of the kiln;

- to investigate the sensitivity of the mass loss of the regenerated carbon to changes in operating conditions of the kiln;

- to investigate the sensitivity of the mass loss of the regenerated carbon to changes in the properties of the activated carbon;

- to investigate the influence of the adsorption capacity of the activated carbon on the rest of the CIP circuit.

Such a model could form the basis for optimizing kiln operation and its development will satisfy a need for such a simulation tool in the industry.

CHAPTER 2

LITERATURE REVIEW

In order to justify the objectives set in Chapter 1 (Section 1.3), a summary of the literature dealing with activated carbon and the principles of its regeneration is presented in this chapter. Literature related to specific problems and parameters will be presented in the respective sections of the appropriate chapters.

2.1 PHYSICAL AND CHEMICAL PROPERTIES OF CARBON

Two of the most common forms of carbon are diamond and graphite. In a diamond, each of the carbon atoms is surrounded by four other carbon atoms in a tetrahedral arrangement. The atoms are bound by strong sigma bonds between the sp^3 orbitals[23]. In graphite, however, each atom is bound to three neighbouring carbon atoms in a plane. The carbon atoms in graphite are sp^2 hybridized. Each of the carbon-carbon bonds consists of a sigma bond plus a third of a p_z-p_z pi-bond, resulting from the resonance between structures with different but equivalent arrangements of the pi-bonds. The distance between successive planes suggests that they are held together by Van der Waals type forces. Graphite is non-isotropic, i.e. its properties such as its electrical and thermal conductivities, as measured along and perpendicular to the planes, are not the same[24,25].

Activated carbon falls in the category of "turbostratic carbon", which has a structure similar to that of graphite. However, this type of carbon is usually isotropic owing to disorder in the structure. Instead of a continuum like ideal graphite, turbostratic carbon consists of separate graphite-like platelets or 'crystallites', a few layers thick and not

more than 100 Å wide, in which the planes are parallel to one another but otherwise rotated at random with respect to one another. The interplanar separation is also slightly greater than that observed in graphite.

Activated carbon has been manufactured from sugar, coconut shells, coffee beans, rubber waste, wood and even blood[1,23,26,27]. Coconut shell and extruded coalbased charcoals are two of the frequently used carbons for gold and silver adsorption applications. The physical and chemical properties of activated carbon are influenced by both the source material and the conditions of activation, i.e. chemical or thermal activation, temperature and the duration of the process.

Carbonization, which is the first step in the production of activated charcoal, is the formation of a char from the raw material. This is conducted by heating carbonaceous base material at temperatures between 400-700°C in the absence of oxidizing gases[28]. The raw material is dehydrated and oxygen and hydrogen containing groups are expelled to leave the carbonized char. At higher temperatures oxygen is eliminated from the structure and aromatization takes place[29]. During this phase graphite-like microcrystallites are formed or enlarged. Although these structures are similar to graphite, they include impurities, tetrahedrally bonded carbon atoms and heterocyclic groups at the edges of the planes[28]. The spaces between the microcrystallites are largely filled with charred residues of the carbonization process.

During the activation step steam or other oxidizing gases are contacted with the charcoal at 750-900°C[1]. The residues are selectively eroded to develop the porous structure within the charcoal. The size of the microcrystallites increases with the temperature of carbonization, which may relate to the adsorption properties of the charcoal since these depend strongly on the temperature of carbonization and activation[1,29]. Oxidation yields a variety of oxygen-containing functional groups on the surfaces such as CO, CO_2 and CH_3OH. There seem to be conflicting opinions as to whether these groups play any role in the adsorption process. Acton[30] stated that these functional groups may play a role, while other authors [31,32] feel that these

groups are of minor importance to the adsorption process. There are various other methods described by Wilson[33] for the activation of charcoal. Duri and Schafer[34] describe a method where no activation step is required. A chemical method for the activation of almond shells was investigated by Ruiz Bevia et al.[35]. The use of $ZnCl_2$, as activating reagent, produced the best results[35].

The porous structure which develops during the activation step, consists of irregularly shaped spaces between the microcrystallites. Activated carbon generally has an extended surface area of between 600 and 1500 m^2/g[27]. Mercury porosimetry and nitrogen adsorption have been used to obtain pore size distributions for different charcoals[28,36]. Although the activation procedure mainly determines the nature of the surface oxides and the surface area of the product, the structure of the pores and the pore-size distribution are, to a large extent, predetermined by the source material[26].

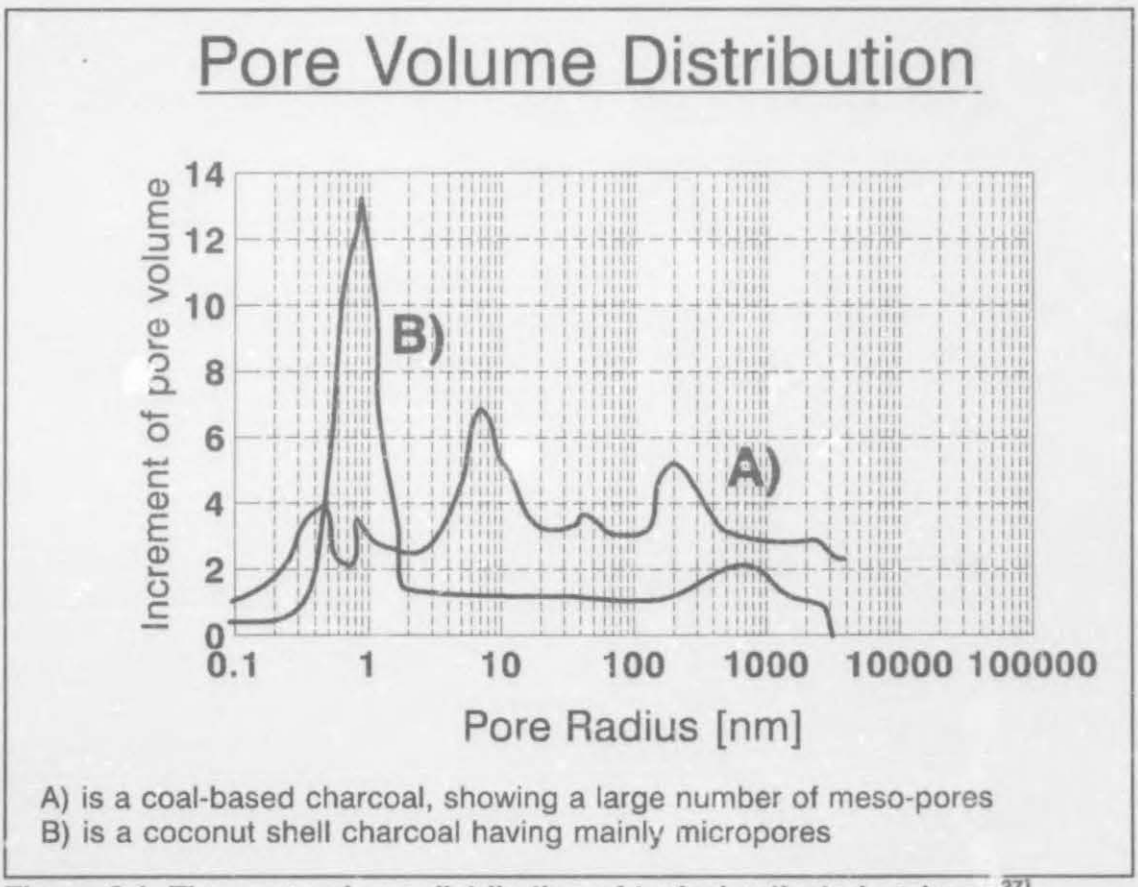

Figure 2.1: The pore volume distribution of typical activated carbons[27].

These differences are apparent in figure 2.1, which shows pore-size distribution data for carbon products manufactured from coconut-shell and bituminous material[27]. These pores are generally classified in terms of their equivalent diameters[27,29]:

macropores	50	-	2000	nm
mesopores	5	-	50	nm
micropores	0.8	-	5	nm

The most important division of activated carbon is into what Steenberg[37] has called the H- and L-carbons. H-carbons are formed at temperatures in excess of 700°C and are characterized by taking up acid on immersion in water. L-carbons are activated well below 700°C, and are characterized by taking up a base on immersion in water. The two types of carbon are completely interconvertible. Heating an H-carbon in air at 400°C will produce an L-carbon and therefore H-carbons must be cooled in an inert atmosphere after activation[2]. Oxygen is irreversibly adsorbed by the carbon and only evolves at high temperatures as CO and CO_2, showing that when is present on the carbon, it is chemically bound to the surface as surface oxides[37]. Although these oxides play an important role in the adsorption process, their identities are not known with certainty. According to McDougall and Hancock[27], the following oxide groups may be present on the surface of the activated carbon, i.e. carboxylic acid, phenolic hydroxyl, quinone-type carbonyl, normal lactones, fluorescein-type lactones, carboxylic acid anhydrides, and cyclic peroxides. Tsuchida et al.[38] suggested that in addition to these groups, chromene-type groups would account for the ion-exchange properties of activated carbon. The temperature and the conditions of activation should alter the ratio of these functional groups and play an important role in determining the overall activity of the carbon[38].

2.2 ACTIVATED CARBON FOULANTS AND THEIR CLASSIFICATION

In gold recovery circuits, carbon is often fouled by $CaCO_3$, resulting from lime added

for pH adjustment and by other inorganic foulants that may be specific to an ore. These inorganic compounds can be removed to a large extent by acid washing. However, thermal regeneration of the spent activated carbon is often required for the complete removal of some of the organic substances. These organic substances originate mainly from wood fibres and the vegetation on sand or slime deposits that are being reclaimed[39]. Organic substances can also enter the solution phase by the alkaline hydrolysis of wood fibres and/or fine vegetation that may be present amongst the activated carbon particles during the elution thereof with hot caustic solution. The water used at plants often contains traces of organic substances like detergents. When a flotation step precedes leaching and gold recovery, flotation reagents also add to the organic substances that could foul the carbon.

Pollutants usually leave different amounts of residue on the carbon after heating in an inert atmosphere. Suzuki et al.[40] studied the amount of residue of 32 different organic substances using gravimetric analysis (TGA) and classified them into three distinct groups[40]:

- Group I - organic substances which are very volatile and easy to desorb, such as n-hexane, benzene and butanol;
- Group II - organic substances which are easy to decompose without leaving residual char, such as poly-ethyleneglycol and benzoic acid;
- Group III - organic substances such as phenol, lignin and humic acid, which leave a relatively large amount of residue upon heating up to 800°C. These carbonaceous residues cannot be removed by mere further heating of the carbon.

(The organic materials belonging to group I, II and III will be referred to as type I, II and III organic materials, respectively.)

The amount of residue, if any, is of great concern, since the residue occupies or obstructs active sites on the activated carbon and reduces its adsorptive capability.

The classification of Suzuki et al.[40] suggests that the organic substances of group III are critical to thermal regeneration, since these foulants cannot be removed by heating only. Wang and Smith[41] confirmed this behaviour with TGA of phenol (a type III organic material) adsorbed on a bituminous-base activated carbon. After heating the carbon to 800°C a residue of 29 per cent of the initial loading was observed. Results obtained for a carbon lloaded with sodium dodecyl-benzene sulphonate (also a type III organic substance) suggest that considerable amounts of carbonaceous residue remain on the carbon upon heating to 850°C in an inert atmosphere[42].

An interesting phenomenon in the results of Suzuki et al.[40] is the combined effect of the aromatic ring and the OH group on the amount of residue. Alcohols, benzene or toluene leave little residue compared with phenol after heating in an inert atmosphere. Suzuki et al.[40] did not explain this specific behaviour in their study. However, the aromatic content, i.e. the fraction of carbon atoms in a molecule which is contained in aromatic rings, and the boiling point were found to be the two main factors influencing the amount of residue which remains on the carbon after heating[40]. Harriott and Cheng[43] supported this result when they observed that the amount of residue left on the carbon after thermal decomposition of the adsorbate at 600°C could be related to the aromatic portion of the adsorbate. It is possibly only the side groups which are lost during heating, while the aromatic portion of the foulants is mainly deposited as a carbonaceous residue. Suzuki et al.[40] summarized their findings as follows: if the boiling point of a substance is above 170°C and its aromatic content is more than 80 per cent, it is very likely to belong to group III. When the aromatic content and the boiling point of an organic material are known, it is thus possible to make a rough prediction as to whether the organic material will leave a residue or not. The precursors used in the manufacturing of the carbon onto which the organic materials were loaded, were found not to influence these findings significantly.

According to Martin and Ng[44], there is a marked correlation between the molecular weight of adsorbates and the efficiency of regeneration: it was found that smaller molecular weights correlate with lower regeneration efficiencies.

It is desirable to prevent the fouling of activated carbon in the CIP circuit. Therefore it is important to predict the amount of residue on the carbon after heating in an inert atmosphere, since this would determine whether thermal regeneration in an inert atmosphere would be adequate to restore the original activity of the carbon. It would be possible to gather enough data from TGA to train a sophisticated mathematical tool like a neural net to learn the relationship between the aromatic number, the boiling point and the molecular weight as inputs, and the amount of residue as output. Such a result would be very interesting and would summarize the work done by Suzuki et al.[40], Wang and Smit[41], Umehara et al.[42], Harriott and Cheng[43] and Martin and Ng[44]. The neural network could then be used to predict the amount of residue for a wide variety of organic materials when the aromatic number, the boiling point and the molecular weights of these organic materials are known. Unfortunately, this information is not usually available. Furthermore, adsorbates which are adsorbed onto carbon in the CIP circuit are unknown, making any predictions of the amount of residue impossible. An alternative method should therefore be investigated to make predictions of this kind.

2.3 KINETICS OF STEAM GASIFICATION

When activated carbon is fouled by one of the type III organic substrates, thermal regeneration in an inert atmosphere alone is not adequate to restore the original activity of activated carbon. Oxidation is necessary for the complete removal of the residual material[42,45] to regain the activity of the carbon.

Steam regeneration is used to remove the residual char left in the pores of the carbon by the more complex (type III) organic compounds in order to restore the original activity of the carbon. Steam, in preference to other oxidizing gases, is used because the steam-carbon reaction is endothermic, which makes it possible to control the reaction temperature. Apparently, the use of oxygen in the temperature range 630-780°C could lead to explosive gas mixtures. Spontaneous ignition of carbon monoxide

and oxygen mixtures has also been observed. Secondary oxidation of the product could also retard the oxidation process[46]. Furthermore, the velocities of the reactions of carbon with oxygen:

$$C + \tfrac{1}{2}O_2 \leftrightarrow CO \quad \textbf{(2-1)}$$

$$C + O_2 \leftrightarrow CO_2 \quad \textbf{(2-2)}$$

are orders of magnitude greater than the steam-carbon reaction 2-3[47,48]. Since these reactions are also exothermic, and therefore selfpromoting, control of the reaction rates is extremely difficult. They would, if allowed to occur, result in aggressive oxidation along the surface of the carbonaceous residue and of the virgin (base) carbon[49]. The pores would widen, the residue would not be removed from the deep pores and, in general, the adsorption sites would not be reactivated[49]. This would result in excessive losses of valuable activated carbon. Therefore, care is taken to exclude air (and thus oxygen) from the atmosphere in the regeneration furnace.

The generation of carbon dioxide as an alternative oxidizing gas is expensive and impractical. Furthermore, large amounts of steam are generated during drying of the wet (feed) carbon in the rotary kiln, which could be used in the oxidation step. This makes steam superior to the other oxidizing gases.

The kinetics of the steam gasification of pyrolysed residues and carbon have been studied in great detail[50-57]. The main reactions that occur during steam-carbon gasification are[49,50,57]:

$$C + H_2O \leftrightarrow CO + H_2 \qquad \Delta H_r = 131.4 \text{ kJ/mol} \quad \textbf{(2-3)}$$

$$CO + H_2O \leftrightarrow CO_2 + H_2 \qquad \Delta H_r = -41 \text{ kJ/mol} \quad \textbf{(2-4)}$$

$$C + CO_2 \leftrightarrow 2CO \qquad \Delta H_r = 172 \text{ kJ/mol} \quad \textbf{(2-5)}$$

$$C + 2H_2 \leftrightarrow CH_4 \qquad \Delta H_r = -89 \text{ kJ/mol} \quad \textbf{(2-6)}$$

$$CO + 3H_2 \leftrightarrow CH_4 + H_2O \qquad \Delta H_r = -206.3 \text{ kJ/mol} \quad \textbf{(2-7)}$$

with reactions 2-3 and 2-4[49,56] being the most significant during gasification.

Harriott and Cheng[43] observed that between 500°C and 640°C, the reaction time of carbonaceous alkyl phenol residues, obtained during the heating of carbon, is twelve times as fast with oxygen as with the base carbon. However, at temperatures above 700°C, which is the temperature range in which steam regeneration is performed, the residues lose their high activity. It was further observed[53] that, between 730°C and 850°C, virgin carbon and spent (used) carbon react with steam at similar rates. Since the reaction is endothermic, the rate of reaction only becomes significant at temperatures in excess of 815°C[53]. Thus, residues can be more reactive than the base carbon at temperatures lower than 700°C, making it possible to selectively gasify the residues and not the carbon. The steam-carbon reaction, however, is too slow at temperatures below 700°C to make use of this property.

The rate expression for the steam-carbon gasification reaction was determined by various researchers[53,57];

$$R = \frac{k_1 p_{H_2O}}{1 + k_2 p_{H_2} + k_3 p_{H_2O}} \qquad (2\text{-}8)$$

where;

$$k_1 = k_1^* \exp\left(\frac{-E_1}{R_0 T}\right)$$

$$k_2 = k_2^* \exp\left(\frac{-\Delta H_{H_2}}{R_0 T}\right) \qquad (2\text{-}9)$$

$$k_3 = constant$$

Equation 2-8 is known as the Langmuir-Hinshelwood equation. Hydrogen, which is a by-product of the reactivation reactions 2-3 and 2-4, will naturally tend to suppress the gasification rate[49,53,58] via the rate equation 2-8. It will also extend the range within which the reaction rate, R, will be sensitive to the steam concentration. The reaction rate changed from first order to zero order as the steam concentration increased[49,53].

The kinetics of the steam-activated carbon reaction were also studied[45] over a wide range of steam pressures (100-10 000 Pa) and temperatures (850-950°C) with virgin carbon samples and with samples previously loaded with phenol. The rate equation which best represented the data was[45]:

$$r = \frac{K_1 p_{H_2O}}{(1 + \sqrt{K_2 p_{H_2O}})^2} \qquad \textbf{(2-10)}$$

Equation 2-10 is only valid if no hydrogen is present in the oxidizing atmosphere. It is therefore not applicable for kinetic calculations in a rotary kiln.

Matsui et al.[58] investigated carbon dioxide gasification rates of coal char. It was observed that the reaction rate is independent of particle size in the size range +44 - 710 μm. Contrary to these results Kasoaka et al.[59] observed during a similar experiment that the rate of gasification is dependent on the type of coal. In view of this contradiction and the fact that no relevant literature could be found, it is not possible to draw any conclusions about the effect of particle size on the rate of gasification of activated carbon at this stage.

2.4 MASS TRANSFER DURING THERMAL REGENERATION

The mass transfer during steam gasification of activated carbon is very complex. No relevant literature investigating this specific problem could be found. Based on experimental results, several authors[53,61] have concluded, however, that at temperatures below 1000°C and in particles up to 1 mm in diameter, the steam carbon reaction is controlled mainly by chemical reaction. Ergun and Mentser[62] also concluded that film-boundary diffusion has no influence on the observed reaction rate below 1100°C and that any possible influence of the intraparticle diffusion in particles up to 1 mm in size might be limited by the presence of macropores. It was also noted that, should a diffusion-controlled regime be encountered, the outward diffusion of carbon monoxide from the carbon pores is the step most likely to determine the reaction rate. It was further pointed out that a change in the slope of an Arrhenius-type plot (Ln(k) vs 1/T), does not necessarily indicate a transition from the chemically to a mass transfer controlled regime. It can also be an indication of, for example, a modification of the carbon structure[62].

The reaction rate for both carbon dioxide and steam with activated carbon was found to be controlled by chemical reaction at temperatures up to 1000°C[59]. During kinetic studies of the carbon-steam reaction, Riede and Hanesian[51] estimated that the diffusion resistance only contributed to about 1-2% of the total resistance in the temperature range 700-900°C.

However, some evidence of the influence of mass transfer was observed[50,53], although these authors also conclude on grounds of the high activation energy, that the reaction is controlled mainly by chemical reaction.

2.5 ACTIVATED CARBON REGENERATION

Van Vliet[22] and Urano et al.[61] summarized carbon regeneration in a rotary kiln as a four-stage process comprising of:

(i)	Drying of spent carbon;	80 - 450°C
(ii)	Vaporization of the volatile adsorbates;	450 - 600°C
(iii)	Pyrolysis of the non-volatile adsorbates;	600 - 750°C
(iv)	Oxidation of the pyrolysed adsorbates;	750 - 830°C

The following undesirable reactions[61] occur simultaneously with processes (i) to (iv):

(v) Thermal decomposition of the activated (base) carbon;
(vi) The gasification of the activated (base) carbon with steam.

The rate and extent of processes (iii), (v), and (vi) are virtually independent of the composition of the surrounding atmosphere, and are mainly a function of the temperature[61].

The vaporization, thermal decomposition and gasification of a wide range of single adsorbates have been studied extensively[40-42,44,45,50,60]. The physical and chemical properties of these adsorbates were known, which made it relatively easy to relate some of the results to these properties. However, in practice, activated carbon is fouled by several unknown organics. The mathematical description of the kinetics of the simultaneous vaporization, decomposition, pyrolysis and gasification of a large number of unidentified adsorbates is a complex problem. A model was developed[54] by which the weight loss of carbon, loaded with a mixture of organic compounds and subjected to a time dependent temperature, can be predicted. The overall rate of mass loss, due to the multiple reactions that take place during the thermal regeneration and gasification of activated carbon, is best described by assuming that a number of first order reactions are taking place simultaneously[54]. The distribution of the activation

energy of these reactions can be derived from the shape of a TGA curve obtained by increasing the sample's temperature at a constant rate[54]. Hashimoto et al.[54] proved that the mass loss of spent carbon due to pyrolysis and gasification can be predicted from appropriate TGA curves. Unfortunately, drying of the wet carbon and the influence of catalysts were not investigated. However, the use of TGA analysis for predicting the overall mass loss of spent carbon during thermal regeneration is a reliable alternative in the situation where the organic adsorbates are unknown.

Van Deventer and Camby[64] correlated the equilibrium capacity and kinetics of adsorption of silver cyanide with carbon regeneration conditions. It was found that the regeneration temperature has the most marked effect on the adsorption behaviour of the carbon. At temperatures between 700°C and 900°C, the carbon was restored to a quality close to or better than that of the virgin carbon, irrespective of the residence time. However, these authors did not report results obtained with residence times shorter than ten minutes. Van Staden[65] repeated these experiments where 20 gram samples of carbon were regenerated in a steam atmosphere with residence times of between 0 and 40 minutes. The results are depicted in figure 2.2. The optimum temperature observed, is about 650°C. However, a relationship between the duration of regeneration and activity does not exist.

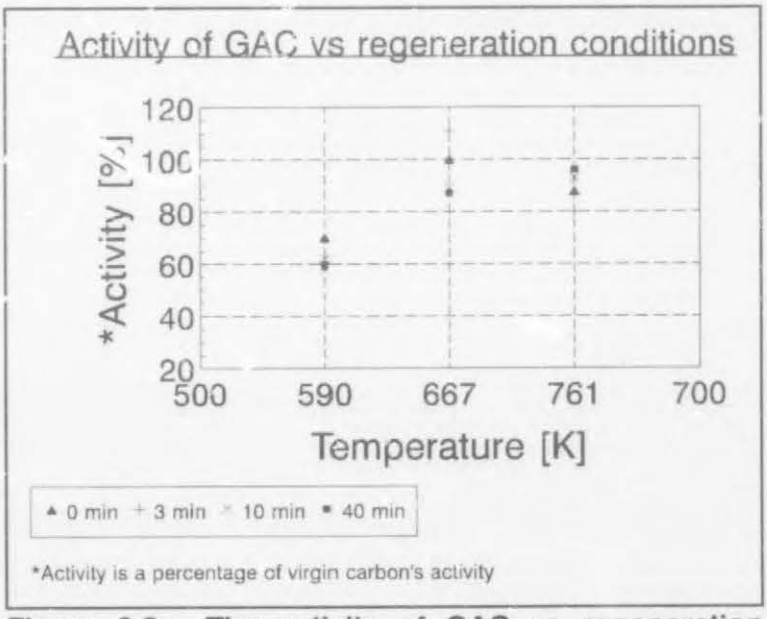

Figure 2.2: The activity of GAC vs regeneration conditions[65].

Umehara et al.[42] found that the adsorption capacity of carbon, containing the

pyrolysed residue of dodecylbenzene sulphonate, can be restored to that of virgin carbon by steam regeneration for 16 minutes at 750°C. Prolonged steam regeneration does not influence the adsorption capacity[42].

2.6 CATALYSTS FOR GASIFICATION

The effects of catalysts are very prominent in the gasification of carbon with oxidizing gases and have been extensively studied by various authors[66-81]. The catalytic effects of alkali metal salts on the gasification of carbon are probably best explained by sequences of cyclic redox processes involving reactions of the salts with the carbon substrate and subsequent re-oxidation by reaction with the oxidizing gaseous environment[71].

Kapteijn et al.[75] conducted a study to obtain the catalytic activity of the earth alkali elements on the gasification of carbonaceous materials in CO_2 atmosphere. Earth alkali elements catalyze the CO_2 gasification of activated carbon in the following order of effectiveness[75]:

$$Be \approx Mg < Ba \approx Sr < Ca$$

It was also shown that, in contrast with some reported results in the literature, the activity of the elements increases with increasing catalyst concentration[75].

Kapteijn et al.[67] showed that the activity of the alkali carbonates increased in the following sequence:

$$Li < Na < K < Rb < Cs$$

Hüttinger and Minges[78] performed similar work for potassium halides. The following results were obtained:

KF > KCl > KBr

Inorganic substances like aluminium[70], minerals of silicon[70], alkali metals[70-79], alkaline earth metals[70,75], iron[70], transition metals[69] and compounds of sulphur[70] have a definite effect on the gasification reaction. Alkali metals, alkaline earth metals and the transition metals promote the gasification rate, especially at low temperatures[70]. However, compounds like sulphur can prevent gasification by poisoning the catalyst, whereas silicon oxide can convert the alkali and other metals to silicates and, thus, the chain of reactions of the metals leading to the promotion of the gasification rate, is interrupted. Although the catalytic effect can be an advantage, an acid wash precedes regeneration to remove most of the calcium carbonate and silica.

2.7 PARAMETERS TO EVALUATE REGENERATION

The parameters used to investigate the efficiency of regeneration of activated carbon are the physical characteristics of the surface area, pore volumes, pore distribution and adsorption data, i.e. the iodine number, phenol number, the capacity of the regenerated carbon to decolourize methylene blue and the adsorptive capacity for gold cyanide of the regenerated carbon.

Laxen and Brown[11] studied the effects of temperature and time during the steam regeneration of an eluted carbon sample from a mine on the micro-, meso- and macropore volumes as well as the activity after regeneration. Figure 2.3 illustrates these results. At a residence time of 10 minutes the micropore volume increased with temperatures up to 850°C[11]. Regeneration with longer residence times (20 and 30 minutes) tended to decrease the micropore volume, since micropores were converted to meso- and macropores. Furthermore, these long regeneration times at high temperatures destroyed the carbon structure, which was undesirable. The activity increased by an increase in both temperature and time. Accordingly, a short

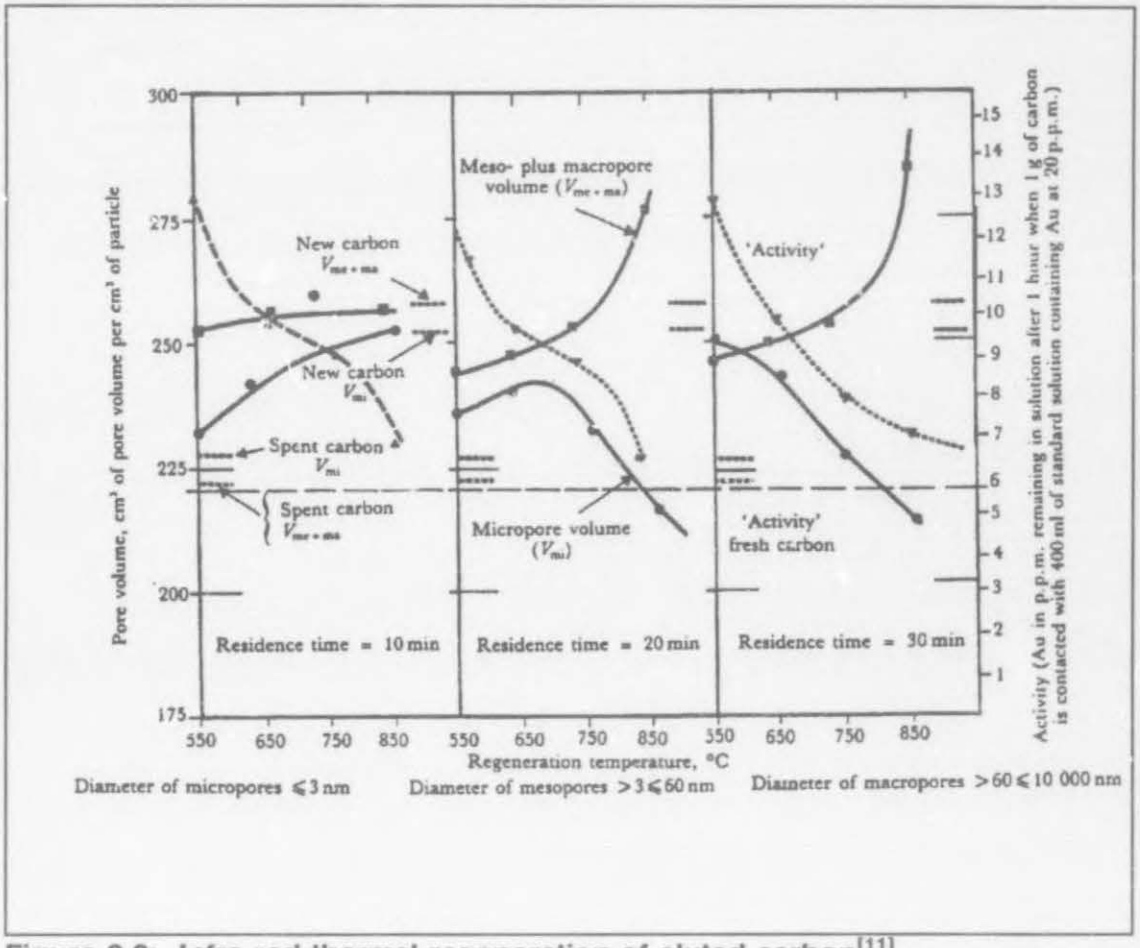

Figure 2.3: Infra-red thermal regeneration of eluted carbon[11].

regeneration time (10 minutes) is favourable for the multicycle use of activated carbon[11]. Van Vliet and Venter[82] obtained similar optimum conditions and proposed regeneration at a temperature of 850°C for 5-10 minutes. These conditions will restore the adsorption capacity, while maintaining the mechanical strength.

Kato et al.[60] studied the relationship between the weight loss by regeneration in a nitrogen and steam-nitrogen atmosphere, and the adsorption capacity, using TGA. The adsorption capacity was estimated by the Iodine number and the capacity of the regenerated carbon to e decolourize methylene blue. It was concluded that the adsorption capacity of the regenerated carbon can be estimated from its weight loss. Furthermore, the Iodine number of the regenerated carbon in the steam-nitrogen

atmosphere was significantly larger than that for the nitrogen atmosphere.

La Brooy et al.[21] examined the effect of inorganic contamination on the activity of the carbon. The criterion for the evaluation of the carbon performance was the carbon activity derived from the adsorptive capacity by the following equation[21]:

$$\frac{dq_{Au}}{dt} = vq_{Au_0}t^{s} \qquad \textbf{(2-11)}$$

where the rate constant v is an indication of the carbon activity.

Since the activity of the carbon is related to its adsorptive capabilities, the parameters of an equilibrium isotherm could also be used to represent the activity. An equilibrium isotherm describes the relationship between the concentration of the adsorbate in the liquid phase and the concentration on the surface of the adsorbent. In aqueous systems the most commonly used single solute isotherms are:

- Linear isotherm:

$$q_e = AC_e \qquad \textbf{(2-12)}$$

- Freundlich isotherm:

$$q_e = AC_e^{n} \qquad \textbf{(2-13)}$$

- Langmuir isotherm:

$$q_e = \frac{AC_e}{B + C_e} \qquad \textbf{(2-14)}$$

where A is the adsorption parameter in equations 2-12, 2-13 and 2-14.

One of the objects of this study was to link the adsorptive capabilities of the regenerated carbon to the mass loss of the carbon during regeneration. An easy and effective method would be to try and relate the constants of equations 2-12 to 2-14 to the mass loss during regeneration.

2.8 HEAT TRANSFER IN A ROTARY KILN

The rotary kiln is a gas-solid reactor that has a long history of use in the metallurgical and chemical industries. Metallurgical processes[83] employing the rotary kiln include the calcination of alumina trihydrate, the incineration and reduction of iron oxide pellets, the Waelz treatment of zinc-lead ores and the treatment of nickel ores and intermediate products. On the chemical side it is used to produce large tonnages of cement and calcined limestone and dolomite in addition to a variety of other solids such as barium sulphide and titanium dioxide[83,84].

Heat transfer in rotary kilns is a very complicated phenome . nuch as heat is transferred simultaneously by conduction, convection and radiation between the gas, kiln wall and the solids. Six heat transfer steps can readily be identified[83]:

(i) gas-to-solids by radiation and convection;
(ii) gas-to-wall by radiation and convection;
(iii) exposed wall-to-solids by radiation;
(iv) covered wall-to-solids by radiation and conduction;
(v) conduction through the kiln wall;
(vi) surface-to-interior of the solid bed by bulk mixing and conduction;

In addition to the six heat transfer steps listed above, a fundamental heat transfer model in a rotary kiln should also account for the following:

- Reflection of the radiative heat from the wall and solids;

- Re-absorption of the reflected radiative heat from the wall and solids by the gas;
- The variation in solid heat transfer area during a change in the solids mass flow;
- Different feed temperatures of the solids and gas.;
- Different types of activated carbon;
- Different water content (weight %) of the solids in the feed;
- Different kiln parameters, such as:
  - slope of the kiln;
  - diameter of the kiln;
  - length of the kiln;
  - outside wall temperature;
  - retention time of the solids;
  - fill height (see Figure 4.4, page 47 for definition);
  - different lining materials;
- The cooling effect during the evaporation of the water;
- The effect of the reaction energy;
- The change of the gas composition during evaporation of the water and the during the gasification reaction to calculate the gas emissivity;
- A real-gas approach for calculating the gas emissivity.

The heat balance calculation is further complicated by the change in the freeboard gas composition, the reaction energy, axial temperature changes of the gas and solids, and the cylindrical temperature variation of the kiln wall.

The effects of rotary kiln operating conditions and design on the solids heat transfer rate as determined by a mathematical model was investigated by Silcox and Pershing[84]. Although the model was developed for a direct-fired kiln, Silcox and Pershing[84] concluded that the temperature profile of the solids can be altered by simply increasing the solids residence time. The moisture content of the feed solids also has a pronounced effect on the temperature profile in the solids. The model does not taken into account the possible changes in the freeboard gas composition. Furthermore, the flame and the surrounding gases are assumed to be grey.

Limestone calcination in a rotary kiln was investigated by Watkinson and Brimacombe[85]. An extensive heat transfer model was developed, but the temperature profile along the kiln axis is needed for the heat transfer rate calculations. Tscheng and Watkinson[86] investigated the convective heat transfer coefficients in a rotary kiln. Their model is only applicable to the reaction-free system in a non-fired rotary kiln where a gas flow is the primary heat source. The axial temperature profile of the gas must be known in order to calculate the heat balances and the heat transfer coefficients. It was also concluded that the angle of kiln inclination, the mass flow rate of the solids and the particle size have no significant effect on the heat transfer rates[86]. These findings, especially the change in mass flow rate, are very doubtful taking into account that a higher mass flow rate would obviously create a bigger heat transfer area of the solids. The same energy input would thus result in a smaller temperature rise. Watkinson and Brimacombe[85] confirmed this contradiction by showing that the gas-to-solid heat flux is a function of the feed rate.

Sass[87] developed a simplified model of the heat transfer phenomena occurring in a cement kiln. The influences of simultaneous chemical reaction and radiative heat transfer have not been taken into account. The fact that convective heat transfer from the kiln wall to the solids was approximated by assuming that radiative heat transfer could be excluded, is not very convincing. In 1979, Ketslakh and Tsibin[88] published a simple radiative heat transfer model. Unfortunately, approximate equations were used to calculate the emissivities which were differ by 20% from published data. Similar work was done by Watkinson and Brimacombe[85] and Barr et al.[89], but the heat flow rates for a direct-fired rotary kiln were again derived from temperature profiles measured in a pilot kiln. The prediction of the temperature profile in the solids is actually one of the objectives of a heat transfer model in order to predict the mass loss of regenerated carbon.

In all these studies[85-89], the accurate prediction of the heat flow and temperature profiles depends on the values of both convective and radiative heat transfer coefficients, which must be specified. Unfortunately, although critical to model success,

previous investigators[85-89] offer little justification for the heat transfer coefficients used in their work. In these studies, convective heat transfer coefficients have either been calculated from untested equations or chosen on a rule-of-thumb basis, while the equations needed to determine the radiative heat-transfer coefficients are either unspecified, incomplete, or in a form which is not easily understood.

Gorog et al.[90] investigated the importance of the regenerative action of the kiln wall in relation to other heat transfer steps. A detailed evaluation of all the heat transfer coefficients was presented in this work. It was also concluded that the freeboard gas should be treated as a real gas. The error introduced by neglecting the grey-gas behaviour may be greater than 20 per cent[90].

A very useful radiative heat transfer model between a non-grey freeboard gas and the interior surfaces of a rotary kiln has been developed by Gorog et al.[91] Direct gas-to-surface heat transfer, reflection of the radiation by the kiln wall and kiln wall-to-solids heat exchange have been considered. This model was used as part of the overall heat transfer model developed in this study (see Chapter 4). It was concluded from the work of Gorog et al.[91] that, as the freeboard gas common to rotary kiln operations contains carbon dioxide and steam, which emit and absorb radiation in distinct bands, the gray-gas approximation is not valid. Although the model[91] was based on a real-gas behaviour, an equimolar carbon dioxide and steam mixture was assumed as the freeboard gas. This is not the situation in real kilns.

2.9 SIGNIFICANCE OF THE LITERATURE REVIEW

It is clear from a review of the literature that, although extensive work regarding activated carbon and its regeneration has been done, only laboratory prepared cases have been investigated. Heat transfer in a rotary kiln itself is a complex interaction of a variety of simultaneous processes, which together with the multiplicity of the effects of carbon foulants and catalysts, must be taken into consideration in predicting the

optimum condotions for regeneration. The need for a mathematical model to predict the optimum regeneration conditions has thus not yet been satisfied. Neither does a model for the simultaneous conductive, convective and real gas radiative heat transfer exist. Such a model could find its application not only for the regeneration of spent activated carbon, but for a variety of applications in a rotary kiln, like the production of cement and titanium dioxide. It is evident from a review of the literature that the regeneration of spent mine samples is complicated by the fact that the types of organic foulants and the loading of these foulants, are unknown. No model has been published for predicting the mass loss of spent activated carbon with an unknown loading of unknown organic foulants during steam regeneration. A detailed analysis of the sensitivity of the adsorption capacity of the regenerated carbon to changes in the kiln design and operating parameters and activated carbon properties, has also not been investigated. The need to measure the performance of a rotary kiln in restoring activity of the spent carbon has not been satisfied. The influence of rotary kiln performance on the adsorption section of the CIP circuit has not been considered.

A mathematical model for the thermal regeneration of spent carbon should be useful in the industry for predicting optimum regeneration conditions.

CHAPTER 3

EXPERIMENTAL PROCEDURES

Thermogravimetric analysis (TGA) was used to determine the kinetics of the drying process of activated carbon. TGA was also used to generate a set of data of mass loss versus temperature. The TGA furnace was used to regenerate spent carbon to relate the mass loss of the regenerated carbon to the adsorptive capacity thereof. Batch adsorption tests have been used to determine the adsorptive capacity of the regenerated carbon. The experimental procedures used to study these phenomena are discussed in this chapter.

3.1 EXPERIMENTAL MATERIALS

Fresh Le Carbone G 210 AS activated carbon was used to determine the kinetics of drying. The carbon was screened at 0.84 mm (20 mesh) which is the screen size for the carbon prior to re-entry to the CIP circuit. Different organic materials were also loaded onto this carbon to investigate the effect of different foulants on the predicted mass loss of the regenerated carbon. A spent G 210 sample with unknown foulants from the CIP plant at President Brand Gold Mine (PB3) was used to investigate the adsorption capacity of regenerated carbon as a function of the mass loss. White phenol was obtained from Analiticals Carlo Erba and had a purity of 99.5%. Dow froth 2000, Aniken 4122, methylene blue, sodium isobutyl xanthate and wattle bark extract were obtained from MINTEK. These organic materials were loaded onto the fresh activated carbon. Potassium aurocyanide obtained from Barry Colne & Co. as a pure crystalline salt was used in the adsorption tests. Potassium cyanide (as a crystalline salt) was used to maintain the level of free cyanide above 250 ppm while potassium

hydroxide was used to alter the pH of the solution during the adsorption tests. Glass distilled deionized water was used in all the experiments.

3.2 EXPERIMENTAL APPARATUS

A schematic diagram of the experimental regeneration apparatus is shown in figure 3.1. Pure nitrogen gas (99.9%) from a gas cylinder was divided into two streams. One stream passed through a rotameter to measure the flow rate. This stream then passed through a coil submerged in a constant-temperature (88°C) water bath and then to a sealed compartment, filled with distilled water and submerged in the same constant-temperature bath. A thin nozzle was used to guide the heated nitrogen gas under the water in the sealed compartment to generate very small nitrogen bubbles. Therefore it was assumed that the nitrogen was saturated with water vapour at the temperature prevailing in the water bath. The partial pressure of the water was then calculated at this temperature. The saturated nitrogen stream passed through a heating jacket where it was superheated to 200°C before flowing through theTGA reactor chamber.

The balance compartment of the TGA apparatus is open to the furnace chamber. The second nitrogen stream was therefore used as a purge gas to protect the very sensitive electronic equipment in the balance chamber. The flow rate of this stream could be read directly from the TGA instrument. The concentration of steam and the flow rate of the purge gas were determined by measuring the flow rates in both streams and the partial pressure of the steam.

The TGA furnace used was a Shimadzu TGA-50. This is a highly sophisticated computer controlled TGA instrument with software support for data analysis. The mass loss of the sample and the corresponding temperature were recorded automatically with accuracies of ± 0.002 mg and ± 5°C respectively.

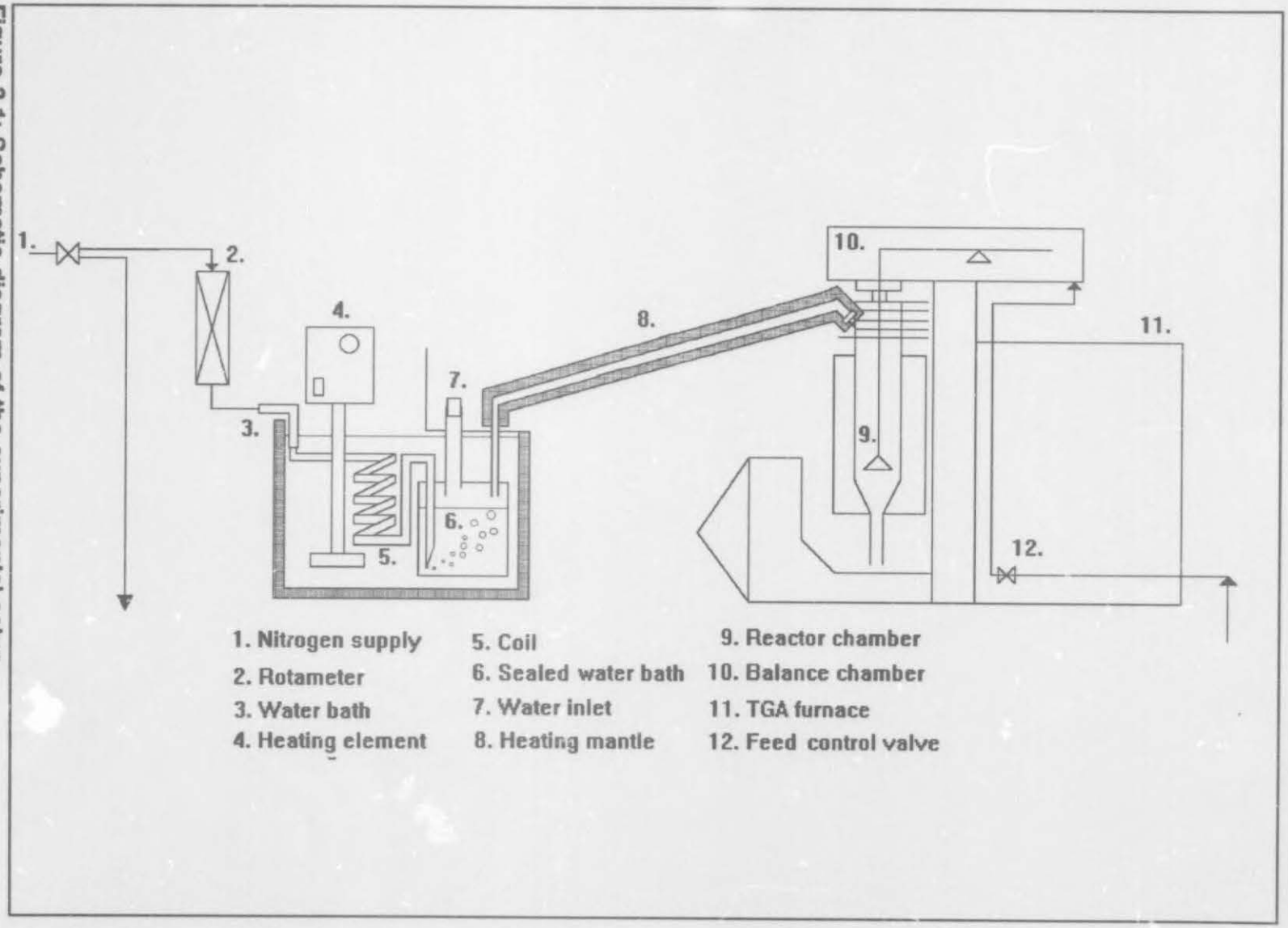

Figure 3.1: Schematic diagram of the experimental setup.

3.3 EXPERIMENTAL PROCEDURES

The experimental procedures for the determination of the drying kinetics, the loading of the organic materials onto the carbon, the determination of the mass loss versus temperature data, the mass loss of spent activated carbon during regeneration and the adsorptive capacity of the regenerated carbon respectively, are discussed below.

3.3.1 Drying kinetics

A representative sample of virgin carbon (G210) was dried for 22 hours at 104°C. Four accurately weighed samples of ±1 gram were then taken, to which accurately weighed amounts of about 0.5, 0.4, 0.3 and 0.2 gram of water were added. The different moisture contents were necessary to investigate their effect on the parameters k^*_d and E_d in equation 6-5 (see Chapter 6, Section 6.3). The slightly wet samples were then left in a sealed container for 60 hours to allow the moisture to be distributed evenly through the sample. One of these mixtures was then thoroughly mixed and a portion of about 50 mg was heated in a TGA furnace (see Section 3.1). The sample was heated in a nitrogen atmosphere, from 20 to 140°C, at a constant rate of 10 °C/min and The mass loss of the sample was recorded as a function of its temperature to obtain a TGA curve.

3.3.2 Mass loss of spent sample

Spent activated carbon (PB3) was dried for 22 hours at 104°C. Approximately 700 mg of the spent carbon was put into a porous quartz glass basket and hung on the suspension wire from the balance in the TGA furnace. Nitrogen purge gas was fed at 10ml/min to the balance chamber. The carbon sample was heated at a rate of 20°C/min up to 102°C. The temperature then remained constant at 102°C for 15 minutes after which individual samples were heated again at 10°C/min to 1400°C,

1300°C, 900°, 750°C, 550°C and 450°C respectively. The constant temperature period of 15 minutes was to ensure that all the water that might be present would evaporate. Different temperatures were used to investigate the effect of different mass losses on the adsorptive behaviour of the regenerated carbon. The steam line was opened for 10 minutes after the constant temperature period of 102°C at a rate of 10ml/min. This procedure would avoid any condensation during the heating stage below 102°C. The partial pressure of the steam was 0.048 atm. The mass loss was determined from the software that controls the TGA furnace.

3.3.3 Batch adsorption experiments

The samples regenerated at 1400°C, 1300°C, 900°C, 750°C, 550°C and 450°C, labelled A, B, C, D, E and F respectively were used in the adsorption experiments. Three (two for sample A) accurately weighed amounts of about 1.0, 0.8 and 0.5 gram from samples A, B, C, D, E and F respectively (see Table D.1, Appendix D), were contacted with 1000ml of gold cyanide solution. A 20 ppm cyanide solution was used. KCN was added to maintain the free cyanide concentration at 250 ppm. This procedure would keep the gold as a soluble gold cyanide complex. The pH was kept above 11 with the addition of KOH as required. These samples were stirred for 48 hours in tank reactors, each fitted with 3 baffles. At the end of the run the equilibrium concentration in the solution phase was determined with atomic absorption spectrophotometry.

3.3.4 Adsorption of materials on the fresh activated carbon

The loading of the organic materials was performed in a rather robust manner, since it unnecessary to know the amount of material loaded. An excess of each of the organic materials was dissolved in 1l water to get a saturated solution. Approximately 10g fresh activated carbon was added and the solution was stirred for 72 hours. The loaded carbon was washed with water for three hours and dried for 22 hours at 104°C

except in case of phenol. To load the phenol, 250g fresh activated carbon was added to 2l of aqueous solution containing 1.3 weight per cent phenol. The solution was stirred for 72 hours after which the concentration of the phenol in the water was determined by spectophotometry. A loading of 150mg phenol/g carbon was obtained.

3.3.5 Experimental procedure for determining the mass loss during decomposition and pyrolysis as a function of the temperature

The samples used for this experiment were dried for 22 hours at 104°C (see Section 3.3.4). Accurately weighted samples of about 40mg each, of the activated carbon loaded with phenol, Dow Froth 2000, Aniken 4122, sodium isobutyl xanthate, wattle bark extract and of the spent sample (PB3), respectively were used. The samples were heated in a nitrogen atmophere from 20°C to 102°C at a constant rate of 10°C/min in the TGA furnace. The temperature remained constant at 102°C for 15 minutes after which the samples were heated again at a rate of 10°C/min to 850°C. The constant temperature period of 15 minutes was again to ensure that all the moisture that might be present would evaporate. The mass loss versus temperature data was then recorded automatically. The data analysis software was used to record the data as the mass loss per initial mass of dry carbon.

3.4 ANALYTICAL METHODS

The analysis of the equilibrium adsorption concentrations was performed by atomic adsorption spectrophotometry, using a Varian AA-1275 instrument with automatic calibration facilities. Three calibration standards, i.e. 20ppm, 10ppm and 5ppm, were used. Gold concentrations were measured at a wavelength of 242.8nm and a slit width of 1nm.

CHAPTER 4

ROTARY KILN SIMULATION MODEL

In this chapter a mathematical model is developed to describe the regeneration process in a rotary kiln. The model is specific for the rotary kiln configuration as described in chapter 1 (see Chapter 1, Section 1.3). The global heat transfer mechanisms needed for the development of the model are described. A conceptual representation of a rotary kiln was assumed for the development of the model. After stating the underlying assumptions for each heat transfer step, a solution was obtained for the overall heat transfer in the rotary kiln. This made it possible to predict the axial temperature profiles of the solids bed, the gas and the kiln wall. The solids bed temperature profile was then used to calculate the mass loss of the carbon due to the decomposition, the pyrolysis and the gasification reaction. Batch adsorption tests were then used to relate the calculated mass loss to the activity of the regenerated carbon for the eluted mine sample (PB3).

4.1 INTRODUCTION

Previous investigators[84-91] represented the heat transfer rate as a global or overall process, i.e. their models could only predict the total heat transfer rate to the burden (solids), gas or wall. Using their approach, the total heat transfer rate to the solids[3] would be calculated as follows:

---

3. The heat transfer rate to the solids is used as an example to illustrate the rationale and is therefore applicable to the gas heat transfer rate as well, although the rate equation may differ to some extent.

$$Q_s = Q_{total_s} \tag{4-1}$$

However, equation 4-1 cannot be used in this form to calculate the burden (solids) temperature as a function of the kiln length. The axial solids temperature profile is critical for calculating the mass loss of the carbon during the regeneration process. In return the mass loss of the carbon is an indication of the extent of foulant removal and thus the regeneration efficiency. Furthermore, the solids temperature is also essential for predicting the rate of water evaporation in the drying zone, the evolution of the volatile matter, decomposition pyrolysis and the gasification reaction. These reactions are needed to predict and calculate the mass loss of the carbon and the gas composition which in turn is required to calculate the thermodynamic properties of the freeboard gas. The heat of reaction for these reactions will also influence the solids and gas temperature profiles. Eventually, predicting the mass loss will regulate the time of regeneration. To summarize, the accurate prediction of the axial solids temperature profile is critical in the development of a successful regeneration model.

The heat transfer rate to the solids must be calculated as a function of the axial position of the kiln. Therefore the total heat transfer rate to the solids should be calculated as follows:

$$Q_s(L) = \int_0^L Q_{total_s} dL \tag{4-2}$$

Equation 4-2 can now be used to calculate the temperature profile of the solids bed as a function of the kiln length. The temperature profile of the freeboard gas can be calculated from a similar equation. The prediction of the axial wall temperature profile will be discussed in Section 4.4.

4.2 CONCEPTUAL REPRESENTATION

Many of the previous models[83,87] used the measured axial temperature profiles to calculate the total heat transfer rates. When the temperature profile has a zero gradient, these models could still be used to calculate the total heat transfer rates. Using this rationale, it is assumed that the kiln could be divided into a number of

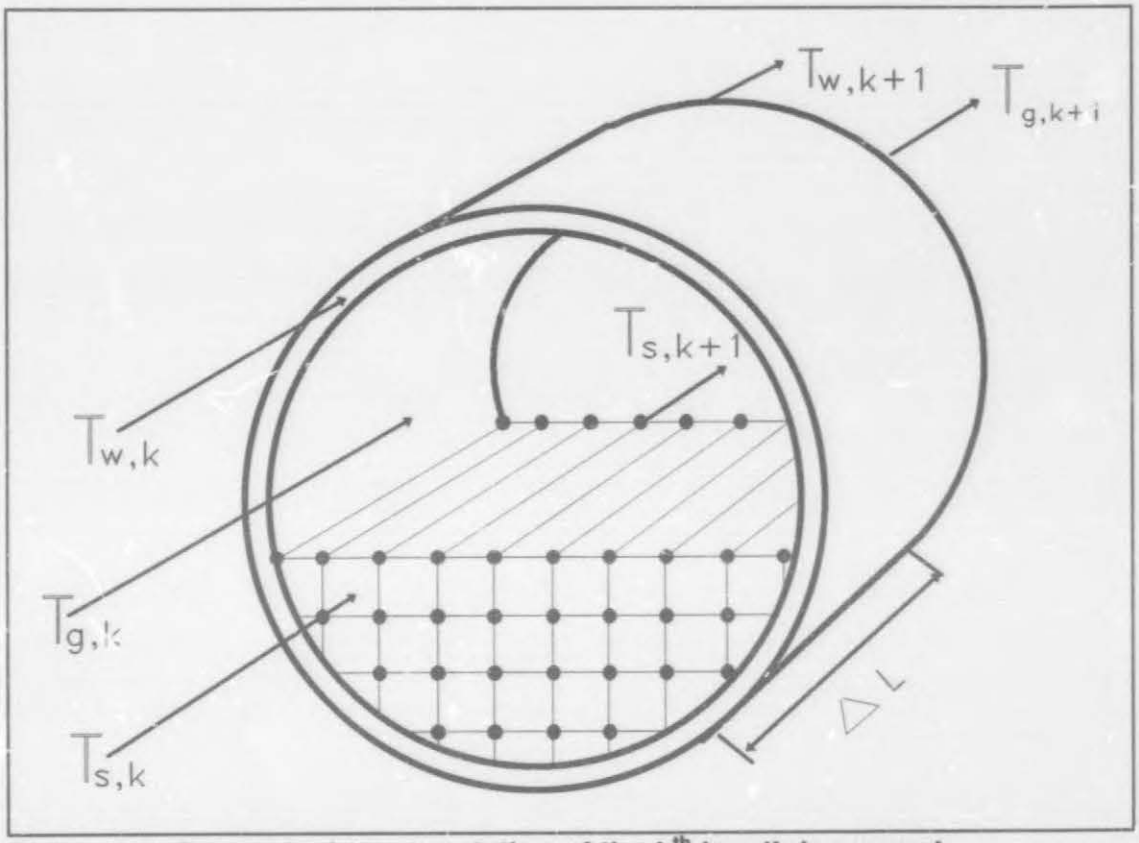

Figure 4.1: Conceptual representation of the k^{th} length increment.

length increments. Provided that the number of increments is sufficiently high, the temperature gradient across a single increment would almost be zero. Figure 4.1 is a conceptual representation of such a length increment. Since the number of increments is high, isothermal conditions in each increment is assumed. This means that the temperatures, $T_{g,k}$, $T_{s,k}$ and $T_{w,k}$ remain constant up to the end of the increment k, when the heat transfer between the solids, gas and wall in that specific

increment, k, will cause a temperature change to $T_{g,k+1}$, $T_{s,k+1}$ and $T_{w,k+1}$, being the new input temperatures for increment k+1.

Since disturbances in the bed of solids are basically limited to only forward motion by the spiral scroll (see Chapter 1, Section 1.3), radial temperature gradients could exist. The bed of solids is thus represented by the nodal structure in figure 4.1, with each node representing the temperature of the solids at that specific point.

Equation 4-2 could thus be discretized as follows:

$$Q_s = \sum_{k=0}^{k=L} Q_{k\ total_s} \qquad (4\text{-}3)$$

Equation 4-3 will be used to calculate the temperature profile of the bed of solids. The same procedure will be used to calculate the heat transfer to the freeboard gas.

4.3 HEAT TRANSFER TO THE SOLIDS

In a rotary kiln, heat is transferred to the solids by two paths, i.e. across the exposed upper surface of the bed of solids and the covered lower surface of the bed. These paths are indicated by figure 4.2. The mechanisms of heat flow to the two surfaces are very different. At the upper surface the solids receive heat directly by radiation (see Section 4.3.1) from the freeboard gas and the inside kiln wall respectively as well as convection (see Section 4.3.2) from the freeboard gas. At the lower surface, heat flows by conduction (see Section 4.3.3) from

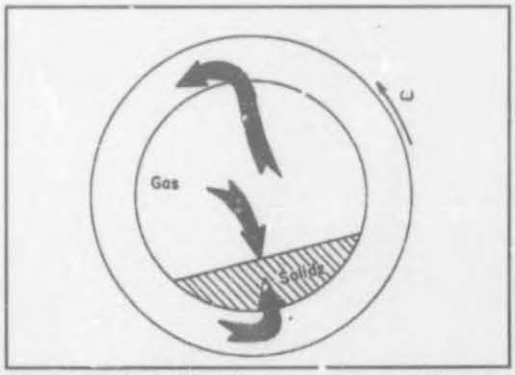

Figure 4.2: Heat transfer paths in the rotary kiln.

the kiln wall to the solids. In the bed of solids, heat flows by means of conduction (see Section 4.3.4). Hence the total rate of heat transfer to the solids is:

$$Q_s = \sum_{k=0}^{k=L} Q_{rad_k} + \sum_{k=0}^{k=L} Q_{cv_k} + \sum_{k=0}^{k=L} Q_{cd_k} \qquad (4\text{-}4)$$

4.3.1 Radiation

Radiation in a rotary kiln is complicated by the reflection of the radiated energy from the kiln wall and the solids, and the re-absorption of reflected energy. Gorog et al.[91] developed a radiative heat transfer model which incorporated these phenomena. However, this model was used with a grey-gas assumption to calculate the radiant heat flux to the kiln wall, the solids and the freeboard gas. The grey-gas approach is erroneous and in the present analysis the real-gas assumption was used. The use of the real-gas assumption is discussed in detail in chapter 6, section 6.1. Consequently the model developed by Gorog et al.[91] was be used to calculate the radiative heat transfer to the solids. The gas was treated as a real gas (see also Chapter 6, Section 6.1).

For the solids, the path of emitted[4] energy is presented in figure 4.3. As can be seen from figure 4.3, radiant energy leaves the solid surface, travels through the gas where a portion is absorbed, and strikes the kiln wall. At the wall surface a portion of the energy is absorbed with the remainder being reflected back through the gas, either to the solids or to the remaining wall. This process is repeated for each reflected ray until all the energy leaving the solids has been absorbed. Two reflections have been considered (shown by the solid lines in Figure 4.3) where the energy remaining after the second reflection was distributed between the solids and the wall as if they were

---

4. Emitted energy, radiation, radiative energy, radiative power and radiant loss are used synonymously in this chapter.

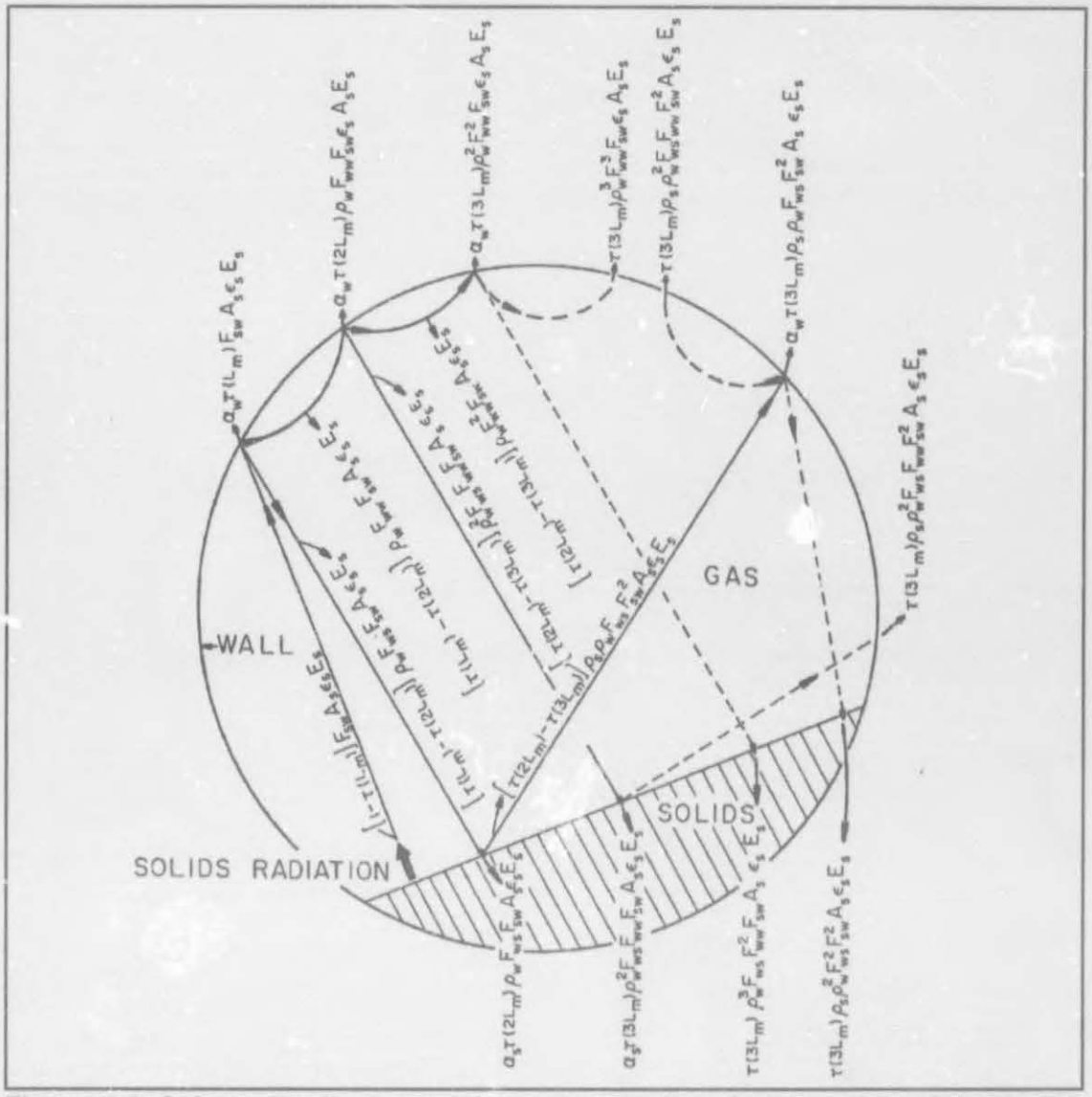

Figure 4.3: Schematic diagram of the cross-section of a rotary kiln showing the path of radiant energy leaving the solids surface[91].

black. The reason that only two reflections are considered is that for a real gas, absorption occurs only within bands bounded by discrete wavelengths[91,93,4]. Therefore, the amount of energy attenuated by successive reflections is decreased, since for each reflection there is less radiant energy lying within the wavelength regions where absorption occurs. Thus, the gas absorbs no radiation after the second reflection since effectively all the radiant energy within the banded regions has been absorbed, i.e. the gas becomes transparent after only two reflections[92]. After two

reflections a large percentage of the radiant energy emitted has either been absorbed by the wall or re-absorbed by the gas[91]. For this reason the radiant energy remaining after two reflections was distributed between the kiln wall and the solids as if they were black as indicated in figure 4.3 by the broken lines. The error introduced by this approximation is small, especially if the solids and wall emissivities are high[91].

The equations for the different heat transfer mechanisms described above (see also Figure 4.3) can be summarized as follows:

- energy emitted by the solids[91]:

$$= -\epsilon_s A_s E_s \tag{4-5}$$

- energy emitted by the solids and re-absorbed by the solids[91]:

$$\begin{aligned} &= \alpha_s \tau_g (2L_m) F_{ws} F_{sw} \rho_w \epsilon_s A_s E_s \\ &+ \alpha_s \tau_g (3L_m) F_{ws} F_{ww} F_{sw} \rho_w^2 \epsilon_s A_s E_s \\ &+ F_{ws} \tau_g (3L_m) F_{ww} F_{sw} \rho_w^3 \epsilon_s A_s E_s \\ &+ F_{ws} \tau_g (3L_m) F_{ws} F_{sw}^2 \rho_s \rho_w^2 \epsilon_s A_s E_s \end{aligned} \tag{4-6}$$

- energy emitted by the wall and absorbed by the solids[91]:

$$
\begin{aligned}
&= \alpha_s \tau_g(L_m) F_{ws} \epsilon_w A_w E_w \\
&+ \alpha_s \tau_g(2L_m) F_{ws} F_{ww} \rho_w \epsilon_w A_w E_{w_k} \\
&+ \alpha_s \tau_{g_k}(3L_m) F_{ws} F_{ww}^2 \rho_w^2 \epsilon_w A_w E_w \\
&+ \alpha_s \tau_g(3L_m) F_{ws}^2 F_{sw} \rho_s \rho_w \epsilon_w A_w E_w \\
&+ F_{ws} \tau_g(3L_m) F_{ww}^3 \rho_w^3 \epsilon_w A_w E_w \\
&+ 2F_{ws} \tau_g(3L_m) F_{ws} F_{ww} F_{sw} \rho_s \rho_w^2 \epsilon_w A_w E_w
\end{aligned}
\tag{4-7}
$$

- energy emitted by the gas and absorbed by the solids[91]:

$$
\begin{aligned}
&= \alpha_s \epsilon_{g_k}(L_m) A_s E_{g_k} \\
&+ \alpha_s F_{ws} \rho_w \dot{\tau}_{g_k}(L_m) \epsilon_{g_k}(L_m) A_w E_{g_k}
\end{aligned}
\tag{4-8}
$$

The net radiative heat transfer to the exposed solid surface in the kth length increment is the sum of equations 4-5, 4-6, 4-7 and 4-8, hence[91]:

$$
\begin{aligned}
Q_{s_k} &= -\epsilon_s A_s E_{s_k} \\
&+ \alpha_s \tau_{g_k}(2L_m) F_{ws} F_{sw} \rho_w \epsilon_s A_s E_{s_k} \\
&+ \alpha_s \tau_{g_k}(3L_m) F_{ws} F_{ww} F_{sw} \rho_w^2 \epsilon_s A_s E_{s_k} \\
&+ F_{ws} \tau_{g_k}(3L_m) F_{ww} F_{sw} \rho_w^3 \epsilon_s A_s E_{s_k} \\
&+ F_{ws} \tau_{g_k}(3L_m) F_{ws} F_{sw}^2 \rho_s \rho_w^2 \epsilon_s A_s E_{s_k} \\
&+ \alpha_s \tau_{g_k}(L_m) F_{ws} \epsilon_w A_w E_{w_k} \\
&+ \alpha_s \tau_{g_k}(2L_m) F_{ws} F_{ww} \rho_w \epsilon_w A_w E_{w_k} \\
&+ \alpha_s \tau_{g_k}(3L_m) F_{ws} F_{ww}^2 \rho_w^2 \epsilon_w A_w E_{w_k} \\
&+ \alpha_s \tau_{g_k}(3L_m) F_{ws}^2 F_{sw} \rho_s \rho_w \epsilon_w A_w E_{w_k} \\
&+ F_{ws} \tau_{g_k}(3L_m) F_{ww}^3 \rho_w^3 \epsilon_w A_w E_{w_k} \\
&+ 2F_{ws} \tau_{g_k}(3L_m) F_{ws} F_{ww} F_{sw} \rho_s \rho_w^2 \epsilon_w A_w E_{w_k} \\
&+ \alpha_s \epsilon_{g_k}(L_m) A_s E_{g_k} \\
&+ \alpha_s F_{ws} \rho_w \dot{\tau}_{g_k}(L_m) \epsilon_{g_k}(L_m) A_w E_{g_k}
\end{aligned}
\tag{4-9}
$$

where:

$$F_{ws} = 1$$

$$F_{ws} = \frac{\sin(\Phi_L)}{\Pi - \Phi_L} \qquad (4\text{-}10)$$

$$F_{ww} = 1 - F_{ws}$$

where Φ_L is defined by figure 4.4:

The reflectivity and emissivity of the kiln wall and the solids respectively, are assumed to be constant.

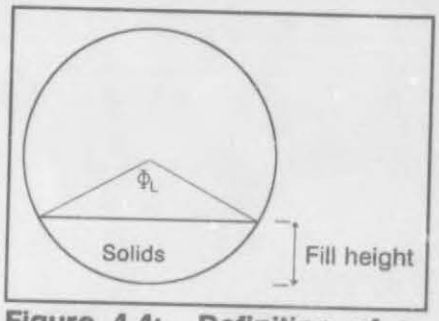

Figure 4.4: Definition of Φ_L and the fill height.

4.3.2 Convection

Although there is no gas flow through the kiln (see Chapter 1, Section 1.3), it is usually considered in published models. Provision should be made for possible gas flow to investigate the influences of an external gas feed, like a flow of extra steam, to enhance the gasification reaction. Of all the heat transfer coefficients, the convective heat transfer coefficient is the least known. Experimental studies[90] indicated that the equation:

$$h_{cv_{g-s}} = 0.4 G_g^{0.62} \qquad (4\text{-}11)$$

fits data for a kiln with measurements of 0.19 to 0.4 meter inside diameter. However, equation 4-11 has not been tested with data from a larger kiln, and thus, its usefulness

in scale-up operations is uncertain. The convective heat transfer rate to the solids is thus represented by equation 4-12.

$$Q_{cv_k} = h_{cv_{g-s}} A_s (T_{g_k} - T_{s_k}) \qquad (4\text{-}12)$$

4.3.3 Conduction

Rotation of the kiln causes a regular cyclic temperature change in the wall as it rotates through the freeboard gas and then passes beneath the burden. The variation of the inner wall temperature is typically between 50 and 100°C[83,90]. The circumferential temperature gradients should be taken into account in calculating the conductive heat transfer rate from the wall to the solids. However, Vaillant[96] has shown the error to be less than 2 per cent of the conductive heat transfer rate to the solids in neglecting these temperature gradients. Gorog et al.[91] also confirmed this result. Calculations indicated that the error introduced by neglecting the circumferential temperature variance is less than 3 per cent. In view of these results the circumferential temperature gradients could be neglected. The temperature of the kiln wall is thus assumed to be constant in a single length increment.

Hence, the heat transfer rate from the inside kiln wall to the solids in the length increment, k, is:

$$Q_{cd_k} = \lambda_s A_s (T_{w_k} - T_{s_k}) \qquad (4\text{-}13)$$

where λ_s is the thermal conductivity of the solids bed.

Equation 4-13 is representative of the total conductive heat transfer rate to the solids. The use of equation 4-13 will be explained in more detail in Section 4.3.5. The use of the thermal conductivity of the solids will also be explained in that section.

4.3.4 Heat transfer in the solids bed

The conduction of heat in the bed itself is a two dimensional problem. Under transient conditions with constant properties and no internal generation, the appropriate form of the heat equation is:

$$\frac{1}{\alpha}\frac{\partial T}{\partial t} = \frac{\partial^2 T}{\partial x^2} + \frac{\partial^2 T}{\partial y^2} \qquad \textbf{(4-14)}$$

where α is the thermal diffusivity.

The assumption of constant thermophysical properties for the bed of activated carbon might seem erroneous, since thermophysical properties vary with temperature. However, isothermal conditions in a length increment of the kiln are assumed (see Section 4.2), provided that the number of increments is sufficiently high. Thus, the assumption of constant properties for the bed of activated carbon is still valid.

4.3.5 Calculation of the temperature distribution in the solids bed

As mentioned in section 4.3, heat is transferred to the solids across the exposed upper surface by radiation, equation 4-9, and convection, equation 4-12, from the freeboard gas. At the lower surface, heat flows by conduction, equation 4-13, from the wall to the solids. A method will now be developed to calculate the temperature of the solids bed as a result of these heat transfer influences.

An explicit finite-difference technique will be used to solve the temperature distribution (Equation 4-14) in the solids bed. The reader is referred to Appendix A for the development of the governing finite-difference equations. The finite difference form of equation 4-14 for the interior nodes of the solids bed in length increment, k, (see Appendix A) is then :

$$T^{p}_{m,n} = T_{m,n} + \frac{\alpha \Delta t}{V}\left[\left(\frac{a+1}{2}\right)(T_{m,n-1} - T_{m,n}) + \left(\frac{b+1}{2}\right)(T_{m-1,n} - T_{m,n})\right] + \frac{\alpha \Delta t}{V}\left[\left(\frac{a+1}{2a}\right)(T_{m+1,n} - T_{m,n}) + \left(\frac{a+1}{2b}\right)(T_{m,n+1} - T_{m,n})\right] \quad \text{(4-15)}$$

The surface of the solids bed is exposed to radiation and possible convection. The total heat transfer rate to the exposed solids surface in a length increment is then the sum of equations 4-9 and 4-12, denoted as q" in equation 4-16. The finite difference form of equation 4-14 for the nodes corresponding to the surface of the solids bed in length increment, k, (see Appendix A) is then:

$$T^{p}_{m,n} = T_{m,n} + \frac{\alpha \Delta t}{V}\left[\left(\frac{b}{2}\right)(T_{m-1,n} - T_{m,n}) + \left(\frac{b}{2a}\right)(T_{m+1,n} - T_{m,n})\right] + \frac{\alpha \Delta t}{V}\left[\left(\frac{a+1}{2b}\right)(T_{m,n+1} - T_{m,n}) + \frac{q''}{\lambda . \Delta L}\right] \quad \text{(4-16)}$$

The temperature of the solids touching the kiln wall and the wall itself were found to be similar, so that heat transfer between the wall and these solids could be ignored[84]. Hence, the temperatures of the m+1 and n+1 nodes which correspond to the kiln wall, are assumed to be equal to the wall temperature. The temperatures $T_{m+1,n}$ and

$T_{m,n+1}$ in equation 4-16 are thus equal to the temperature of the inside kiln wall. Therefore the use of the thermal conductivity of the solids bed is appropriate in equation 4-13.

The nodal temperature distribution of the solids bed can now be calculated from equations 4-15 and 4-16. The average grid temperature of the solids bed is used in equations 4-9 (to calculated the emmisive power) and 4-12. The number of nodal gridpoints is calculated as follows:

1) an arbitrary number of gridpoints is used to calculate the nodal temperature distribution of the solids;
2) then the average temperature of the solids is calculated;
3) more gridpoints are then chosen and steps (1) and (2) are repeated;
4) if there is a large difference between the solids temperature calculated in steps (2) and (3), more gridpoints are chosen until the difference is sufficiently small.

4.4 HEAT TRANSFER TO THE KILN WALL

Heat is transferred to the kiln wall by three separate mechanisms, i.e. by radiation, convection and from electric elements. A loss of convective heat transfer to the surrounding atmosphere, also affects the total heat transfer rate to the kiln wall. These elements are fitted around the outside kiln wall and with proper process control keep the wall temperature constant at a preselected value. These elements are usually divided into three or more sections (see Chapter 1, Section 1.3) each with its own control unit. It is, thus, possible to select a different temperature for each section to create an axial wall temperature profile. Although this facility is hardly ever used in practise, the influence of a sectional temperature profile was investigated (see chapter 7 Section 7.3).

4.5 HEAT TRANSFER TO THE GAS

Heat is transferred to the gas by radiation from the solids and the kiln wall. The model developed by Gorog et al.[91] (see also Section 4.3.1) was used to calculate the radiative heat transfer to the gas.

For the freeboard gas the path of emitted energy is shown in figure 4.5. As seen in figure 4.5 the radiant energy emitted by the gas is received by both the wall and the solids. At the wall and the solids a portion of this incident radiation is absorbed with the remainder being reflected. Since the absorptivity of a real gas for its own radiation is high, only one reflection needs to be considered[91]. The energy remaining after the second reflection is completely absorbed by the freeboard gas.

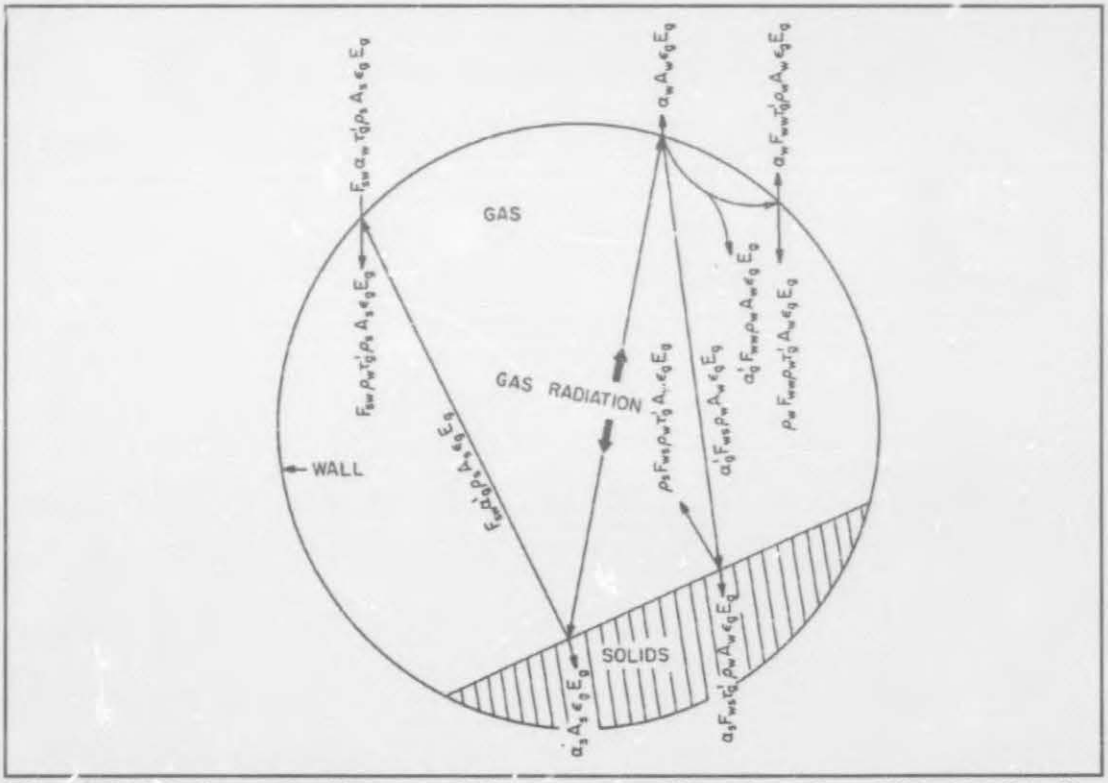

Figure 4.5: Schematic diagram of the cross-section of a rotary kiln showing the path of radiant energy emitted from the freeboard gas[91].

The appropriate equations are:

- energy emitted by the gas[91]:

$$= -\epsilon_g(L_m)A_gE_g \tag{4-17}$$

- energy emitted by the solids and absorbed by the gas[91]:

$$\begin{aligned} &= [1-\tau_g(L_m)]F_{sw}\epsilon_s A_s E_s \\ &+ [\tau_g(L_m)-\tau_g(2L_m)]F_{sw}\rho_w\epsilon_s A_s E_s \\ &+ [\tau_g(2L_m)-\tau_g(3L_m)]F_{ww}F_{sw}\rho_w^2\epsilon_s A_s E_s \\ &+ [\tau_g(2L_m)-\tau_g(3L_m)]F_{ws}F_{sw}^2\rho_s\rho_w\epsilon_s A_s E_s \end{aligned} \tag{4-18}$$

- energy emitted by the wall and absorbed by the gas[91]:

$$\begin{aligned} &= [1-\tau_g(L_m)]\epsilon_w A_w E_w \\ &+ [\tau_g(L_m)-\tau_g(2L_m)]F_{ww}\rho_w\epsilon_w A_w E_w \\ &+ [\tau_g(2L_m)-\tau_g(3L_m)]F_{ww}^2\rho_w^2\epsilon_w A_w E_w \\ &+ [\tau_g(2L_m)-\tau_g(3L_m)]F_{ws}F_{sw}\rho_s\rho_w\epsilon_w A_w E_w \\ &+ [\tau_g(2L_m)-\tau_g(3L_m)]F_{ws}F_{ww}F_{sw}\rho_s\rho_w\epsilon_w A_w E_w \\ &+ [\tau_g(L_m)-\tau_g(2L_m)]F_{ws}F_{sw}\rho_s\epsilon_w A_w E_w \end{aligned} \tag{4-19}$$

- energy emitted by gas and reabsorbed by the gas[91]:

$$\begin{aligned} &= \acute{\alpha}_g\rho_w\epsilon_g(L_m)A_wE_g \\ &+ [\rho_wF_{ww}+\rho_sF_{ws}]\rho_w\acute{\tau}_g(L_m)\epsilon_g(L_m)A_wE_g \\ &+ [\acute{\alpha}_g+\rho_w\acute{\tau}_g(L_m)]F_{sw}\rho_s\epsilon_g(L_m)A_sE_g \end{aligned} \tag{4-20}$$

The net radiative heat transfer in the length increment, k, could be calculated as follows[91]:

$$
\begin{aligned}
Q_{g_k} = & -\epsilon_{g_k}(L_m)A_g E_{g_k} \\
& + \left[1-\tau_{g_k}(L_m)\right]F_{sw}\epsilon_s A_s E_{s_k} \\
& + \left[\tau_{g_k}(L_m)-\tau_{g_k}(2L_m)\right]F_{sw}\rho_w\epsilon_s A_s E_{s_k} \\
& + \left[\tau_{g_k}(2L_m)-\tau_{g_k}(3L_m)\right]F_{ww}F_{sw}\rho_w^2\epsilon_s A_s E_{s_k} \\
& + \left[\tau_{g_k}(2L_m)-\tau_{g_k}(3L_m)\right]F_{ws}F_{sw}^2\rho_s\rho_w\epsilon_s A_s E_{s_k} \\
& + \left[1-\tau_{g_k}(L_m)\right]\epsilon_w A_w E_{w_k} \\
& + \left[\tau_{g_k}(L_m)-\tau_{g_k}(2L_m)\right]F_{ww}\rho_w\epsilon_w A_w E_{w_k} \\
& + \left[\tau_{g_k}(2L_m)-\tau_{g_k}(3L_m)\right]F_{ww}^2\rho_w^2\epsilon_w A_w E_{w_k} \\
& + \left[\tau_{g_k}(2L_m)-\tau_{g_k}(3L_m)\right]F_{ws}F_{sw}\rho_s\rho_w\epsilon_w A_w E_{w_k} \\
& + \left[\tau_{g_k}(2L_m)-\tau_{g_k}(3L_m)\right]F_{ws}F_{ww}F_{sw}\rho_s\rho_w\epsilon_w A_w E_{w_k} \\
& + \left[\tau_{g_k}(L_m)-\tau_{g_k}(2L_m)\right]F_{ws}F_{sw}\rho_s\epsilon_w A_w E_{w_k} \\
& + \dot{\alpha}_g\rho_w\epsilon_{g_k}(L_m)A_w E_{g_k} \\
& + \left[\rho_w F_{ww}+\rho_s F_{ws}\right]\rho_w\dot{\tau}_{g_k}(L_m)\epsilon_{g_k}(L_m)A_w E_{g_k} \\
& + \left[\dot{\alpha}_{g_k}+\rho_w\dot{\tau}_{g_k}(L_m)\right]F_{sw}\rho_s\epsilon_{g_k}(L_m)A_s E_{g_k}
\end{aligned}
\qquad \text{(4-21)}
$$

4.6 KINETICS DURING STEAM REGENERATION

The heat transfer rates to calculate the solids bed and gas temperature profiles have been developed. The reactions during steam regenerating is a result of the temperature of the solids bed. The processes involved in the steam regeneration operation may be divided into the production of steam (see Section 4.6.1) and the production of a variety of other gases (see Section 4.6.2). Steam originates from the evaporation of water during the drying stage. The other gaseous products result from the evaporation of the highly volatile adsorbates during the drying stage, the evaporation of the volatile adsorbates, the decomposition of the unstable adsorbates, the pyrolysis of the non-volatile adsorbates and the products of the steam-carbon reaction. These reactions are important in:

- predicting the composition of the freeboard gas in order to calculate the gas properties;
- predicting the effect of the reaction heat on the solids temperature;
- calculating the mass loss of the carbon.

4.6.1 Water evaporation

The evaporation of water during the drying of the spent carbon had been investigated by an experimental study. It was assumed that the rate of water removal during the drying of the activated carbon could be treated as a first order process (with respect to the amount of remaining moisture on the carbon). The theory, experimental procedures and the results are discussed and presented in detail in chapter 6, section 6.3. From chapter 6, the rate of water removal is:

$$R_d = k_d^* \exp\left(\frac{-E_d}{RT}\right) w \qquad (4\text{-}22)$$

where k_d^* and E_d are functions of the weight per cent moisture loaded onto the carbon (see Chapter 6, Sectior 6.3).

4.6.2 Other freeboard gases

Apart from steam, the freeboard gas also consists of other gases. The prediction of the composition of the freeboard gas is virtually impossible if the adsorbates on the activated carbon are unknown.

Chin et al.[56], however, confirmed that the rates of CO and CO_2 production during

vaporization and pyrolysis, which are of major concern for the calculation of the gas properties (see Chapter 6, Section 6.1), are less than one tenth of those during steam gasification. In practice, the original loading of adsorbate is less than that experienced during experimental studies and the contribution should be even smaller. Evaporation of the volatile adsorbates, the decomposition of the unstable adsorbates and the pyrolysis of the non-volatile adsorbates stop after all the adsorbates have been converted to residual carbon and volatiles. The gasification reaction, however, will carry on until all the carbon has been gasified, provided that a sufficient amount of steam is available. The duration of the gasification reaction is therefore longer with a higher production rate. Futhermore, simulation runs with different freeboard gas compositions indicated that the calculated solids bed temperature, and hence the mass loss is not very sensitive to the fraction of CO and CO_2 in the gas (see Chapter 7, Section 7.3). The major fraction of the freeboard gas is made up of steam which originates from the drying of the activated carbon and possible external feed gas. Thus, the contribution to the freeboard gas by the evaporation of the highly volatile and volatile adsorbates, the decomposition of the unstable adsorbates and the pyrolysis of the non-volatile adsorbates during steam regeneration is negligible compared to the contribution by gasification. However, the mass loss as a result of these reaction cannot be ignored (see Section 4.7).

The main reactions that take place during steam-carbon gasification (see Chapter 2, Section 2.3) are:

$$C + H_2O \leftrightarrow CO + H_2 \quad (4\text{-}23)$$

$$CO + H_2O \leftrightarrow CO_2 + H_2 \quad (4\text{-}24)$$

$$C + CO_2 \leftrightarrow 2CO \quad (4\text{-}25)$$

$$C + 2H_2 \leftrightarrow CH_4 \quad (4\text{-}26)$$

$$CO + 3H_2 \leftrightarrow CH_4 + H_2O \quad (4\text{-}27)$$

The carbon-oxygen reaction has not been considered since the carbon will be regenerated in a steam atmosphere for the reasons outlined in chapter 2, Section 2.3.

Nitrogen also forms part of the freeboard gas atmosphere; however, it is assumed that it does not take part in any reaction. The formation of methane according to reactions 4-26 and 4-27 is thermodynamically unfavoured at the conditions which normally prevail in regeneration furnaces. It occurs slowly at atmospheric pressure and in the absence of a catalyst[47]. Rotary kilns operate at atmospheric pressure and the effect of catalysts can be decreased by acid washing before carbon regeneration. Chin et al.[56] showed that the production of methane is very small compared to the other components. In view of these findings, the formation of methane was taken as negligible.

The Boudouard reaction, reaction 4-25, becomes significant at high temperatures and would dictate the ratio of CO_2/CO since these two gases are simultaneously in equilibrium with the base carbon. It is expected that more CO than CO_2 will be present in the freeboard gas at high temperatures. This is also evident from the equilibrium constant for this reaction (see Appendix B and also Equation 4-32). Previous investigators[56,65] used the water-gas shift equilibrium, reaction 4-24, to calculate the gas composition. This approach is erroneous since conditions in the kiln do not always guarantee sufficient steam for the stoichiometric reaction, while steam could also be introduced to the freeboard gas. These situations occur frequently in practice. Since the amount of CO and CO_2 is simultaneously in equilibrium with the base carbon, the Boudouard equilibrium, reaction 4-25, will prevail.

The rotary kiln operating pressure would not deviate much from one atmosphere with both ends open to the atmosphere (see Chapter 1, Section 1.3). The gas temperature would vary between 25 and 900°C. Under these conditions of low pressure and high gas temperature, the ideal gas law is assumed to be valid. Furthermore, it is assumed that a radial gas temperature gradient does not exist. In any event Gorog et al.[91] have that radial gas temperature gradients do not influence the heat flux to the solids.

Experimental simulation runs performed with the simulator model indicated that the gas pressure would vary from 1 atmosphere at the at the inlet to 1.4 atmosphere at the

outlet. The pressure gradient would introduce a flow of gas to the low pressure regions situated at the feed end of the kiln. It is assumed that with both ends open, together with the diffusion of the gaseous products to regions of low concentration and temperature, the pressure distribution would create a well-mixed freeboard gas. Even if external gas is added, the freeboard gas is still assumed to be in mixed flow, since gas would flow from the high pressure region at the discharge end to the low pressure feed end. External feed gas if required is fed co-current with this flow. However the gas flow rate should not vary much from the flow rate of the solids. The assumptions concerning the composition of the freeboard gas are summarized as follows:

- the gaseous products produced of vaporization and pyrolysis are negligible;
- the formation of methane can be ignored;
- the Boudouard equilibrium, reaction 4-25, is maintained;
- the ideal gas law hold;
- radial temperature gradient does not exist;
- the freeboard gas is ideally mixed;
- the kiln operates at atmospheric pressure.

Thus, the gasification reactions are:

$$C^* + H_2O \leftrightarrow CO + H_2 \qquad \Delta H_r = 131.4 \text{ kJ/mol} \qquad (4\text{-}26)$$

$$CO + H_2 \leftrightarrow CO_2 + H_2 \qquad \Delta H_r = -41 \text{ kJ/mol} \qquad (4\text{-}29)$$

$$C^* + CO_2 \leftrightarrow 2CO \qquad \Delta H_r = 172 \text{ kJ/mol} \qquad (4\text{-}30)$$

Since the residual carbon is more reactive than the virgin (base) carbon[49], it is expected to be oxidised preferentially. It should be noted that the virgin carbon is not excluded from gasification, but would react slowly in comparison to the residual carbon. However, Chihara et al.[53] observed a similar rate for the gasification of residual char (from sucrose deposits) and virgin carbon. In view of this contradiction no conclusion regarding the difference in reaction rates could be made. Thus, C^*

would mean the carbon that reacts.

The overall gasification reaction is then:

$$n_{C^*}C^* + n_{H_2O}H_2O \leftrightarrow n_{H_2}H_2 + n_{CO_2}CO_2 + n_{CO}CO \quad (4\text{-}31)$$

4.6.2.1 Calculation of the gas composition

Reaction 4-31 is not the simple stoichiometric sum of reactions 4-28, 4-29 and 4-30, since the conditions prevailing in a kiln do not guarantee a simple stoichiometric reaction and thus, equilibrium. Accordingly it is possible to cater for and identify situations where the amount of steam is insufficient.

The stoichiometric coefficients in equation 4-31 are calculated from the Boudouard equilibrium and a carbon mass balance. The equilibrium constant for the Boudouard reaction was determined as follows (see Appendix B):

$$K_p = \exp\left[28.5 + \frac{1}{R}\left(-\frac{42952.9}{T} - 1.07Ln(T) - 0.00111T - \frac{392000}{T^2}\right)\right] \quad (4\text{-}42)$$

where K_p is defined as:

$$K_p = \frac{n_{CO}^2}{n_{CO_2}} \quad (4\text{-}33)$$

Then, from a carbon mass balance, the amount of CO and CO_2 can be calculated. Thus from the Boudouard reaction, reaction 4-30:

$$n_{CO_2} + n_{CO} = n_{C^*} \tag{4-34}$$

Solving equations 4-33 and 4-34:

$$n_{CO} = \frac{-K_p + \sqrt{K_p^2 + 4K_p n_{C^*}}}{2}$$

$$n_{CO_2} = \frac{\left(-K_p + \sqrt{K_p^2 + 4K_p n_{C^*}}\right)^2}{4K_p} \tag{4-35}$$

n_{c*} can be calculated from the Langmuir-Hinshelwood rate equation 2-8 (see Chapter 2, Section 2.3) for the gasification reaction, reaction 4-31. Hence:

$$n_{C^*} = t\left(\frac{k_1 p_{H_2O}}{1 + k_2 p_{H_2} + k_3 p_{H_2O}}\right) \tag{4-36}$$

where t is the time the carbon remains at the specific temperature of reaction, and can be calculated from the stability criterion, equation A-15 (see Appendix A).

The amount of steam reacting can be calculated from an oxygen balance, Hence from reaction 4-31:

$$n_{H_2O} = 2n_{CO_2} + n_{CO} \tag{4-37}$$

Similarly, from a hydrogen balance:

$$n_{H_2} = n_{H_2O} \tag{4-38}$$

The freeboard gas composition can thus be calculated using equations 4-35 to 4-38.

4.6.2.2 Heat of reaction

The endothermic gasification reaction will influence the temperature of the solids. To quantify this influence, the endothermic reaction heat for the gasification reaction 4-31 should be calculated.

Assume that x, y and z are the stoichoimetric constants of reactions 4-28, 4-29 and 4-30 respectively to give the gasification reaction, reaction 4-31. These constants can then be calculated from a mole balance of each component. Hence:

$$x = n_{CO_2} + \frac{1}{2}(n_{C^*} + n_{CO_2} - n_{CO})$$

$$y = n_{CO_2} + \frac{1}{2}(n_{C^*} + n_{CO_2} - n_{CO}) \tag{4-39}$$

$$z = \frac{1}{2}(n_{C^*} + n_{CO_2} - n_{CO})$$

Having calculated the stoichiometric coefficients according to equation 4-39, the heat of reaction for the gasification reaction, reaction 4-31, can be calculated from the different heats of reaction of the individual reactions, reactions 4-28, 4-29 and 4-30.

The heat of reaction ΔH_r for the gasification reaction, reaction 4-31, is then:

$$\Delta H_r = 131.4x - 41y - 172z \qquad (4\text{-}40)$$

It is assumed that the energy of the solids in a length increment will decrease (endothermic reaction) by the total amount of heat absorbed by the gasification reaction in that section, hence equation 4-40. It is also assumed that the heat of reaction is not temperature dependent.

4.7 Mass loss of the carbon

The mass loss of spent carbon during steam regeneration is influenced by a variety of simultaneous processes and reactions (see Chapter 2). The mass loss results from the evaporation of the highly volatile adsorbates during the drying stage, the evaporation of the less volatile adsorbates, the decomposition of the unstable adsorbates, the pyrolysis of the non-volatile adsorbates and the products of the steam-carbon reaction. Decomposition of the virgin (base) was also observed[40,43,62,92]. Various investigators[40-45,64] succeeded in deriving mathematical models to calculate the mass loss of a single component loaded onto activated carbon during thermal regeneration. They simulated the evaporation of the highly volatile adsorbates, the evaporation of the less volatile adsorbates, the decomposition of the unstable adsorbates and the pyrolysis of the non-volatile adsorbates. These reactions have been taken as being first order. There was a satisfactory correlation between the calculated and the experimental results. These models, however, are only applicable for carbon loaded with a specific amount of a single known organic material. Adsorbed materials on industrial carbons are difficult to identify, but usually originate from oils, flotation reagents, wood fibres and vegetation substances from the sand or slime deposits that are being reclaimed and other organics in the gold plant solution[59]. The exact loading of these foulants is unknown. A model needed to be developed to

calculate the mass loss of spent carbon fouled with an unknown amount of unknown organic materials. Such a model should be universal, to account for different organic foulants. It is inevitable that such a model would not use experimental data as its basis.

Van Deventer and Camby[92] developed a model to calculate the mass loss of spent carbon regenerated in a fluidized bed at a constant temperature. The decompostition and pyrolysis reactions were assumed to follow first order kinetics. Hence, the reaction rate is[92]:

$$\frac{d(q-q_\infty)}{dt} = -k_{dp}(q-q_\infty) \qquad \textbf{(4-41)}$$

with the boundary conditions $q = q_0$ at $t = 0$, and $q = q_\infty$ at $t = \infty$.

The total mass loss due to decomposition and pyrolysis is then:

$$M_{dp} = (q_0 - q_\infty)[1 - e^{k_{dp}t}] \qquad \textbf{(4-42)}$$

where:

$$k_{dp} = k^*_{dp} e^{\frac{E_{dp}}{RT}} \qquad \textbf{(4-43)}$$

However, the value of (q_0-q_∞) in equation 4-42 is unknown. Van Deventer and Camby[92] defined a fractional mass loss, ξ, where:

$$\xi = \frac{(q_0 - q_\infty)}{q_\infty} \qquad (4\text{-}44)$$

The parameter, ξ, was assumed to be independent of the initial loading, q_0. Little has been published on the realtionship between ξ and temperature. Furthermore, non-isothermal conditions are normally used to determine ξ. Van Deventer and Camby[92] assumed that, within a limited temperature range, ξ can be approximated by:

$$\xi = \xi^*(T - T_0) \qquad (4\text{-}45)$$

where T_0 is the temperature at which decomposition and pyrolysis begin.

Sustitution of equations 4-46 and 4-45 in equation 4-43 gives the required mass loss equation for the decomposition and pyrolysis reactions:

$$M_{dp} = q_0\xi^*(T - T_0)\left[1 - 9^{-tk^*_{dp}e^{\left(\frac{-E_{dp}}{RT}\right)}}\right] \qquad (4\text{-}46)$$

Equation 4-46 is however limited to a very small temperature range. Van Deventer and Camby[92] stated that equation 4-46 was valid to calculate only the mass loss due to decomposition and pyrolysis carbon loaded with phenol and an eluted mine sample, at temperatures above 500°C. An attempt to fit equation 4-46 to TGA data of the mass loss by carbon loaded with 150mg phenol/g carbon (see Chapter 3, Section 3.3.4) proved to be impossible over the temperature range, since ξ is a not a linear function of temperature in the low temperature regions, as had been previously assumed. The result of this comparison is depicted in figure 4.6. The parameters $q_0\xi^*$, T_0, k^*_{dp} and E_{dp} in equation 4-46 were estimated (for figure 4.6) from a regression analysis (see Chapter 6, Section 6.4).

The parameters were also calculated for the temperature ranges above 500°C and 700°C. Significant improvement was attained, but this was not sufficient to providean adequate model for the experimental data. These results are shown in figure E.1 (see Appendix E). The temperature, T_0, where decomposition and pyrolysis starts could have any value, since $q_0\xi^*$ is calculated from a regression analysis and the mass loss is then recalculated. It is thus concluded that equation 4-46 can not be used to calculate the mass loss due to decomposition and pyrolysis from TGA data over the full temperature range. The reason is believed to be the fact that the temperature is a function of the time of regeneration in the present TGA methods, whereas Van Deventer and Camby[92] used a constant regeneration temperature. An alternative was therefore investigated for calculating the mass loss due to decomposition and pyrolysis when the nature and quantity of the intial loading of organic adsorbates is unknown.

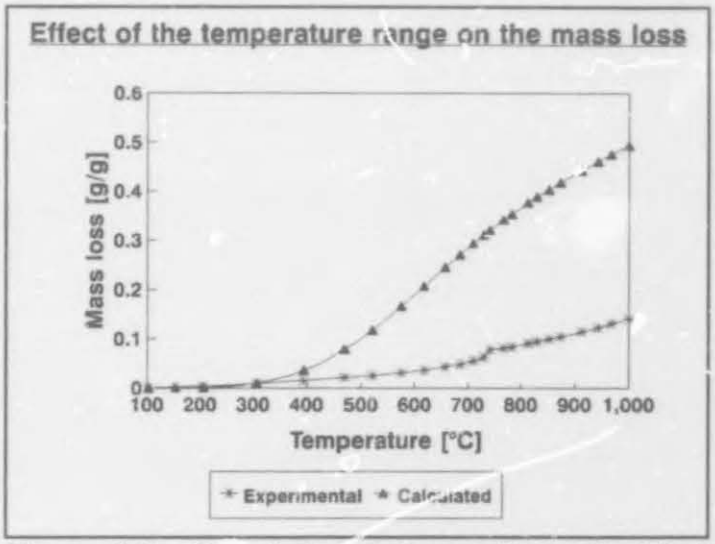

Figure 4.6: Correlation between the calculated and experimental mass loss (carbon + phenol).

The following method is proposed for calculating the mass loss due to decomposition and pyrolysis. TGA in an inert atmosphere shows the mass loss due to evaporation of the highly volatile adsorbates during the drying stage, the evaporation of the less volatile adsorbates, the decomposition of the unstable adsorbates and the pyrolysis of the non-volatile adsorbates as a function of the temperature of the carbon sample which in turn is also a function of time. The mass loss can be presented as the mass loss per mass of the initial loaded sample. It is thus possible to have a set of data available to predict the loss per unit mass as a result of decomposition and pyrolysis

provided that the carbon temperature is available. The mathematical model developed in this chapter utilises this relationship. The temperature of the carbon is calculated and the mass loss be predicted from the mass loss versus temperature data. This approach makes it possible to calculate the mass loss of the spent carbon fouled by unknown organic materials, provided that TGA data (in an inert atmophere) are available for the specific spent sample. The set of TGA data is representative of all the possible reactions, the decomposition of the active groups of the base carbon and the effect of catalysts, if any. It is assumed that the composition of the surrounding gas does not influence the mass loss due to decomposition and pyrolysis.

When activated carbon is fouled by a type III organic material (see Chapter 2, Section 2.2), thermal regeneration in an inert atmosphere alone, is inadequate to restore the original activity of the activated carbon. Steam regeneration is used to remove the residual char left in the pores of the carbon by the more complex (Type II and III) organic materials. Chihara et al.[53] and Umehara et al.[53] studied the kinetics of the reaction between steam and thermally regenerated (in an inert atmosphere) carbon containing dodecylbenzene sulfonate and sucrose, respectively. It was concluded that the steam-carbon reaction follows Langmuir-Hinshelwood kinetics. The rate constants and the activation energies calculated for the Hishelwood equation in these studies, were not the same. Urano et al.[61] indicated that the observed reaction rate depends on the type of carbon and the type of residue on it. However, Umehara et al.[63] concluded during their investigation that Na_2SO_4 catalysed the steam-carbon reaction.

The catalytic effect of inorganic species has been studied by various authors[66-81] and it is generally concluded that the inorganic species could have a pronounced effect on the gasification reaction. However, a model quantifying their effects is not available. (This phenomenon is currently being investigated at the University of Stellenbosch). Umehara et. al.[63] observed that the catalytic effect could be reduced by washing the carbon with water prior to gasification. In a real CIP circuit, an acid wash precedes the regeneration process to remove as much mineral matter as possible. In view of these findings, it is assumed in developing the model that the effect of inorganic catalysts on

the steam-carbon reaction is negligible. In practice, however, the steam-carbon reaction is always catalysed to an extent by mineral matter.

Klei et al.[50] observed that the reaction between activatedd carbon and steam is not very sensitive to variations in the gas flow rate, and that external mass transfer does not control overall reaction dynamics. Furthermore, Chihara et al.[53] showed that intraparticle diffusion is not very likely to affect the overall kinetics at the temperatures normally used: the measured reaction rate was the same for both residual and virgin carbon.

The assumptions made to predict the mass loss during the steam regeneration of spent carbon fouled with an unknown amount of a type I, II or III organic material, are summarized as follows:

- the mass loss due to decomposition and pyrolysis could be predicted from the representative set of mass loss versus temperature data, obtained during TGA;
- the steam-carbon reaction follows Langmuir-Hishelwood kinetics;
- the effect of inorganic catalysts is negligible.

The mass loss of the spent sample regenerated in a steam atmosphere is then the sum of the mass loss due to decomposition and pyrolysis and the loss due to the steam-carbon reaction. Hence, the mass loss in the length increment, k, is:

$$M_k = M_{dp_k}(T) + t\left(\frac{k_1 p_{H_2O}}{1 + k_2 p_{H_2} + k_3 p_{H_2O}}\right)_k \qquad (4\text{-}47)$$

In equation 4-47, the mass loss, M_k, is a function of the time, temperature, the partial pressure of steam, the partial presure of hydrogen, the physical and chemical properties of the foulant(s) and the initial loading of the foulant(s).

Suzuki et al.[40] classified organic foulants into three distinct types (see Chapter 2, Section 2.2). It was pointed out that type III organic foulants leave a larger residual char than those of types I and II during regeneration in an inert atmosphere. The influences of typical type I, II and III organic materials, frothers, collectors and dispersors are investigated in the simulation runs in chapter 7, section 7.4. The different TGA curves to calculate $M_{dp}(T)$ in equation 4-47 were obtained as explained in chapter 3, section 3.3.5.

CHAPTER 5

COMPUTATIONAL PROCEDURES

In this chapter, the procedures for predicting the mass loss of the regenerated carbon according to the mathematical model developed in chapter 4, will be discussed. A method is then proposed to relate the calculated mass loss of the regenerated carbon to the adsorptive capacity of this carbon.

5.1 INTRODUCTION

A computer program was written in Turbo Pascal 6.0 implementing the mathematical model developed in chapter 4 to predict the mass loss of spent activated carbon during steam regeneration. The intention was to write a program that could be used in the industry to satisfy the need for a simulator tool to optimize rotary kiln operation. Therefore a user-friendly package was written and no skill apart from a limited computer knowledge is required to use this program. However, the user must be able to interpret the results.

5.2 HARD- AND SOFTWARE REQUIREMENTS

Since the program can be used for other applications apart from the regeneration of activated carbon (see Chapter 8), the user should be able to change the program code. It is therefore available as a Turbo Pascal 6 program. The software requirements is a copy of Borland's Turbo Pascal 5 or an updated version.

The program can run on any personal computer with a mathematical coprocessor. If a coprocessor is unavailable, Turbo Pascals emulation mode may be used. However, a 486 computer is recommended to manage the substantial numerical computations in an acceptable running time.

5.3 COMPUTATIONAL PROCEDURE

Figure 5.1 shows the main flow diagram of the computer program.

The program starts with the main menu appearing on the screen. In this menu three options are given:

[1] to go to the kiln design, operating and carbon parameters menu (see Section 5.3.1);

[2] to calculate the temperature profiles and the mass loss during regeneration using the values that have been stored in the data files from the kiln design, operating and carbon parameters menu (see Section 5.3.2);

[3] to quit the program.

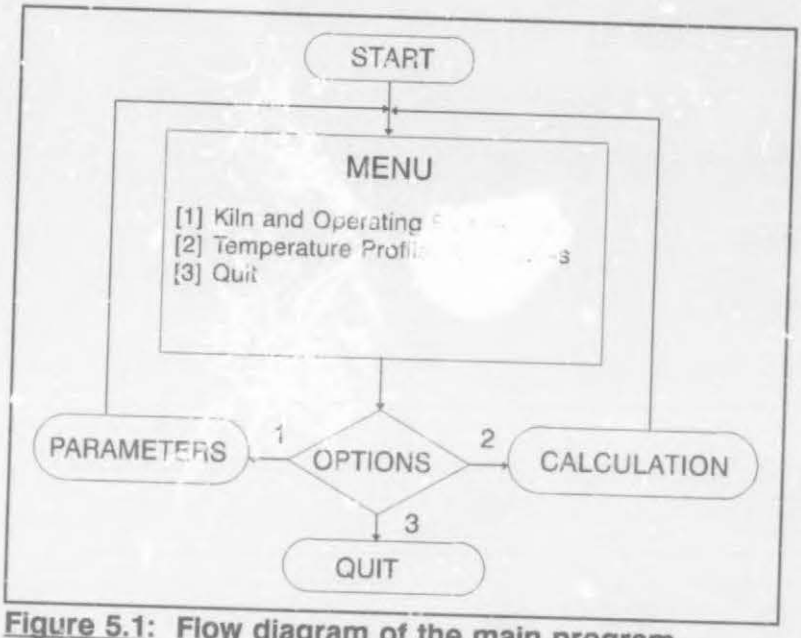

Figure 5.1: Flow diagram of the main program.

5.3.1 Menu for Kiln design, operating and carbon parameters

Option 1 (Number 1 in Figure 5.1) should be selected to go to a new menu where the values of kiln design, operating and activated carbon parameters are set. The format of this menu is represented in figure 5.2.

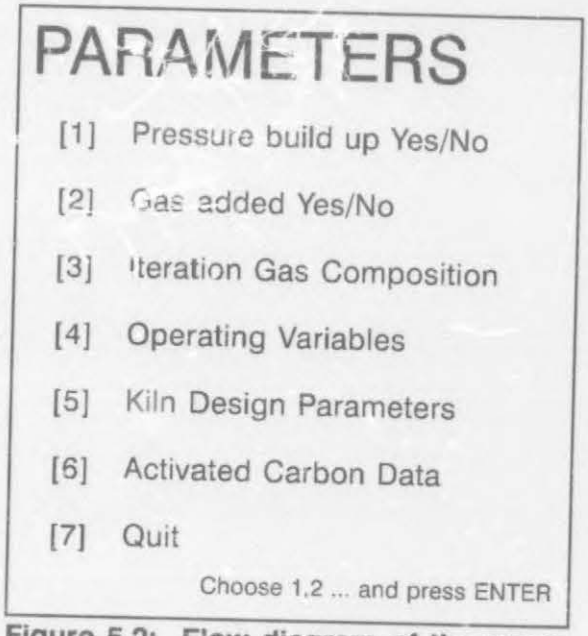

Figure 5.2: Flow diagram of the menu for kiln design, operating and carbon parameters.

When an option is selected, the values of certain parameters or the status of different conditions are requested. In the sequence of the options in figure 5.2, the requested values or status are:

[1] Allow for a pressure build up or not (if atmospheric conditions do not prevail);

[2] Is external gas added to the freeboard gas (Y/N). If gas is added, the fractions of steam, carbon dioxide, carbon monoxide, hydrogen and nitrogen are requested;

[3] The equilibrium composition of the freeboard gas is necessary to start the iteration procedure (see Section 5.3.3 for an explanation). The different fractions wanted are the same as stated above ([2]);

[4] The values for the operating conditions are set in this option. They are:

- outside kiln wall temperature;
- temperature of the solids;
- the equilibrium temperature of the gas (see Section 5.3.3);
- *inside kiln wall temperature;
- mass flow rate of the solids;
- mass flow rate of the external gas (the mass flow rate of this gas is only requested if the "external gas added" in option

2 was " Yes");

- the inclination of the kiln to the horizontal;
- the rotating speed of the kiln;
- moisture in the carbon feed (mass per cent).

[5] The kiln design parameters wanted are:

- *number of layers of which the wall is constructed;
- diameter of the kiln;
- *conductivity of each of the layers;
- *specific heat capacity of each layer;
- *density of each layer;
- *thickness of each layer;
- length of the kiln;
- fill height of the kiln (see Chapter 4 Figure 4.4);

[6] In this option the bulk density and *mean solids diameter are requested;

[7] Quit the menu.

The variables marked with an asterisk (*) are not required for the rotary kiln configuration investigated in this study (see Chapter 1, Section 1.3). However, these values are required for convenience if the program is to be adjusted to incorporate other applications (see Chapter 8). The values requested in the design, operating and carbon parameters menu are read from the keyboard input and then stored in data files. These values are used in option 2 of the main menu, (see Figure 5.3) to calculate the mass loss. (see Section 5.3.2).

5.3.2 Temperature profiles and the mass loss

The flow diagram for the calculation of the temperature profiles of the solids bed and the gas, and the mass loss of the regenerated carbon (see Option 2 in Figure 5.1) is depicted in figure 5.3. The individual flow diagrams and a discussion for each of the calculation procedures depicted in figure 5.3, are presented in Appendix F.

It is evident from chapter 4 that the calculation of the mass loss is dependent on the accurate prediction of the temperature of the solids bed as a function of the kiln length. The total mass loss is then the sum of the calculated mass losses in each length increment. The calculation procedure will now be discussed.

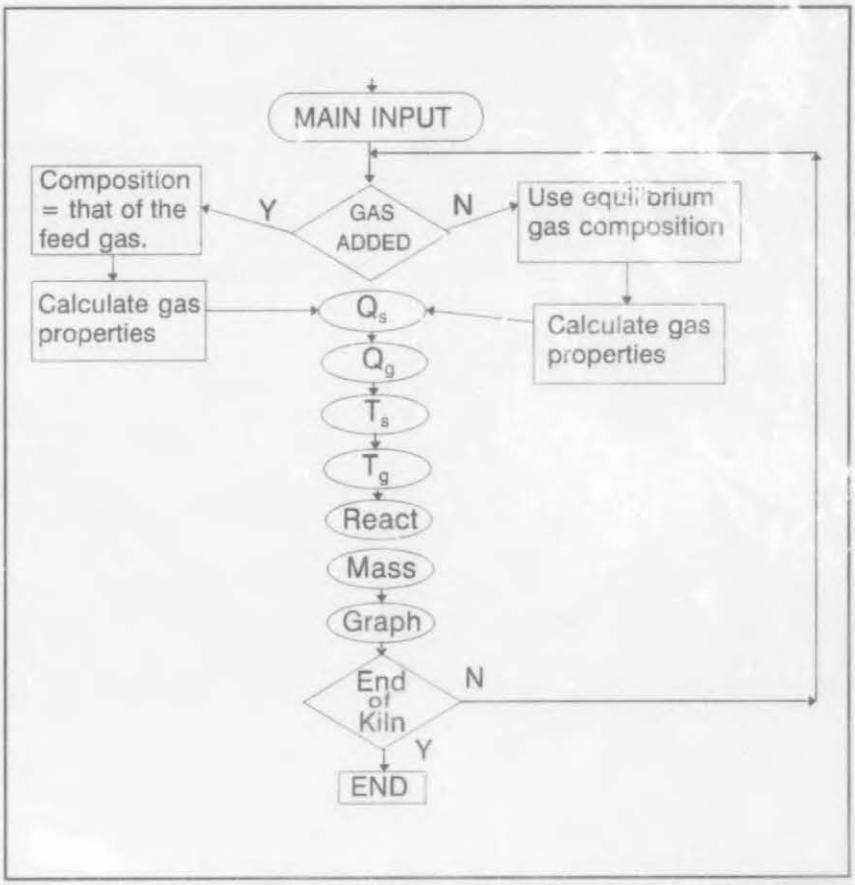

Figure 5.3: Flow diagram of the main calculation procedure.

The procedure starts with a "Main Input" procedure (see Appendix F, Section F.1) where all the initial values are calculated from the values of the kiln design, operating and activated carbon parameters. These are the values stored in data files in the kiln design, operating and carbon parameters menu (see Section 5.3.1). It is important to note that in this procedure, the kiln is also divided into a number of length increments (see Appendix F, Section F.1). The appropriate data file is then checked to see whether external feed gas is used. If external feed gas is used, there is no need to iterate the equilibrium compostion and temperature of the freeboard gas (see Section 5.3.3), since the equilibrium composition of the freeboard gas will be the same as that of the feed gas. If external feed gas is not used, the equilibrium freeboard gas composition and temperature should be calculated (see Section 5.3.3). These options

are shown in figure 5.3. The freeboard gas emissivity, adsorptivity and transmissivity is then calculated. This is a lengthy and complicated procedure, as the real gas approach has been used, and is discussed in Appendix F, section F.2.

The radiative and possible convective heat transfer rates to the solids, " Q_s", and the radiative heat transfer rate to the gas, "Q_g", in a length increment, is then calculated. The calculation procedures are discussed in Appendix F, section F.3. The new temperatures of the solids, "T_s", and the gas, " T_g", as a result of the heat transfer, are then calculated. These calculations are discussed in detail in Appendix F, sections F.4 and F.5, respectively. The temperature of the wall remains the same.

The calculations that follow are all performed in procedure, "React", of figure 5.3 (see Appendix F, Section F.6). At the new temperature of the solids the mass loss due to decomposition, pyrolysis and the steam-carbon reaction is calculated according to equation 4-47. This mass loss represents the mass loss of the regenerated carbon in the specific length increment. Using equations 4-32 to 4-38, the new composition of the freeboard gas is calculated as a result of the gasification reaction and together with the amount of water evaporated (see Appendix F, Section F.4), represents the new freeboard gas composition.

The decrease in the temperature of the solids as a result of the endothermic reaction is then calculated according to equation 4-40 (see Appendix F, Section F.7).

The "Graph" procedure is the procedure that plots the calculated temperature profiles on the computer screen. This procedure will not be discussed.

The calculated freeboard gas composition, temperatures of the solids bed, gas and wall (with the temperature remaining constant), are then used as the input values for the next length increment where the above described procedure is repeated, until the last length increment is reached. The overall mass loss is then the sum of the individual mass losses calculated in each of the length increments.

5.3.3 Calculation of the equilibrium gas temperature and composition

The initial gas temperature and freeboard gas compostion is unknown. These values are calculated by an iterative procedure. An educated guess is made to select the initial freeboard gas composition and temperature (see Option "3" and "4" of the kiln design, operating and carbon parameters menu, Section 5.3.1). The procedure described above (see Section 5.3.2) is then used to calculate the mass loss of the solids. The final freeboard gas composition and temperature can then be found. These values are compared with the initial values. If a difference does occur, the necessary changes are made and the procedure is repeated until equilibrium is reached. The calculation of the equilibrium gas composition is only necessary if no external feed gas is added but the calculation of equilibrium temperature is needed for both cases, i.e. feed gas and no feed gas. This procedure is only valid if the kiln operates under steady state conditions.

5.4 RELATIONSHIP THE CAPACITY OF REGENERATED CARBON AND THE CALCULATED MASS LOSS

The performance of a rotary kiln should be measured in its ability to restore the activity of the spent carbon to that of virgin carbon. The simulation program can be used to calculate the mass loss of the regenerated carbon as explained above. However, it is impossible to evaluate the regeneration performance of a rotary kiln alone. In this section a method is proposed to using the calculated mass loss to evaluate rotary kiln performance.

Since the activity of the carbon is related to its adsorptive capabilities, the parameters of an equilibrium isotherm can be used to quantify the capacity of the regenerated carbon. A number of equilibrium isotherms (see Equations 2-12, 2-13 and 2-14, Chapter 2, Section 2.7) can be used to describe the relationship between the

concentration of the adsorbate in the liquid phase and the concentration on the surface of the adsorbent.

The Freundlich isotherm:

$$q_e = AC_e^n \qquad (5\text{-}1)$$

can be used to correlate data for the equilibrium adsorption of gold cyanide on activated carbon.

The parameter, A, then represents the equilibrium adsorption capacity of the carbons. It is argued that this approach is of more practical use than merely the determination of the surface area[53] or the iodine number[60]. It is expected that the adsorption capacity of the regenerated carbon would increase and reach a maximum if regenerated under increasing temperatures. Van Camby[92] confirmed this behaviour of activated carbon. The mass loss would obviously differ during regeneration under different temperatures. This phenomenon can thus be used to correlate the mass loss of the regenerated carbon under different temperatures to the adsorption capacity, A, of the carbon. It is expected that the capacity would be a function of the mass loss. Furthermore, a maximum capacity should be reached with an increasing mass loss, since an excessive mass loss would be indicative of a loss of valuable virgin (base) carbon. Eventually it is possible to select the optimum kiln conditions for regeneration. In support of this approach, Kato et al.[60] stated that the relative adsorption capacity was determined only by the mass loss, regardless of the carbon, adsorbate or temperature.

5.4.1 Results

The details for the experimental procedures to relate the mass loss of the regenerated carbon to its adsorptive capacity, are presented in chapter 3, section 3.3.2 to 3.3.3.

As was expected, the mass loss of the spent carbon increased with an increase in the regeneration temperature. The total mass losses recorded for the different regeneration temperatures are listed in Table 5.1. The Freundlich parameters were then calculated from the adsorption data. The experimental results and the calculated equilibrium loading are listed in Table D.1, Appendix D. A curve fit program was used to fit equation 5-1 to the equilibrium concentration in the liquid phase, C_e, and the equilibrium loading on the carbon, q_e, to find the Freundlich parameters A and n. The calculated A and n parameters of equation 5-1 are listed in Table 5.2. It was found that the parameter n is inversely proportional to the parameter A (see Figure D.1, Appendix D). Equation 5-1 can thus be written as follows:

Table 5.1: Experimental mass loss data.

Temperature [°C] [°C]	Mass loss [kg/kg]
1400	0.62
1300	0.54
900	0.34
750	0.29
550	0.12
450	0.06

Table 5.2: The calculated Freundlich parameters.

Temperature [°C]	Mass loss [kg/kg	A [g_{Au}/kg]	n
1400	0.62	9.2	0.20
1300	0.54	10.3	0.21
900	0.34	11.4	0.21
750	0.29	10.1	0.23
550	0.12	8.6	0.25
450	0.06	6.9	0.30

$$q_e = AC_e^{b1*A+b2} \qquad (5\text{-}2)$$

The functional relationship between the parameters A and n is given in equation D-1 (see Appendix D). Van der Merwe[104] also confirmed the inverse proportionality. It is also more convenient to relate the a single parameter to the mass loss of the carbon.

The calculated and experimental loading of gold cyanide, q_e, is depicted in figure 5.4 as a function of the concentration of the goldcyanide in the liquid phase, C_e (see Appendix D for the original data). The calculated values in figure 5.4 have been

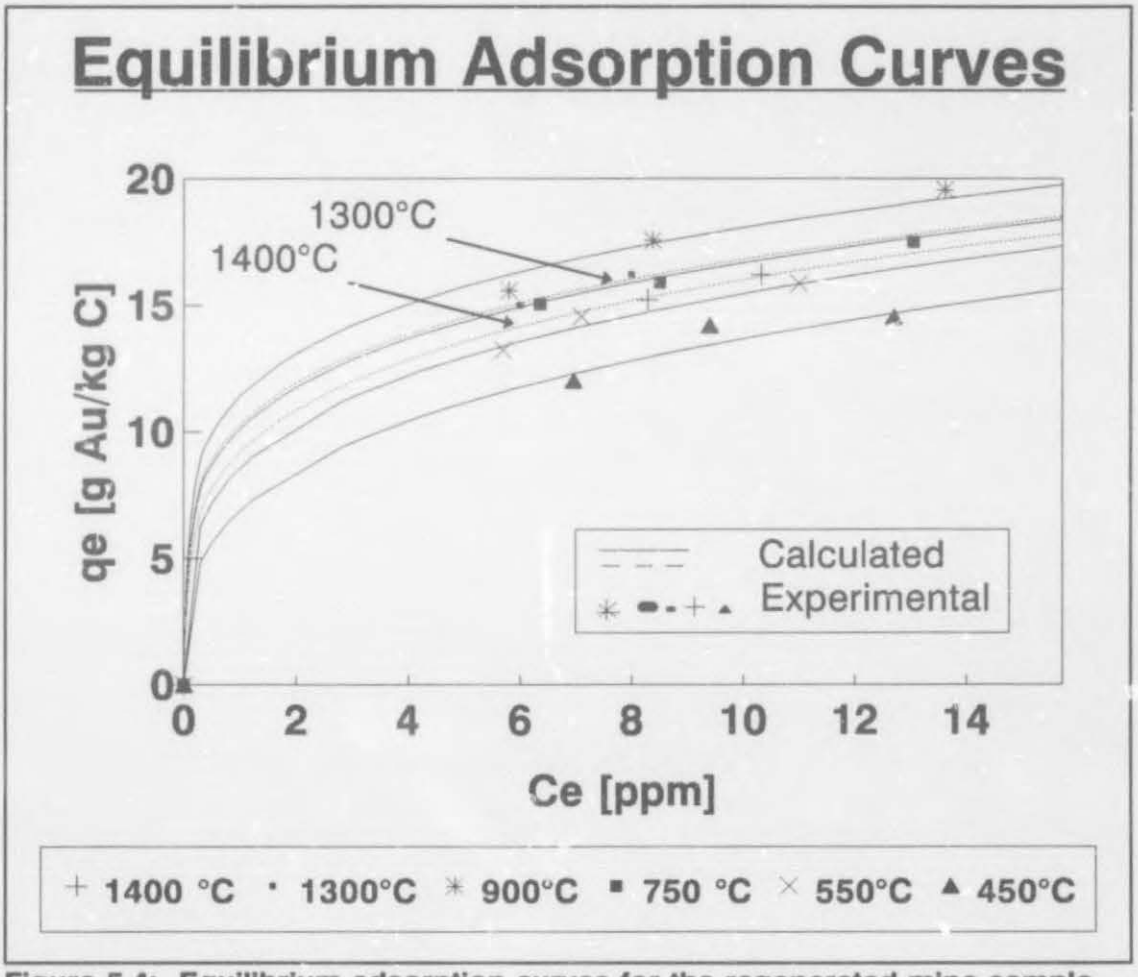

Figure 5.4: Equilibrium adsorption curves for the regenerated mine sample.

determined with the modified Freundlich equation, equation 5-2. The A parameters of table 5.2 and the n parameters from equation D-1 (see Appendix D) have been used. Figure 5.4 illustrates that a Freundlich isotherm can be used to predict the equilibrium loading of gold on activated carbon. The Freundlich parameter, A, can therefore be used with confidence to represent the adsorptive capacity of regenerated carbon.

The relationship between the Freundlich A parameters, i.e the capacity of the regenerated carbon and the mass loss of the carbon is depicted in figure 5.5. The results are in agreement with those found in the literature[92]. The adsorptive capacity of the regenerated carbon increases with increasing temperature as more of the organic foulants are removed. However, a maximum is reached when all the organic foulant and the residual material have been removed. Regeneration at even higher

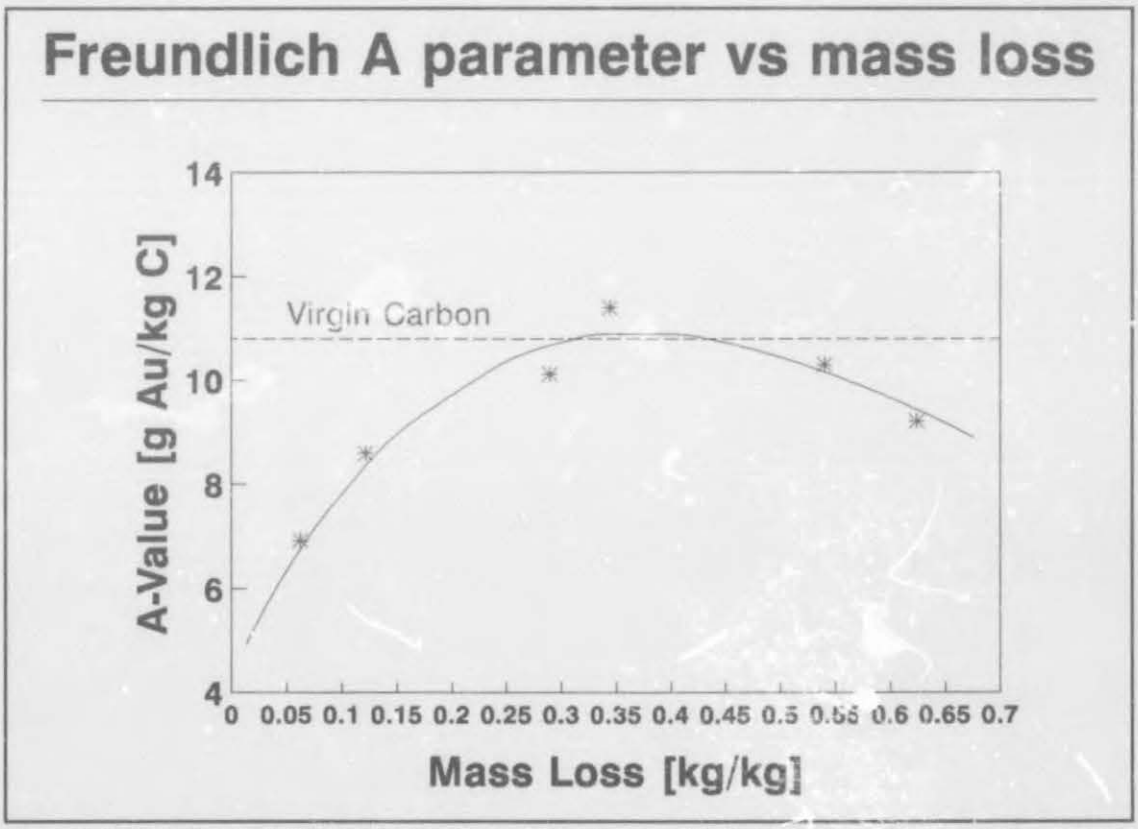

Figure 5.5: The relationship between the Freundlich A parameter and the mass loss of the regenerated mine sample.

temperatures would then result in the oxidation of valuable base carbon and would reduce the capacity of the carbon[49]. The capacity of the regenerated mine sample reached a maximum at a mass loss of between 0.3kg/kg and 0.45 kg/kg carbon. The Figure 5.5 indicates that the adsorption capacity could be restored completely, and even improved. The mass loss of 0.62kg/kg at the regeneration temperature of 1400°C might appear to be low, but one should bear in mind that regeneration with a gradually increasing temperature has been used and equilibrium at the maximum temperature might not have been reached (see Chapter 3, Section 3.3.2). The use of figure 5.5 is thus an indication of the capacity of the regenerated carbon and is by no means exact. The objective is to show the possibility of the use of such a relationship. This relationship makes it possible to use the developed mathematical model (see Chapter 4) to calculate the mass loss of the regenerated carbon (PB3 carbon) under specific rotary kiln operating conditions and then predict the capacity of the regenerated carbon from figure 5.5. The aim would be to adjust the operating conditions to obtain a mass loss of between 0.3 and 0.45 kg/kg carbon. The optimum regeneration conditions could thus be found. A method has thus been established for evaluating the performance of a rotary kiln using the mass loss during regeneration as measured by TGA and the adsorptive properties of the regenerated carbon.

Figure 5.5 is only applicable to evaluate the rotary kiln performance for the regeneration of the spent (PB3) activated carbon. The procedure described in this section should be repeated to examine other samples of activated carbon fouled by different organics. This procedure would make the use of the mathematical model rather tedious in evaluating the performance of a rotary kiln in the industry. In practice, however, it is expected that organic foulants are typical for a period of mining, since foulants originating from the organic reagents used in the plant solution and the vegetation of the sand or slime being reclaimed are unlikely to change eratically. It is assumed that the relationship between adsortive capacity and mass loss found for such a sample would be representative of the spent carbon for a period of mining. This relationship could be determined from time to time to update the data base.

CHAPTER 6

DETERMINATION OF THE PARAMETERS REQUIRED FOR THE SIMULATION OF A ROTARY KILN

Certain physical and chemical parameters are required for the simulation of the rotary kiln by means of the mathematical model developed in chapter 4. In this chapter the values for the parameters, which could not readily be obtained from the literature or measurement, or which need to be calculated, were determined as explained below.

6.1 EMISSIVITY, ABSORPTIVITY AND TRANSMISSIVITY OF GAS

The freeboard gas common to rotary kiln operation contains mainly CO_2 and H_2O mixtures generated by the evaporation of water from the wet carbon and the gasification of the residual product on the spent carbon. Because these gases emit and absorb radiative energy in distinct wavelength intervals (called bands), the use of a gray-gas approximation[4] for calculating the emissivity and absorptivity of the gas is not valid. The error introduced by the gray-gas assumption may be greater than 20 per cent[90]. The freeboard gas should therefore be treated as a real gas during the calculation of the gas properties.

4. That is to assume that the absorptivity (and emissivity) of a gas is independent of wavelength[94,97], and thus equal and constant at a given temperature.

6.1.1 Models for calculating gas emissivity, absorptivity and transmissivity

Advancing length increment by length increment along the rotary kiln axis during operation, the composition and temperature of the gas would change for each of the increments. It should therefore be possible to calculate the emissivity and absorptivity of various gas compositions at different temperatures.

Hottel and Sarofirm[94] and Eckert et al.[97] published a review of experimental and theoretical methods for the determination of the emissivity and absorptivity of gases. Hottel and Sarofirm[94] also reported their findings of a literature survey of recent developments in the calculation of gas properties.

Emissivity charts, derived from experimental measurements of the absorption spectra of gases, form the basis for the calculation of gas properties. Gas emissivities are presented on these charts as a function of temperature, partial pressure and mean beam length. Hottel and Sarofirm[94] suggest that gas radiation can be visualized as being due to the weighted sum of a sufficient number of gray and clear gas components to approximate the banded characteristics of a real gas. The reader is referred to their original work for the detail of this method[94]. Thus, according to their approach, the gas emissivity may be represented by:

$$\epsilon = \sum_i a_i (1 - e^{-k_i p L_m}) \qquad \textbf{(6-1)}$$

subject to the restrictions that a_i are all positive for all values of i, and that:

$$\sum_i a_i = 1 \qquad \textbf{(6-2)}$$

since emissivity approaches 1 with increasing pL_m.

Accordingly, the emissivity of a gas can be calculated provided that an appropriate emissivity chart is available. This is the method used by Gorog et al.[91] (see Chapter 2, Section 2.8), but as stated, it has limitations which will be discussed.

The success of Hottel and Sarofirm's[94] method depends on the availability of appropriate emissivity charts. Unfortunately, these charts do not cater for all the possible options of partial pressure, mean beam length and temperature. Furthermore, the number of gases for which these charts are available, is limited. Calculation of the emissivity for gas mixtures from these charts was virtually impossible until Hadvig[95] proposed a method for calculating the emissivity of mixtures of carbon dioxide and steam. Hadvig[95] calculated the emissivities for CO_2/H_2O ratios of 1 and 2. The reader is referred to their original paper for details on this method. It is not clear from the original paper whether this method is applicable to gas mixtures other than CO_2 and H_2O. Hadvig's procedure is very lengthy and the calculation of the gas properties for a large number of different gas compositions at different temperatures will take up a lot of computer time (even on a 486). Data for the correction ($\Delta\epsilon$) due to spectral overlap for CO_2 and H_2O mixtures is available at only three different temperatures. In addition to the uncertainty regarding the accuracy of these correction factors[93], interpolation between the three temperatures for the calculation of $\Delta\epsilon$ would thus be unreliable. In view of these limitations, the use of Hottel and Sarofirm's method could not be considered.

Subsequent to the empirical development of gas emissivity charts, attempts to calculate CO_2 and H_2O emissivities purely from knowledge of the molecular structure were determined[94]. The ideal scenario would be to construct a quantum-mechanical model to avoid erroneous results due to accuracy in experimental measurements and certain assumptions (like those in the model of Hottel and Sarofirm[94]). Eckert et al.[97] developed such a model. Although this model is very complicated, it is superior to the model proposed by Hottel and Sarofirm[94] as emissivities, absorptivities and transmissivities can be calculated for:

- different temperatures;
- different gas compositions;
- different gas geometries.

The gas composition is limited to a mixture of CO_2, H_2O, CO, NO, SO_2 and CH_4 since only the quantum mechanical data for these gases is available in the literature. For the purpose of calculating gas properties in a rotary kiln this is not a limitation, since the freeboard gas contains mainly a mixture of CO_2, H_2O and CO mixtures (see Chapter 4, Section 4.6). In view of these advantages with special regard to the limitations of Hottel's model[94], the method of Eckert et al.[97] was used to calculate the gas properties.

The detailed calculation for calculating the gas properties according to the procedure of Eckert et al.[97] is outlined in Appendix C. Inspection of this method in Appendix C would indicate that it is a rather involved numerical exercise. The procedure uses up considerable computer running time (up to 5 minutes for a single gas composition). The effort, however, seemed worthwhile in view of the limitations of the other alternatives.

6.2 THE EFFECTIVE THERMAL CONDUCTIVITY OF COAL

The heat flow, Q, by conduction in the direction, x, can be determined from:

$$Q = -\lambda A \frac{dT}{dx} \qquad (6\text{-}3)$$

The factor, λ, is the thermal conductivity, which is generally temperature dependent.

Heat can be conducted through solids by electrons, lattice vibrations (photons),

magnetic excitations or electromagnetic radiation[98]. All these factors contribute to some extent to the thermal conductivity of the solid[98]. In metals and alloys, the heat is usually conducted by free electrons[98]. However, in non-metals, the contribution of the photons is usually the dominant factor, especially at high temperatures[98]. In a bed of granular carbon, the carbon-carbon contact contributes to the resistance to the conduction from one particle to another. Furthermore, heat transfer by radiation across the voids between the particles, and the pores inside the particles, contribute to the apparent thermal conductivity at high temperatures.

Tsotsas and Martin[99] published a review of experimental and theoretical methods for the determination of the thermal conductivity of packed beds. Fine and Glasser[100] reported findings from a literature survey of different theoretical models to predict the effective thermal conductivity of a packed bed. Their experimental data was fitted to various theoretical models.

Experimental determination of the thermal conductivity usually involves the measurement of the temperature profile associated with a known heat flow. (see Laubitz[101]). Owing to the temperature dependence of the thermal conductivity, the temperature gradient needs to be kept as small as possible without seriously affecting the precision of the experimental measurements. The experimental determination of the thermal conductivity of GAC was done by Fine and Glasser[100]. Only a summary of their work is presented below.

The experimental approach adopted by Fine and Glasser[100] was to derive the thermal conductivity for the temperature gradient associated with the steady state rate of radial heat loss from a cylindrical bed of GAC. The results obtained by Fine and Glasser[100] are depicted in figure 6.1. The results can be fitted well to a straight line in the temperature range 400-1200 K. The apparatus and experimental procedure used by Fine and Glasser[100] had a few limitations. The most serious of these was the accuracy with which the rate of heat loss could be measured, i.e. the required heat input to maintain steady state, and the uneven heating of the bed of GAC. They

estimated the overall accuracy of the results obtained, to be about ±25 per cent. In view of the limited data and the fact that published values for solid carbon at 25°C are 1.52[102] and 1.6[103] [W/m.K] respectively, which should be lower for porous GAC, the

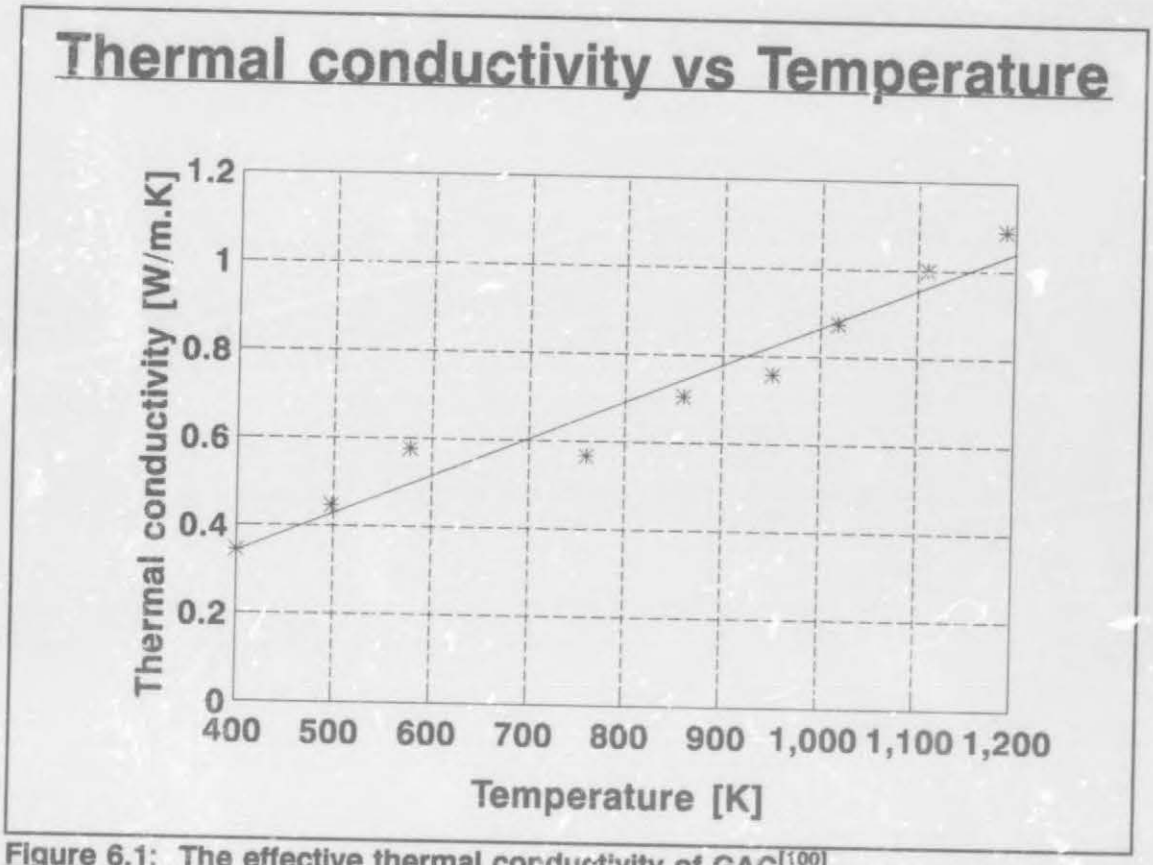

Figure 6.1: The effective thermal conductivity of GAC[100].

use of their published thermal conductivity was regarded as acceptable.

Accordingly, equation 6-4, fitted to the data in figure 6.1, was used to calculate the thermal conductivity of the bed of activated carbon.

$$\lambda_s = 8.7 * 10^{-4} * T - 9.4 * 10^{-3} \qquad (6\text{-}4)$$

6.3 THE KINETICS OF DRYING

A number of heat transfer phenomena occurs during the drying of solid material. Whichever phenomenon limits the rate of drying depends on the moisture content and the drying conditions[103]. However these phenomena were not investigated in detail for the purpose of this study. Van Staden[65] suggested that the rate of water removal during the drying of the activated carbon could be treated as a first order process (with respect to the amount of remaining moisture on the carbon). Van Staden[65], however, did not investigate the effect of different amounts of water loaded on the activated carbon. The water content of activated carbon entering the rotary kiln varies between 10 and 50 weight per cent of moisture. Although some surface moisture does exist, it is assumed that moisture of GAC entering the kiln is almost entirely contained in the carbon's macro- and meso pores. Therefore it is assumed that the drying of the spent carbon occurs within the falling rate regime, where the rate of drying decreases with decreasing moisture content. Hence, for the rate of water removal the following relationship is assumed:

$$R_d = k_d(w - w_e) \tag{6-5}$$

where k_d is a factor with an Arrhenius temperature dependence:

$$k_d = k_d^* \exp\left(\frac{-E_d}{RT}\right) \tag{6-6}$$

The equilibrium moisture content w_e is a function of the conditions prevailing in the rotary kiln. Since the temperature in a rotary kiln is well above the boiling point of water, the equilibrium moisture content is assumed to be zero. Hence equation 6-4 can be simplified to:

$$R_d = k_d w \qquad (6\text{-}7)$$

The object is therefore to determine the parameters k^*_d also called the frequency factor, and E_d the activation energy. The procedure used by Suzuki et al.[40] to determine first order rate expressions for the desorption of organic substances from activated carbon is used. The reader is referred to the original publication (see References) for the rationale from which the procedure was developed. Its application is illustrated in section 6.3.1.

6.3.1 Results

The details concerning the experimental procedures to investigate the drying kinetics of activated carbon are discussed in chapter 3, section 3.2.1.

The mass of the different samples starts to decrease notably at between 40°C and 60°C. In all of the experimental runs, the total mass loss of the samples was equal to the amount of moisture loaded onto the dried carbon. From the original amounts of water loaded and the TGA data, the TGA curves of figures 6.2, 6.3, 6.4 and 6.5 were constructed. A tangent was drawn to the curve at the point where the relative moisture content, q/q_0, is equal to 0.5. The temperature corresponding to that point, $T_{½}$, as well as the difference between the temperature corresponding to the two ends of the tangent, ΔT, were found as shown in figures 6.2, 6.3, 6.4 and 6.5.

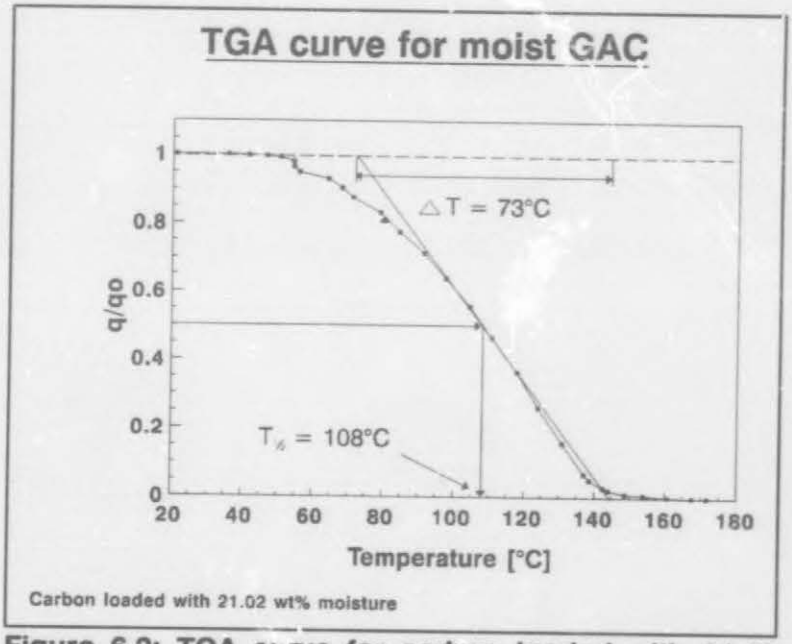

Figure 6.2: TGA curve for carbon loaded with 21.02 weight per cent water.

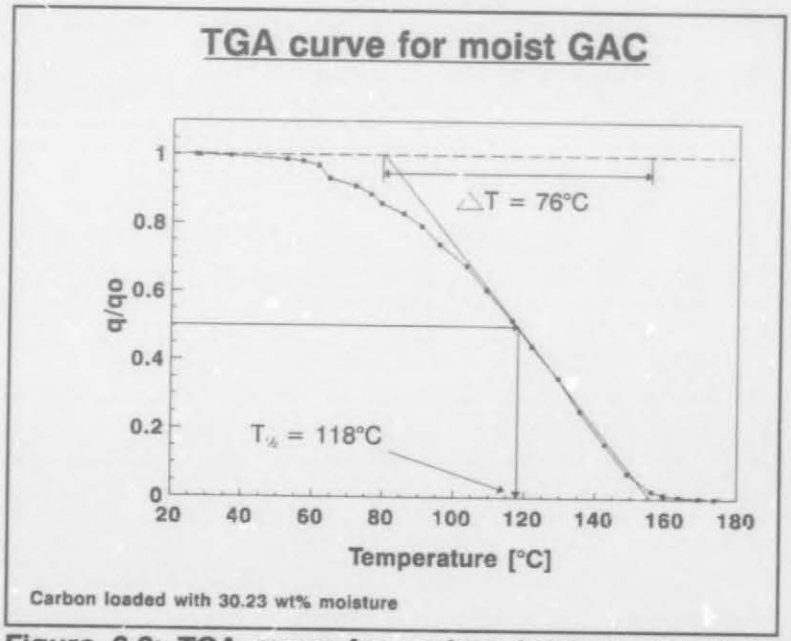

Figure 6.3: TGA curve for carbon loaded with 30.23 weight per cent water.

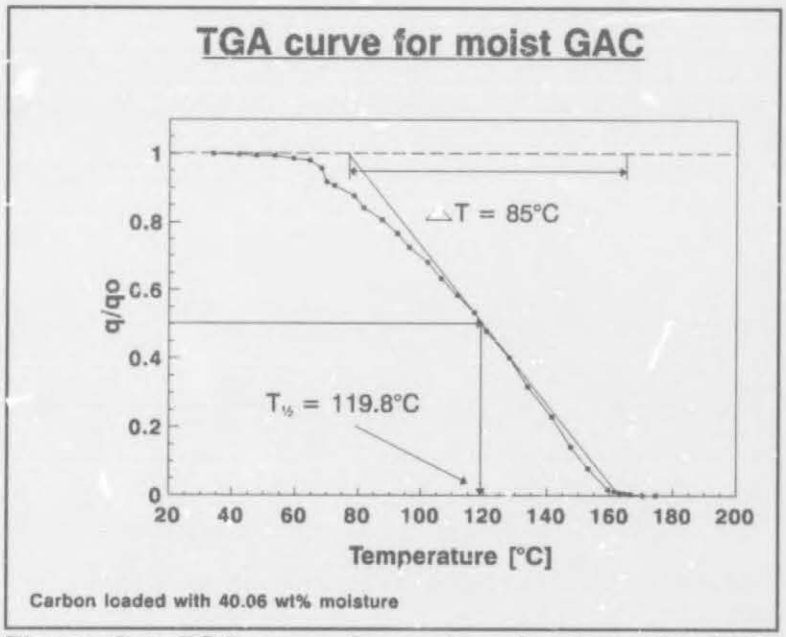

Figure 6.4: TGA curve for carbon loaded with 40.06 weight per cent water.

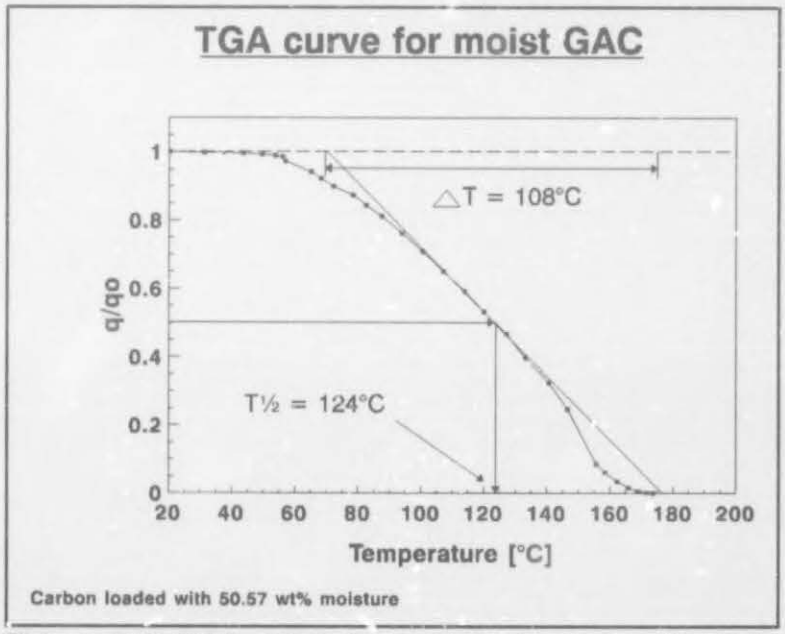

Figure 6.5: TGA curve for carbon loaded with 50.57 weight per cent water.

Suzuki et al.[40] showed that:

$$\frac{\Delta T}{T_{1/2}} = \frac{2\Psi}{\ln(2)} \tag{6-8}$$

and:

$$k_d^* = \frac{2m'}{\Delta T}\exp\left(\frac{E_d}{RT_{1/2}}\right) \tag{6-9}$$

The parameter Ψ was derived by Suzuki et al.[40] as a function of x, where:

$$x = \frac{E_d}{RT_{1/2}} \tag{6-10}$$

This relationship is depicted in figure 6.6.

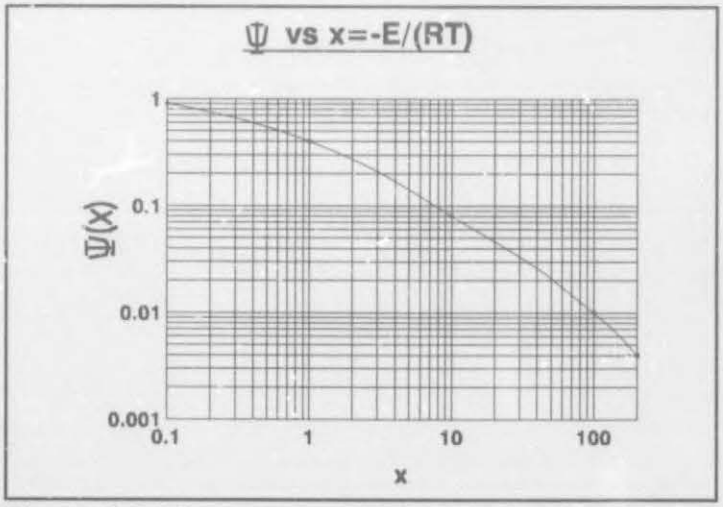

Figure 6.6: Diagram for obtaining $x = E/RT_{1/2}$ from $\Psi(x)$.

From figure 6.2 it is found that $T_{½}$ = 108°C and ΔT = 73°C. Therefore, from equation 6-8:

$$\frac{\Delta T}{T_{1/2}} = \frac{2\psi}{\ln(2)}$$

$$\frac{73}{381} = \frac{2\psi}{\ln(2)}$$

$$\therefore \psi = 0.066$$

From figure 6.6 with Ψ = 0.066, x is equal to 14.3. The activation energy can be calculated from equation 6-10:

$$14.3 = \frac{E_d}{RT_{1/2}}$$

$$\therefore E_d = 14.3 * 8.314 * 381$$

$$E_d = 45250 \qquad [J/mol]$$

and from equation 6-9:

$$k_d^* = \left(\frac{2*0.167}{73}\right)\exp\left(\frac{-45250}{8.314*381}\right)$$

$$= 7317 \qquad [\frac{1}{s}]$$

Similarly, from figures 6.3, 6.4 and 6.5 the frequency factor and the activation energy for the drying of activated carbon loaded with different amounts of water can be

calculated. The results are summarized in Table 6.1.

Table 6.1: Acitivation energies and frequence factors.

wt %	E_d [J/mol]	E_d [kJ/kg]	k_d^* [s^{-1}]
21.02	45250	2513	7317
30.23	40447	2247	1283
40.06	35923	1996	233
50.57	27395	1522	12

The functional relationships have been calculated from Table 6.1 to predict the activation energy and the frequence factor for activated carbon loaded with different amounts of water. The expressions for the activation energy as a function of the water content is:

$$E_d = -8.25(wt\%)^2 + 48629 \qquad \textbf{(6-11)}$$

and for the frequency factor:

$$k_d^* = 2.25 * 10^{10}(wt\%)^{-4.9} \qquad \textbf{(6-12)}$$

Using equations 6-11 and 6-12, the activation energy and the frequency factor can be calculated for the drying of activated carbon loaded with any amount of water between 20 and 50 weight per cent.

The expression for the rate of water desorption from activated carbon as a function of the water content and the temperature can therefore be calculated as follows:

$$R_d = k_d^* \exp\left(\frac{-E_d}{RT}\right) w \qquad \textbf{(6-13)}$$

The magnitude of the apparent activation energy, E_d, (see Table 6.1) corresponds more or less with the heat of vaporization of water, i.e. 2200 kJ/kg[103]. Therefore it is further concluded that the moisture is not strongly adsorbed in the macro-, meso- and micropores of the carbon and that the heat of adsorption of the moisture is negligible. The decrease in the activation energy for an increase in the moisture content might seem contradictory. Since all the dry carbon samples were given the same time for water absorption, the extent of equilibrium moisture distribution between the macro-, meso- and micropores would be the same, i.e if moisture in the sample loaded with 40.06 weight per cent water reached the micropores, they would also reach the micropores for the sample loaded with 21.02 weight per cent water. However, the sample loaded with more water will obviously have its meso- and/or macropores filled with water. On the contrary, the sample loaded with less water could have its micropores filled with moisture, but only part of the mesopores. Upon heating, the resistance to water removal from the pores increases from macro- to micropores, so that the activation energy for the removal of the moisture from the micropores (less wt% moisture) would be more than from the meso- and macropores. Although the drying of activated carbon is treated analogously to a chemical reaction, the vaporization of water is still a physical phenomenon.

6.4 DETERMINATION OF THE PARAMETERS OF EQUATION 4-46

The parameters $q_0\xi^*$, T_0, k^*_{dp} and E_{dp} in equation 4-46, can be estimated from a regression analysis. TGA data was used for this purpose. The detailed experimental procedures for acquiring the necessary data for the calculation of these parameters are discussed in chapter 3, section 3.3.5. The parameters were estimated for the sample loaded with phenol (see chapter 3, Section 3.3.4). The TGA curve is depicted in figures 6.7.

The activation energy, E_{dp}, and the frequence factor, k_{dp}, were determined with the procedure developed by Suzuki et.al.[40] (as used in Section 6.3.1 above). Similarly

from section 6.3.1, the activation energies and the frequency factor for the decomposition and pyrolysis reactions of the foulants are summarized in Table 6.2. T_0 is the temperature where decomposition starts, hence from figure 6.7, T_0 = 100°C. The parameter $q_0\xi^*$ was calculated from a regression analysis and is listed in Table 6.2.

Table 6.2: Parameters for equation 4-46.

Organic material	$q_0\xi^*$	T_0 [°C]	k_{dR}^* [s^{-1}]	E_{dp} [kJ/mol]
Phenol	0.091	110	0.25	24.8

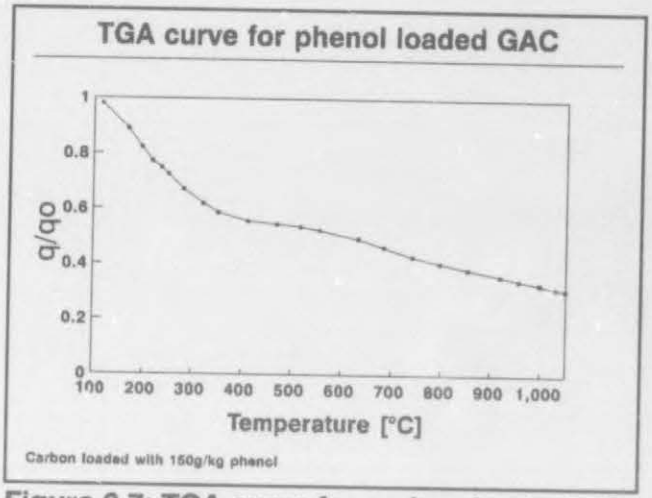

Figure 6.7: TGA curve for carbon loaded with 150mg/g phenol.

CHAPTER 7

SIMULATION

In this chapter the mathematical model developed in chapter 4, was used to simulate the dynamic behaviour of the regeneration of spent activated carbon in a rotary kiln. Since the unit mass loss of the spent carbon during regeneration is an indication of its adsorptive capacity (see Chapter 5, Section 5.4), it was employed to evaluate the kiln performance under different design and operating conditions and with alternative carbon properties. The simulation runs were classified as follows:

- a sensitivity analysis of the mass loss to changes in the physical properties of the activated carbon (see Section 7.1);
- the influence of the design parameters of the rotary kiln on the mass loss (see Section 7.2);
- the influence of the operating conditions on the mass loss (see Section 7.3);
- the effect of properties of activated carbon on the mass loss (see Section 7.4).

Finally, the influence of the capacity of the regenerated carbon was investigated on the rest of the CIP circuit.

7.1 SENSITIVITY ANALYSIS

In this section, the sensitivity of the mass loss to changes in the physical properties of the activated carbon was investigated.

7.1.1 Thermal conductivity, specific heat capacity and the bulk solids density

It is evident from chapter 6, section 6.2 that the estimated accuracy of the thermal conductivity of activated carbon is about 25 per cent. Furthermore, published average values of the specific heat capacity and the mean bulk density of the solids were used. It is expected that these properties are very specific for the type of carbon used, however, no relevant literature in this regard could be found. The sensitivity of the mass loss to a ±10, ±25 and ±35 per cent change in the values of the physical properties of the activated carbon was investigated. Average parameters from rotary kilns in the industry have been used. The values of the operating parameters, the design parameters and the activated carbon properties

Table 7.1: Parameters used for the base simulation run.

DESIGN PARAMETERS	
Kiln Length	5m
Diameter	0.9m
Fill height	0.2m
Reflectivity of inner wall	0.8
OPERATING PARAMETERS	
Temperatures:	
- solids	17°C
- gas*	600°C
- wall	650°C
Initial gas composition*:	
- H_2O	0.33%
- CO_2	0.006%
- CO	0.003%
- H_2	0%
- N_2	0.661%
Speed of rotation	0.5rev/min
Feed rate of the solids	250kg/hr
External gas flow rate	none
ACTIVATED CARBON DATA	
Bulk solid density	587kg/m^3
Weight moisture loaded	50%
Fouled by:	unknown foulants (PB3 mine sample)

* These values are not the iterated equilibrium values (see Chapter 5, Section 5.3.3)

for the base simulation run, are summarized in Table 7.1. For each sensitivity analysis the values of the parameters differing from these reference values are listed in the applicable sections. The freeboard gas temperature and composition used, were not the equilibrium calculated values, since accurate values are not necessary to show the tendencies during different sensitivity runs. These values should not differ much from the equilibrium ones, however, reliable estimates have been used.

The calculated mass loss of the regenerated mine sample (PB3) using the base values of Table 7.1and the computer program was 0.0365 kg/kg. (The four digit decimal does not indicate an accuracy of four digits, but is merely used for the sensitivity analysis).

The mass loss was calculated with the parameter values of Table 7.1, hence referred to as the base value. A change is then made to one parameter only and the mass loss is recalculated. The results of the sensitivity analysis on an individual basis, i.e. only one parameter value changed during a sensitivity run, are depicted in figure 7.1. It is clear that the mass loss is sensitive to changes in the values of the physical parameters. The worst influence was a 6% change to the base value when the thermal conductivity of the solids was decreased by 35%. The increase in the mass loss when the thermal conductivity increase is a direct influence of the thermal diffusivity, α;

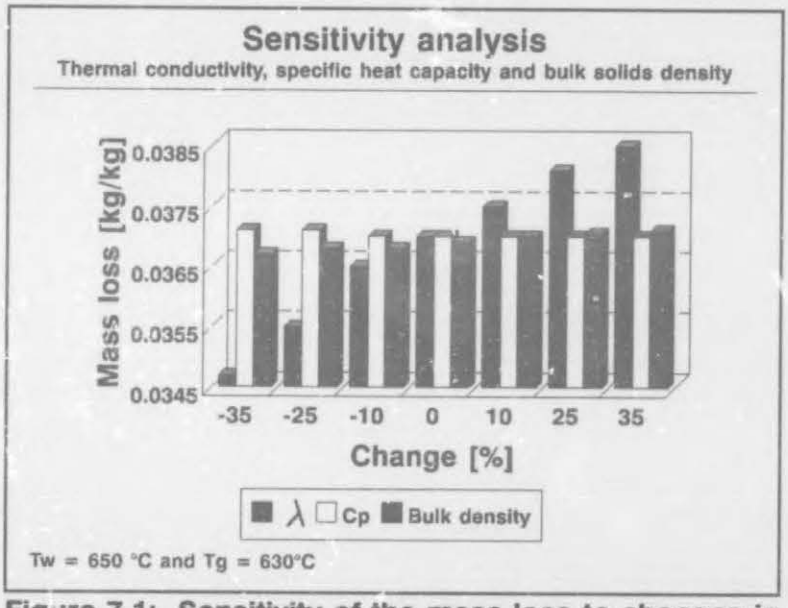

Figure 7.1: Sensitivity of the mass loss to changes in the values of the physical properties of the carbon.

$$\alpha = \frac{\lambda_s}{Cp_s \varrho_s} \qquad (7\text{-}1)$$

in the conductive heat transfer equations, equation 4-15, and 4-16. An increase in the thermal conductivity would increase α, and thus the conductive heat transfer rate (see equations 4-15 and 4-16). The opposite was expected for the bulk solids density and the specific heat capacity. An increase in the value of Cp_s and λ_s would lower the value of α in equation 7-1. A smaller α would result in a smaller conductive heat transfer rate to the solids, a smaller solids temperature and eventually, a smaller mass loss. However, this was not the case. The mass loss remained virtually constant for changes in the specific heat capacity and increased only by a very small amount when the values of the bulk solids density increased. An investigation of this phenomenon indicated that this result could be expected, since the decrease in the solids temperature as a result of a smaller α, was counteracted by the fact that an increase in Cp_s made the decrease of the solids temperature smaller due to the heat of reaction. An increase in the bulk density reduces α and thus the conductive heat transfer rate. The eventual temperature of the solids bed should therefore be smaller. However, for the same solids flow rate, an increase in the bulk density would lower the volume of the solids. The volume of the freeboard gas would therefore increase with an increase in the bulk density of the solids. The resulting partial pressure of the steam would be bigger and would result in an increase in the amount of carbon gassified (see the Langmuir-Hinshelwood equation, equation 2-8). It is expected that this effect should be more pronounced at higher temperatures. This is indeed the case (see Figure 7.2). It could therefore be expected that mass loss would be sensitive to the partial pressure of the steam and thus the dimensions of the oven (see Section 7.2 and 7.3).

It is provisionally accepted that the primary influence on the mass loss is the temperature of the kiln wall. The sensitivity runs were therefore repeated with different wall and freeboard gas temperatures of 750°C, 850°C and 950°C and 720°C, 820°C

and 920°C respectively. (Since the wall temperature changed, the gas temperature will also change). The temperature values used for the gas were not the calculated equilibrium temperatures, but estimated values. The rest of the parameter values were the same as in Table 7.1. The results with the temperature of the wall and the freeboard gas equal to 950°C and 920°C respectively, are depicted in figure 7.2. The effect of the changes in the values of the physical parameters showed the same trend as in figure 7.1, though the effects on the mass loss were more pronounced at the higher wall temperature. The maximum mass loss of 39% occurred when the value of the thermal conductivity was decreased by 35 %. It is evident that the mass loss is more sensitive to changes in the physical parameters when the temperature of the kiln wall and hence, the solids, is higher. This effect is shown in figure 7.3. During the sensitivity analysis, the mass loss was most sensitive to a -35% change in the value of all the physical parameters. Therefore the percentage difference in the mass loss when the value of one parameter changed with -35% was used to show the influence of temperature on the sensitivity of the mass loss in figure 7.3.

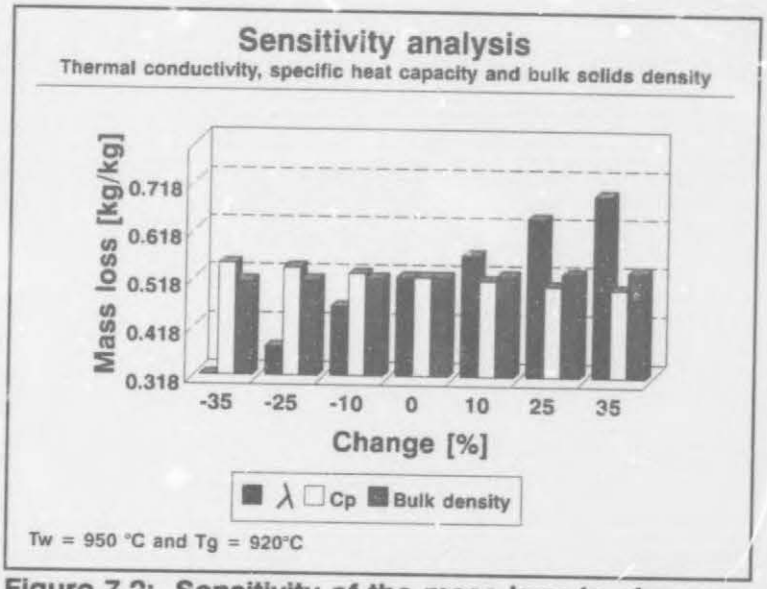

Figure 7.2: Sensitivity of the mass loss to changes in the values of the physical properties of the carbon.

Figure 7.3 indicates that the mass loss is not very sensitive to changes in the physical parameters of the activated carbon at low temperatures. At higher temperatures, the influence of individual changes becomes more substancial. However, the sensitivity of the mass loss to changes in the bulk density and the specific heat capacity is

negligible compared to the influence of changes in the thermal conductivity. In view of the overall accuracy of the simulator model, the sensitivity of the mass loss to changes in the physical parameters of the activated carbon is negligible. At temperatures above 750°C, however, the influence on the mass loss cannot be ignored.

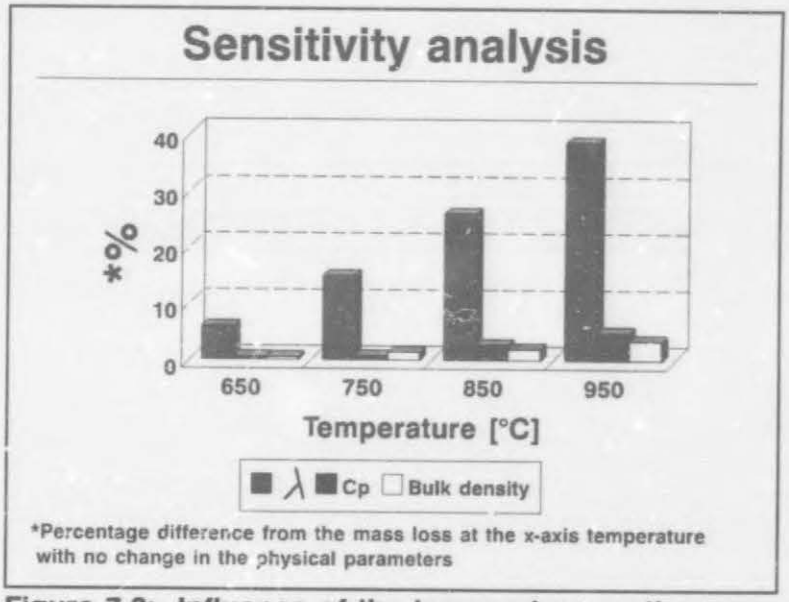

Figure 7.3: Influence of the temperature on the mass loss sensitivity.

Based on the individual sensitivity runs it can be concluded that the mass loss is only sensitive to changes in the thermal conductivity, however, individual changes are not sufficient to support a conclusion of this nature. The sensitivity analysis was therefore expanded to incorporate changes to more than one

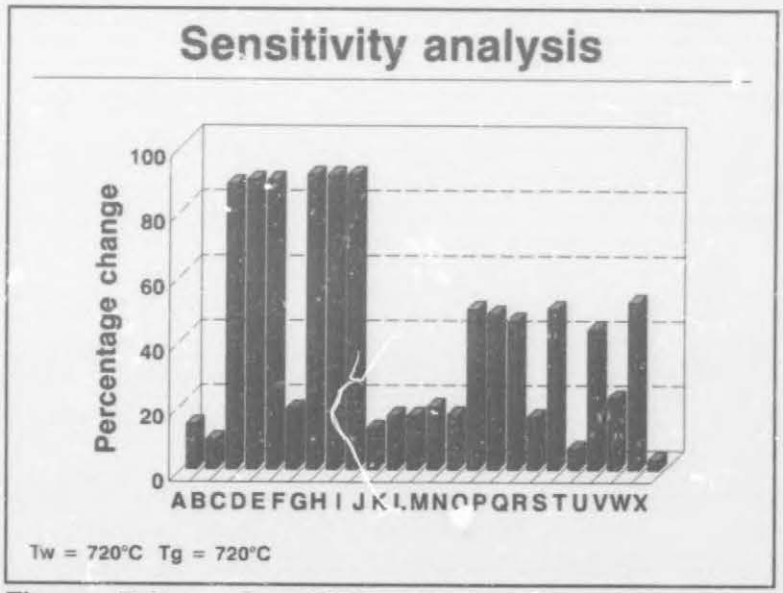

Figure 7.4: Sensitivity of the mass loss to a combination of changes to the physical parameters of the carbon.

parameter value at a time. Only changes of +35% and -35% have been considered. These results are depicted in figure 7.4. The legend for the x-axis is listed in Table 7.2.

The maximum influence on the mass loss was observed during runs C, D, E, G, H, and I. The influence during run C (see Table 7.2) is expected. It is evident from figure 7.4 that the influence of a change in the thermal conductivity is more pronounced on the mass loss at high temperatures than the influence due to a change in the bulk density and the specific heat capacity.

The bulk density of the activated carbon is the one parameter which can be calculated with a high degree of accuracy. The sensitivity of the mass loss to changes in the thermal conductivity and the specific heat capacity only, was thus investigated. Maximum influences were encountered when the thermal conductivity changed during runs G and H. When comparing runs G and H it was evident that the influence of the thermal conductivity is more

Table 7.2: X-axis legend.

LABEL	λ	Cp	ϱ
A	+35%	-	-
B	+35%	+35%	-
C	+35%	+35%	+35%
D	-	+35%	+35%
E	-	-	+35%
F	-	+35%	-
G	-35%	-	-
H	-35%	-35%	-
I	-35%	-35%	-35%
J	-	-35%	-35%
K	-	-	-35%
L	-	-35%	-
M	+35%	-35%	-
N	+35%	-35%	-35%
O	-35%	+35%	-
P	-35%	+35%	+35%
Q	-35%	-	+35%
R	+35%	-	+35%
S	-35%	-	-35%
T	+35%	-	-35%
U	-35%	-35%	+35%
V	+35%	-35%	+35%
W	-35%	+35%	-35%
X	+35%	+35%	-35%

pronounced than the influence of the specific heat capacity. The same situation occurred during runs S and U. Once again it shows that the mass loss was more sensitive to the thermal conductivity. However, a comparison between runs M and O showed that the higher specific heat capacity in run O could have a pronounce effect, since it lowered α as well as the heat loss of the solids due to the endothermic gasification reaction. The effect however, was not so strong in comparison with the influence of the thermal conductivity.

In view of these observations it is concluded that:

- the mass loss becomes sensitive to the thermal conductivity, the specific heat capacity and the bulk solids density at a solids temperature higher than 750°C;
- the mass loss is more sensitive to changes in the physical parameters at a higher temperature of the solids;
- the mass loss is more sensitive to a change in the thermal conductivity than to changes in the specific heat capacity and the bulk density of the solids;
- for the use of the simulator model in the industry, only the bulk density of the solids and the thermal conductivity for the carbon used, need to be determined.

7.1.2 Emissivity of the solids

The emissivity of the solids bed is another parameter that can influence the mass loss of the activated carbon. Figure 7.5 depicts the behaviour of the mass loss when the emissivity changes. The parameter values of Table 7.1 have been used, with the wall and freeboard gas temperatures as indicated in figure 7.5.

The effect of the emissivity of the inside kiln wall is also included in figure 7.5. The mass loss decreased with an increase in the emissivity of the solids. This result was expected since the radiative energy emitted by the solids would increase with an increasing emissivity (see Equation 4-9, Chapter 4, Section 4.3.1). The opposite is

true for the emissivity of the kiln wall. The influence on the mass loss of a change in the emissivity of the solids was bigger than for a change in the emissivity of the inside kiln wall. Although not tested, it is expected that these influences would be less at lower temperatures, since the same tendency that applied to the kiln wall reflectivity, should be applicable to the emissivities (see Section 7.2, Figure 7.7). However, the maximum influence on the mass loss was a 6% and 9% change from the mass loss calculated with the parameter values from Table 7.1 and the wall and gas temperatures indicated in figure 7.5. This influence is regarded as negligible in view of the overall accuracy of the simulation model. Estimated values for the emissivity of the kiln wall and the solids are regarded as acceptable.

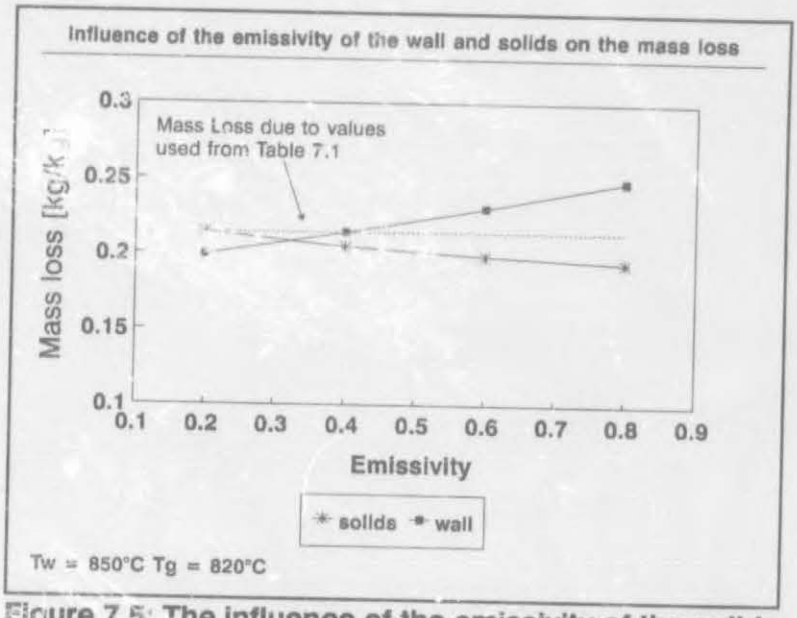

Figure 7.5: The influence of the emissivity of the solids and the inside kiln wall on the mass loss.

7.2 DESIGN PARAMETERS

In this section the influence of the design parameters on the predicted mass loss and hence the capacity of the regenerated carbon, is reported. This section can also be regarded as a type of sensitivity analysis. The parameter values of Table 7.1 were used with the exception of the wall and gas temperatures being 900°C and 827°C respectively. The influence on the mass loss was investigated to changes in the kiln diameter, length and the reflectivity of the kiln wall.

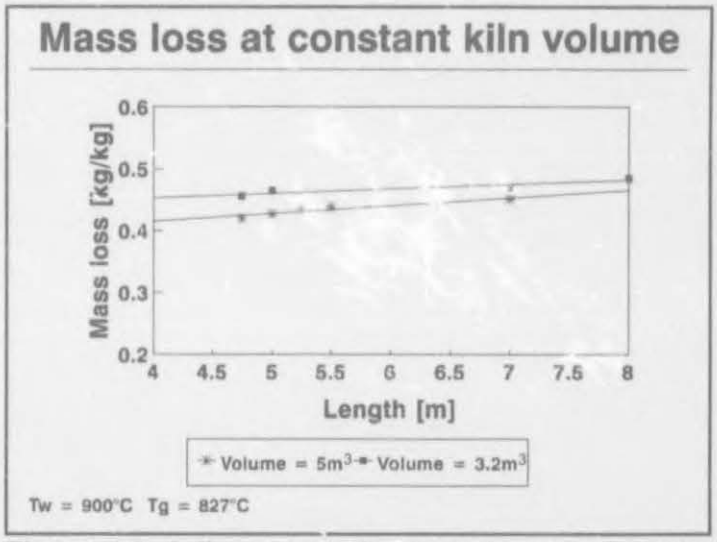

Figure 7.6: Influence on the mass loss to changes in the kiln length at constant volume.

The influence of the kiln length for a constant volume is indicated in figure 7.6. The mass loss shows a linear growth with increasing kiln length. However, the mass loss was slightly smaller for the smaller volume kiln. The solids mass per length increment for a kiln with a smaller diameter would be less than that for a larger diameter kiln. Therefore, the temperature of the solids bed in the small diameter kiln would increase at a faster rate than in a larger diameter kiln. Since the mass loss is a function of the solids bed temperature, it is expected that the mass loss of the solids in the longer kiln would be greater. Furthermore, the bed of solids in a longer, smaller diameter kiln would reach the gasifcation reaction temperature sooner than in a shorter wider kiln. This phenomenon should be considerred in detail during the design of a rotary kiln. Figure 7.6 also illustrates that an optimum length for a constant volume exists. A further increase in the kiln length would have no beneficial influence on the mass loss with regard to the increase in regeneration time. This is also true from a mathematical point of view. However, the length where the optimum is reached, may be inpractically long. This effect should be investigated in more detail during the design of a rotary kiln before making any decisions about the kiln dimensions.

The influence of the reflectivity of the wall is depicted in figure 7.7. Figure 7.7 shows an increase in the mass loss with an increase in the reflectivity of the kiln wall. This influence is, however, negligible at low temperatures. The larger influence at the higher temperature can be explained by the fact that the radiative energy transfer to the solids is a function of the temperature of the solids bed and the inside kiln wall. Thus, the

radiative heat transfer contribution to the overall heat transfer rate becomes more pronounce at higher temperatures of the solids and the kiln wall.

Although the influence is small, it appears that the heat transfer efficiency could be enhanced by covering the inside kiln wall with a highly reflective inner lining.

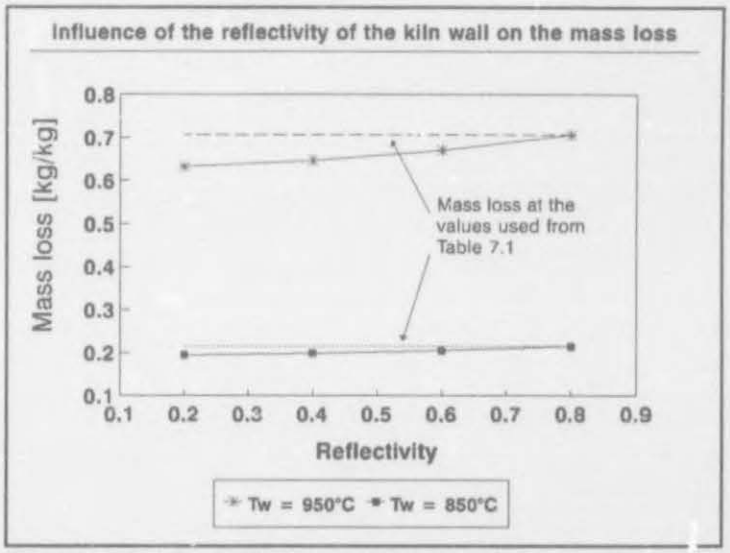

Figure 7.7: Sensitivity of the mass loss to changes in the reflectivity of the kiln wall.

7.3 OPERATING CONDITIONS

In this section the simulation model is used in a demonstrative manner to investigate the influence of different operating conditions. The parameter values of Table 7.1 were used as initial values. However, a non-ideal initial gas composition was selected. The freeboard gas composition is listed in Table 7.3. Except for the freeboard gas composition, the operating conditions were the same as those of the rotary kiln operating at the gold recovery plant of the President Brand mine in the Orange Free State. This was also the plant from which the mine sample (PB3) was obtained.

Table 7.3: Initial gas composition.

Initial gas composition:	
- H_2O	0.18%
- CO_2	0.006%
- CO	0.003%
- H_2	0.15%
- N_2	0.661%

7.3.1 Speed of rotation

It is evident from figure 5.5 (see Chapter 5, Section 5.4.1) that a mass loss of between 0.3kg/kg and 0.45kg/kg should be attained for the maximum adsorption capacity of the regenerated carbon. However, a single simulation run to iterate the equilibrium freeboard gas temperature and composition (see Chapter 5, Section 5.3.3) showed that a mass loss of only 0.0369kg/kg was obtained. Even a reduction of 50% in the rotation speed of the kiln to 0.25rev/min resulted in a mass loss of only 0.0371kg/kg.

The relationship between the mass loss and the speed of rotation is depicted in figure 7.8. The influence due to the reduction in the speed of rotation is negligible at the operating conditions prevailing. However, when the wall temperature is increased to 700°C and 900°C, respectively, a significant influence on the mass loss can be obtained by reducing the speed of rotation. A reduction in the speed of rotation would also lower the production rate of the kiln. The regeneration time increased from 24 minutes to 62 minutes when the speed of rotation reduced from 0.5rev/min to 0.2rev/min. In view of the lower production rate it is concluded that, at a wall temperature less than 900°C, the speed of rotation should not be reduced to obtain a higher mass loss. However, this situation may change at higher wall temperatures. The asymptotic behaviour of the

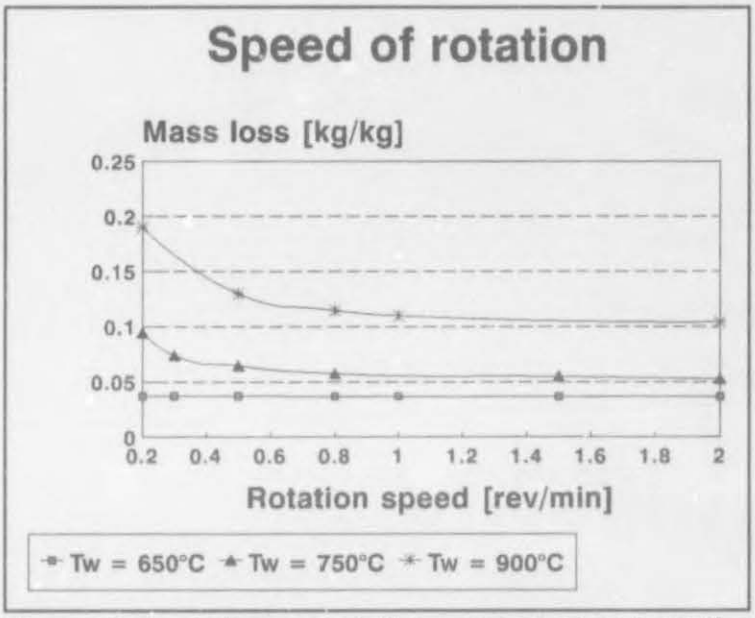

Figure 7.8: Influence of the rotation speed on the mass loss at different wall temperatures.

mass loss, on the other hand is an indication of a minimum regeneration time for the specific operating conditions. Care should therefore be taken when selecting the speed of rotation. The influence of the wall temperature as the only heat source is again very prominent in figure 7.8. It is evident that the wall temperature is the one parameter which should be selected with care.

7.3.2 Freeboard gas composition

The final solids bed temperatures during the two simulation runs in section 7.3.1 were 619°C (0.5rev/min) and 623°C (0.25rev/min) respectively. It is evident from the literature[11,42,65,82] that these temperatures are too low for proper regeneration. Regeneration temperatures of between 650°C and 850°C have been listed. Furthermore, it was shown that the steam-carbon reaction only becomes significant at temperatures in excess of 815°C [53]. Accordingly, the temperature of the wall, as the only heat source, should be increased to obtain the required mass loss of between 0.3kg/kg and 0.45kg/kg (see Figure 5.5, Chapter 5, Section 5.4.1) for proper regeneration.

The simulation run was repeated after selecting a wall and gas temperature of 750°C and 700°C, respectively. The parameter values of Table 7.1 were used. The initial gas composition was that of Table 7.3. A mass loss of only 0.056kg/kg was attained. Since the mass loss was less that the required mass loss, the wall temperature was increased to 900°C. The calculated mass loss during the first run was 0.1281kg/kg. However, a strange phenomenon was observed when the equilibrium freeboard gas temperature and composition were calculated (see Chapter 5, Section 5.3.3). The calculated mass loss increased with every iteration. It was observed that steam accumulated in the oven. The results for the first 19 iterations are shown in figure 7.9. A larger quantity of water evaporated during the drying stage than that used during the gasification reaction. Therefore, the fraction of steam in the freeboard gas increased. Accordingly, the partial pressure of the steam increased during every

iteration. A higher partial pressure of the steam enhances the gasification reaction. The fraction of hydrogen also increased with every iteration, however, at a smaller rate. Hydrogen retards the gasification reaction (see the Langmuir-Hinshelwood equation, equation 2-8). However, the mass loss still increased with every iteration, since the increase in the amount of hydrogen is less than that of steam. The fraction of steam will increase until equilibrium is reached for the conditions prevailing. One should be careful when selecting the wall temperature to obtain a certain mass loss. The iterative procedure to calculate the gas composition should be repeated until equilibrium conditions are obtained. A big difference in the intial and the equilibrium conditions could exists.

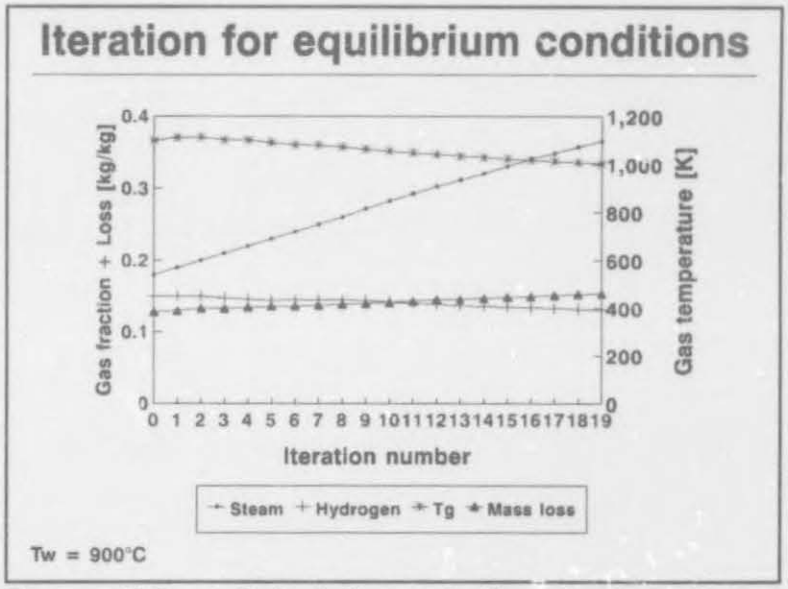

Figure 7.9: Calculation of the freeboard gas composition.

The fraction of hydrogen, as a product of the gasification

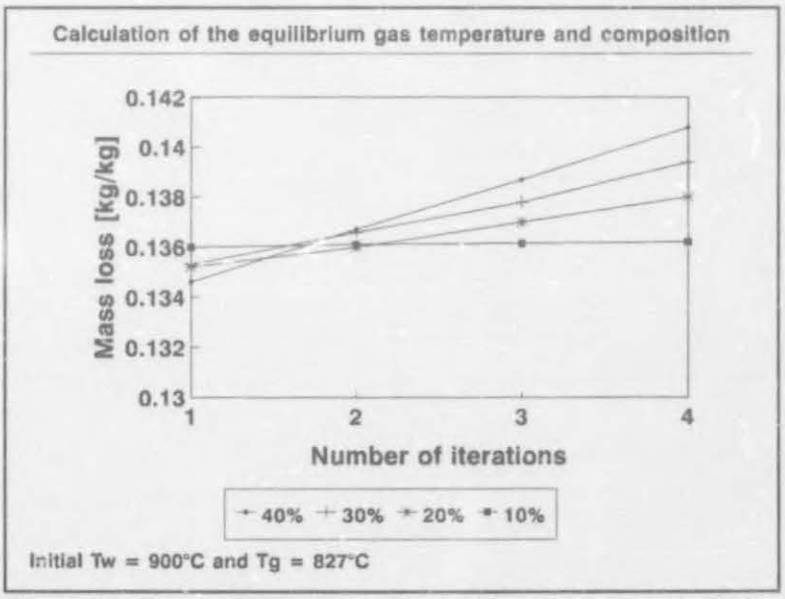

Figure 7.10: Influence on the moisture content of the carbon on the mass loss.

reaction (see reaction 4-31), increases at a rate slightly lower than that of the steam. However, the moisture content on the solids was 50 per cent. A decrease in the moisture content of the solids could thus eventually lead to a situation where the increase in the fraction of steam in the gas phase is less than the increase of hydrogen. A situation could also occur where the fraction of steam is less than the amount needed for the gasification reaction. This scenario is investigated in figure 7.10. The moisture content of the solids was taken as 40%, 30%, 20% and 10% respectively. The mass loss during thew first four iterations is shown in figure 7.10. Figure 7.10 illustrates that the fraction of steam cannot be maintained for moisture content less than 10% (for the conditions prevailing). Hydrogen will accumulate and will eventually slow the reaction rate to such an extent that the activity of the carbon will not be restored. A situation where the water content of the carbon is less than 10% is unlikely to occur.

Drying of the carbon prior to regeneration is thus fatal unless additional steam is not introduced into the furnace. Such an operating condition would be expensive and is not recommended, since enough steam is generated in the drying zone (if the moisture content of the carbon is high). However, if excess heat and steam is available, such an option can be considered.

During other simulation runs (not listed here) it was observed that the mass loss is not sensitive to the concentration of carbon dioxide and carbon monoxide.

Important conclusions for the condition prevailing, could be made:

- the evaporation of water in the drying zone of the kiln provides enough steam for the gasification reaction except for carbon with a moisyure content less than 10%;
- drying of the carbon prior to regeneration is not recomended;
- the mass loss is very sensitive to the fraction of hydrogen and steam in the freeboard gas;

- extra steam is not needed if the moisture content of the carbon is not enough;
- the simulator is able to identify problematic freeboard gas compositions.

These results are in agreement with experience in practise at the gold recovery plant of the President Brand Gold Mine.

7.3.3 Temperature of the kiln wall

During the simulation runs it was evident that the temperature of the kiln wall is the most important parameter. It was also expected, since the temperature of the kiln wall is the only heat source to the regenerative system.

Figure 5.5 (see Chapter 5, Section 5.4.1) indicated that a mass loss of between 0.3kg/kg and 0.45kg/kg should be attained for the proper regeneration of the spent mine sample (PB3). One operating strategy would be to select simply a wall temperature on a rule of thumb basis. This is usually the option taken at numerous gold recovery plants. On the other hand, however, the simulation model could be used to deal with this problem. The generation of heat is an expensive process and the selection of a wall temperature that is too high, is not economically viable. The simulation model was used in an illustrative manner to deal with this problem as discussed in Section 7.3.3.1.

7.3.3.1 Temperature profile

It is possible to introduce a temperature profile in the kiln wall, since the heating elements are usullally divided into a number of sections (see Chaper 1, Section 1.3). Three sections were considered with two different temperature profiles. In one simulation the sections were maintained at 750°C, 850°C and 950°C and in another the sections were maintained at 850°C, 950°C and 1050°C. These profiles are numbered step1 and step2 respectively in Table 7.4. The calculated mass loss was compared

with that obtained with the full length of the kiln wall maintained at the selected temperatures listed in Table 7.4. The results are listed in Table 7.4. Although two simulation runs are not sufficient to reach a definite conclusion, it appears that the use of a step temperature profile has no advantage over a constant temperature profile. An economic investigation into the heat requirements could determine which wall temperature profile to use. The temperature profile, "step1", is depicted in figure 7.11.

Table 7.4: Comparison of wall temperature profiles.

Mass loss [kg/kg]	Temperature [°C]
0.0708	750
0.1500	Step1
0.4092	Step2
0.2099	850
0.6760	950

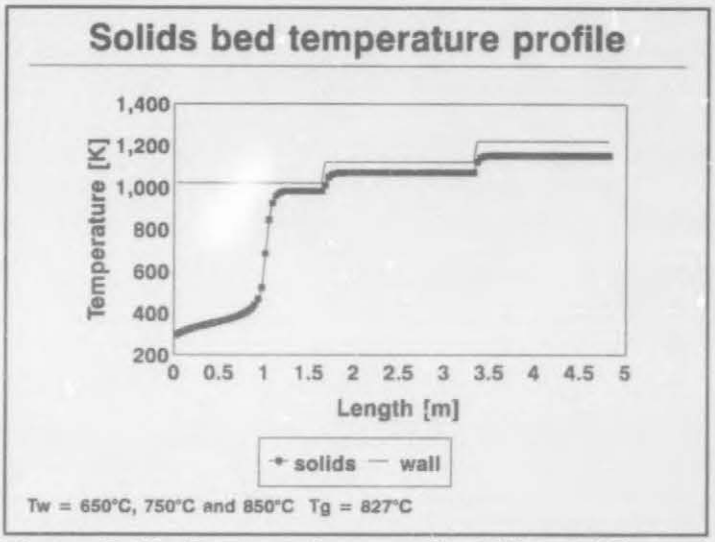

Figure 7.11: Temperature profile of the solids and kiln wall.

7.3.4 Mass flow of the solids

The influence of the mass flow rate of the solids is investigated in this section. It is obvious that a decrease in the mass loss can be expected. The same heat flow rate would result in a lower temperature of the solids when the rate increases. This result is depicted in figure 7.12. The influence of the mass flow rate of the solids was not very pronounced in the region investigated.

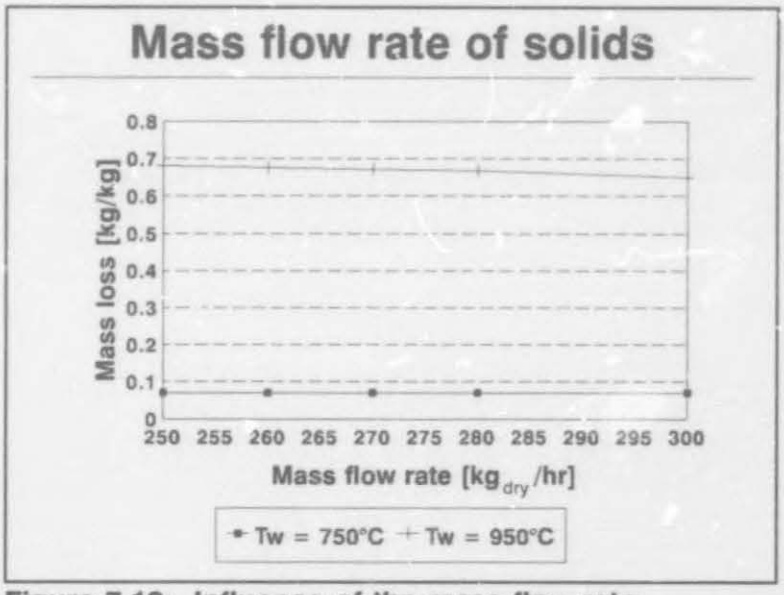

Figure 7.12: Influence of the mass flow rate.

7.4 CARBON PARAMETERS

Suzuki et al.[40] classified organic foulants into three distinct types (see Chapter 2, Section 2.2). Type III organic foulants are of particular concern for the regeneration process. The influence of different foulants on the mass loss of the regenerated carbon was investigated. Carbon loaded with Dow Froth 2000, Aniken 4122, sodium isobutyl xanthate (SIBX) and wattle bark extract (see Chapter 3, Section 3.3.4) was used. The relationship between the mass loss and adsorptive capacity was determined only for the eluted mine sample (PB3). Unfortunately, conclusions on the capacity of the regenerated carbon which had been fouled by the different organic materials cannot be made. The objective was to provide an illustration of the capability of the simulation model to incorporate carbon which had been fouled by different organic materials. The mass loss was calculated for the different samples regenerated under the same operating conditions. The parameter values used, were the same as those in Table 7.1. However, wall and gas temperatures of 900°C and 827°C respectively, were used. The results are listed in Table 7.5.

Different mass losses were obtained for the different samples. The differences in predicted mass loss results from different mass losses during the decomposition and pyrolysis reactions of the foulants. The mass loss of the different samples cannot be used to evaluate the capacity of the regenerated samples, since the mass loss capacity relationship was not determined for samples other than the eluted mine sample. Table 7.5 merely illustrates that the simulator can be used for carbon fouled by any type of organic material, provided that the mass loss versus temperature relationship has been determined as outlined in chapter 4, section 4.7. In order to predict the capacity, the mass loss versus capacity relationship should be determined as explained in chapter 5, section 5.4.

Table 7.5: Mass loss for different foulants.

Foulant	Mass loss [kg/kg]
Mine sample	0.3663
Anniken 4122	0.5580
Dow froth 2000	0.6598
SIBX	0.2709
Wattle bark extract	0.6384

7.5 INFLUENCE OF THE FREUNDLICH A PARAMETER ON THE CIP CIRCUIT

In this section the influence of the capacity of the regenerated carbon on the rest of the CIP circuit was investigated. The mathematical model developed in this study evaluates the regeneration process in terms of the capacity of the regenerated carbon. Moreover, the capacity is quantified as the Freundlich A parameter.

Van der Walt and Van Deventer[105] developed a simulator algorithm in order to predict the dynamic behaviour in a CIP/CIL circuit. The simulator was developed in Turbo C^{++}. A modified version of Van der Walt's program was used to predict the influence of the Freundlich A parameter of the regenerated mine carbon on the rest of the CIP

circuit. A brief discussion on the basis of the simulation model will be given.

7.5.1 CIP simulator

The simulator uses a simple film phase diffusion model. Solid phase diffusion has not been considered. The phenomenon of preg-robbing was considered to be essentially an adsorption process and was also modelled by film diffusion. A multi-component Langmuir isotherm was used to simulate the multi-component adsorption from leached slurries. The phenomenon of fouling was modelled by a gradual decrease in loading owing to direct competition of other complexes. The well-known Mintek empirical equation was used for leaching.

Since the adsorptive capacity of the regenerated carbon in this study was expressed in terms of the Freundlich A parameter, the acquired computer program had to be modified. The adsorption process was changed to a single component system where the Freundlich isotherm, equation 5-2, was used to simulate the adsorption process. Furthermore, leaching and preg-robbing were considered.

7.5.2 Results

The rotary kiln simulator developed in this study could then be used in combination with the modified CIP simulator to predict the performance of a rotary kiln. The values of the operating pararameters used for CIP simulation are listed in Table 7.6.

Improper operating conditions of the rotary kiln would result in a lower capacity of the regenerated carbon. The capacity of the regenerated carbon was quantified in chapter 5 in terms of the Freundlich A parameter. Assume thus that three different operating conditions resulted in a mass loss of 0.001kg/kg, 0.15kg/kg and 0.35kg/kg of the spent carbon (PB3). The capacity, in terms of the Freundlich A parameter, of the regenerated samples are: 4g/kg, 6g/kg and 12 g/kg (see Figure 5.5, Chapter 5,

Section 5.4.1).

Table 7.6: Values for the operating parameters in the simulation runs.

Number of stages	: 6
Total simulation time	: 300hr
Carbon transfer cycles	: 12hr
Carbon transfer period during each cycle	: 0.5hr
Volume of stages	: $750m^3$
Volumetric flow rate of slurry entering stage 1	: $750m^3.hr^{-1}$
Densities:	
carbon	: $587kg.m^{-3}$
ore	: $2550kg.m^{-3}$
slurry	: $1400kg.m^{-3}$
Film diffusion coefficient for adsorption	: $10^{-5}m.s^{-1}$
Concentration of gold in feed	: $6g.m^{-3}$
Gold grade of ore	: $10^{-3}g_{Au}.kg^{-1}$
Loading of adsorbates on eluted carbon	: $0g.kg^{-1}$
Freundlich isotherms on the carbon surface, equation 5-2 (see Chapter 5, Section 5.4.1)	: A = 4, 8, 12

These values of the Freundlich A parameter were used in the modified CIP simulator to calculate the loading of the carbon in each adsorption section and the concentration of gold in solution. The results are summarized in figure 7.13 and 7.14 respectively.

As expected, Figure 7.13 shows that a lower capacity (Freundlich A parameter = 4) results in a significant decrease in the loading of gold on the product carbon and a concomitant increase in the gold lost in the solution leaving the last stage (Figure 7.14). Moreover, the poor regeneration affects the profile of gold loading on the carbon throughout the cascade. This results in a larger gold holdup in the cascade. This has a detrimental effect on the overall economy of the CIP circuit, since it has a retarded effect on the selling of gold. The influence of effetive regeneration is apparent in figures 7.13 and 7.14. The increase in the capacity of the regenerated carbon results in an increase in the loading of the carbon and a decrease in the gold holdup and the gold lost in the solution leaving the last stage. This programme demonstrates clearly why activated carbon should be regenerated efficiently in order to remove organic foulants. Nevertheless, it is surprising that many plants do not even measure the activity of the regenerated carbon.

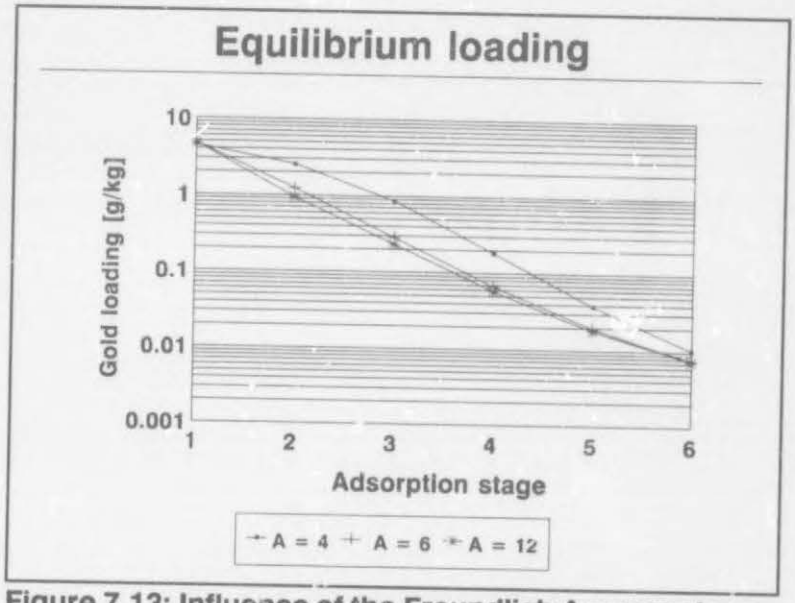

Figure 7.13: Influence of the Freundlich A parameter on the equilibrium gold loading on regenerated carbon in the CIP cascade.

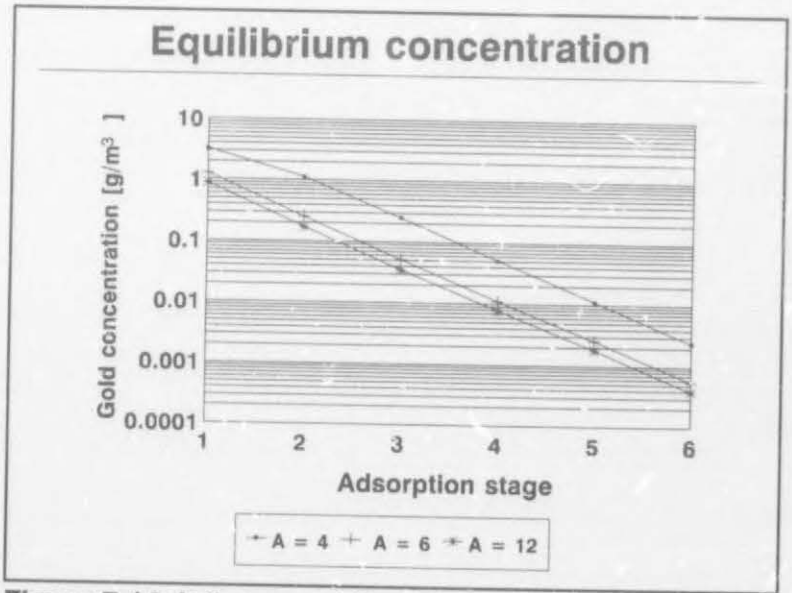

Figure 7.14: Influence of the Freundlich A parameter on the equilibrium concentration of gold in the solution of the CIP cascade.

The regeneration model developed in this study is a useful simulator tool to optimize regeneration in a rotary kiln and to attain the optimum adsorption capacity of the regenerated carbon. The regeneration simulation program can be used with economic models, and simulators for the elution, acid washing and CIP adsorption cascade (as illustrated) so as to optimise the operation of the entire plant.

CHAPTER 8

CONCLUSIONS AND SIGNIFICANCE

- A literature survey revealed that the need for a mathematical model to predict the optimum regeneration conditions had not been satisfied. The effect of the design parameters, the operating conditions and the activated carbon properties on the capacity of the regenerated carbon had not been investigated. No attempt had been made to quantify the performance of a rotary kiln and to evaluate the performance not only in terms of the enhanced capacity of the regenerated carbon, but also in terms of the influence on the CIP circuit. These phenomena have been satisfied in this study.

- The Freundlich A parameter was found adequate to relate the mass loss during regeneration to the adsorption capacity of the regenerated carbon.

- Experimental results showed that an optimum mass loss during regeneration corresponds to a maximum adsorption capacity exists for regenerated carbon.

- A rotary kiln simulator model was developed to predict the performance of a rotary kiln in terms of the calculated mass loss and the associated adsorptive capacity of the regenerated carbon.

- A sensitivity analysis showed that the mass loss is most sensitive to changes in the temperature of the kiln wall. The mass loss is also

sensitive to changes in the thermal conductivity and the density of the solids in the kiln. This phenomenon is more pronounced at higher temperatures. These two parameters should be determined when the type of carbon used, is changed.

- A highly reflective lining material is likely to improve the radiative heat transfer rate to the solids bed.

- The influence of a reduction in the rotational speed becomes significant only at wall temperatures greater than 900°C .

- The fractions of hydrogen and steam in the freeboard gas is critical for effective regeneration.

- A feed of external steam is not required for the regeneration of carbon loaded with more than 10% moisture.

- Drying of the activated carbon prior to regeneration is not recommended for carbon loaded with water.

- Proper control of the wall temperature of the kiln is essential for optimum operation of the regeneration process.

- An increase in the flow rate of the solids reduces the mass loss.

- The simulator model could be used to evaluate the regeneration of spent activated carbon fouled by an unknown amount of unknown organic materials.

- The model confirmed mathematically that insufficient regeneration would result in a gold loss in the solution leaving the last stage of the CIP

cascade, since the loading on the carbon decreases when the capacity of the regenerated carbon decreased. Furthermore, the degree of gold holdup in the CIP cascade would increased with a decrease in the capacity of the carbon.

- With minor alterations, the developed model can also be used to simulate processes in rotary kilns other that the regeneration of carbon.

- A more comprehensive mathematical model than was previously available has been developed.

REFERENCES

1. HASSLER, J.W., Purification with activated carbon, Chemical Publishing Co., Inc., New York, 1974, p. 3.

2. HASBASHI, F., Principles of the Extractive Metallurgy, Gordon and Breach Science Publishers, New York, 1970, p. 184.

3. LAXEN, P.A., BECKER, G.S.M. and RUBIN, R., Developments in the application of carbon-in-pulp to the recovery of gold from South African ores, J. S. Afr. Inst. Min. Metall., vol. 79, no. 11, 1979, pp. 315-326.

4. ZADRA, J.B., A process for the recovery of gold from activated carbon by leaching and electrolysis, U.S. Bureau of Mines Report of Investigations, no. 4672, 1950. Also abstracted in Chemical Abstracts, 4837b, vol. 44, no. 11, June 10, 1950.

5. FLEMING, C.A., Recent developments in the carbon-in-pulp technology in South Africa, Hydrometallurgy: Research, Development, and Plant Practice, K. Osseo-Asare and J.D. Miller (editors), The Metallurgical Society of AIME, New York, 1983, pp. 839-857.

6. HALL, K.B., Homestake uses carbon-in-pulp process to recover gold from slimes, World Mining, vol. 27, no. 12, Nov. 1974, pp. 44-49.

7. MENNE, D., Optimization of full-scale circuits for the carbon-in-pulp recovery of gold, Proceedings, 12th CMMI Congress, H.W. Glen (editor), Johannesburg, S.

Afr. Inst. Min. Metall., 1982, pp. 569-574.

8. FINKELSTEIN, N.P., The chemistry of the extraction of gold from ores, in: Gold Metallurgy in South Africa, Adamson, P. (editor.), Chamber of Mines of South Africa, Johannesburg, 1972, p. 305.

9. LAXEN, P.A., FLEMING, C.A., HOLTUM, D.A. and RUBIN, R., A review of pilot-plant testwork conducted on the carbon-in-pulp process for the recovery of gold, Proceedings, 12th CMMI Congress, Glen, H.W. (editor), Johannesburg, S. Afr. Inst. Min. Metall., 1982, pp. 551-561.

10. LAXEN, P.A. and BROWN, T.D., The carbon-in-pulp plant at Rand Mines Milling and Mining Company Limited: Problems encountered and developments introduced, Paper B7/2: MINTEK 50, International conference on recent advances in mineral science and technology, Paper B7/2, Sandton, 26-30 March 1984.

11. BRIGGS, A.P.W., Problems encountered during the commisioning of the carbon-in-pulp plant at Beisa Mine, J.S. Afr. Inst. Min. Metall., vol. 83, no. 10, 1983, pp. 246-253.

12. DAHYA, A.S. and KING, D.J., Developments in carbon-in-pulp technology for gold recovery, CIM Bulletin, September 1983, pp. 55-61.

13. LAMMERS, J.H. The process design of the OK Tedi project, Paper IV: First International Symposium on Precious Metal Recovery, June 10-14, 1984, Reno, Nevada.

14. ZADRA, J.B., ENGEL, A.L. and HEINEN, H.J., Process for recovering gold and silver from activated carbon by leaching and electrolysis, U.S. Bureau of Mines Report of Investigation, no. 4843, 1952.

15. JHA, M.C., Recovery of gold and silver from cyanide solutions: a comparative study of various processes, Paper XXI: First International Symposium on Precious Metals Recovery, June 10-14, 1984, Reno, Nevada.

16. DAVIDSON, R.J. and DUNCANSON, D., The elution of gold from activated carbon using deionized water, J.S. Afr. Inst. Min. Metall., vol. 77, no. 12, 1977, pp. 254-261.

17. DAVIDSON, R.J. and VERONESE, V., Further studies on the elution of gold from activated carbon using water as the eluant, J.S. Afr. Inst. Min. Metall., vol. 79, no. 10, 1979, pp. 437-445.

18. TODD, L.R. and ANDERSON, A.R., Gold and silver processing at Duval's Battle Mountain, Nevada Operation, Paper II: First International Symposium on Precious Metals Recovery, June 10-14, 1984, Reno, Nevada.

19. ADAMSON, R.J. (editor), Gold Metallurgy in South Africa, Chamber of Mines of South Africa, Johannesburg, 1972, pp. [illegible].

20. OLIVIER, P. and BARBERY, G., Development of a carbon-in-pulp process for clayey gold ores, Paper: XIV International Mineral Processing Congress, October 17-23, 1982, Toronto, Canada.

21. LA BROOY, S.R., HOSKING, J.W., MUIR, D.M., RUANE, M., SMITH, I and HINCHLIFFE, W.D., Studies on the fouling and regeneration of activated carbon, Symposium Series: Aus. Inst. Min. Metall, vol. 39, October 1984, pp. 257-269.

22. VAN VLIET, B.M., Carbon regeneration in South Africa, Prog. Wat. Tech., vol. 10, nos. 1&2, 1978, pp. 555-563.

23. SPAIN, I.L., The electronic transport properties of graphite, carbons and related

materials, in: Chemistry and Physics of Carbon, Walker, P. L. and Thrower, P.A. (editors), vol. 16, New York: Marcel Dekker Inc., 1981, pp. 119-304.

24. KELLY, B.T. and TAYLOR, R., The thermal properties of graphite, in: Chemistry and Physics of Carbon, Walker, P.L. and Thrower, P.A. (editors), vol. 10, New York: Marcel Dekker inc., 1969, pp. 119-215.

25. COTTON, F.A. and WILKINSON, G., Advanced Inorganic Chemistry, Third ed., New York: Interscience Publishers, 1972.

26. YEHASKEL, A., Activated Carbon: Manufacture and Regeneration, Noyes Data Corporation, New Jersey, 1978, 328 p.

27. McDOUGALL, G.J. and HANCOCK, R.D., Activated carbons and gold - a literature survey, Minerals Sci. Engng., vol.12, no. 2, 1980, pp. 24-27.

28. PEEL, R.G., The roles of slow adsorption kinetics and bioactivity in modelling of activated carbon adsorbers, Ph.D Thesis, McMaster University, 1979.

29. McDOUGALL, G.J., Adsorption on activated carbon, Chem SA, 1982, pp.24-27.

30. ACTON, C.F., The technology of gold and silver extraction, A.I.Ch.E Symposium Series, no. 216, vol. 78, 1982, pp. 127-137.

31. JONES, W.G., KLAUBER, C. and LINGE, H.G., Loading of $Au(CN)_2^-$-solution onto activated carbon, The AusIMM 1989 Annual Conference, Perth-Kalgoorlie, Western Australia, 1989, pp. 225-228.

32. CHEREMISINOFF, P.N. and MORRESI, A.C., Carbon adsorption, in: Carbon Adsorption Handbook, Cheremisinoff, P.N. and Ellerbush, F. (editors), Michigan: Ann Arbor Science Publishers Inc., 1978, pp. 1-53.

33. WILSON, J., Active carbons from coals, Fuel, vol. 60, 1981, pp. 823-831.

34. DURIE, R.A. and SCHAFER, H.N.S., The production of activated carbon from brown coal in high yields, Fuel, vol. 58, 1980, pp. 472-476.

35. RUIZ BEVIà, F., PRATS RICO, D. and MARCILLA GOMIS, A.F., Activated carbon from almond shells. Chemical activation. 1. Activating reagent selection and variables influence, Ind. Eng. Chem. Prod. Res. Dev., vol. 23. no. 2, 1984, pp. 266-271.

36. WATANABE, F., YAMADA, Y., HASATANI, M. and SUGIYAMA, S., Effect of pore size distributions of original carbonized materials on the development of pores during activation, J. Chem. Eng. Japan, vol. 9, no. 4, 1976, pp. 314-316.

37. STEENBERG, B., Adsorption and Exchange of ions on Activated Carbon Upsala, Almqvist and Wiksells, 1944.

38. TSUCHIDA, N., RUANE, M. and MUIR, D.M., Studies on the mechanism of gold adsorption on carbon, MINTEK 50, International conference on recent advances in mineral science and technology, Paper B6/2, Sandton, 1984.

39. LEE, A.F., BROWN, T.D. and LAXEN, P.A., The distribution of humic substances in the dumps and carbon-in-pulp plant circuits at Rand Mines Milling and Mining, Gold 100, Proceedings of the international conference on gold, vol. 2: Extractive metallurgy of gold, Johannesburg, SAIMM, 1986, pp. 367-381.

40. SUZUKI, M, MISIC, D.M., KOYAMA, O. and KAWAZOE, K., Study of thermal regeneration of spent activated carbons: Thermogravimetric measurement of various single component organics loaded on activated carbon, Chem. Eng. Sc., vol. 33, 1978, pp. 271-279.

41. WANG, J. and SMITH, J.M., Thermal regeneration of the phenol-carbon system, AIChE Journal, vol. 31, no. 3, 1985, pp.496-498.

42. UMEHARA, T., HARRIOTT, P. and SMITH, J.M., Regenerating of activated carbon. Part I: Thermal decomposition of adsorbed sodium dodecylbenzene sulphonate, AIChE Journal, vol. 29, no. 5, 1983, pp. 732-737.

43. HARRIOTT, P. and CHENG, A.T., Kinetics of spent activated carbon regeneration, AIChE Journal, vol. 34, no. 10, 1988, pp. 1656-1662.

44. MARTIN, R.J. and NG, W.J., Chemical regeneration of exhausted activated carbon - II, Water Res., vol. 19, no. 2, 1985, pp. 1527-1535.

45. KREBS, C. and SMITH, J.M., Kinetics of steam regeneration of virgin and phenol-loaded activated carbon, Carbon, vol. 33, no. 2, 1985, pp. 223-235.

46. AHMED, S. and BACK, M.H., 1987, The effect of water vapour and inert gases on the carbon-oxygen reaction, Carbon, vol. 25, no. 6, pp. 783-789.

47. MCKEE, D.W., The catalysed gasification ractions of carbon, in: Chemistry and Physics of Carbon, Walker, P.L. and Thrower, P.A. (editors), vol. 16, New York: Marcel Dekker Inc., 1981, pp. 1-118.

48. MATSUI, I, MISIC, D.M. and SUZUKI, M., Caparison of steam gasification rates of various activated carbons by TGA method, J. Chem. Engng Japan, vol. 17, no. 1, 1984, pp. 13-18.

49. VAN VLIET, B.M., The regeneration of activated carbon, J. S Afr. Inst. Min. Metall, vol. 91, no. 5, 1991, pp. 159-167.

50. KLEI, H.E., SAHAGIAN, J. and SUNDSTROM, D.W., Kinetics of the activated

carbon-steam reaction, Ind. Eng. Chem., Process Des. Dev., vol. 14, no. 4 1975, pp. 470-473.

51. RIEDE, B.E. and HANESIAN, D., Kinetic study of carbon-steam reaction, Ind. Eng. Chem., Process Des. Dev., vol. 14, no. 1, 1975, pp. 70-74.

52. KASAOKA, S., SAKATA, Y., SHIMADA, M. and MATSUTOMI, T., A new kinetic model for the temperature programmed thermogravimetry and its applications to the gasification of coal chars with steam and carbon dioxide, J. Chem Engng. Japan, vol. 18, no.5, 1985, pp.426-432.

53. CHIHARA, K., MATSUI, I. and SMITH, J.M., Regeneration of activated carbon. Part II: Steam-carbon reaction kinetics, AIChE Journal, vol. 27, no. 2, 1981, pp. 220-225.

54. HASHIMOTO, K., MIURA, K. and WATANABE, T., Kinetics of thermal regeneration reaction of activated carbons used in waste water treatment, AIChE Journal, vol. 28, no. 5, 1982, pp. 737-746.

55. SAFFER, M., OCAMPO, A. and LAGUERIE, C., Gasification of coal in a fluidized bed in the presence of water vapour and oxygen; an experimental study and a first attempt at modelling the reactor, Int. Chem. Engng, vol. 28, no. 1, January 1988, pp. 46-61.

56. CHIN, G., KIMURA, S., TONE, S. and OTAKE, T., Gasification of coal char with steam. Part 3. Effect of potassium carbonate catalyst on the rate of gasification, regeneration conditions on the adsorptive behaviour of activated carbon, Int. Chem. Engng, vol. 24, no. 2, 1984, pp. 346-354.7

57. JÜNTGEN, H., Reactivities of carbon to steam and hydrogen and applications to technical gasification processes - a review, Carbon, vol. 19, 1981, pp. 167-

173.

58. MATSUI, I., KUNII, D. and FURUSAWA, T., Study of char gasification by carbon dioxide. 1. Kinetic study by thermogravimetric analysis, Ind. Eng. Chem. Res, vol. 26. no. 1, 1987, pp. 91-95.

59. KASAOKA, S., SAKATA, Y. and TONG, C., Kinetic evaluation of the reactivity of various coal chars for gasification with carbon dioxide in comparison with steam, Int. Chem. Eng., vol. 25, no. 1, 1985, pp. 160-175.

60. KATO, K., MATSUURA, K., SAWAMURA, Y., MORI, H. and HANZAWA, T., The thermal regeneration of spent activated carbon, J. Chem. Eng. Japan, vol. 13, no.3, 1980, pp. 214-219.

61. URANO, K., YAMAMOTO, E. and TAKEDA, H., The regeneration rates of granular activated carbons containing adsorbed matter, Ind. Eng. Chem. Process. Des. Dev., vol. 21, no. 1, 1982, pp. 180-185.

62. ERGUN, S. and MENTSER, M., Reaction of carbon with carbon dioxide and steam, in: Chemistry and Physics of Carbon, Walker, P.L. and Thrower, P.A. (editors), vol. 1, New York: Marcel Dekker Inc., 1965, pp. 204-263.

63. UMEHARA, T., HARRIOTT, P. and SMITH, J.M., Regenerating of activated carbon. Part II: Gasification kinetics with steam, AIChE Journal, vol. 29, no. 5, 1983, pp. 737-741.

64. VAN DEVENTER, J.S.J. and CAMBY, B.S., Technical note: The influence of regeneration conditions on the adsorptive behaviour of activated carbon, Min. Engng, vol. 1, no. 2, 1988, pp. 157-163.

65. VAN STADEN, P.J., Parameters governing the performance of a continuous,

direct resistance heating, carbon regeneration furnace, M-Thesis, University of the Witwatersrand 1990.

66. HUH, F., KLEIN, J. and JÜNTGEN, H., Investigation on the alkali-catalysed steam gasification of coal: kinetics and interactions of alkali catalyst with carbon, Fuel, vol. 62, 1983, pp. 196-199.

67. KAPTEIJN, F., ABBEL, G. and MOULIJN, J.A., CO_2 gasification of carbon catalysed by alkali metals; reactivity and mechanism, Fuel, vol. 63, 1984, pp. 1036-1042.

68. SUZUKI, T., MIDHIMA, M., KITAGUCHI, J., ITOH, M. and WATANABE, Y., The catalytic steam gasification of one Australian and three Japanese coals using potassium and sodium carbonates, Fuel Processing Technology, vol. 8, 1984, pp. 205-212.

69. HOLSTEIN, W.L., and BOUDART, M., Transition metal and metal oxide catalysed gasification of carbon by oxygen, water and carbon dioxide, Fuel, vol. 63, 1983, pp. 162-165.

70. DOUCHANOV, D. and ANGELOVA, G., Effect of catalysis and inlet gas on coal gasification, Fuel, vol. 62, 1983, pp. 231-233.

71. MCKEE, D., Mechanisms of the alkali metal catalysed gasification of carbon, Fuel, vol. 62, 1983, pp. 170-175.

72. WIGMANS, T., VAN DOORN, J. and MOULIJN, J.A., Temperature-programmed desorption study of Na_2CO_3-containing activated carbon, Fuel, vol. 62, 1983, pp. 190-195.

73. YUH, S.J. and WOLF, E.E., FTIR studies of potassium catalyst-treated gasified

coal chars and carbons, Fuel, vol. 62, 1983, pp. 252-255.

74. MCKEE, D.W., SPIRO, C.L., KOSKY, P.G. and LAMBY, E.J., Catalysis of coal char gasification by alkali metal salts, Fuel, vol. 62, 1983, pp. 217-220.

75. KAPTEIJN, F., PORRE, H. and MOULIJN, J.A., CO_2 Gasification of activated carbon catalysed by earth alkaline elements, AIChE Journal vol. 32, no. 4, pp. 691-695.

76. SPIRO, C.L., MCKEE, D.W., KOSKY, P.G. and LAMBY, E.J., Catalytic CO_2-gasification of graphite versus coal char, Fuel, vol. 62, 1983, pp. 180-184.

77. MIMS,C.A. and PABST, J.K., Role of surface complexes in alkali-catalysed carbon gasification, Fuel, vol. 62, February 1983, pp. 176-179.

78. HÜTTINGER, K.J. and MINGES, R., Catalytic activity of potassium halides in water vapour gasification of graphite, Fuel, vol. 63, 1984, pp. 9-12.

79. KAPTEIJN, F. and MOULIJN, J.A., Kinetics of the potassium carbonate-catalysed CO_2 gasification of activated carbon, Fuel, vol. 62, February 1983, pp. 221-225.

80. FURIMSKY, E., Catalytic effect of mineral matter of high ash Onakawana lignite on steam gasification, Can. J. Chem. Engng, vol. 64, 1986, pp. 293-298.

81. FIGUEIREDO, J.L., ORFÃO, J.J.M. and FERRAZ, M.C.A., Catalytic gasification of chars, Fuel, vol. 63, pp. 1059-1060.

82. VAN VLIET, D.A. and VENTER, L., Infrared thermal regeneration of spent activated carbon from water reclamation, Wat. Sci. Tech., 1984, vol. 17, pp. 1029-1042.

83. BRIMACOMBE, J.P. and WATKINSON, A.P., Heat transfer in a direct-fired rotary kiln: I. Pilot plant and experimentation, Metallurgical Transactions B, vol. 9B, 1978, pp. 201-208.

84. SILCOX, G.D. and PERSHING, D.W., The effect of rotary kiln operating conditions and design on burden heating rates as determined by a mathematical model of rotary kiln heat transfer, J. Air Wast Manage. Assoc., vol. 40, no. 3, 1990, pp. 337-344.

85. WATKINSON, A.P. and BRIMACOMBE, J.K., Heat transfer in a direct-fired rotary kiln: II. Heat flow results and their interpretation, Metallurgical Transactions B, vol. 9B, 1978, pp. 209-219.

86. TSCHENG, S.H. and WATKINSON, A.P., Convective heat transfer in a rotary kiln, Can. J. Chem. Engng., vol. 57, 1979, pp. 433-443.

87. SASS, A., Simulation of the heat transfer phenomena in a rotary kiln, I&EC Process Design and Development, vol. 6,no. 4, 1967, pp. 532-536.

88. KETSLAKH, G.A. and TSIBIN, I.P., Heat transfer by radiation in rotary kilns, Heat Engineering, Translated from Ogneupory, no. 1, 1978, pp. 17-19.

89. BARR, P.V., BRIMACOMBE, J.K. and WATKINSON, A.P., A heat transfer model for the rotary kiln: Part I. Pilot kiln trails, Metallurgical Transaction B, vol. 20B, 1989, pp. 391-402.

90. GOROG, J.P., ADAMS, T.N. and BRIMACOMBE, J.K., Regenerative heat transfer in rotary kilns, Metallurgical Transactions B, vol. 13B, 1982, pp. 153-163.

91. GOROG, J.P., BRIMACOMBE, J.K. and ADAMS, T.N., Radiative heat transfer

in rotary kilns, Metallurgical Transactions B, vol.12, 1981 pp. 55-70.

92. VAN DEVENTER, J.S.J. and CAMBY, B.S., Kinetics of thermal regeneration of activated carbon in a fluidized bed, Themochimica Acta vol. 136, 1988, pp. 170-189.

93. INCROPERA, F.P. and DE WITT, D.P., Fundamentals of heat transfer, Second edition, John Wiley and Sons, Ney York, 1985, pp. 579-580.

94. HOTTEL, H. and SAROFIRM, A., Radiative Transfer, McGraw-Hill Book Company, New York, 1967, pp. 199-296.

95. HADVIG, S., Gas Emissivity and absorptivity: A thermodynamic study, Journal of the Institute of Fuel, April 1970, pp. 129-135.

96. VAILLANT, A., PhD Thesis, Faculty of Mechanical Engineering, Columbia University, 1965.

97. ECKERT, E.R.G., TIEN, C.L. and EDWARDS, D.K., Radiation, in: Handbook of Heat Transfer Fundamentals, Second Edition, Rohsenow, W.M., Hartnett, J.P and Ganić, E.N., (editors), McGraw-Hill Book Company, New York, 1985, pp. 14.1-14.127

98. TOULOUKIAN, Y.S., POWELL, R.W. and KLEMENS, P.G., Thermophysical Properties of Matter: Thermal Conductivity, Non-metallic Solids, New York: IFI/Plenum Data Corporation, 1970.

99. TSOTSAS, E. and MARTIN, H., Thermal conductivity of packed beds: A review, Chem. Engng. Prog, vol. 22, no. 1, 1987, pp. 19-37.

100. FINE, D. and GLASSER, B., The Measurement and Modelling of the Effective

Thermal Conductivity of a Packed Bed of Activated Carbon, Undergraduate project, University of the Witwatersrand, Johannesburg, 1989.

101. Laubitz, M.J., Thermal conductivity of powders, Canadian Journal of Physics, vol. 37, 1959, pp. 798-807.

102. HIMMELBLAU, D.M., Basic Principles and Calculation in Chemical Engineering, Prentice-Hall Inc., New Jersey, 1962, pp. 493-498.

103. PERRY, R.H. and GREEN, D., (Editors), Perry's Chemical Engineers' Handbook, Sixth Edition, McGraw-Hill, New York, 1988.

104. VAN DER MERWE, P.F., Fundamentals of the elution of gold cyanide on activated carbon, PhD-Thesis, University of Stellenbosch, 1989.

105. VAN DER WALT, T.J. and VAN DEVENTER, J.S.J., Non-ideal behaviour in counter-current in-pulp adsorption cascades, Min. Engng, vol. 5, Nos. 10-12, pp. 1401-1420.

APPENDIX A

THE FINITE-DIFFERENCE HEAT EQUATION

The determination of the temperature distribution numerically dictates that an appropriate conservation equation should be written for each of the points in the nodal network, representing the solids bed. The resulting set of equations may then be simultaneously solved for the temperature at each node. For any interior node of a two-dimensional system with no heat generation and a uniform thermal conductivity, the exact form of the energy conservation requirement is given by the heat equation, equation A-1:

$$\frac{1}{\alpha}\frac{\partial T}{\partial t} = \frac{\partial^2 T}{\partial x^2} + \frac{\partial^2 T}{\partial y^2} \qquad \textbf{(A-1)}$$

However, if the system is characterized in terms of a nodal network, it is necessary to work with a finite-difference form of equation A-1. To obtain the finite-difference form of this equation, the central-difference approximations to the spatial derivatives will be used, hence the value of the second derivative at the m, n nodal point may be approximated as:

$$\frac{\partial^2 T}{\partial x^2}\Big|_{m,n} \approx \frac{\frac{\partial T}{\partial x}\Big|_{m+\frac{1}{2},n} - \frac{\partial T}{\partial x}\Big|_{m-\frac{1}{2},n}}{\Delta x} \qquad \textbf{(A-2)}$$

The temperature gradients may in turn be expressed as a function of the nodal

temperatures. That is:

$$\frac{\partial T}{\partial x}\Big|_{m+\frac{1}{2},n} \approx \frac{T_{m+1,n} - T_{m,n}}{\Delta x} \qquad \text{(A-3)}$$

and:

$$\frac{\partial T}{\partial x}\Big|_{m-\frac{1}{2},n} \approx \frac{T_{m,n} - T_{m-1,n}}{\Delta x} \qquad \text{(A-4)}$$

Substituting equations A-3 and A-4 into A-2, we obtain:

$$\frac{\partial^2 T}{\partial x^2}\Big|_{m,n} \approx \frac{T_{m,n+1} + T_{m,n-1} - 2T_{m,n}}{(\Delta x)^2} \qquad \text{(A-5)}$$

Proceeding in a similar fashion, it is readily shown that:

$$\frac{\partial^2 T}{\partial y^2}\Big|_{m,n} \approx \frac{T_{m,n+1} + T_{m,n-1} - 2T_{m,n}}{(\Delta y)^2} \qquad \text{(A-6)}$$

The problem must also be discretized in time. The integer, p, is introduced for this purpose, where:

$$t = p\Delta t \qquad \text{(A-7)}$$

and the finite-difference approximation to the time derivative in equation A-1 is expressed as:

$$\frac{\partial T}{\partial t}\Big|_{m,n} = \frac{T^{p}_{m,n} - T_{m,n}}{\Delta t} \qquad \text{(A-8)}$$

The superscript, p, is used to denote the time dependence of the temperature, T, and the time derivative is expressed in terms of the difference in temperatures associated with the new (T^p) and previous (T) times. Hence calculations must be performed at successive times separated by the interval, Δt.

The finite difference equation for the interior nodes and the nodes on the solids may be obtained by applying the conservation of energy to a control volume about the nodal region. During the development of these equations it is assumed that all the heat flows into the node. Such a condition is impossible, but if the rate equations are expressed in a manner consistent with this assumption, the correct form of the finite-difference equation is obtained.

Consider applying equation A-1 to a control volume about the interior node m,n of figure A.1. Then:

$$\begin{aligned} \varrho Cp V\frac{(T^{p}_{m,n} - T_{m,n})}{\Delta t} &= T_{m,n} \\ &+ \lambda\left(\frac{\Delta y}{2} + \frac{b\Delta y}{2}\right)\frac{(T_{m-1,n} - T_{m,n})}{\Delta x} \\ &+ \lambda\left(\frac{a\Delta x}{2} + \frac{\Delta x}{2}\right)\frac{(T_{m,n-1} - T_{m,n})}{\Delta y} \\ &\lambda\left(\frac{a\Delta x}{2} + \frac{\Delta x}{2}\right)\frac{(T_{2} - T_{m,n})}{b\Delta y} \\ &+ \lambda\left(\frac{b\Delta y}{2} + \frac{\Delta y}{2}\right)\frac{(T_{1} - T_{m,n})}{a\Delta x} \end{aligned} \qquad \text{(A-9)}$$

where:

$$T_2 = T_{m+1,n}$$
$$T_1 = T_{m,n+1} \qquad \text{(A-10)}$$

and λ is the thermal conductivity with units [W/m.K]

The temperatures $T_{m+1,n}$ and $T_{m,n+1}$ are again equal to the temperature of the wall, T_w, and $\Delta x = \Delta y$.

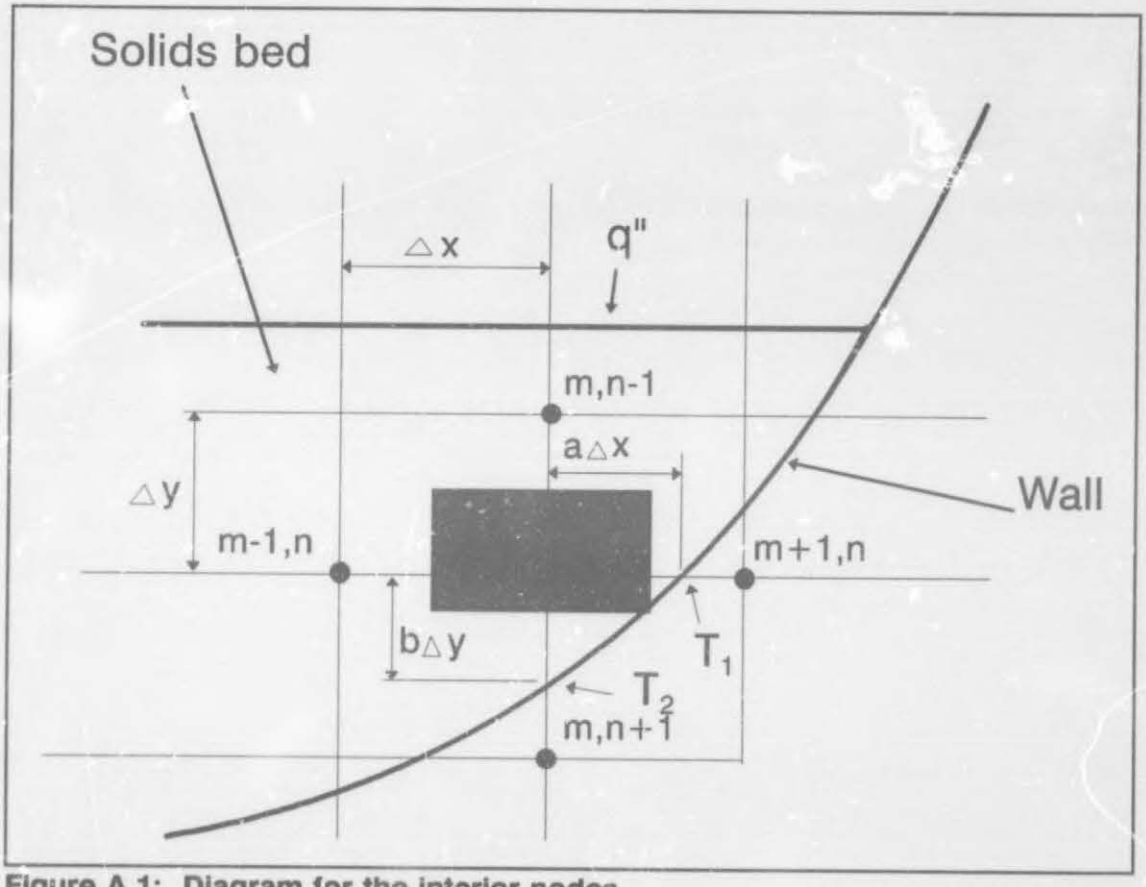

Figure A.1: Diagram for the interior nodes.

Solving for T^p in equation A-9 gives the required finite difference equation of the interior nodes, hence:

$$T^{p}_{m,n} = T_{m,n} + \frac{\alpha \Delta t}{V}\left[\left(\frac{a+1}{2}\right)(T_{m,n-1} - T_{m,n}) + \left(\frac{b+1}{2}\right)(T_{m-1,n} - T_{m,n})\right] + \frac{\alpha \Delta t}{V}\left[\left(\frac{a+1}{2a}\right)(T_{m+1,n} - T_{m,n}) + \left(\frac{a+1}{2b}\right)(T_{m,n+1} - T_{m,n})\right]$$

where:

$$V = \frac{\Delta x^2}{4}[1 + a + b + ab]$$

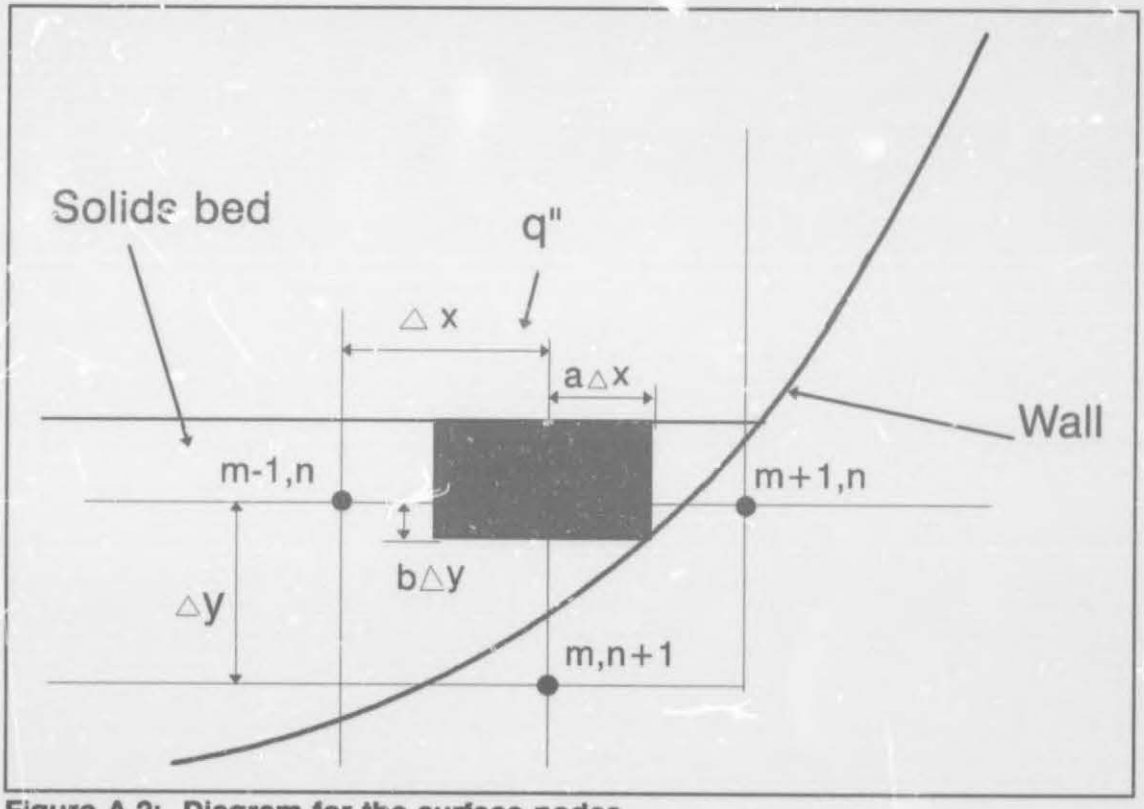

Figure A.2: Diagram for the surface nodes.

Similarly,from figure A.2, the finite-difference equation for the nodes corresponding to the solids surface:

$$T^{p}_{m,n} = T_{m,n} + \frac{\alpha \Delta t}{V}\left[\left(\frac{b}{2}\right)(T_{m-1,n} - T_{m,n}) + \left(\frac{b}{2a}\right)(T_{m+1,n} - T_{m,n})\right] + \frac{\alpha \Delta t}{V}\left[\left(\frac{a+1}{2b}\right)(T_{m,n+1} - T_{m,n}) + \frac{q''}{\lambda . \Delta L}\right] \quad \text{(A-13)}$$

where:

$$V = \frac{\Delta x^2}{4}(b + ab) \quad \text{(A-14)}$$

The explicit method of solution will be used, i.e. the new temperatures (T^p) are evaluated using the values of the previous temperatures (T).

An undesirable feature of the explicit method is that it is not unconditionally stable. The solution may be characterized by numerically induced oscillations, which are physically impossible. The oscillations may become unstable, causing the solution to diverge from the actual steady-state conditions. To prevent such erroneous results, the prescribed value of Δt must be maintained below a certain limit, which depends on Δx, Δy and other physical parameters of the system. The stability criteria for equations A-10 and A-12 are such that:

$$\sum \textit{ of the coefficients of } T_{m,n} \geq 0 \quad \text{(A-15)}$$

For the nodal structure of figure 4.1, chapter 4, Δx and Δy at the boundaries of the nodal network, i.e. near the kiln wall, are not equal to Δx and Δy at the interior nodes.

This would mean that smallest Δx and Δy should be used to calculate Δt to satisfy the stability criteria, equation A-14. In the simulation program this is done in procedure "Stability" (see Appendix E and F).

APPENDIX B

EQUILIBRIUM BOUDOUARD CONSTANT

The Boudouard reaction can be represented by[50,56]:

$$C + CO_2 \leftrightarrow 2CO \qquad \Delta H_r = 172 \text{ kJ/mol} \qquad \textbf{(B-1)}$$

From the literature[102,103] the following are postulated at 25°C:

Species	Cp-Value	$\Delta H_r°$	$\Delta G_f°$
C*	4.17 + 1.02E-3T - 2.1E5/T^2	0	0
CO	6.79 + 0.98E-3T - 0.11E5/T^2	-26.416	-32.808
CO_2	10.55 + 2.16E-3T - 2.04E5/T^2	-94.052	-94.26

At 25°C the free energy of formation of CO can be calculated as follows:

$$\begin{aligned} \Delta G^\circ &= \Sigma(\nu_i G_i^\circ) \\ &= 2*(-32.808) - (-94.26) \\ &= 28.644 \text{ kcal/mol} \end{aligned} \qquad \textbf{(B-2)}$$

and

$$\ln(K_p) = \frac{-\Delta G^\circ}{RT} \qquad \textbf{(B-3)}$$

Thus, with R = 1.987 kcal/mol at 25°C:

$$\therefore \ln(K_p) = \frac{-28.644 * 1000}{1.987 * 298} \qquad \text{(B-4)}$$

$$= -48.37$$

The heat of formation of CO at 25°C:

$$\begin{aligned} \Delta H^{\circ} &= \Sigma(\nu_i H_i^{\circ}) \\ &= 2*(-26.416) - (-94.052) \\ &= 41.22\ kcal/mol \end{aligned} \qquad \text{(B-5)}$$

At any other temperature,T:

$$\Delta H = C_0 + \int_0^T (\Sigma_i \nu_i Cp_i)\, dT \qquad \text{(B-6)}$$

where C_0 is the integration constant.

Thus:

$$\begin{aligned}\Delta H &= C_0 + \int_0^T 2(6.79 + 0.98E\text{-}3T - \frac{0.11E5}{T^2})dT \\ &\quad - \int_0^T (10.55 + 2.16E\text{-}3T - \frac{2.04E5}{T^2})dT \\ &\quad - \int_0^T (4.1 + 2.02E\text{-}3T - \frac{2.1E5}{T^2})dT \\ &= C_0 + \int_0^T (-1.07 - 0.00222T + \frac{392000}{T^2})dT \\ &= C_0 + -1.07T - 0.00111T^2 - \frac{392000}{T}\end{aligned} \qquad \text{(B-7)}$$

Substituting B-5, with T = 25°C, in equation B-7, the integration constant, C_0, can be calculated.

$$\begin{aligned}41220 &= C_0 - 1.07T - 0.00111T^2 - \frac{392000}{T} \\ 41220 &= C_0 - 1.07*298 - 0.00111*298^2 - \frac{392000}{298} \\ \therefore C_0 &= 42952.9 \quad [cal/mol]\end{aligned} \qquad \text{(B-8)}$$

Substituting B-8 in B-7, the heat of formation at any temperature, T, is:

$$\Delta H = 42952.9 - 1.07T - 0.00111T^2 - \frac{392000}{T} \quad [cal/mol] \qquad \text{(B-9)}$$

and:

$$\ln(K_p) = C_1 + \frac{1}{R}\int_0^T \frac{\Delta H}{T^2}dT \qquad \text{(B-10)}$$

Thus:

$$Ln(K_p) = C_1 + \frac{1}{R}\int_0^T \left(\frac{42952.9}{T^2} - \frac{1.07}{T} - 0.00111 - \frac{392000}{T^3} \right) dT$$
$$= C_1 + \frac{1}{R}\left[-\frac{42952.9}{T} - 1.07Ln(T) - 0.00111T + \frac{196000}{T^2} \right] \quad \text{(B-11)}$$

Substituting equation B-4 in B-11 the integration constant, C_1, is obtained:

$$-48.374 = C_1 + \frac{1}{1.987}\left[-\frac{42952.9}{298} - 1.07\ln(298) - 0.00111 * 298 - \frac{196000}{298^2} \right]$$

$$\therefore C_1 = 28.5 \quad \text{(B-12)}$$

Therefore,at any temperature,T:

$$K_p = \exp\left[28.5 + \frac{1}{R}\left(-\frac{42952.9}{T} - 1.07Ln(T) - 0.00111T - \frac{196000}{T^2} \right) \right] \quad \text{(B-13)}$$

This relationship is depicted in figure B1.

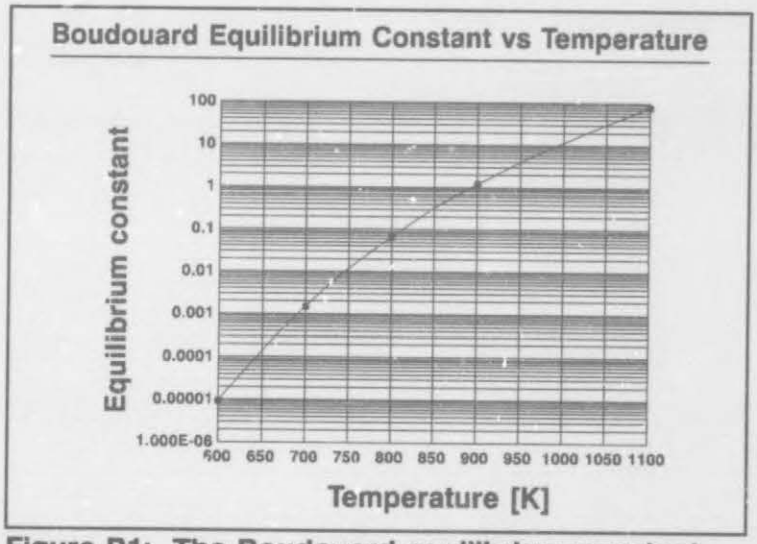

Figure B1: The Boudouard equilibrium constant.

APPENDIX C

CALCULATION OF GAS PROPERTIES

It is not the objective of this study to deal with the various features leading to and arising from the calculation of gas properties. However, this calculation needs some attention, and only a brief discussion will be given. This approach might lead to situations where the reader will find it difficult to understand the equations. In these cases the reader should refer to the original papers (see References).

C.1 THEORETICAL BACKGROUND

Molecular gases absorb a photon (or a quantum) of radiative energy during a transition from a lower to a higher energy level and emit it during the reverse process. In general, the energy levels are electronic, vibrational and rotational in nature[97]. The frequencies of the absorption or emission occur in the ultraviolet and visible range for transitions between electronic levels. These frequencies could also occur in the far infra-red range for transitions between rotational energy levels or closely grouped in narrow wavelength regions in the infra-red, referred to as bands, for the simultaneous transitions in the vibrational and rotational energy levels[93]. At rotary kiln operating temperatures, the transitions of major concern are the simultaneous vibrational and rotational ones[97].

The vibrations and/or rotations must have an oscillating electric dipole to be radiatively active. Monatomic gases (like He, Ne, etc.) and symmetric diatomic gases (like H_2, N_2, etc.) are not radiatively active at ordinary temperatures and pressures[97]. These gases are essentially transparent to thermal radiation[93].

At very high pressures, a pressure-induced dipole becomes evident[97], but is of no concern during normal rotary kiln operation. Vibrations in asymmetrical diatomic gases (like CO_2, H_2O, NO,CO,etc.) or ions, give rise to radiative absorption and emission. For these gases matters are complicated by the fact that, unlike radiation from a solid which is distributed continuously, with wavelength, gaseous radiation is concentrated in specific wavelength intervals, called bands, as stated above. Moreover, gaseous radiation is not a surface phenomenon, but a volumetric phenomenon instead.

C.2 ECKERT ET AL.[97] PROCEDURE FOR CALCULATING GAS PROPERTIES

The crux of Eckert's procedure lies in the division of the spectrum into spectral blocks, dictated by the gas bands, i.e. the wavelength intervals where absorption and/or emission occur. First, the radiating species are identified and the temperature, pressure and path length of interest fixed. Then, for each gas species, the band absorption values and band transmissivities are found. From the corresponding band absorption and band transmissivity values, each bandwidth is found and located. In the spectral blocks where bands overlap, the block transmissivity is taken as the product. The final result is a non-overlapping set of spectral blocks in each of which gas transmissivity is known. The emissivity and absorptivity are calculated from the known transmissivity.

C.3 EQUATIONS FOR CALCULATING THE GAS PROPERTIES

The procedure starts with finding, α_k, β_k and ω_{bk}. The following rather complex equation gives the required α_k, ω_{bk} and β_k parameters versus temperature based on experimental correlation parameters α_{0k}, β_{0k} and ω_{b0k}, and spectroscopic assignments of vibrational quantum number differences $\pm\delta_j$ and associated wave numbers. (The parameters ω_j, α_{0k}, β_{0k}, ω_{b0k} and $\pm\delta_j$ are available in the literature[97]):

$$\alpha_k(T) = \alpha_{k0}\frac{[1-\exp(-\Sigma\pm\delta\mu_j)]\Psi(T)}{[1-\exp(-\Sigma\pm\delta\mu_{0j})]\Psi(T_0)} \qquad \text{(C-1)}$$

$$\beta_k(T) = \beta_{k0}\left(\frac{T}{T_0}\right)^{-\frac{1}{2}}\frac{\Phi(T)}{\Phi(T_0)} \qquad \text{(C-2)}$$

$$\omega_{bk}(T) = \omega_{bok}\left(\frac{T}{T_0}\right)^{\frac{1}{2}} \qquad \text{(C-3)}$$

with:

$$\Psi(T) = \frac{\prod_{j=1}^{m}\sum_{\upsilon_j=\upsilon_{0j}}^{\infty}\frac{(\upsilon_j+g_j+\delta_j-1)!}{(g_j-1)!\upsilon_j!}\exp^{-u_j\upsilon_j}}{\prod_{j=1}^{m}\sum_{\upsilon_j=0}^{\infty}\frac{(\upsilon_j+g_j-1)!}{(g_j-1)!\upsilon_j!}\exp^{-u_j\upsilon_j}} \qquad \text{(C-4)}$$

and:

$$\Phi(T) = \frac{\left[\prod_{j=1}^{m}\sum_{\upsilon_j=\upsilon_{0j}}^{\infty}\left(\frac{(\upsilon_j+g_j+\delta_j-1)!}{(g_j-1)!\upsilon_j!}\exp^{-u_j\upsilon_j}\right)^{\frac{1}{2}}\right]^2}{\prod_{j=1}^{m}\sum_{\upsilon_j=0}^{\infty}\frac{(\upsilon_j+g_j+\delta_j-1)!}{(g_j-1)!\upsilon_j!}\exp^{-u_j\upsilon_j}} \qquad \text{(C-5)}$$

where:

$$u_j = \frac{hc\omega_j}{kT}, \qquad u_{0j} = \frac{hc\omega_j}{kT_0} \qquad \text{(C-6)}$$

and T_0 = 100 K.

The average mean beamlength, L_m, is the parameter accounting for the geometrical shape of the gas volume. Based on the procedure as outlined by Hottel and

Sarofirm[94], Gorog et al.[91] determined the average mean beamlength as follows:

$$L_m = 0.95D\left(1 - \frac{F}{D}\right) \qquad \text{(C-7)}$$

Then, knowing ρ_a, L_m, P and χ_a, the values of P_e, n_k and τ_{Hk} are calculated according to equations C-8, C-9 and C-10:

$$P_e = \left(\frac{P}{P_0}\right)^n \left[1 + \chi_a(b-1)\right]^n \qquad \text{(C-8)}$$

$$\eta_k = \beta_k P_e \qquad \text{(C-9)}$$

$$t_{Hk} = \frac{\alpha_k \rho_k L_m}{\omega_{bk}} \qquad \text{(C-10)}$$

Having calculated n_k and t_{Hk}, the region of the four-region expression is identified and the sought after ω^*_{ak} and τ_g are found. The four-region expression is:

- Linear region ($t_{Hk} \leq 1$ and $t_{Hk} \leq n_k$) with:

$$\omega^*_{ak} = t_{Hk} \qquad \text{(C-11)}$$

$$\tau_{gk} = 0.9 \qquad \text{(C-12)}$$

- Square-root region ($n_k \leq 1$ and $n_k \leq t_{HK} \leq 1/n_k$) with:

$$\omega^{*}_{ak} = (4\eta_k t_{Hk})^{1/2} - \eta_k \qquad \text{(C-13)}$$

$$\tau_{gk} = 0.5\left(1 + \frac{\eta_k}{\omega^{*}_{ak}}\right) \qquad \text{(C-14)}$$

- Log-root region ($\eta_k \leq 1$ and $t_{Hk} > 1/\eta_k$) with:

$$\omega_{ak}^{*} = \ln(t_{Hk}\eta_k) + 2 - \eta_k \qquad \text{(C-15)}$$

$$\tau_{gk} = \frac{1}{\omega^{*}_{ak}} \quad (\textit{but less than } 0.9) \qquad \text{(C-16)}$$

- Log region ($\eta_k > 1$ and $t_{Hk} > 1$) with:

$$\omega^{*}_{ak} = \ln(t_{Hk}) + 1 \qquad \text{(C-17)}$$

$$\tau_{gk} = \frac{1}{\omega^{*}_{ak}} \quad (\textit{but less than } 0.9) \qquad \text{(C-18)}$$

The quantity τ_{gk} is a spectral block transmissivity to be employed in the following equations to calculate the emissivity and the absorptivity. Having calculated τ_{gk} in each spectral block, the bandwidths and band limits should be calculated. Thus the

assigned bandwidths are then:

$$\Delta\omega_k = \frac{\omega_{gk}}{1-\tau_{gk}} \qquad \text{(C-19)}$$

and the assigned band limits are:

$$\omega_{uk} = \omega_{0k} + \frac{\Delta\omega_k}{2} \qquad \text{(C-20)}$$

$$\omega_{lk} = \omega_{uk} - \Delta\omega_k \qquad \text{(C-21)}$$

The total emissivity of a length, L_m, of absorbing gas with partial pressure, P_a, at equivalent broadening pressure, P_e, and at temperature, T_g, is defined as:

$$\epsilon_g(T_g, P_a L_m, P_e) = \sum_k (1-\tau_{gk}) \left[f\left(\frac{T_g}{\omega_{lk}}\right) - f\left(\frac{T_g}{\omega_{uk}}\right) \right] \qquad \text{(C-22)}$$

Similarly, the total absorptivity for radiation from a wall at T_w is defined as:

$$\alpha_g(T_w, T_g, P_a L_m, P_e) = \sum_k (1-\tau_{gk}) \left[f\left(\frac{T_w}{\omega_{lk}}\right) - f\left(\frac{T_w}{\omega_{uk}}\right) \right] \qquad \text{(C-23)}$$

with the fractional function f:

The term $i_{b,\,0\to\infty}$, the intensity of radiation emitted by a blackbody at a temperature, T, in the wavelength range from 0 to ∞ is obtained by integrating over all wavelengths.

$$f\left(\frac{T}{\omega}\right) = \frac{1}{\sigma T^4}\int_{\omega}^{\infty} e_{b\omega}(T)\,d\omega = \frac{i_{b,0\to\lambda}/C_5 T^4}{i_{b,0\to\infty}/C_5 T^4} \qquad \text{(C-24)}$$

The result is:

$$i_b = \int_0^{\infty} i_{\lambda,b}\,d\lambda = \frac{\sigma}{\pi} T^4 \qquad \text{(C-25)}$$

Substituting C-25 in C-24 one obtains:

$$f\left(\frac{T}{\omega}\right) = \frac{i_{b,0\to\lambda}/C_5 T^4}{\frac{\sigma}{\pi C_5]}} \qquad \text{(C-26)}$$

The relationship between the parameters $\lambda T/C_2$ and $i_{b,0\to\lambda}/C_5T^4$ and the values of C_5 and is available in the literature[97]. Since $\lambda T = T/\omega$, the value for the fractional function, as defined in equation C-24, can be calculated for each spectral block,k. Thus, having calculated the block transmissivity and the fractional functions for the lower and upper limit of the wavenumber, the emissivity and absorptivity can be calculated according to equations C-24 and C-25 respectively.

Eckert's procedure has been used in the simulation program for calculating the gas properties. This is explained in Appendix E and Appendix F,section 2. The reader can also refer to the Turbo Pascal Unit "EmiesOne.TPU" in the listing of the computer program (see Appendix F, Section F.2). Simulation runs show the calculated gas properties using the computer program within an accuracy of 0.27 % from the

published[97] data.

APPENDIX D

Table D.1: Adsortption data.

Sample	Mass of Carbon [g]	C_0 [ppm]	C_e [ppm]	q_e [g Au/kg C]
A1	0.5064	16.00	8.29	15.23
A2	0.2185	13.70	13.85	16.20
B1	1.0012	21.00	6.00	15.00
B2	0.8001	21.00	8.00	16.20
B3	0.4998	21.80	13.00	17.60
C1	1.0000	21.38	5.80	15.58
C2	0.7525	21.60	8.38	17.58
C3	0.5000	23.40	13.62	19.56
D1	1.0000	21.40	6.36	15.04
D2	0.7993	21.20	8.50	15.89
D3	0.4999	21.80	13.05	17.50

Sample	Mass of Carbon [g]	C_0 [ppm]	C_e [ppm]	q_e [g Au/kg C]
E1	1.0049	19.00	5.70	13.24
E2	0.8006	18.75	7.10	14.55
E3	0.5048	19.00	11.00	15.85
F1	1.0016	19.00	6.96	12.02
F2	0.7047	19.40	9.40	14.19
F3	0.5026	20.00	12.70	14.52

Table D.2: Freundlich parameters.

Sample	A	n
A	9.21	0.20
B	10.3	0.21
C	11.4	0.21
D	10.12	0.21
E	8.59	0.25
F	6.92	0.30

The relationship between the parameters A and n is shown in figure D.1.

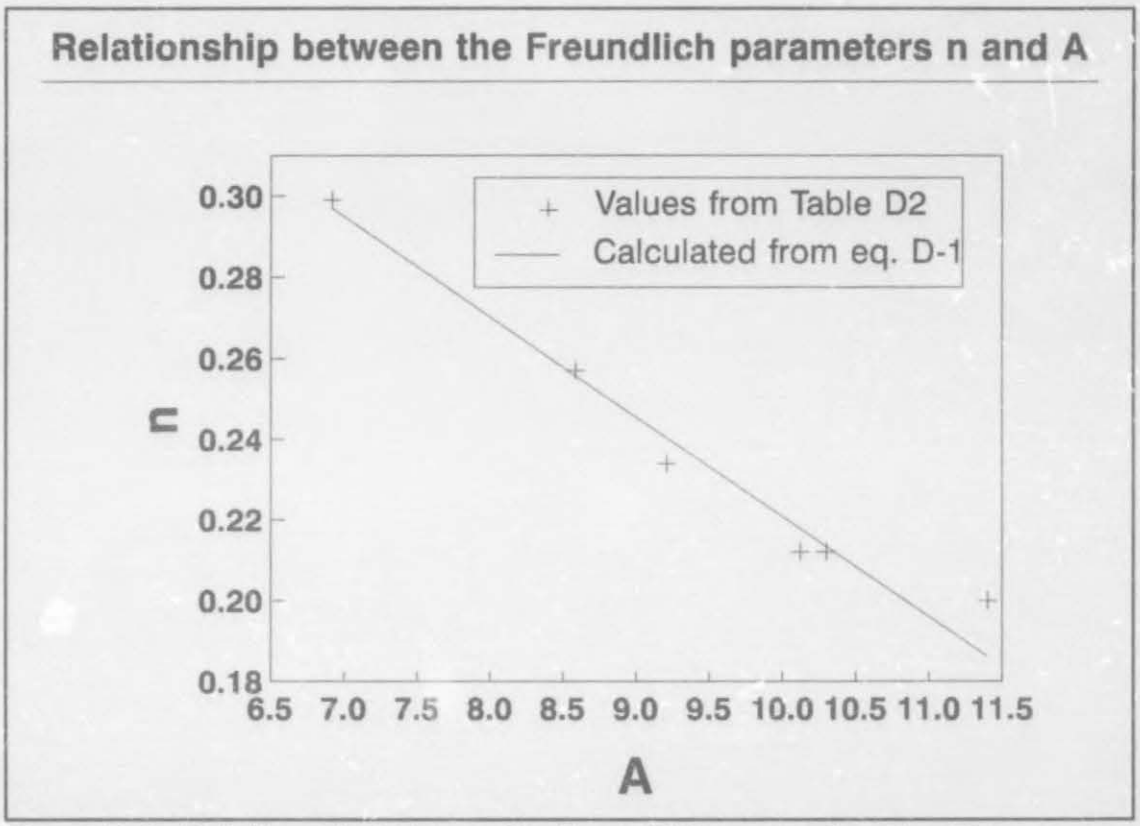

Figure D.1: Relationship between the Freundlich parameters A and n.

It is clear that there is an inversely proportional relationship between n and A respectively. The functional relationship is:

$$n = -0.0247 * A + 0.4678 \qquad \text{(D-1)}$$

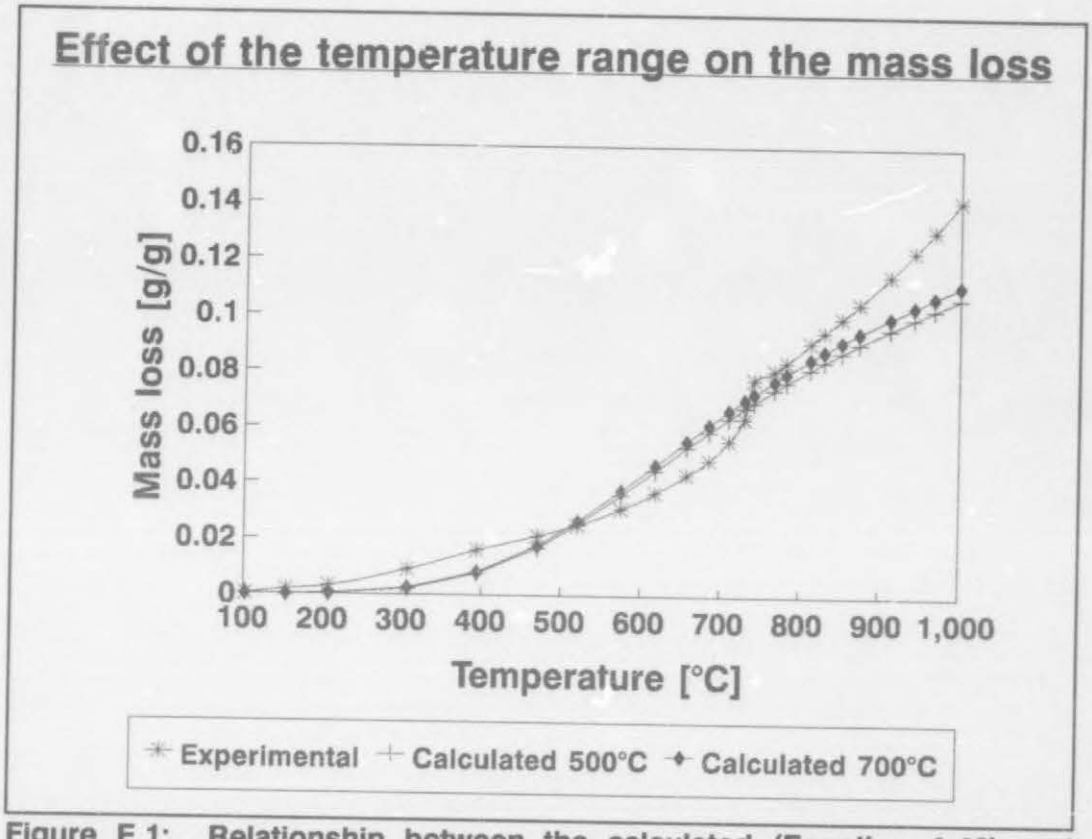

Figure E.1: Relationship between the calculated (Equation 4-46) and experimental mass loss.

APPENDIX F

FLOW DIAGRAMS

The detailed computational procedures in chapter 5, figure 5.2 for calculating the mass loss of regenerated carbon are discussed in this section. It is not the intention to explain the computational skills or methods employed in the procedures to calculate the mass loss. The reader is referred to the program listing in Appendix G to investigate these methods. The names of the procedures will be used as they are employed in the computer program and will be printed in "inverted commas". The calculation procedures will be discussed with the aid of appropriate flow diagrams.

F.1 PROCEDURE "MAININPUT"

The flow diagram for the "MainInput" procedure (see, Chapter 5, Section 5.3.2, Figure 5.4 and the program listing in Appendix G, Section G.1) is depicted in figure F.1.

Figure F.1 indicates the calculation steps when option 2 of figure 5.1 is selected to calculate the

Figure F.1: Flow diagram to calculate the intial values.

temperature profiles and the mass loss of the regenerated carbon (see Chapter 5, Section 5.3). The calculation begins with the initiation of all the initial values in procedure "Initial". These are the values stored in the data files under the kiln design, operating and carbon data parameters menu, option 1, of the main menu (see Figure 5.1, Chapter 5, Section 5.3.2). These values are:

- The pressure of the gas;
- If external gas is added to the freeboard gas,the fraction of the steam, carbon dioxide, carbon monoxide, hydrogen and nitrogen isrequested;
- The equilibrium composition of the freeboard gas;
- The outside kiln wall temperature;
- Temperature of the solids;
- The equilibrium temperature of the gas;
- Inside kiln wall temperature;
- Mass flow rate of the solids;
- Mass flow rate of the external gas if external gas is used;
- The inclination of the kiln to the horizontal;
- The spedd of rotation;
- Weight per cent moisture in the carbon feed;
- Diameter of the kiln;
- Length of the kiln;
- Fill height of the kiln (see Figure 4.4, Chapter 4, Section 4.3.1);
- The bulk density.

These values are used to calculate the other initial parameters.

The bed of solids is divided into a number of nodes in procedure "NodalLength".

In procedure "Stability", the stability criterium, equation A-15 is used to calculate the maximum time interval. This time interval represents the time that the solids spend in one length increment.

The residence time of the solids in the kiln is calculated in procedure "ResidenceT" from the appropriate equation. This empirical equation is usually specific for a rotary kiln. The equation used for the kiln in this study was derived from the number of screws of the scroll-shaped flights and the length of the kiln. Hence:

$$r_t = \frac{12.2046}{rot} + \frac{L}{5} \qquad \text{(F-1)}$$

In procedure "NumberZones", the number of length increments into which the kiln is divided is calculated as the residence time (Equation F-1) divided by the maximum time that the solids spend in a section of the kiln (Equation A-15) .

The remaining initial values are calculated in procedure "InitialThree". These values are:

- The average mean beam length, L_m from equation C-7;
- The view factors, F_{ww}, F_{ws} and F_{sw} from equation 4-10;
- The areas A_w, A_g and A_s;
- The frequency factor and the activation energy of the drying reaction are calculated with equations 6-11 and 6-12 respectively.

The equilibrium or feed gas composition is read from the appropriate data file in procedure "GasCompIn". The gas properties are then calculated with this composition in procedure "EmiesOne" (see Section E.2). The procedures that follow are the same as those described in chapter 5, section 5.3.2. The energy flow to the gas and the solids is calculated. The temperature changes of the solids and the gas are then calculated. The mass loss,as a result of the temperature of the solids in the first length increment is calculated. These values are the initial values for the next length increment.

F.2 PROCEDURE "EMIESONE"

The main flow diagram for the calculation of the gas properties, i.e. the emissivity, adsorptivity and the transmissivity, is depicted in figure F.2:

The gas properties are calculated in the Turbo Pascal Unit "EmiesOne.TPU" (see Appendix G.2). The procedure starts when the fraction of each gas species, i, (where i = 1, 2 and 3 for H_2O, CO_2 and CO respectively) in each length is used to calculate ("Calc.", see Section F.2.1) the gas transmissivity in each block in a set of nonoverlapping spectral blocks (see also Appendix C). From the spectral blocks, the gas properties are calculated in procedures "UpperBand" (see Section F.2.2) and "Fraction" (see Section F.2.3) respectively.

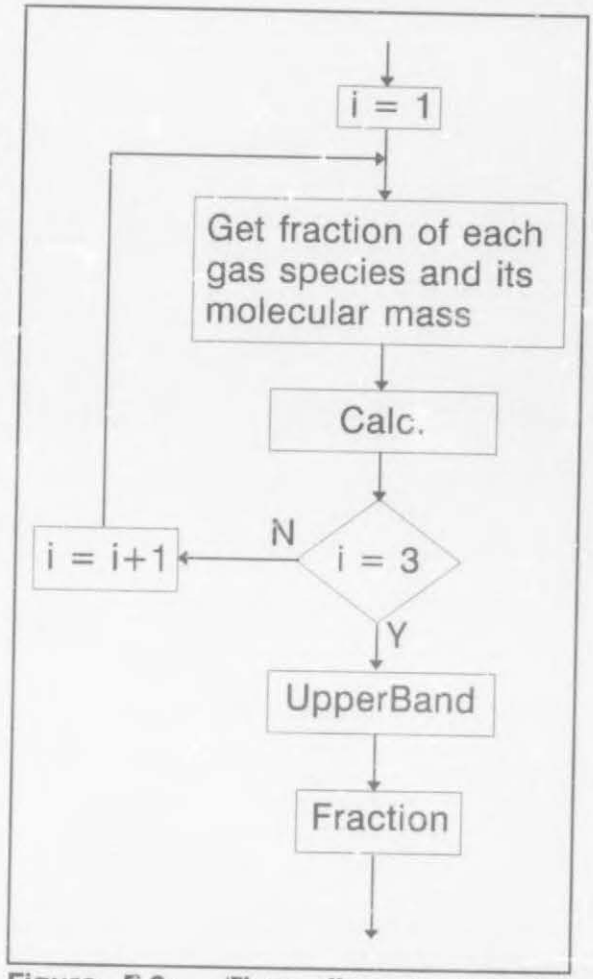

Figure F.2: Flow diagram for the calculation of the gas properties.

F.2.1 Procedure "Calc."

The flow diagram for the procedure "Calc. is depicted in figure F.3. The rationale behind this procedure is quite involved with regard to the actual programming of the mathematical equations.

The procedure starts when the quantum-mechanical data for each gas species are

read from the appropriate data file. The quantum-mechanical data are available in the literature[97] (see Appendix C, Section C.3). The number of spectral adsorption bands for each species is also identified from a data file.

The integrated intensity of the k^{th} band, α_k, is calculated according to equation C-1 followed by the calculation of the line-width to spacing parameter, β_k, and the bandwidth parameter, ω_{bk}, according to equations C-2 and C-3 respectively. The equivalent broadening pressure, P_e, as a function of the gas fraction is calculated with equation C-8. The associated line width to spacing parameter, η, for an arbitrary P_e is then calculated (see equation C-9). The optical depth, τ_{Hk}, as a function of the average mean beam length (see equation C-7) is calculated. In the next procedure the line-width to spacing parameter and the optical depth are used to locate and calculate the band width adsorptance (Equations C-11 to C-18) and the gas transmissivity of the spectral band.

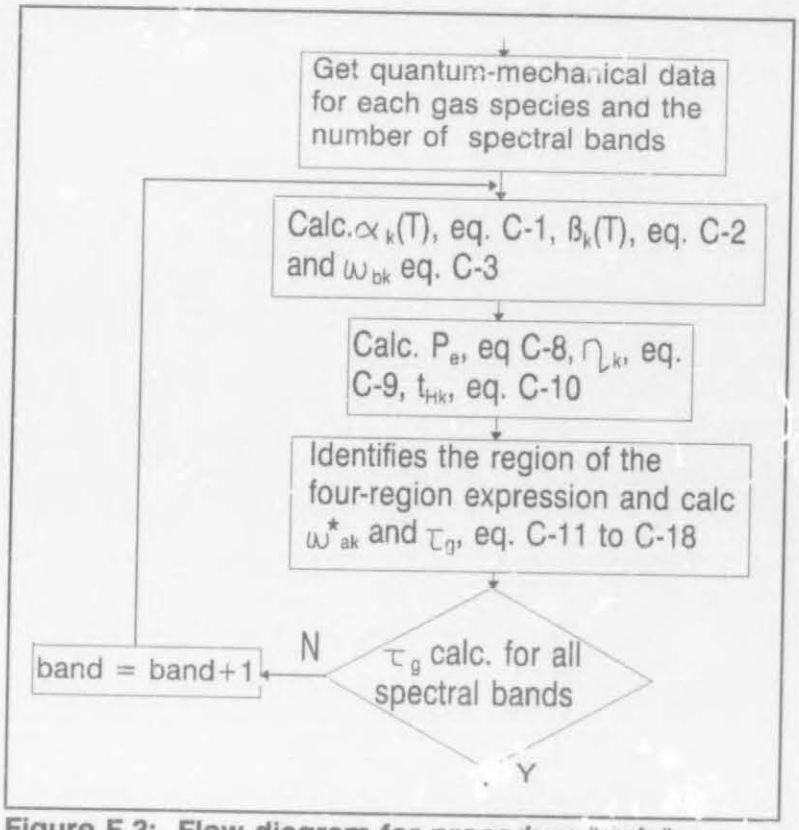

Figure F.3: Flow diagram for procedure "Calc".

This procedure is repeated for all the adsorption bands for each gas species as identified from the data files.

F.2.2 PROCEDURE "UPPERBAND"

In procedure "Calc. (see figure F.3) the band adsorption values and the band transmissivity of each gas species have been calculated. In procedure "UPPERBAND", the spectrum of adsorption bands is divided into a set of non-overlapping spectral blocks. Accordingly, the bandwidths are calculated using equation C-19 and the calculation of the band limits requires equations C-20 and C-21.

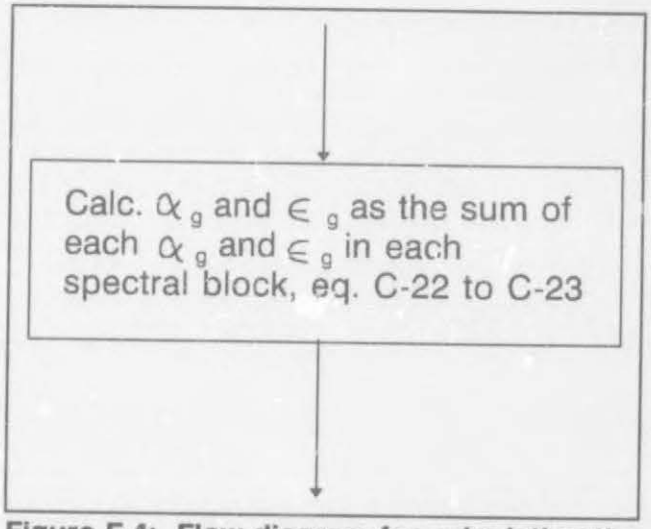

Figure F.4: Flow diagram for calculating the gas properties.

F.2.3 PROCEDURE "FRACTION"

In procedure "UPPERBAND the spectrum has been divided into a number of spectral blocks. The location of these blocks, as well as the band adsorption values and the band transmissivity of each gas species in these blocks have been calculated. The total adsorptivity and emissivity of the gas can now be calculated using equations C-22 and C-23 respectively (see Figure F.4). The total transmissivity is the average of the transmissivity in each of the spectral blocks.

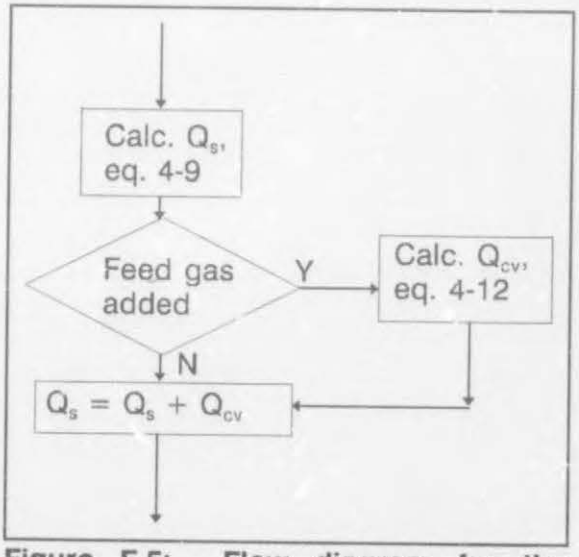

Figure F.5: Flow diagram for the calculation of the heat transfer rate to the solids.

F.3 HEAT TRANSFER RATES TO THE SOLIDS AND GAS

The procedure for calculating the heat transfer rate of the solids and the gas is explained in this section. The calculation procedures are very simple. Figures F.5 and F.6 are diagrams representing the calculation procedures. The heat transfer rate to the solids is calculated according to equation 4-9. If external feed gas is added, the convective heat transfer rate is calculated using equation 4-12. The total heat transfer rate to the solids is then the sum of the radiative heat transfer rate and the convective heat transfer rate (if applicable).

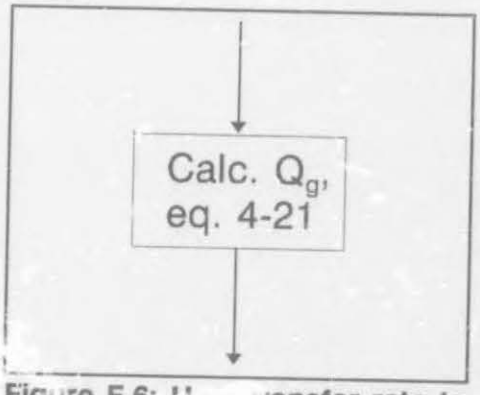

Figure F.6: ... transfer rate to the gas.

The radiative heat transfer rate to the gas is simply calculated using equation 4-21.

F.4 PROCEDURE "NodalTemp"

The flow diagram for procedure "NodalTemp" for the calculation of the temperature of the solids bed is depicted in figure F.7.

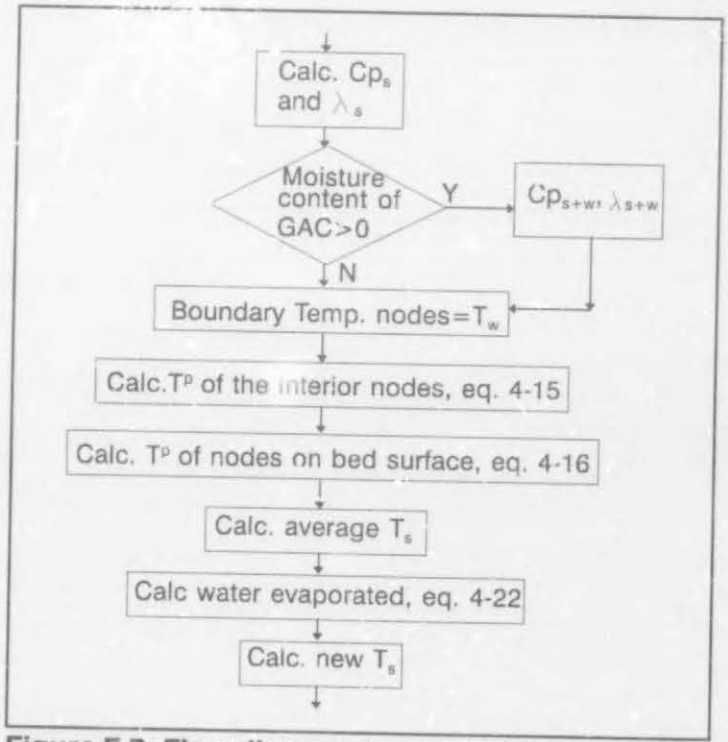

Figure F.7: Flow diagram for calculating the solids temperature.

The procedure starts with the calculation of the specific heat capacity and the thermal conductivity of the actitvated carbon and the associated moisture (if the carbon is still wet). The temperature of the boundary nodes (see Figure 4.1, Chapter 4, Section 4.2). The temperature distribution of the interior and boundary nodes is then calculated according to equations 4-15 and 4-16 respectively. The average temperature of the bed, T1, is then calculated on an area basis, i.e. the sum of the product of the temperature of a node and the area it represents, divided by the total area.. Having the temperature of the solids bed the amount of water evaporated can be calculated from equation 4-22. The decrease in the energy of the solids bed as a result of the water evaporation is then calculated as the product of mass of evaporated water and the latent heat of evaporation for water. A new average temperature, T2, for the solids is then calculated as the old average temperature, T1, less the temperature decrease equivalent to the energy loss. The temperature of each node is then decreased by a very small amount. The average temperature, T3, is then calculated on the area basis as described above. This routine is repeated until the average temperature, T3, equals T2.

F.5 PROCEDURE "TempChangeGas"

The fractions of the different gas species are identified. If external feed gas is used, the gas composition is that of the feed gas. If not, the gas composition is the composition of the freeboard gas. The specific heat capacities for the different gas species in the freeboard gas, i.e. nitrogen, hydrogen, steam, carbon monoxide and carbon dioxide are calculated from correlations in the literature[102,103]. The new gas temperature is then calculated from the heat transfer rate to the gas as indicated in figure F.8.

F.6 PROCEDURE "React"

The flow diagram for calculating the gas composition as a result of pyrolisis and the

gasification reaction is depicted in figure F.9. The calculation procedure is simple. It starts with the gas composition of the freeboard gas. The mass loss as a result of decomposition, pyrolysis and the gasification reaction is calculated according to equation 4-47. The new gas composition, as a result of the gasification reaction, is then calculated according to equations 4-32 to 4-38.

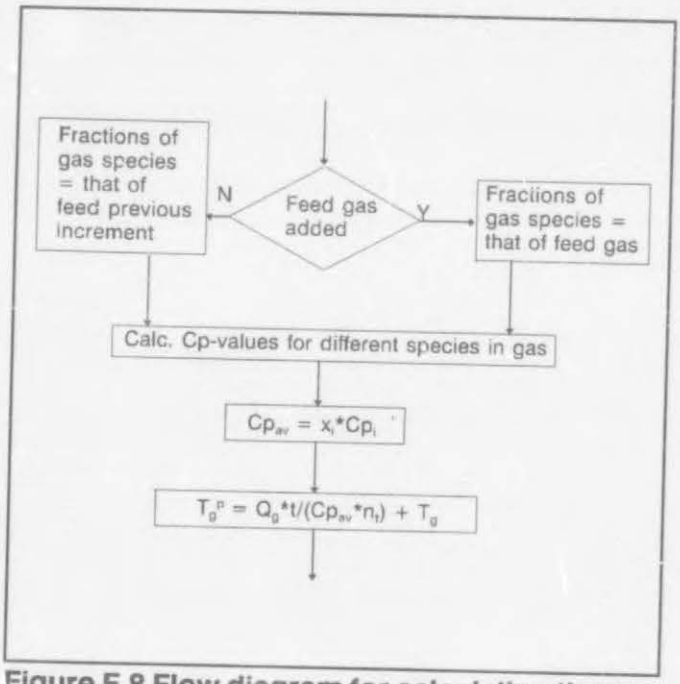

Figure F.8 Flow diagram for calculating the gas temperature.

F.7 PROCEDURE "ReactHeat"

In this procedure the decrease in the temperature of the solids bed is calculated. The heat of reaction is calculated from equation 4-40. A method, similarly to that employed to calculate the temperature of the solids bed as a result of the water evaporation, is used to calculated the new temperature of the solids bed as a result of the endothermic reaction (see Section F.4).

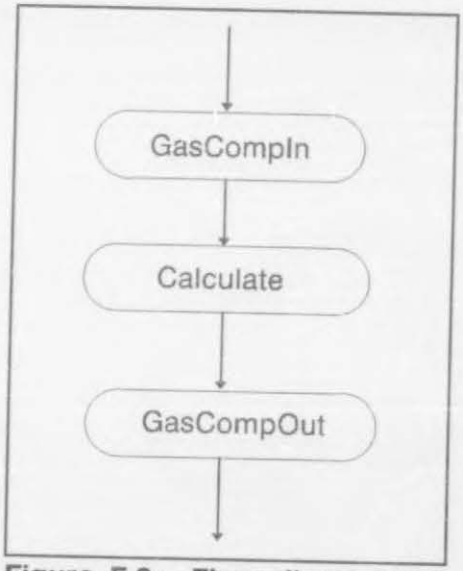

Figure F.9: Flow diagram for procedure "React."

APPENDIX G

SIMULATION PROGRAM

G.1 THE MAIN PROGRAM, "Regen.pas"

The main program code is listed in this section.

```
Program RegenNew;

{$N+,R+}

Uses Crt,Graph,Menu,EmiesOne,KilnOp,React,Grid,QSolid,QGas;

Const
  nr=5;
  Rgas=8.314;                {* [kJ/kMol.K]                *}
  Po=1;                      {* [N/m^2] or [atm.]          *}
  sigma=5.67E-8;

Type
  Posisie = Record
    Xp:integer;
```

```
    Yp:integer;
  End;
  MdpLoss = Record
    mx:real;
    my:real;
  End;

  RoosterThree = Array [1..2, 1..30] of integer;
  RoosterOne   = Array [1..20] of integer;
  RoosterTwo   = Array [0..8] of real;
  Rooster      = Array [1..20,1..20] of real;
  RoosterEen   = Array [1..20,1..20] of real;


Var

  Datas : MdpLoss;
  Data  : File of MdpLoss;       {* File for decomposition and pyrolysis  *}
  C_x,C_y    : File of integer;  {* File for number of grid points        *}
  XY_x,XY_y  : File of real;     {* File for nodal grid lengths           *}
  OutKiln    : File of real;     {* File for kiln construction parameters *}
  OutOp      : File of real;     {* File for kiln operational  parameters *}
  OutGComp   : File of real;     {* File for Feed gas composition         *}
  OutGAC     : File of real;     {* File for GAC parameters               *}
  OutSame    : File of real;     {* File for Freeboardgas composition     *}
  OutGEx     : File of real;     {* File for Feed gas composition         *}
  Pup        : File of char;     {* File for Pressure build up Yes/No     *}
  OutMP      : File of char;     {* File for Mixed or Plug flow of the gas*}
  OutGasYN   : File of char;     {* File for external gas flow Yes/No     *}

toetsone,move,XPix,YPix,opt,c,b,m,kan,lr,kx,ky,na,aa,wall,cnt  : integer;
```

```
  i,kp,MaxX,MaxY,j,kpp,GraphDriver,GraphMode,ErrorCode,cnt2,kere : integer;
  PosqoB22,PosqoB11                                              : integer;
  GradePerPix,LengtePerPix,Rtin e,Time,zone,DelL,Twi,Two,Stabiel : real;
  Area,L,lengte,slope,rot,Dp,P,X,Y,DelY,rad,Vgas,lgth,F,D,Alfaas : real;
  Ks,DencityS,AwExp,Aw,Ag,As,AlfaS,Fws,Fww,Fsw,Alfa,EmW,EmG,EmS  : real;
  Fox,Foy,TauGLm,TauG2Lm,TauG3Lm,TauAcLm,Lm,Row,Ros,Teta,Ts,Tg   : real;
  AlfaGAc,Qg,Qw,Qs,AlfaW,nH2O,nCO2,nCO,nN2,nt,MassS,MassG,exN2   : real;
  Wtper,CpH2O,CpCO2,CpCO,CpN2,CpAv,Qw1,Qw2,xH2O,xCO2,xCO,xN2,absg:
real;
  nH2,CpS,CpH2,DelTemp,H2OMass,H2Oved, PH2O,PH2,xH2,H2ved,CO2ved :
real;
  H2OMNew,Qver,lgth1,Two1,L1,Test,COved,exH2O,exCO2,exCO,exH2    : real;
  TemHeat,Ts2,TestTem,TestTs,TotA,Mg,k_des,E_des,Step,RHeat,xreag: real;
  EmG1,TauGLm1,TauG2Lm1,TauG3Lm1,TauAcLm1,meter,Los,yreag,zreag  : real;
  Area2,Maal,Vol,QA,ax,by,TestQcon,TestQrad,qoBSoek,qoBT22,SoekT : real;
  qoB22,qoBT11,qoB11,droogte,QTOETS,Mdp,Mreg,massDryS,hcvgw,Pr,Re: real;
  Aseg,ksH2O                                                     : real;

  Yy,Xx                                                  : Rooster;
  Tp,T                                                   : RoosterEen;
  Cx,Cy                                                  : RoosterOne;
  ScPos                                                  : RoosterThree;
  Cond,Den,radius,Cp,U                                   : RoosterTwo;
  eL,qxN2,qxH2,qxH2O,qxCO2,qP,qxCO,uTs,uTg,uTw,S         : String;
  opdie,verder,name, change                              : char;
```

{ ** THIS PROCEDURE READ THE INPUT DATA FROM THE DATAFILES ** }

```
Procedure InitialOne;
 Begin
  Assign(OutKiln,'KilnPar.dat');
  Reset(Outkiln);
  read(Outkiln,rad);
  lr:=Round(rad);
  read(OutKiln,rad);
  D:=rad;
  FOR j:=1 TO lr DO
   Begin
    read(OutKiln,rad);
    Cond[j]:=rad;
   End;
 FOR j:=1 TO lr DO
  Begin
   read(OutKiln,rad);
   Cp[j]:=rad;
  End;
FOR j:=1 TO lr DO
 Begin
  read(OutKiln,rad);
  Den[j]:=rad;
 End;
radius[1]:=D/2;
FOR j:=2 TO lr+1 DO
 Begin
  read(OutKiln,rad);
  radius[j]:=Radius[j-1]+rad;
 End;
read(OutKiln,rad);lgth:=rad;
read(OutKiln,rad);F:=rad;
```

```
  Close(OutKiln);
  Assign(OutGasYN,'KilnYN.dat');
  Reset(OutGasYN);
  Read(OutGasYN,name);
  Close(OutGasYN);
  CASE name OF
  'n','N':
        Begin
         Assign(OutOp,'KilnOp.dat');
         Reset(OutOp);
         read(OutOp,rad);Two:=rad;   read(OutOp,rad);Ts:=rad;
         read(OutOp,rad);Tg:=rad;    read(OutOp,rad);Twi:=rad;
         read(OutOp,rad);MassS:=rad; read(OutOp,rad);rot:=rad;
         read(OutOp,rad);slope:=rad; read(OutOp,rad);Wtper:=rad;
         Close(Outop);
        End;
 'y','Y':
        Begin
         Assign(OutOp,'KilnOpG.dat');
         Reset(OutOp);
         read(OutOp,rad);Two:=rad;   read(OutOp,rad);Ts:=rad;
         read(OutOp,rad);Tg:=rad;    read(OutOp,rad);Twi:=rad;
         read(OutOp,rad);MassS:=rad; read(OutOp,rad);MassG:=rad;
         read(OutOp,rad);slope:=rad; read(OutOp,rad);rot:=rad;
         read(OutOp,rad);Wtper:=rad;
         Close(OutOp);
        End;
    End;
Assign(OutGAC,'GAC.dat');
Reset(OutGAC);
read(OutGAC,rad);DencityS:=rad;
```

```
  read(OutGAC,rad);Dp:=rad;close(OutGAC);
  Assign(OutGComp,'KilnGas.dat');
  Reset(OutGComp);
  read(OutGComp,rad);exH2O:=rad; read(OutGComp,rad);exCO2:=rad;
  read(OutGComp,rad);exCO:=rad;  read(OutGComp,rad);exH2:=rad;
  read(OutGComp,rad);exN2:=rad;
  close(OutGComp);
  FOR j:=1 TO 20 DO
    Begin
      FOR kx:=1 TO 20 DO
      Begin
        xx[kx,j]:=0;
        yy[kx,j]:=0;
      End;
    End;
  FOR j:=1 TO 20 DO
    Begin
      FOR kx:=1 TO 20 DO
      Begin
        T[kx,j]:=Ts;
        Tp[kx,j]:=Ts
      End;
    End;
  Mg:=0;
  xreag:=0;
  yreag:=0;
  zreag:=0;
End;
```

```
{ ** THIS PROCEDURE READ THE NODAL GRIDPOINTS FROM UNIT GRID.TPU
** }

Procedure Lengths;
 Begin
  delY:=F/(nr-1);
  Assign(C_x,'C:\Cx.dat');
  Reset(C_x);
  b:=0;
  REPEAT
   Begin
    b:=b+1;
    Read(C_x,Cx[b]);
   End;
  UNTIL b=(nr-1);
  Close(C_x);
  Assign(C_y,'C:\Cy.dat');
  Reset(C_y);
  b:=0;
  REPEAT
   Begin
    b:=b+1;
    Read(C_y,Cy[b]);
   End;
  UNTIL b=Cx[1];
  Close(C_y);
  Assign(XY_x,'C:\XGrid.dat');
  Reset(XY_x);
  FOR kan:=1 to nr-1 DO
   Begin
    FOR j:=1 to Cx[kan] DO
```

```
        Begin
          read(XY_x,Xx[kan,j]);
        End;
    End;
  Close(XY_x);
  Assign(XY_y,'C:\YGrid.dat');
  Reset(XY_y);
  FOR kan:=1 to (nr-1) DO
    Begin
      FOR j:=1 to Cx[kan] DO
        Begin
          read(XY_y,Yy[kan,j]);
        End;
    End;
  Close(XY_y);
End;
```

```
{ ** THE INITIAL CONDITION ARE CALCULATED IN THE PROCEDURE ** }

Procedure InitialThree;
  Begin
    droogte:=0;
    P:=1.2;
    Ln:=0.95*D*(1-F/D);
    Teta:=Arctan((D*D-(D-F)*(D-F))/(D-F));
    Fsw:=1;
    Fws:=(D*D-(D-F)*(D-F))/D/(pi-Teta);
    Fww:=1-Fws;
    L:=D*Arctan((D/2-F)/(exp(0.5*Ln(exp(2*Ln(D/2))-exp(2*Ln(D/2-F))))))+D/2*pi;
```

```
    AwExp:=L*DelL;
    Aw:=2*pi*radius[1]*DelL;
    As:=2*(exp(0.5*Ln(exp(2*Ln(D/2)) - exp(2*Ln(D/2-F)))))*DelL;
    k_des:=exp(-2.949E-3*sqr(wtper) + 10.073);
    E_des:=-8.25*sqr(wtper)+48629;
    Ag:=(As+AwExp);
  End;


{ ** MAXIMUM TIME IS CALCULATED FROM THE STABILITY CRITERION ** }

Procedure Stability;
Label Hier;
  Begin
    YPix:=1;
    tIME:=0.01;
    CpS:=(500+(-0.44 +
4.92E-3*Twi-3.6E-6*Twi*Twi+9.59E-10*Twi*Twi*Twi)*1000);
    ks:=1.35*((8.69497E-4*Twi-9.43737E-3));
    Alfaas:=ks/CpS/DencityS;
    REPEAT
      Begin
        REPEAT
          Begin
            FOR aa:=2 TO nr-1 DO
              Begin
                IF Xx[aa,Cx[aa]]=0
                THEN
                  wall:=Cx[aa]-1
                ELSE
```

```
        wall:=Cx[aa];
      FOR b:=2 TO wall DO
       Begin
        Stabiel:=1-2*Alfaas*Time/sqr(Xx[aa,b]);
        Stabiel:=Stabiel-2*Alfaas*Time/sqr(Yy[aa,b]);
        IF Stabiel<=0
        THEN
         Begin
          Goto Hier;
         End
        ELSE
       End;
    End;
  End;
  CASE step

     Begin
      Step:=0.01;
     End;
    2:
     Begin
      Step:=0.001;
     End;
    3:
     Begin
      Step:=0.0001;
     End;
    End;
  Time:=Time+Step;
  Hier:
UNTIL Stabiel<=0;
```

```
        Time:=Time-4*Step;
        YPix:=YPix+1;
      End;
    UNTIL YPix = 4;
  End;


{ ** RESIDENCE  TIME CALCULATED FOR THE KILN ** }

Procedure ResidenceT;
 Begin

   RTime:=12.2046/rot*60*lght/5;
 End;



Procedure NumberZones;
 Begin
   zone:=RTime/Time;
   DelL:=lgth/zone;
 End;



{ ** FUNCTION FOR CALCULATED THE WATER EVAPORATED ** }
```

```
Function Dry(kdes,Edes,Tem:real) : real;
  Begin
    Dry:=kdes*exp(-Edes/Rgas/Tem);
  End;


{** PROCEDURE FOR CALCULATING THE SOLIDS BED TEMPERATURE ** }

Procedure NodalTemp;
Label Nou;
  Begin
    CpS:=(500 + (-0.44 + 4.92E-3*Ts - 3.6E-6*Ts*Ts +
9.59E-10*Ts*Ts*Ts)*1000);
    ks:=1.35*((8.69497E-4*Ts - 9.43737E-3));
    IF H2OMass>=0
    THEN
      Begin
        CpH2O:=75.4*1000/18;
        ksH2O:=-6.1258E-6*(Ts-1.897)+5.002E-3*(Ts-4.486)-3.196E-1;
        CpS:=MassDryS/(MassDryS+H2OMass)*CpS +
H2OMass/(MassDryS+H2OMass)*CpH2O;
        ks:=MassDryS/(MassDryS+H2OMass)*ks +
H2OMass/(MassDrYS+H2OMass)*ksH2O;
        Alfaas:=ks/CpS/((1-H2OMass/(H2OMass+MassDryS)*DencityS +
H2OMass/(MassDrYS+H2OMass)*1000));
      End
    ELSE
    Alfaas:=ks/CpS/DencityS;
    FOR aa:=1 TO nr-1 DO
      Begin
```

```
      IF Xx[aa,Cx[aa]]=0
      THEN
        Begin
          T[aa,Cx[aa]]:=Twi;
          T[aa,Cx[aa]+1]:=Twi;
          Tp[aa,Cx[aa]]:=Twi;
          Tp[aa,Cx[aa]+1]:=Twi;
        End
      ELSE
      IF Xx[aa,Cx[aa]] > 0
      THEN
        Begin
          T[aa,Cx[aa]+1]:=Twi;
          Tp[aa,Cx[aa]+1]:=Twi;
        End;
    End;
  T[nr,1]:=Twi;
  Tp[nr,1]:=Twi;
  FOR b:=1 TO nr-1 DO
    Begin
      i:=0;
      REPEAT
        Begin
          IF (Yy[b,Cx[b]-i] > 0) AND (Yy[b,Cx[b]-i] < DelY)
          THEN
            Begin
              T[b+1,Cx[b]-i]:=Twi;
              Tp[b+1,Cx[b]-i]:=Twi;
              i:=i+1;
            End
          ELSE
```

```
        Begin
          i:=i+1;
        End
      End;
    UNTIL i=Cx[b]
  End;


{** THE INTERIOR NODES **}

  FOR aa:=2 TO nr-1 DO
   Begin
    IF Xx[aa,Cx[aa]]=0
    THEN
     wall:=Cx[aa]-1
    ELSE
     wall:=Cx[aa];
    FOR b:=2 TO wall DO
     Begin
      ax:=Xx[aa,b]/DelY;
      by:=Yy[aa,b]/DelY;
      Vol:=sqr(delY)/4*(1+ax+by+ax*by);
      Maal:=Alfaas*Time/Vol;
      Tp[aa,b]:=T[aa,b] + Maal*((ax+1)/2*(T[aa-1,b] - T[aa,b]));
      Tp[aa,b]:=Tp[aa,b] + Maal*((by+1)/2*(T[aa,b-1] - T[aa,b]));
      Tp[aa,b]:=Tp[aa,b] + Maal*((by+1)/(2*ax)*(T[aa,b+1] - T[aa,b]));
      Tp[aa,b]:=Tp[aa,b] + Maal*((ax+1)/(2*by)*(T[aa+1,b] - T[aa,b]));
     End;
  End;
```

```
{** THE NODES ON THE SYMETRY LINE **}


  FOR aa.=2 TO (nr-1) DO
    Begin
      Tp[aa,1]:=T[aa,b] + 2*Alfaas*Time/sqr(DelY)*(T[aa-1,b] - 4*T[aa,b] +
T[aa+1,b] + 2*T[aa,b+1])
    End;


{** THE NODES ON THE SOLID BED SURFACE **}


  FOR b:=2 TO Cx[1] DO
    Begin
      ax:=Xx[1,b]/DelY;
      by:=Yy[1,b]/DelY;
      QA:=-Qs/As*sqr(delY)/4*(by+ax*by);
      Vol:=sqr(delY)/4*(by+ax*by);
      Maal:=Alfaas*Time/Vol;
      Tp[1,b]:=T[1,b] + Maal*by/2*(T[1,b-1] - T[1,b]);
      Tp[1,b]:=Tp[1,b] + Maal*by/(2*ax)*(T[1,b+1] - T[1,b]);
      Tp[1,b]:=Tp[1,b] + Maal*((ax+1)/(2*by)*(T[1+1,b] - T[1,b]));
      Tp[1,b]:=Tp[1,b] + Maal*QA/ks;
    End;


{** THE TOP [1,1] NODE **}


  QA:=-Qs/As*sqr(DelY/2);
```

```
Vol:=Sqr(DelY);
Tp[1,1]:=T[1,1] + 4*Alfaas*Time/Vol*(T[1,2j + T[2,1] - 2*T[1,1] + QA/ks);
Ts:=0;
cnt:=0;
Area:=0;
TotA:=0;
FOR kan:=2 TO nr-1 DO
 Begin
  FOR j:=2 TO Cx[kan]  DO
   Begin
    Area:=(Xx[kan,j-1]+Xx[kan,j])/2*(Yy[kan,j]+Yy[kan-1,j])/2;
    Ts:=Tp[kan,j]*Area+Ts;
    TotA:=TotA+Area;
    cnt:=cnt+1;
   End;
  End;
 Ts:=2*Ts;
 Ts2:=0;
 TotA:=2*TotA;
 cnt:=2*cnt;
 Area2:=0;
 Ts2:=0;
 cnt2:=0;
 FOR j:=2 TO Cx[kan]  DO
  Begin
   Area:=(Xx[1,j-1]+Xx[1,j])/2*DelY/2;
   Ts2:=Tp[1,j]*Area+Ts2;
   Area2:=Area2+Area;
   cnt2:=Cnt2+1;
  End;
 Ts:=Ts+2*Ts2;
```

```
TotA:=TotA+2*Area2;
cnt:=cnt+2*Cnt2;
TotA:=TotA+DelY*DelY/2;
Ts:=Tp[1,1]*DelY*DelY/2+Ts;
cnt:=cnt+1;
FOR aa:=2 TO (nr-1) DO
  Begin
    Area:=DelY*DelY;
    Ts:=Tp[aa,1]*Area+Ts;
    TotA:=TotA+Area;
    cnt:=Cnt+1;
  End;
Ts:=Ts/TotA;
TestTs:=Ts;
H2OMNew:=H2OMass;
DelTemp:=0.00001;
IF H2OMass > 0
THEN
  Begin
    H2Oved:=Dry(k_des,E_des,Ts)*H2OMass/MassS*Time;
    H2OMass:=H2OMNew-H2Oved;
    IF H2OMass <=0
    THEN
      Begin
        H2OMass:=0;
        H2Oved:=0;
        Goto Nou;
      End
    ELSE
      Qver:=2200*H2Oved*1000;  {J}
      TestTem:=Qver/(75.4/18*1000);
```

```
IF TestTem < 0.5
THEN
  Begin
    Goto Nou;
  End
ELSE
REPEAT
  Begin
    FOR kan:=1 TO nr-1 DO
      Begin
        FOR j:=1 TO Cx[kan]  DO
          Begin
            Tp[kan,j]:=Tp[kan,j]-DelTemp;
          End;
      End;
    Tp[nr,1]:=Tp[nr,1]-DelTemp;
    Ts:=0;
    cnt:=0;
    Area:=0;
    TotA:=0;
    FOR kan:=2 TO nr-1 DO
      Begin
        FOR j:=2 TO Cx[kan]  DO
          Begin
            Area:=(Xx[kan,j-1]+Xx[kan,j])/2*(Yy[kan,j]+Yy[kan-1,j])/2;
            Ts:=Tp[kan,j]*Area+Ts;
            TotA:=TotA+Area;
            cnt:=cnt+1;
          End;
      End;
    Ts:=2*Ts;
```

```
        Ts2:=0;
        TotA:=2*TotA;
        cnt:=2*cnt;
        Area2:=0;
        Ts2:=0;
        cnt2:=0;
        FOR j:=2 TO Cx[kan]  DO
          Begin
            Area:=(Xx[1,j-1]+Xx[1,j])/2*DelY/2;
            Ts2:=Tp[1,j]*Area+Ts2;
            Area2:=Area2+Area;
            cnt2:=Cnt2+1;
          End;
        Ts:=Ts+2*Ts2;
        TotA:=TotA+2*Area2;
        cnt:=cnt+2*Cnt2;
        TotA:=TotA+DelY*DelY/2;
        Ts:=Tp[1,1]*DelY*DelY/2+Ts;
        cnt:=cnt+1;
        FOR aa:=2 TO (nr-1) DO
          Begin
            Area:=DelY*DelY;
            Ts:=Tp[aa,1]*Area+Ts;
            TotA:=TotA+Area;
            cnt:=Cnt+1;
          End;
        Ts:=Ts/TotA;
      End;
    UNTIL (TestTs-Ts)<TestTem;
  End
ELSE;
```

```
        NCU:
        FOR kan:=1 TO 20 DO
         Begin
           FOR aa:=1 TO 20 DO
            Begin
              T[aa,kan]:=Tp[aa,kan];
            End;
         End;
       FOR kan:=1 TO 20 DO
         Begin
           FOR aa:=1 TO 20 DO
            Begin
              T[aa,kan]:=Tp[aa,kan];
            End;
         End;

  End;



{ ** PROCEDURE CALCULATING THE TEMPERATURE CHANGE OF THE GAS **
}

Procedure TempChangeGas;
  Begin
    Tg:=Tg-273;
    CpH2:=(28.84 + 0.00756E-2*Tg + 0.3288E-5*Tg*Tg -0.3698E-9*Tg*Tg*Tg);
    CpN2:=(29.00 + 0.2199E-2*Tg + 0.5723E-5*Tg*Tg -2.871E-9*Tg*Tg*Tg);
    CpH2O:=(33.46 + 0.688E-2*Tg + 0.7604E-5*Tg*Tg -3.593E-9*Tg*Tg*Tg);
    CpCO2:=(33.11 + 4.233E-2*Tg - 2.887E-5*Tg*Tg + 7.464E-9*Tg*Tg*Tg);
```

```
    CpCO:=(28.95 + 0.411E-2*Tg + 0.3548E-5*Tg*Tg - 2.22E-9*Tg*Tg*Tg);
    CpAv:=1000*(xH2*CpH2 + xN2*CpN2 + xH2O*CpH2O + xCO2*CpCO2 +
xCO*CpCO);
    Tg:=-Qg*Time/(CpAv*nt) + Tg;
    Tg:=Tg+273;
  End;



{ ** PROCEDURE CALCULATING THE TEMPERATURE CHANGE OF THE
SOLIDS ** }
{ ** AS A RESULT OF THE EDOTHERMIC REACTION                    ** }

Procedure ReactHeat;
 Begin
   RHeat:=1000000*(xreag*131.4-41*yreag+172*zreag);
   CpS:=(500 + (-0.44 + 4.92E-3*Ts-3.6E-6*Ts*Ts+9.59E-10*Ts*Ts*Ts)*1000);
   TestTs:=Ts;
   Ts:=0;
   cnt:=0;
   Area:=0;
   TotA:=0;
   DelTemp:=0.01;
   Temheat:=RHeat/(CpS*MassDryS);
   REPEAT
    Begin
     FOR kan:=1 TO nr-1 DO
      Begin
       FOR j:=1 TO Cx[kan]  DO
        Begin
         T[kan,j]:=T[kan,j]-DelTemp;
```

```
      End;
    End;
  T[nr,1]:=T[nr,1]-DelTemp;
  Ts:=0;
  cnt:=0;
  Area:=0;
  TotA:=0;
  FOR kan:=2 TO nr-1 DO
   Begin
     FOR j:=2 TO Cx[kan]  DO
       Begin
         Area:=(Xx[kan,j-1]+Xx[kan,j])/2*(Yy[kan,j]+Yy[kan-1,j])/2;
         Ts:=T[kan,j]*Area+Ts;
         TotA:=TotA+Area;
         cnt:=cnt+1;
       End;
    End;
  Ts:=2*Ts;
  Ts2:=0;
  TotA:=2*TotA;
  cnt:=2*cnt;
  Area2:=0;
  Ts2:=0;
  cnt2:=0;
  FOR j:=2 TO Cx[kan]  DO
   Begin
     Area:=(Xx[1,j-1]+Xx[1,j])/2*DelY/2;
     Ts2:=T[1,j]*Area+Ts2;
     Area2:=Area2+Area;
     cnt2:=Cnt2+1;
   End;
```

```
        Ts:=Ts+2*Ts2;
        TotA:=TotA+2*Area2;
        cnt:=cnt+2*Cnt2;
        TotA:=TotA+DelY*DelY/2;
        Ts:=T[1,1]*DelY*DelY/2+Ts;
        cnt:=cnt+1;
        FOR aa:=2 TO (nr-1) DO
          Begin
            Area:=DelY*DelY;
            Ts:=T[aa,1]*Area+Ts;
            TotA:=TotA+Area;
            cnt:=Cnt+1;
          End;
      Ts:=Ts/TotA;
    End;
  UNTIL (TestTs-Ts)>TemHeat;
End;


{ ** PROCEDURE READING THE INITIAL GAS COMPOSITION ** }

Procedure GasCompIn;
  Begin
    Assign(OutGasYN,'KilnYN.dat');
    Reset(OutGasYN);
    Read(OutGasYN,name);
    Close(OutGasYN);
    CASE name OF
    'y','Y':
          Begin
```

```
            move:=trunc(zone)-1;
            Assign(OutGEx,'ExGas.dat');
            Reset(OutGEx);
            read(OutGEx,rad);xH2O:=rad;     read(OutGEx,rad);xCO2:=rad;
            read(OutGEx,rad);xCO:=rad;      read(OutGEx,rad);xH2:=rad;
            read(OutGEx,rad);xN2:=rad;
            Close(OutGEx);
            Vgas:=pi/4*exp(2*Ln(D))*lgth/zone*move - 0.6*MassS*Time/DencityS;
            nt:=1.2*101.325*Vgas/(Rgas*Tg);

nH2:=xH2*nt;nN2:=xN2*nt;nH2O:=xH2O*nt;nCO2:=xCO2*nt;nCO:=xCO*nt;
          End;
    'n','N':
          Begin
            Assign(OutSame,'KilnGas.dat');
            Reset(OutSame);
            read(OutSame,rad);xH2O:=rad;    read(OutSame,rad);xCO2:=rad;
            read(OutSame,rad);xCO:=rad;     read(OutSame,rad);xH2:=rad;
            read(OutSame,rad);xN2:=rad;
            Close(OutSame);
            Vgas:=pi/4*exp(2*Ln(D))*lgth - MassS*Time*zone/DencityS;
            nt:=1.2*101.325*Vgas/(Rgas*Tg);

nH2:=xH2*nt;nN2:=xN2*nt;nH2O:=xH2O*nt;nCO2:=xCO2*nt;nCO:=xCO*nt;
          End;
      End;
    H2OMass:=Wtper/100*MassS*Time;
    MassdryS:=(100-Wtper)/100*MassS*Time;
    H2Oved:=0;
  End;
```

```
{ ** PROCEDURE CALCULATING THE MASS LOSS DUE TO DECOMPOSITION
AND PYROLYSIS ** }

Procedure Look;
 Begin
  Assign(Data,'Mine.dat');
  Reset(Data);
  REPEAT
   Begin
    Read(Data,Datas);
    WITH Datas DO
     Begin
      qoBT22:=mx;
     End;
   End;
 UNTIL (qoBT22>=SoekT);
 PosqoB22:=FilePos(Data);
 PosqoB11:=PosqoB22-1;
 Seek(Data,PosqoB22-1);
 Read(Data,Datas);
 WITH Datas DO
     Begin
      qoBT22:=mx;
      qoB22:=my;
     End;
 Seek(Data,PosqoB11-1);
 Read(Data,Datas);
 WITH Datas DO
     Begin
      qoBT11:=mx;
```

```
            qoB11:=my;
          End;
    qoBsoek:=(SoekT-qoBT11)/(qoBT22-qoBT11)*(qoB22-qoB11)+qoB11;
    Close(Data);
  End;



Procedure Put_Pix(Lgg,Too : real; kleur : word);
  Begin
    XPix:=Trunc(Lgg/LengtePerPix);
    YPix:=Trunc(Too/GradePerPix);
    YPix:=MaxY-YPix;
    PutPixel(XPix+30,YPix-30,kleur);
  End;



{ ** MAIN PROCEDURE FOR CALCULATING THE INITIAL VALUES ** }

Procedure MainInPut;
  Begin
    InitialOne;          {* Set kiln parameters *}
    NodalLength;         {* Call Unid Grid.TPU to calculate nodal lengths *}
    Lengths;
    Stability;           {* Calculate the stability kriteria *}
    ResidenceT;
    NumberZones;         {* Calculate the number of length increments *}
                         {* using the retention time as setpoint *}
```

```
InitialThree;        {* Calculates the variables for the heatbalance *}
GasComposIn;         {* Gas Composition for iteration start *}
mg:=0;
clrscr;
L1:=Lm;
FOR c:=1 TO 3 DO
 Begin
  Lm:=c*L1;
  Invoer(xH2O,xCO2,xCO,Lm,P,Tg,Twi);
  Running;           {* Call Unit EmiesOne.TPU to calculate the emmissivity *}
  Answer(EmG,absg);{* with the parameters of Invoer *}
  CASE c OF
  1:
   Begin
    TauGLm:=1-absg;
    EmG:=EmG;
    AlfaGAc:=0.7;
    TauAcLm:=TauGLm/24;
   End;
 2:
   Begin
    TauG2Lm:=1-absg;
   End;
 3:
  Begin
    TauG3Lm:=1-absg;

  End;
 End;
End;
```

```
EInS(Ts,Twi,TauGLm,TauG2Lm,TauG3Lm,Fws,Fsw,Fww,As,AwExp,EmG,TauAcLm,
MassG,D,Tg,zone,move);
   SolidQs;
   EtoS(Qs);

EInG(Ts,Twi,TauGLm,TauG2Lm,TauG3Lm,Fws,Fsw,Fww,As,AwExp,EmG,TauAcLm,
MassG,D,Tg,Ag,AlfaGAc,zone,move);
   GasQg;
   EtoG(Qg);
   NodalTemp;
   TempChangeGas;

ReactIn(Ts,H2Oved,Vgas,Tg,nN2,nH2,nH2O,nCO2,nCO,Time,MassdryS,P,droogte);
   Reaction;

ReactOut(nN2,nH2,nH2O,nCO2,nCO,xN2,xH2,xH2O,xCO2,xCO,Los,xreag,yreag,zre
ag,droogte);
   Mg:=Mg+Los;
 End;
```

```
{ ** THE MAIN PROCEDURE FOR THE CALCULATIONS STARS HERE ** }

Procedure TempGraph;
Label voort;
 Begin
   MainInPut;
```

```
GraphDriver:=detect;
InitGraph(GraphDriver,GraphMode,'C:\TP\BGI');
ErrorCode :=GraphResult;
IF ErrorCode <> grOK
THEN
  Begin
    Writeln('Graphics Error:',GraphErrorMsg(ErrorCode));
    Halt;
  End;
MaxX:=GetMaxX;
MaxY:=GetMaxY;
Line(30,MaxY-30,30,0);
Line(30,MaxY-30,MaxX,MaxY-30);
GradePerPix:=(Twi)/(MaxY-30);
LengtePerPix:=lgth/(MaxX-30);
lgth1:=lgth;
Two1:=Two;
lgth:=lgth1;
Two:=Two1;
SetTextStyle(3,1,3);
OutTextXY(1,90,'Temperature [K]' );
SetTextStyle(3,0,3);
OutTextXY(250,450,'Length [m]' );
Assign(OutGasYN,'KilnYN.dat');
Reset(OutGasYN);
Read(OutGasYN,name);
Close(OutGasYN);
meter:=1/lgth*trunc(zone);
Lm:=0.95*D*(1-F/D);
L1:=Lm;
EmG1:=xH2O;
```

```
FOR kp:=1 TO trunc(zone) DO
 Begin
  IF (xH2O/EmG1>1.13) OR (xH2O/EmG1<0.87)
  THEN
   Begin
    FOR c:=1 TO 3 DO
     Begin
      Lm:=c*L1;
      Invoer(xH2O,xCO2,xCO,Lm,P,Tg,Twi);
      Running;          {* Call Unit EmiesOne.TPU to calculate the
emmissivity *}
      Answer(EmG,absg);
      CASE c OF
      1:
       Begin
        TauGLm:=1-absg;
        EmG:=EmG;
        AlfaGAc:=0.7;
        TauAcLm:=TauGLm/24;
       End;
      2:
       Begin
        TauG2Lm:=1-absg;
       End;
      3:
       Begin
        TauG3Lm:=1-absg;
       End;
     End;
   End;
End
```

```
        ELSE;

EInS(Ts,Twi,TauGLm,TauG2Lm,TauG3Lm,Fws,Fsw,Fww,As,AwExp,EmG,TauAcLm,
MassG,D,Tg,zone,move);
        SolidQs;      { ** CALL UNIT QSOLIDS.TPU ** }
        EtoS(Qs);

EInG(Ts,Twi,TauGLm,TauG2Lm,TauG3Lm,Fws,Fsw,Fww,As,AwExp,EmG,TauAcLm,
MassG,D,Tg,Ag,AlfaGAc,zone,move);
        GasQg;        { ** CALL UNIT QGAS.TPU ** }
        EtoG(Qg);
        NodalTemp;
        TempChangeGas;
        EmG1:=xH2O;

ReactIn(Ts,H2Oved,Vgas,Tg,nN2,nH2,nH2O,nCO2,nCO,Time,MassdryS,P,droogte);
        Reaction;     { ** CALL UNIT REACT.TPU. ** }
        ReactOut(nN2,nH2,nH2O,nCO2,nCO,xN2,xH2,xH2O,xCO2,
        xCO,Los,xreag,yreag,zreag,droogte);
        Mg:=Mg+Los;
        Ts:=Ts-273;
        IF (Ts<105) OR (Ts>990)
        THEN
         Begin
          Mdp:=0;
          Goto voort;
         End
       ELSE
         Begin
          SoekT:=Ts;
          Look;
```

```
        Mdp:=qoBSoek;
      End;
    Voort:
    Mreg:=Mg+Mdp;
    Ts:=Ts+273;
    nt:=nN2+nH2+nH2O+nCO2+nCO;
    Assign(PuP,'Pbuild.dat');
    Reset(Pup);
    read(Pup,opdie);
    Close(Pup);
    CASE opdie OF
    'n','N':
          Begin
            P:=1.2;
          End;
    'y','Y':
          Begin
            P:=nt*Rgas*Tg/Vgas/101.325;
          End;
    End;
    ReactHeat;
    Lengte:=kp*DelL;
    Put_Pix(Lengte,Ts-200,lightblue);
    Put_Pix(Lengte,Tg-200,lightmagenta);
    Put_Pix(Lengte,Twi-200,yellow);
  End;
 readln;
 CloseGraph;
End;
```

```
Procedure Options;
Label
  Hier;
  Begin
    Hier:
    CASE opt OF
    1:
      Begin
        KilnOperate;
        Screen;          {*Call Unit Menu.TPU*}
        Choice(opt);     {*From Unit Menu.TPU*}
        Goto Hier;
      End;
   2:
      Begin
        TempGraph;
        Screen;          {*Call Unit Menu.TPU*}
        Choice(opt);     {*From Unit Menu.TPU*}
        Goto Hier;
      End;
   3:
      Begin
        Halt;
        Goto Hier;
      End;
  End;
End;
```

```
{** THE MAIN PROGRAM STARTS HERE ** }

BEGIN
  Screen;          {*Call Unit Menu.TPU*}
  Choice(opt);     {*From Unit Menu.TPU*}
  Options;
  Clrscr;
  Screen;          {*Call Unit Menu.TPU*}
  Choice(opt);     {*From Unit Menu.TPU*}
END.
```

G.2 UNIT "Menu.TPU"

This is the unit for setting the main menu.

```
Unit Menu;

{$R+}

InterFace
        Procedure Screen;
        Procedure Choice(Var keuse : integer);

Implementation

Uses Crt,Graph;

Var
```

```
  ken,MaxX,MaxY,GraphDriver,GraphMode,ErrorCode,k0,k2 : integer;
  S : String;


Procedure SetScreen;
  Begin
    GraphDriver:=Detect;
    InitGraph(GraphDriver,GraphMode,'D:\TURBO6\BGI');
    ErrorCode :=GraphResult;
    IF ErrorCode <> grOK
    THEN
      Begin
        Writeln('Graphics Error:',GraphErrorMsg(ErrorCode));
        Halt;
      End;
    MaxX:=GetMaxX;
    MaxY:=GetMaxY;
    SetColor(Red);
    SetTextStyle(0,0,7);
    OutTextXY(130,20,'Menu'  );
    Setcolor(Lightblue);
    k0:=TextHeight('default') + 60;
    SetTextStyle(0,0,2);
    OutTextXY(30,k0,'[1]');
    OutTextXY(130,k0,'Kiln and Operation Parameters');
    k2:=k0 + TextHeight('Default') + 30;
    OutTextXY(30,k2,'[2]');
    OutTextXY(130,k2,'Temperature Profiles/Mass Loss');
    k2:=k2 + TextHeight('Default') + 30;
    OutTextXY(30,k2,'[3]');
    OutTextXY(130,k2,'Quit');
```

```
    SetColor(Yellow);
    SetTextStyle(0,0,1);
    s:='Choose [1], [2]... and press ENTER ';
    OutTextXY(MaxX-TextWidth(S),MaxY-TextHeight(S),S);
    GotoXY(whereX,whereY);
    Readln(ken);
    CloseGraph;
  End;


Procedure Choice;
  Begin
    keuse:=ken;
  End;


Procedure Screen;
  Begin
    SetScreen;
  End;
END.
```

G.3 UNIT "EmiesOne.TPU"

This is the unit for calculating the properties of the freeboard gas.

```
Unit EmiesOne;
```

```
{ ** THIS UNIT CALCULATES THE GAS PROPERTIES ** }


{$R+,N+}

InterFace
  Procedure Running;
  Procedure Answer (Var Ant,AntT:real);
  Procedure Invoer (Var Wat,Kdiok,KMon,BeamLm,Pres,Tempgas,Tempwall:real);
                {H2O,CO2,CO,NO,SO2 en CH4 composition last three not cal-}
                {culated}


Implementation
  Uses Crt;

Const
  h=6.625E-34;
  kb=1.38E-23;
  speed=2.9977E8;
  R=82.05;
  C2=1.4387;
  Po=1;
  MrH2O=18;
  MrCO2=44;MrCO=28;MrNO=30;
  MrSO2=64;MrCH4=16;MrN2=28;
  T0=100;          {K}
  mH2O=3;mCO2=3;mCO=1;
  mNO=1;mSO2=3;mCH4=4;
  BandH2O=5;BandCO2=6;BandCO=2;
  BandSO2=5;BandCH4=4;BandNO=1;
```

```
Type

  Em1 = Record
    wf:integer;
    gf:integer;
  End;
  Em2 = Record
    bnd:integer;
    delt1:integer;
    delt2.integer;
    delt3:integer;
    nn:real;
    bb:real;
  End;
  Em3 = Record
    wnul:real;
    Alfanul:real;
    Betanul:real;
    wbnul:real;
End;
Em4 = Record
   bnd:integer;
   delt1:integer;
   delt2:integer;
   delt3:integer;
   delt4:integer;
   nn:real;
   bb:real;
End;
Em5 = Record
  bnd:integer;
```

```
    delt1:integer;
    nn:real;
    bb:real;
  End;
  Em6 = Record
    LamF:real;
    C5TF:real;
  End;
  Fil = Record
    wlkf:real;
    wrkf:real;
    emf :real;
  End;

  Plekke = Array[0..200] of real;
  Rooster1 = Array [1..8] of real;
  Rotor = Array[1..50] of integer;
  Matriks = Array [1..8,1..10] of integer;

Var

  Datas1 : Em1;
  Datas2 : Em2;
  Datas3 : Em3;
  Datas4 : Em4;
  Datas5 : Em5;
  Datas6 : Em6;
  DataFil : Fil;
  Data1 : File of Em1;
  Data2 : File of Em2;
  Data3 : File of Em3;
```

```
  Data4 : File of Em4;
  Data5 : File of Em5;
  Data6 : File of Em6;
  BandWave : File of Fil;
  Wave,Vergelyk : File of real;

  ou,i,o,Band,k,count,a,Typegas,c,mValue,z    : integer;
  PosFrak22,PosFrak11,Block,Pos,Getal,fak,Vkk : integer;
  FrakSeek,Error,DSumOne,SumFi,Upsum,DSumTwo,Somasie,xxH2O:double;
  xxCO2,xxCO,xxNO,xxSO2,xxCH4,FiT,FiT0,TetaT,Teta0,SommT  :real;
  Somm0,xMr,xGas,RealAlfa,RealBeta,FrakRight,FrakLeft     :real;
  LamT22,TC522,LamT11,TC511,Tw,Wuk,Wlk,PiTTemp,PiTNul     :real;
  PiNoemT,PiNoem0,P,Pe,Ro,nk,Lm,Tg,TauH      : real;
  BetaT,w,Al,Bet,w0,Alfa0,n,b,Uk,Uk0,SigTTemp: Rooster1;
  SigTNul,Beta0,wster,DelWk,AlfaT,wa,wbT,wb0 : Rooster1;
  ProdTNul,ProdTTemp,ProdTelT,TauG: Rooster1;
  Poss,Vk,Vk0,m,g                 : Rotor;
  Absorp,Emisie,BndLimit,DelF     : Plekke;
  Del     : Matriks;
  FileNaam1,FileNaam2,FileNaam3   : String [14];


Procedure Invoer;
 Begin
  xxH2O:=Wat;
  xxCO2:=Kdiok;
  xxCO:=KMon;
  Lm:=BeamLm;
  P:=Pres;
  Tg:=Tempgas;
  Tw:=Tempwall;
```

```
 End;


Procedure Gas;
 Begin
  CASE ou OF
 1:
  Begin
   Typegas:=1;
   xGas:=xxH2O;
   xMR:=MrH2O;
  End;
 2:
  Begin
   Typegas:=2;
   xGas:=xxCO2;
   xMR:=MrCO2;
  End;
 3:
  Begin
   Typegas:=3;
   xGas:=xxCO;
   xMR:=MrCO;
  End;
 4:
  Begin
   Typegas:=4;
   xGas:=xxNO;
   xMR:=MrNO;
  End;
 5:
```

```
      Begin
        Typegas:=5;
        xGas:=xxSO2;
        xMR:=MrSO2;
      End;
    6:
      Begin
        Typegas:=6;
        xGas:=xxCH4;
        xMR:=MrCH4;
      End;
    End;
  End;

Procedure TipeGas;
  Begin
    IF Typegas=2
    THEN
      Begin
        Error:=1E-3;
      End
    ELSE
      Begin
        Error:=1E-6;
      End;
  End;


Procedure GetData;
Label
  Kick;
```

```
Begin
  CASE typegas OF
  1:
    Begin
      FileNaam1:='DataH2O1.dat';
      FileNaam2:='DataH2O2.dat';
      FileNaam3:='DataH2O3.dat';
      mValue:=mH2O;
      Band:=BandH2O;
    End;
  2:
    Begin
      FileNaam1:='DataCO21.dat';
      FileNaam2:='DataCO22.dat';
      FileNaam3:='DataCO23.dat';
      mValue:=mCO2;
      Band:=BandCO2;
    End;
  3:
    Begin
      FileNaam1:='DataCO1.dat';
      FileNaam2:='DataCO2.dat';
      FileNaam3:='DataCO3.dat';
      mValue:=mCO;
      Band:=BandCO;
    End;
  4:
    Begin
      FileNaam1:='DataNO1.dat';
      FileNaam2:='DataNO2.dat';
      FileNaam3:='DataNO3.dat';
```

```
      mValue:=mNO;
      Band:=BandNO;
    End;
  5:
    Begin
      FileNaam1:='DataSO21.dat';
      FileNaam2:='DataSO22.dat';
      FileNaam3:='DataSO23.dat';
      mValue:=mSO2;
      Band:=BandSO2;
    End;
  6:
    Begin
      FileNaam1:='DataCH41.dat';
      FileNaam2:='DataCH42.dat';
      FileNaam3:='DataCH43.dat';
      mValue:=mCH4;
      Band:=BandCH4;
    End;
End;
Assign(Data1,FileNaam1);
Reset(Data1);
FOR c:=1 TO mValue DO
  Begin
    Read(data1,datas1);
    WITH datas1 DO
      Begin
        w[c]:=wf;
        g[c]:=gf;
      End;
  End;
```

```
  Close(Data1);
  IF FileNaam2='DataCO2.dat'
  THEN
   Begin
    Assign(Data5,FileNaam2);
    Reset(Data5);
    FOR c:=1 TO Band DO
     Begin
      Read(data5,datas5);
      WITH datas5 DO
       Begin
        Del[c,1]:=delt1;
        n[c]:=nn;
        b[c]:=bb;
       End;
     End;
    Close(Data5);
    GoTo Kick;
   End
ELSE
IF FileNaam2 ='DataNO2.dat'
THEN
 Begin
   Assign(Data5,FileNaam2);
   Reset(Data5);
   FOR c:=1 TO Band DO
    Begin
     Read(data5,datas5);
     WITH datas5 DO
      Begin
       del[c,1]:=delt1;
```

```
            n[c]:=nn;
            b[c]:=bb;
          End;
      End;
    Close(Data5);
    GoTo Kick;
  End;
IF FileNaam2='DataCH42.dat'
THEN
  Begin
    Assign(Data4,FileNaam2);
    Reset(Data4);
    FOR c:=1 TO Band DO
      Begin
        Read(data4,datas4);
        WITH datas4 DO
          Begin
            Del[c,1]:=delt1;
            Del[c,2]:=delt2;
            Del[c,3]:=delt3;
            Del[c,4]:=delt4;
            n[c]:=nn;
            b[c]:=bb;
          End;
      End;
    Close(Data4);
    GoTo Kick;
  End;
Assign(Data2,FileNaam2);
Reset(Data2);
FOR c:=1 TO Band DO
```

```
    Begin
      Read(data2,datas2);
      WITH datas2 DO
        Begin
          Del[c,1]:=delt1;
          Del[c,2]:=delt2;
          Del[c,3]:=delt3;
          n[c]:=nn;
          b[c]:=bb;
        End;
    End;
  Close(Data2);
  Kick:
  Assign(Data3,FileNaam3);
  Reset(Data3);
  FOR c:=1 TO Band DO
    Begin
      Read(data3,datas3);
      WITH datas3 DO
        Begin
          w0[c]:=wnul;
          Alfa0[c]:=Alfanul;
          Beta0[c]:=Betanul;
          wb0[c]:=wbnul;
        End;
    End;
  Close(Data3);
End;

Procedure Choice;
 Begin
```

```
IF (TauH <=1) AND (TauH<=nk)
THEN
  Begin
    wster[k]:=TauH;
    TauG[k]:=0.9;
  End
ELSE
IF (nk<=1)
THEN
  Begin
    IF (TauH>=nk) AND (TauH<=1/nk)
    THEN
      Begin
        wster[k]:=sqrt(4*nk*TauH)-nk;
        TauG[k]:=0.5*(1+nk/wster[k]);
      End
    ELSE
  End;
IF (nk<=1) AND (TauH>1/nk)
THEN
  Begin
    wster[k]:=Ln(TauH*nk)+2-nk;
    TauG[k]:=1/wster[k];
  End
ELSE
IF (nk>1) AND (TauH>1)
THEN
  Begin
    wster[k]:=Ln(TauH)+1;
    TauG[k]:=1/wster[k];
    IF TauG[k]>0.9
```

```
      THEN
        Begin
          TauG[k]:=0.9
        End;
    End
  ELSE
End;

Procedure Fundamental;
 Begin
  count:=0;
  FOR a:=1 TO mValue DO
    Begin
      IF Del[k,a]=1
      THEN
        Begin
          count:=count+1;
        End;
    End;
 End;

Procedure Fakulteit;
 Begin
  Fak:=0;
  IF SumFi=0
  THEN
    Begin
      Fak:=0;
    End
  ELSE
  REPEAT
```

```
      Begin
        fak:=fak+1;
      End;
    UNTIL Fak=SumFi
  End;

Procedure Total;
  Begin
    IF fak=0
    THEN
      Begin
        Somasie:=1;
      End
    ELSE
      Begin
        Somasie:=1;
        FOR i:=1 TO fak DO
          Begin
            Somasie:=Somasie*i;
          End;
      End;
  End;

Procedure AlfaTemp;
  Begin
    FOR z:=1 TO mValue DO
      Begin
        Uk[z]:=h*speed*w[z]*100/kb/Tg;          {Om na cm te kry}
        Uk0[z]:=h*speed*w[z]*100/kb/T0;
        IF Del[k,z]>=0
        THEN
```

```
      Begin
        Vk0[z]:=0;
      End
    ELSE
    IF Del[k,z]<0
    THEN
      Begin
        Vk0[z]:=Abs(Del[k,z]);
      End;
  End;
FOR z:=1 TO mValue DO
  Begin
    ProdTTemp[z]:=0;
    ProdTNul[z]:=0;
  End;
FOR z:=1 TO mValue DO      {Vir die teller van fi(T)}
  Begin
    Vkk:=Vk0[z];
    REPEAT
      Begin
        SumFi:=Vkk+g[z]+Del[k,z]-1;
        Fakulteit;
        Total;
        UpSum:=Somasie;
        SumFi:=g[z]-1;
        Fakulteit;
        Total;
        DSumOne:=Somasie;
        SumFi:=Vkk;
        Fakulteit;
        Total;
```

```
            DSumTwo:=Somasie;

ProdTTemp[z]:=UpSum/DSumOne/DSumTwo*exp(-Uk[z]*Vkk)+ProdTTemp[z];

ProdTnul[z]:=UpSum/DSumOne/DSumTwo*exp(-Uk0[z]*Vkk)+ProdTNul[z];
          End;
          Vkk:=Vkk+1;
        UNTIL (UpSum/DSumOne/DSumTwo*exp(-'.    *Vkk))<=1E-6;
      End;
      PiTTemp:=1;
      PiTNul:=1;
      FOR z:=1 TO mValue DO
        Begin
          PiTTemp:=ProdTTemp[z]*PiTTemp;
          PiTNul:=ProdTNul[z]*PiTNul;
        End;
    FOR z:=1 TO mValue DO
      Begin
        ProdTTemp[z]:=0;
        ProdTNul[z]:=0;
      End;
    FOR z:=1 TO mValue DO      {Vir die noemer van fi(T)}
      Begin
        Vkk:=Vk0[z];
        REPEAT
          Begin
            SumFi:=Vkk+g[z]-1;
            Fakulteit;
            Total;
            UpSum:=Somasie;
            SumFi:=g[z]-1;
```

```
            Fakulteit;
            Total;
            DSumOne:=Somasie;
            SumFi:=Vkk;
            Fakulteit;
            Total;
            DSumTwo:=Somasie;

ProdTTemp[z]:=UpSum/DSumOne/DSumTwo*exp(-Uk[z]*Vkk)+ProdTTemp[z];

ProdTNul[z]:=UpSum/DSumOne/DSumTwo*exp(-Uk0[z]*Vkk)+ProdTNul[z];
          End;
          Vkk:=Vkk+1;
        UNTIL (UpSum/DSumOne/DSumTwo*exp(-Uk[z]*Vkk))<=1E-6;
      End;
    PiNoemT:=1;
    PiNoem0:=1;
    FOR z:=1 TO mValue DO
      Begin
        PiNoemT:=ProdTTemp[z]*PiNoemT;
        PiNoem0:=ProdTNul[z]*PiNoem0;
      End;
    FiT:=PiTTemp/PiNoemT;
    FiT0:=PiTNul/PiNoem0;
    SommT:=0;
    Somm0:=0;
    FOR z:=1 TO mValue DO
      Begin
        SommT:=Del[k,z]*Uk[z]+SommT;
        Somm0:=Del[k,z]*Uk0[z]+Somm0;
      End;
```

```
  End;


Procedure BetaTemp;
 Begin
  FOR z:=1 TO mValue DO
   Begin
    Uk[z]:=h*speed*w[z]*100/kb/Tg;    {om na cm te kry * 100}
    Uk0[z]:=h*speed*w[z]*100/kb/T0;
    IF Del[k,z]>=0
    THEN
     Begin
      Vk0[z]:=0;
     End
   ELSE
   IF Del[k,z]<0
   THEN
    Begin
     Vk0[z]:=Abs(Del[k,z]);
    End;
  End;
FOR z:=1 TO mValue DO
 Begin
  ProdTTemp[z]:=0;
  ProdTNul[z]:=0;
 End;
FOR z:=1 TO mValue DO      {Vir die teller van fi(T)}
 Begin
  Vkk:=Vk0[z];
  REPEAT
   Begin
```

```
            SumFi:=Vkk+g[z]+Del[k,z]-1;
            Fakulteit;
            Total;
            UpSum:=Somasie;
            SumFi:=g[z]-1;
            Fakulteit;
            Total;
            DSumOne:=Somasie;
            SumFi:=Vkk;
            Fakulteit;
            Total;
            DSumTwo:=Somas e;

ProdTTemp[z]:=sqrt(UpSum/DSumOne/DSumTwo*exp(-Uk[z]*Vkk))+ProdTTemp
[z];

ProdTNul[z]:=sqrt(UpSum/DSumOne/DSumTwo*exp(-Uk0[z]*Vkk))+ProdTNul[z];
          End;
          Vkk:=Vkk+1;
        UNTIL sqrt(UpSum/DSumOne/DSumTwo*exp(-Uk[z]*Vkk))<=Error;
      End;
      PiTTemp:=1;
      PiTNul:=1;
      FOR z:=1 TO mValue DO
         Begin
           PiTTemp:=ProdTTemp[z]*PiTTemp;
           PiTNul:=ProdTNul[z]*PiTNul;
         End;
      PiTTemp:=exp(2*Ln(PiTTemp));
      PiTNUl:=exp(2*Ln(PiTNul));
      FOR z:=1 TO mValue DO
```

```
  Begin
    ProdTTemp[z]:=0;
    ProdTNul[z]:=0;
  End;
FOR z:=1 TO mValue DO      {Vir die noemer van fi(T)}
  Begin
    Vkk:=Vk0[z];
    REPEAT
      Begin
        SumFi:=Vkk+g[z]+Del[k,z]-1;
        Fakulteit;
        Total;
        UpSum:=Somasie;
        SumFi:=g[z]-1;
        Fakulteit;
        Total;
        DSumOne:=Somasie;
        SumFi:=Vkk;
        Fakulteit;
        Total;
        DSumTwo:=Somasie;

ProdTTemp[z]:=UpSum/DSumOne/DSumTwo*exp(-Uk[z]*Vkk)+ProdTTemp[z];

ProdTNul[z]:=UpSum/DSumOne/DSumTwo*exp(-Uk0[z]*Vkk)+ProdTNul[z];
      End;
      Vkk:=Vkk+1;
    UNTIL (UpSum/DSumOne/DSumTwo*exp(-Uk[z]*Vkk))<=1E-6;
  End;
  PiNoemT:=1;
  PiNoem0:=1;
```

```
    FOR z:=1 TO mValue DO
     Begin
      PiNoemT:=ProdTTemp[z]*PiNoemT;
      PiNoem0:=ProdTNul[z]*PiNoem0;
     End;
  TetaT:=PiTTemp/PiNoemT;
  Teta0:=PiTNul/PiNoem0;
End;

Procedure Kwantum;
 Begin
  CASE o OF
 1:
  Begin
   Del[3,1]:=0;
   Del[3,2]:=2;
   Del[3,3]:=0;
   Alfa0[3]:=0.19;
  End;
 2:
  Begin
   Del[3,1]:=1;
   Del[3,2]:=0;
   Del[3,3]:=0;
   Alfa0[3]:=2.3;
  End;
 3:
  Begin
   Del[3,1]:=0;
   Del[3,2]:=0;
   Del[3,3]:=1;
```

```
      Alfa0[3]:=22.4;
    End;
  End;
End;

Procedure CalcOne;
 Begin
   AlfaT[k]:=Alfa0[k]*(exp(-5*sqrt(T0/Tg)));
   BetaT[k]:=Beta0[k]*sqrt(T0/Tg);
   wbT[k]:=wb0[k]*sqrt(Tg/T0);
   b[k]:=8.6*(sqrt(T0/Tg))+0.5;
   Pe:=(exp(n[k]*Ln(P/Po)))*(exp(n[k]*Ln(1+xGas*(b[k]-1))));
   nk:=BetaT[k]*Pe;
   Ro:=xGas*P*xMr/R/Tg;
   TauH:=AlfaT[k]*Ro*Lm*100*10000/wbT[k];
   Choice;
   wa[k]:=wster[k]*wbT[k];
   TauG[k]:=TauG[k];
 End;

Procedure CalcTwo;
 Begin
   AlfaT[k]:=Alfa0[k];
   wbT[k]:=wb0[k]*sqrt(Tg/T0);
   BetaTemp;
   BetaT[k]:=Beta0[k]*sqrt(T0/Tg)*TetaT/Teta0;
   IF Typegas=1
   THEN
     Begin
       b[k]:=8.6*(sqrt(T0/Tg))+0.5;
     End;
```

```
    Pe:=(exp(n[k]*Ln(P/Po)))*(exp(n[k]*Ln(1+xGas*(b[k]-1))));
    nk:=BetaT[k]*Pe;
    Ro:=P*xGas*xMr/R/Tg;
    TauH:=AlfaT[k]*Ro*Lm*100*10000/wbT[k];
    Choice;
    wa[k]:=wster[k]*wbT[k];
    TauG[k]:=TauG[k];
  End;

Procedure CalcThree;
  Begin
    AlfaTemp;
    AlfaT[k]:=Alfa0[k]*((1-exp(-1*SommT))/(1-exp(-1*Somm0)))*(FiT/FiT0);
    BetaTemp;
    BetaT[k]:=Beta0[k]*sqrt(T0/Tg)*TetaT/Teta0;
    wbT[k]:=wb0[k]*sqrt(Tg/T0);
    IF Typegas=1
    THEN
      Begin
        b[k]:=8.6*(sqrt(T0/Tg))+0.5;
      End;
    Pe:=(exp(n[k]*Ln(P/Po)))*(exp(n[k]*Ln(1+xGas*(b[k]-1))));
    nk:=BetaT[k]*Pe;
    Ro:=xGas*P*xMr/R/Tg;
    TauH:=AlfaT[k]*Ro*Lm*100*10000/wbT[k];
    Choice;
    wa[k]:=wster[k]*wbT[k];
    TauG[k]:=TauG[k];
  End;
```

```
Procedure Calculate;
Label
  Stop,
  CalcEnd,
  Ready;
  Begin
    GetData;
    FOR k:=1 TO Band DO    {vir die geval van  Typegas =1 To band DO}
     Begin
       IF (k=1) AND (Typegas=1)
       THEN
         Begin
           CalcOne;
           GoTo Stop;
         End
     ELSE
     IF (k=3) AND (Typegas=1)  {vir die 2.7 band van H2O}
     THEN
       Begin
         FOR o:=1 TO 3 DO
           Begin
             Kwantum;
             Fundamental;
             IF count=1
             THEN
               Begin
                 AlfaT[k]:=Alfa0[k];
                 BetaTemp;
                 GoTo CalcEnd;
               End
             ELSE
```

```
    Begin
      AlfaTemp;
      BetaTemp;
    End;
  CalcEnd:
  IF count=1
  THEN
    Begin
      AlfaT[k]:=Alfa0[k];
      GoTo Ready;
    End
  ELSE
  FOR z:=1 TO mValue DO
    Begin
      Uk[z]:=h*speed*w[z]*100/kb/Tg;          {Om na cm te kry}
      Uk0[z]:=h*speed*w[z]*100/kb/T0;
    End;
  SommT:=0;
  Somm0:=0;
  FOR z:=1 TO 3 DO
    Begin
      SommT:=Del[k,z]*Uk[z]+SommT;
      Somm0:=Del[k,z]*Uk0[z]+Somm0;
    End;
  AlfaT[k]:=Alfa0[k]*((1-exp(-1*SommT))/(1-exp(-1*Somm0)))*(FiT/FiT0);
  ready:
  Al[o]:=AlfaT[k];
  Beta0[3]:=0.13219;
  BetaT[k]:=Beta0[k]*sqrt(T0/Tg)*TetaT/Teta0;
  Bet[o]:=BetaT[k];
End;
```

```
    RealAlfa:=0;
    RealBeta:=0;
    FOR c:=1 TO 3 DO
      Begin
        RealAlfa:=Al[c]+RealAlfa;
        RealBeta:=sqrt(Bet[c]*Al[c])+RealBeta;
      End;
    RealBeta:=exp(2*Ln(RealBeta))/RealAlfa;
    wbT[k]:=wb0[k]*sqrt(Tg/T0);
    b[k]:=8.6*(sqrt(T0/Tg))+0.5;
    Pe:=(exp(n[k]*Ln(P/Po)))*(exp(n[k]*Ln(1+xGas*(b[k]-1))));
    nk:=RealBeta*Pe;
    Ro:=xGas*P*xMr/R/Tg;
    TauH:=RealAlfa*Ro*Lm*100*10000/wbT[k];
    Choice;
    wa[k]:=wster[k]*wbT[k];
    TauG[k]:=TauG[k];
    GoTo Stop;
  End;
Fundamental;
IF count=1
THEN
  Begin
    CalcTwo;
    GoTo Stop;
  End
ELSE
CalcThree;
Stop:
DelWk[k]:=wa[k]/(1-TauG[k]);
Wuk:=w0[k]+DelWk[k]/2;   {Hier is i die tipe gas en k=band}
```

```
      Wlk:=Wuk-DelWk[k];
      IF Wlk<0
      THEN
        Begin
          Wlk:=0;
        End;
      write(Wave,Wlk);
      write(Wave,Wuk);
      WITH DataFil DO
        Begin
          wlkf:=Wlk;
          wrkf:=Wuk;
          emf:=TauG[k];
        End;
      Write(BandWave,DataFil);
    End;
  End;


Procedure Eliminate;
  Begin
    BndLimit[Block]:=FiT;
    IF Round(BndLimit[Block])=Round(BndLimit[Block-1])
    THEN
      Begin
        Block:=Block-1;
        BndLimit[Block]:=FiT;
      End;
    Pos:=FilePos(Wave);
    Seek(Wave,Pos-1);
    FiT:=15000;
```

```
    write(Wave,FiT);
    Fak:=Fak+5;
    Block:=Block+1;
  End;


Procedure UpperBand;
  Begin
    Fak:=0;
    Block:=1;
    BndLimit[0]:=0;
    SumFi:=0;
    Assign(Wave,'DataWave.dat');
    Reset(Wave);
    Getal:=FileSize(Wave);
    Close(Wave);
    SumFi:=Getal*15000.0;
    REPEAT
      Begin
        Somasie:=0;
        Assign(Wave,'DataWave.dat');
        Reset(Wave);
        FOR z:=1 TO Getal DO
          Begin
            Read(Wave,FiT);
            Somasie:=Somasie+FiT;
            IF Fak>=FiT
            THEN
              Begin
                Eliminate;
              End
```

```
          ELSE
         End;
       Fak:=Fak+9;
       Close(Wave);
     End;
   UNTIL Somasie>=SumFi;
   BndLimit[Block]:=10000.0;
 End;

Procedure Seeker;
Label Hier;
 Begin
   Assign(Data6,'DataFrak.dat');
   Reset(Data6);
   REPEAT
     Begin
       Read(Data6,Datas6);
       WITH Datas6 DO
         Begin
           LamT22:=LamF;
         End;
     End;
    IF LamT22>=2.9
    THEN
      Begin
        LamT22:=3.0;
        Goto Hier;
      End
    ELSE
  UNTIL (LamT22>=FrakSeek);
  Hier:
```

```
PosFrak22:=FilePos(Data6);
PosFrak11:=PosFrak22-1;
Seek(Data6,PosFrak22-1);
Read(Data6,Datas6);
WITH Datas6 DO
     Begin
       LamT22:=LamF;
       TC522:=C5TF;
     End;
IF PosFrak11=0
THEN
  Begin
    Seek(Data6,PosFrak11);
    Read(Data6,Datas6);
    WITH Datas6 DO
      Begin
        LamT11:=LamF;
        TC511:=C5TF;
      End;
  End
ELSE
Seek(Data6,PosFrak11-1);
Read(Data6,Datas6);
WITH Datas6 DO
     Begin
       LamT11:=LamF;
       TC511:=C5TF;
     End;
IF LamT22=2.9
 THEN
  Begin
```

```
        FrakSeek:=6.49393;
      End
    ELSE

  FrakSeek:=(FrakSeek-LamT11)/(LamT22-LamT11)*(TC522-TC511)+TC511;
  Close(Data6);
End;

Procedure WaveLook;
 Begin
  Assign(BandWave,'DatBndWve.dat');
  Reset(BandWave);
  Count:=FileSize(BandWave);
  Somasie:=1;
  FOR i:=1 TO Count DO
   Begin
    Read(BandWave,DataFil);
    WITH DataFil DO
     Begin
      UpSum:=wlkf;
      DSumOne:=wrkf;
      SumFi:=emf;
     End;
    IF (DSumOne>=BndLimit[z]) AND (UpSum<=BndLimit[z-1])
    THEN
     Begin
      TauH:=SumFi;
     End
    ELSE
     Begin
      TauH:=1;
```

```
        End;
      Somasie:=Somasie*TauH;
    End;
  Close(BandWave);
  Somasie:=1-Somasie;
End;


Procedure Fraktion;
 Begin
  BndLimit[0]:=0;
  Emisie[0]:=0;
  Absorp[0]:=0;
  FOR z:=1 TO Block DO
   Begin
    WaveLook;
    IF z=1
    THEN
     Begin
      FrakLeft:=1.0;
      FrakSeek:=Tg/BndLimit[z]/C2;
      Seeker;
      FrakRight:=FrakSeek/6.49381;    {sigma/pi/C5}
      DelF[z]:=FrakLeft-FrakRight;
      Emisie[z]:=DelF[z]*Somasie;
      FrakLeft:=1.0;
      FrakSeek:=Tw/BndLimit[z]/C2;
      Seeker;
      FrakRight:=FrakSeek/6.49381;
      DelF[z]:=FrakLeft-FrakRight;
      Absorp[z]:=DelF[z]*Somasie;
```

```
    End
  ELSE
  IF z=Block
  THEN
    Begin
      FrakSeek:=Tg/BndLimit[z-1]/C2;
      Seeker;
      FrakLeft:=FrakSeek/6.49381;
      FrakRight:=0.05;
      DelF[z]:=FrakLeft-FrakRight;
      Emisie[z]:=DelF[z]*Somasie;
      FrakSeek:=Tw/BndLimit[z-1]/C2;
      Seeker;
      FrakLeft:=FrakSeek/6.49381;
      FrakRight:=0.012;
      DelF[z]:=FrakLeft-FrakRight;
      Absorp[z]:=DelF[z]*Somasie;
    End
  ELSE
    Begin
      FrakSeek:=Tg/BndLimit[z-1]/C2;
      Seeker;
      FrakLeft:=FrakSeek/6.49381;
      FrakSeek:=Tg/BndLimit[z]/C2;
      Seeker;
      FrakRight:=FrakSeek/6.49381;    {sigma/pi/C5}
      DelF[z]:=FrakLeft-FrakRight;
      Emisie[z]:=DelF[z]*Somasie;
      FrakSeek:=Tw/BndLimit[z-1]/C2;
      Seeker;
      FrakLeft:=FrakSeek/6.49381;
```

```
            FrakSeek:=Tw/BndLimit[z]/C2;
            Seeker;
            FrakRight:=FrakSeek/6.49381;
            DelF[z]:=FrakLeft-FrakRight;
            Absorp[z]:=DelF[z]*Somasie;
          End;
        Emisie[z]:=Emisie[z]+Emisie[z-1];
        AbSorp[z]:=Absorp[z]+Absorp[z-1];
      End;
  End;

Procedure Answer;
  Begin
    Ant:=Emisie[z];
    AntT:=AbSorp[z];
  End;

{*********************************************************************}
{ THIS IS THE MAIN PROCEDURE FOR CALCULATING THE EMMISSIVITY OF
THE  }
{ GAS MIXTURE IN A LENGTH INCREMENT OF THE KILN                       }
{*********************************************************************}

Procedure Running;
  Begin
    Assign(Wave,'DataWave.dat');
    Rewrite(Wave);
    Assign(BandWave,'DatBndWve.dat');
    Rewrite(BandWave);
    FOR ou:=1 TO 3 DO   {must be 6 for all types of gases}
      Begin
```

```
        Gas;
        TipeGas;
        Calculate;
      End;
    Reset(Wave);
    While not Eof(Wave) do
      Begin
        read(Wave,FiT);
      End;
    Close(Wave);
    Close(BandWave);
    UpperBand;
    Fraktion;
  End;
END.
```

G.4 UNIT "KilnOp.TPU"

This is the unit for obtaining the kiln and operating parameters and saving them in a data file.

```
Unit KilnOp;

{$R+}

Interface
      Procedure KilnOperate;

Implementation
```

```
Uses Crt,Graph;

Var

 OutGCompEx,OutGAC,OutOp,
 OutGComp,OutKiln  : File of real;   {* File to store kiln operating settings *}
 Pup,OutMP,OutGasYN  : File of Char;

 k0,k2,MaxX,MaxY,GraphDriver,x,y,i,par,opt,x1,y1,GraphMode,ErrorCode:integer;
 rad          : real;
 cha,name,ch : char;
 ek,s         : String;
 Fk           : Boolean;



Procedure Screen;
 Begin
  GraphDriver:=Detect;
  InitGraph(GraphDriver,GraphMode,'C:\Tp\BGI');
  ErrorCode :=GraphResult;
  IF ErrorCode <> grOK
  THEN
    Begin
      Writeln('Graphics Error:',GraphErrorMsg(ErrorCode));
      Halt;
    End;
  MaxX:=GetMaxX;
  MaxY:=GetMaxY;
  SetColor(Red);
  SetTextStyle(0,0,7);
```

```
OutTextXY(24,20,'Parameters'  );
Setcolor(LightBlue);
k0:=TextHeight('default') + 60;
SetTextStyle(0,0,2);
OutTextXY(60,k0,'[1]');
OutTextXY(160,k0,'Pressure build up ');
k2:=k0 + TextHeight('Default') + 30;
OutTextXY(60,k2,'[2]');
OutTextXY(160,k2,'Gas added Yes/No ');
k2:=k2 + TextHeight('Default') + 30;
OutTextXY(60,k2,'[3]');
OutTextXY(160,k2,'Iteration Gas Composition');
k2:=k2 + TextHeight('Default') + 30;
OutTextXY(60,k2,'[4]');
OutTextXY(160,k2,'Operating Variables');
k2:=k2 + TextHeight('Default') + 30;
OutTextXY(60,k2,'[5]');
OutTextXY(160,k2,'Kiln Parameters');
k2:=k2 + TextHeight('Default') + 30;
OutTextXY(60,k2,'[6]');
OutTextXY(160,k2,'Activated Carbon Data');
k2:=k2 + TextHeight('Default') + 30;
OutTextXY(60,k2,'[7]');
OutTextXY(160,k2,'Quit');
SetColor(Yellow);
SetTextStyle(1,0,1);
s:='Choose 1, 2 ... and press ENTER ';
OutTextXY(MaxX-TextWidth(S)-10,MaxY-TextHeight(S)-12,S);
x1:=WhereX;
y1:=WhereY;
GotoXY(x1,y1);
```

```
    ReadIn(opt);
    CloseGraph;
  End;


Procedure SkermGas;
  Begin
    Gotoxy(1,2);write('Molar fraction of Steam     : ');
    Gotoxy(38,2);write('fraction of Carbondioxide :');
    Gotoxy(1,3);write('fraction of Carbon Monoxide : ');
    Gotoxy(38,3);write('fraction of Hydrogen       : ');
    Gotoxy(1,4);write('fraction of Nytrogen        :');
  End;


Procedure Skerm;
  Begin
    Gotoxy(1,2);write('Outside wall temperature [K] : ');
    Gotoxy(38,2);write('Solids temperature [K]      : ');
    Gotoxy(1,3);write('Temperature of the Gas   [K] : ');
    Gotoxy(38,3);write('Inside wall temperature [K] : ');
    Gotoxy(1,4);write('Mass flowrate-solids [kg/s]  : ');
    Gotoxy(38,4);write('Kiln revolutions [rev/min]  : ');
    Gotoxy(1,5);write('Slope of kiln-horizon [°]    : ');
    Gotoxy(38,5);write('Weight % water in carbon feed: ');

  End;
```

```
Procedure SkermG;
 Begin
  Gotoxy(1,2);write('Outside wall temperature [K] : ');
  Gotoxy(38,2);write('Solids temperature [K]       : ');
  Gotoxy(1,3);write('Temperature of the Gas   [K] : ');
  Gotoxy(38,3);write('Inside wall temperature [K]  : ');
  Gotoxy(1,4);write('Mass flowrate-Solids [kg/s]  : ');
  Gotoxy(38,4);write('Mass flowrate-Gas   [kg/s]   : ');
  Gotoxy(1,5);write('Slope of kiln-horizon [°]    : ');
  Gotoxy(38,5);write('Kiln revolutions [rev/min]   : ');
  Gotoxy(1,6);write('Weight % water in carbon feed: ');
 End;


Procedure SkermKiln;
 Begin
  Gotoxy(1,2);write('Number of layers in the wall: ');
  Gotoxy(39,2);write('Diameter of the Kiln [m]   : ');
  FOR i:=1 TO par DO
  Begin
   Gotoxy(1,2+i);write('Conductivity [W/m.K] layer ',i,': ');
  End;
  FOR i:=1 TO par DO
  Begin
   Gotoxy(39,2+i);write('Cp-Value [kJ/kg/K] layer ',i,' : ');
   y:=WhereY;
   x:=y
  End;
  FOR i:=1 TO par DO
  Begin
```

```
    Gotoxy(1,y+i);write('Density [kg/m3] of layer ',i,'  : ');
  End;
  FOR i:=1 TO par DO
  Begin
    Gotoxy(39,x+i);write('Thichness [m] of layer ',i,'  : ');
    y:=WhereY;
  End;
  Gotoxy(1,y+1);write('Length [m] of the Kiln      : ');
  Gotoxy(39,y+1);write('Fill height [m] of the Kiln: ');
End;


Procedure SkermGAC;
 Begin
   GotoXY(1,2);write('Bulk Solid Density [kg/m3] : ');
   GotoXY(40,2);write('Mean Solid diameter [μm] : ');

 End;


Procedure scr_put(rad : real; x:integer; y:integer);
 Begin
   GotoXY(x,y);
   write(rad:0:0);
 End;
```

```
Procedure scr_put1(rad : real; x:integer; y:integer);
 Begin
  GotoXY(x,y);
  write(rad:0:1);
 End;


Procedure scr_put2(rad : real; x:integer; y:integer);
 Begin
  GotoXY(x,y);
  write(rad:0:2);
 End;


Procedure scr_put3(rad : real; x:integer; y:integer);
 Begin
  GotoXY(x,y);
  write(rad:0:3);
 End;


Procedure scr_get(var rad : real: x,y:integer);
 Begin
  GotoXY(x,y);
  read(rad);
 End;
```

```
Procedure ScrRead;
  Begin
    Assign(OutOp,'KilnOp.dat');
    Rewrite(OutOp);
    scr_get(rad,32,2);
    write(OutOp,rad);
    scr_get(rad,69,2);
    write(OutOp,rad);
    scr_get(rad,32,3);
    write(OutOp,rad);
    scr_get(rad,69,3);
    write(OutOp,rad);
    scr_get(rad,32,4);
    write(OutOp,rad);
    scr_get(rad,69,4);
    write(OutOp,rad);
    scr_get(rad,32,5);
    write(OutOp,rad);
    scr_get(rad,69,5);
    write(OutOp,rad);
    Close(OutOp);
  End;


Procedure ScrReadG;
  Begin
```

```
    Assign(OutOp,'KilnOpG.dat');
    Rewrite(OutOp);
    scr_get(rad,32,2);
    write(OutOp,rad);
    scr_get(rad,69,2);
    write(OutOp,rad);
    scr_get(rad,32,3);
    write(OutOp,rad);
    scr_get(rad,69,3);
    write(OutOp,rad),
    scr_get(rad,32,4);
    write(OutOp,rad);
    scr_get(rad,69,4);
    write(OutOp,rad);
    scr_get(rad,32,5);
    write(OutOp,rad);
    scr_get(rad,69,5);
    write(OutOp,rad);
    scr_get(rad,32,6);
    write(OutOp,rad);
    Close(OutOp);
  End;



Procedure ScrReadGas;
  Begin
    Assign(OutGComp,'KilnGas.dat');
    Rewrite(OutGComp);
    scr_get(rad,32,2);
```

```
    write(OutGComp,rad);
    scr_get(rad,69,2);
    write(OutGComp,rad);
    scr_get(rad,32,3);
    write(OutGComp,rad);
    scr_get(rad,69,3);
    write(OutGComp,rad);
    scr_get(rad,32,4);
    write(OutGComp,rad);
    Close(OutGComp);
  End;



Procedure ScrReadExGas;
  Begin
    Assign(OutGCompEx,'ExGas.dat');
    Rewrite(OutGCompEx);
    scr_get(rad,32,2);
    write(OutGCompEx,rad);
    scr_get(rad,69,2);
    write(OutGCompEx,rad);
    scr_get(rad,32,3);
    write(OutGCompEx,rad);
    scr_get(rad,69,3);
    write(OutGCompEx,rad);
    scr_get(rad,32,4);
    write(OutGCompEx,rad);
    Close(OutGCompEx);
  End;
```

```
Procedure ScrReadKiln;
 Begin
  Assign(OutKiln,'KilnPar.dat');
  Rewrite(OutKiln);
  GotoXY(32,2);
  Read(rad);
  par:=round(rad);
  write(Outkiln,rad);
  scr_get(rad,70,2);
  write(Outkiln,rad);
  FOR i:=1 TO par DO
  Begin
   scr_get(rad,32,2+i);
   write(Outkiln,rad);
  End;
  FOR i:=1 TO par DO
  Begin
   scr_get(rad,70,2+i);
   write(Outkiln,rad);
   y:=WhereY;
   x:=y;
  End;
  FOR i:=1 TO par DO
  Begin
   scr_get(rad,32,y+i-1);
   write(Outkiln,rad);
  End;
  FOR i:=1 TO par DO
```

```
    Begin
      scr_get(rad,70,x+i-1);
      write(Outkiln,rad);
      y:=WhereY;
    End;
    Gotoxy(1,y);
    scr_get(rad,32,y);
    write(Outkiln,rad);
    scr_get(rad,70,y);
    write(Outkiln,rad);
    close(OutKiln);
  End;


Procedure ScrReadGAC;
  Begin
    Assign(OutGAC,'GAC.dat');
    Rewrite(OutGAC);
    scr_get(rad,32,2);
    write(OutGAC,rad);
    Scr_get(rad,69,2);
    write(OutGAC,rad);
    Close(OutGAC);
  End;


Procedure ScrWrite;
```

```
  Begin
    Assign(OutOp,'KilnOp.dat');
    Reset(OutOp);
    read(OutOp,rad);
    scr_put(rad,32,2);
    read(OutOp,rad);
    scr_put(rad,69,2);
    read(OutOp,rad);
    scr_put(rad,32,3);
    read(OutOp,rad);
    scr_put(rad,69,3);
    read(OutOp,rad);
    scr_put3(rad,32,4);
    read(OutOp,rad);
    scr_put1(rad,69,4);
    read(OutOp,rad);
    scr_put1(rad,32,5);
    read(OutOp,rad);
    scr_put1(rad,69,5);
    close(OutOp);
  End;



Procedure ScrWriteG;
  Begin
    Assign(OutOp,'KilnOpG.dat');
    Reset(OutOp);
    read(OutOp,rad);
    scr_put(rad,32,2);
```

```
    read(OutOp,rad);
    scr_put(rad,69,2);
    read(OutOp,rad);
    scr_put(rad,32,3);
    read(OutOp,rad);
    scr_put(rad,69,3);
    read(OutOp,rad);
    scr_put3(rad,32,4);
    read(OutOp,rad);
    scr_put3(rad,69,4);
    read(OutOp,rad);
    scr_put1(rad,32,5);
    read(OutOp,rad);
    scr_put1(rad,69,5);
    read(OutOp,rad);
    scr_put1(rad,32,6);
    close(OutOp);
  End;



Procedure ScrWriteGas;
  Begin
    Assign(OutGComp,'KilnGas.dat');
    Reset(OutGComp);
    read(OutGComp,rad);
    scr_put2(rad,32,2);
    read(OutGComp,rad);
    scr_put2(rad,69,2);
    read(OutGComp,rad);
```

```
    scr_put2(rad,32,3);
    read(OutGComp,rad);
    scr_put2(rad,69,3);
    read(OutGComp,rad);
    scr_put2(rad,32,4);
    close(OutGComp);
  End;



Procedure ScrWriteExGas;
  Begin
    Assign(OutGCompEx,'ExGas.dat');
    Reset(OutGCompEx);
    read(OutGCompEx,rad);
    scr_put2(rad,32,2);
    read(OutGCompEx,rad);
    scr_put2(rad,69,2);
    read(OutGCompEx,rad);
    scr_put2(rad,32,3);
    read(OutGCompEx,rad);
    scr_put2(rad,69,3);
    read(OutGCompEx,rad);
    scr_put2(rad,32,4);
    close(OutGCompEx);
  End;
```

```
Procedure ScrWriteKiln;
 Begin
  Assign(OutKiln,'KilnPar.dat');
  Reset(OutKiln);
  read(OutKiln,rad);
  scr_put(rad,32,2);
  read(OutKiln,rad);
  scr_put1(rad,70,2);
  FOR i:=1 TO par DO
  Begin
   read(OutKiln,rad);
   scr_put1(rad,32,2+i);
  End;
  FOR i:=1 TO par DO
  Begin
   read(OutKiln,rad);
   scr_put1(rad,70,2+i);
   y:=WhereY;
   x:=y;
 End,
 FOR i:=1 TO par DO
 Begin
  read(OutKiln,rad);
  scr_put(rad,32,y+i);
 End;
 FOR i:=1 TO par DO
 Begin
  read(OutKiln,rad);
  scr_put3(rad,70,x+i);
  y:=WhereY;
End;
```

```
    read(OutKiln,rad);
    scr_put1(rad,32,y+1);
    read(OutKiln,rad);
    scr_put3(rad,70,y+1);
    close(OutKiln);
  End;


Procedure ScrWriteGAC;
 Begin
   Assign(OutGAC,'GAC.dat');
   Reset(OutGAC);
   read(OutGAC,rad);
   scr_put(rad,32,2);
   read(OutGAC,rad);
   scr_put(rad,69,2);
   Close(OutGAC);
End;


Procedure KeyEnterNO;
 Begin
  IF (ch =#13)
  THEN
    Begin
      Fk:=True;
    End
```

```
    ELSE
    IF (ch =#110)
    THEN
      Begin
        Fk:=False;
      End;
  End;



Procedure KeyYN;
 Begin
   IF (ch = #121) or (ch = #110)
   THEN
     Begin
       Fk:=True;
     End
   ELSE
     Begin
       Fk:=False;
     End;
 End;



Procedure InKey(Var Fk: Boolean; Var ch: char);
 Begin
   CASE opt OF
  1:
```

```
      Begin
        KeyYN;
      End;
    2:
      Begin
        KeyYN;
      End;
    3:
      Begin
        KeyEnterNo;
      End;
    4:
      Begin
        KeyEnterNo;
      End;
    5:
      Begin
        KeyEnterNo;
      End;
    6:
      Begin
        KeyEnterNo;
      End;
    7:
      End;
  End;


Procedure OpOne;
```

```
Begin
  Assign(Pup,'PBuild.dat');
  Rewrite(Pup);
  REPEAT
    Begin
      GotoXY(16,12);
      write('Allow for a pressure build up (Y)es or (N)o :');
      ch:=ReadKey;
      write(Pup,ch);
      InKey(Fk,ch);
    End;
  UNTIL Fk = True;
  Close(Pup);
End;



Procedure OpTwo;
 Begin
  Assign(OutGasYN,'KilnYN.dat');
  rewrite(OutGasYN);
  REPEAT
    Begin
      GotoXY(16,14);
      write('Is external gas added to the freeboardgas (Y/N) : ');
      ch:=ReadKey;
      el:=ch;
      write(OutGasYN,ch);
      InKey(Fk,ch);
    End;
```

```
UNTIL Fk = True;
Close(OutGasYN);
GotoXY(16,14);
IF ek = ('y')
THEN
 Begin
  REPEAT
   Begin
    ScrWriteExGas;
    SkermGas;
    GotoXY(16,14);
    write('                                                    ');
    GotoXY(7,20);
    write('IF YOU WANT TO CHANGE THE GAS COMPOSITION PRESS
ENTER ... ');
    GotoXY(24,22);
    write('IF NOT, TYPE (N)O : '):
    ch:=readkey;
    KeyEnterNo;
    IF fk = True
    THEN
     Begin
      GotoXY(7,20);
      write('                                                    ');
      GotoXY(24,22);
      write('                    ');
      GotoXY(16,14);
      write('Give the correct variables .... ');
      ScrReadExGas;
     End
    ELSE
```

```
        End;
      UNTIL ch = 'n';
    End
  ELSE
End;



Procedure OpThree;
 Begin
  Assign(OutGComp,'KilnGas.dat');
  GotoXY(16,14);
  REPEAT
   Begin
    ScrWriteGas;
    SkermGas;
    GotoXY(16,14);
    write('                              ');
    GotoXY(7,20);
    write('IF YOU WANT TO CHANGE THE GAS COMPOSITION PRESS ENTER
... ');
    GotoXY(24,22);
    write('IF NOT, TYPE (N)O : ');
    ch:=readkey;
    InKey(fk,ch);
    IF fk = True
    THEN
     Begin
      GotoXY(7,20);
      write('                                                  ');
```

```
            GotoXY(24,22);
            write('                    ');
            GotoXY(16,14);
            write('Give the correct variables .... ');
            ScrReadGas;
          End
        ELSE
      End;
    UNTIL ch = 'n';
  End;



Procedure OpFour;
  Begin
    Assign(OutGasYN,'KilnYN.dat');
    Reset(OutGasYN);
    read(OutGasYN,name);
    Close(OutGasYN);
    CASE name OF
  'N','n':
      Begin
        Skerm;
        ScrWrite;
      End;
  'Y','y':
      Begin
        SkermG;
        ScrWriteG;
      End;
```

```
End;
REPEAT
 Begin
  GotoXY(16,14);
  write('                              ');
  GotoXY(7,20);
  write('IF YOU WANT TO CHANGE THE OPERATING PARAMETERS PRESS
ENTER ... ');
  GotoXY(24,22);
  write('IF NOT, TYPE (N)O : ');
  ch:=readkey;
  InKey(fk,ch);
  IF fk = True
  THEN
   Begin
    GotoXY(7,20);
    write('                                                    ');
    GotoXY(24,22);
    write('                    ');
    GotoXY(16,14);
    write('Give the correct variables .... ');
    CASE name OF
     'N','n':
           Begin
            Skerm;
            ScrRead;
           End;
    'Y','y':
          Begin
           SkermG;
           ScrReadG;
```

```
                End;
              End;
            End
          ELSE;
        End;
    UNTIL ch = 'n'
End;



Procedure OpFive;
  Begin
    Assign(OutKiln,'KilnPar.dat');
    Reset(OutKiln);
    read(OutKiln,rad);
    par:=round(rad);
    Close(OutKiln);
    REPEAT
      Begin
        SkermKiln;
        ScrWriteKiln;
        GotoXY(16,14);
        write('                              ');
        GotoXY(7,20);
        write('IF YOU WANT TO CHANGE THE KILN PARAMETERS PRESS ENTER
... ');
        GotoXY(24,22);
        write('IF NOT, TYPE (N)O : ');
        ch:=readkey;
        InKey(fk,ch);
```

```
        IF fk = True
        THEN
          Begin
            GotoXY(7,20);
            write('                                                    ');
            GotoXY(24,22);
            write('                    ');
            GotoXY(16,14);
            write('Give the correct variables .... ');
            SkermKiln;
            ScrReadKiln;
          End
        ELSE;
      End;
    UNTIL ch = 'n'
  End;



Procedure OpSix;
  Begin
    Assign(OutGAC,'GAC.dat');
    Reset(OutGAC);
    read(OutGAC,rad);
    par:=round(rad);
    Close(OutGAC);
    REPEAT
      Begin
        SkermGAC;
        ScrWriteGAC;
```

```
        GotoXY(16,14);
        write('                                    ');
        GotoXY(7,20);
        write('IF YOU WANT TO CHANGE THE KILN PARAMETERS PRESS ENTER
... ');
        GotoXY(24,22);
        write('IF NOT, TYPE (N)O : ');
        ch:=readkey;
        InKey(fk,ch);
        IF fk = True
        THEN
         Begin
          GotoXY(7,20);
          write('                                                    ');
          GotoXY(24,22);
          write('                    ');
          GotoXY(16,14);
          write('Give the correct variables .... ');
          SkermGAC;
          ScrReadGAC;
         End
       ELSE;
     End;
  UNTIL ch = 'n'
End;



Procedure Options;
Label Hier;
```

```
Begin
  Hier:
  CASE opt of
  1:
    Begin
      OpOne;
      Screen;
      Goto Hier;
    End;
  2:
    Begin
      OpTwo;
      Screen;
      Goto Hier;
    End;
  3:
    Begin
      OpThree;
      Screen;
      Goto Hier;
    End;
  4:
    Begin
      OpFour;
      Screen;
      Goto Hier;
    End;
  5:
    Begin
      OpFive;
      Screen;
```

```
      Goto Hier;
    End;
  6:
    Begin
      OpSix;
      Screen;
      Goto Hier;
    End;
  7:
   End;
 End;


Procedure KilnOperate;
 Begin
   Clrscr;
   Screen;
   Options;
   clrscr;
 End;
END.
```

G.5 UNIT "React.TPU"

```
Unit React;

{$R+,N+}


InterFace
        Procedure ReactIn( Var Tss,mWt,Vol,TpG,N2in,H2Oin,
                           CO2in,COin,Tyd,mSflow,Pressure,ekke  real);
        Procedure Reaction;
        Procedure ReactOut ( Var outN2,outH2,outH2O,outCO2,outCO,
                             compN2,compH2,compH2O,compCO2,
                             compCO,Cre,xps,yps,zps,noun:real);

Implementation

Uses Crt;

Const

Ro=8.314;   {[kJ/kmol.K]}

Var

 Hoeveel: File of real;

 Ener,Time,molCO,molCO2,molH2O,molH2,MolN2,Wverd,Tgas,TSTS,parH2O,parH2
: real;

k3,V,R,frakN2,frakH2,frakH2O,frakCO2,frakCO,Kpw,Solid,mS,mCreac,mH2Oreac,Cr
e   : real;
```

```
 verlies,Pres,xhs,yhs,zhs,co2OLD,coOLD,mH2reac,TolMol,outH2O,outCO2,outCO :
real;
 k1k,k2k:double;


Procedure ReactIn;
 Begin
  TSTS:=Tss;
  Wverd:=mWt;
  V:=Vol;
  Tgas:=TpG;
  molN2:=N2in;
  molH2:=H2in;
  molH2O:=H2Oin;
  molCO2:=CO2in;
  molCO:=COin;
  Time:=Tyd;
  mS:=mSflow;
  Pres:=Pressure;
  verlies:=ekke;
 End;


Procedure GasCompIn;
 Begin
  molH2O:=molH2O+Wverd/18;  {k.mol}
  parH2O:=molH2O/(molN2+molH2+molH2O+molCO2+molCO)*Pres*101325;
{Pa}
  parH2:=molH2/(molN2+molH2+molH2O+molCO2+molCO)*Pres*101325;
{Pa}
 End;
```

```
Procedure Calculate;
  Begin

    k1k:=1.65E4*exp(-2.27E5/8.314/TsTs);
    k2k:=2.84E-7*exp(1.02E5/8.314/TsTs);
    k3:=1.18E-3;
    R:=k1k*parH2O/(1+k2k*parH2+k3*parH2O)*Time;   {kgresidue/kgCarbon}
    Solid:=R*mS;  {Kg carbon reacted}
    Verlies:=R;
  End;


Procedure GasCompOut;
  Begin
    mCreac:=Solid/12;  {kmol}

Kpw:=exp(28.51+1/1.987*(-42952.9/Tgas-1.07*Ln(Tgas)-0.00111*Tgas-196000/T
gas/Tgas));
    CO2OLD:=molCO2;
    COOLD:=molCO;
    molCO2:=sqr(-Kpw+sqrt(sqr(Kpw)+4*mCreac*Kpw))/4/Kpw;
    molCO:=(-Kpw+sqrt(sqr(Kpw)+4*mCreac*Kpw))/2;
    xhs:=mCreac+0.5*(mCreac+molCO2-molCO);
    yhs:=molCO2+0.5*(mCreac+molCO2-molCO);
    zhs:=0.5*(mCreac+molCO2-molCO);
    mH2Oreac:=2*molCO2+molCO;
    molH2:=molH2+mH2Oreac;
    molCO2:=CO2OLD+molCO2;
```

```
    molCO:=COOLD+molCO;
    molH2O:=molH2O-mH2Oreac;
    IF MolH2O<=0
    THEN
     Begin
      MolH2O:=0;
     End
    ELSE
    TolMol:=molN2+molH2+molH2O+molCO2+molCO;
    frakN2:=molN2/TolMol;
    frakH2:=molH2/TolMol;
    frakH2O:=molH2O/TolMol;
    frakCO2:=molCO2/TolMol;
    frakCO:=molCO/TolMol;
  End;

Procedure ReactOut;
 Begin
   outN2:=molN2;
   outH2:=molH2;
   outH2O:=molH2O;
   outCO2:=molCO2;
   outCO:=molCO;
   compN2:=frakN2;
   compH2:=frakH2;
   compH2O:=frakH2O;
   compCO2:=frakCO2;
   compCO:=frakCO;
   cre:=R;
   xps:=xhs;
   yps:=yhs;
```

```
    zps:=zhs;
    noun:=verlies;
  End;


Procedure Reaction;
  Begin
    GasCompIn;
    Calculate;
    GasCompOut;
  End;
END.
```

G.6 UNIT "Grid.TPU"

This is the unit where the bed of solids is divided into a number of nodes.

```
Unit Grid;



{$R+}

InterFace
      Procedure NodalLength;

Implementation

Uses Crt;
```

```
Const
  num=5;

Type

  RoosterOne   = Array [1..20] of integer;
  Rooster      = Array [1..20,1..20] of real;

Var

  OutKiln : File of real;     {** File for kiln construction parameters **}
  XY_x    : File of real;
  XY_y    : File of real;
  C_x     : File of integer;
  C_y     : File of integer;

  i,kan,C,lr,j,m,kx,ky,na      :integer;
  DelL,P,X,Y,DelY,rad,lgth,F,D : real;

  Yy,Xx : Rooster;
  Cx,Cy : RoosterOne;


Procedure Initial;
  Begin
    Assign(OutKiln,'KilnPar.dat');
    Reset(Outkiln);
    read(Outkiln,rad);
    lr:=Round(rad);
    read(OutKiln,rad);
    D:=rad;
```

```
    FOR j:=1 TO lr DO
     Begin
      read(OutKiln,rad);
     End;
    FOR j:=1 TO lr DO
     Begin
      read(OutKiln,rad);
     End;
    FOR j:=1 TO lr DO
     Begin
      read(OutKiln,rad);
     End;
    FOR j:=2 TO lr+1 DO
     Begin
      read(OutKiln,rad);
     End;
   read(OutKiln,rad);
   lgth:=rad;
   read(OutKiln,rad);
   F:=rad;
   Close(OutKiln);
End;


Procedure Calclength;
 Begin
  delY:=F/(num-1);
  kx:=0;
  REPEAT
  Begin
```

```
        m:=1;
        na:=1;
        kx:=kx+1;
        X:=exp(0.5*Ln(exp(2*ln(D/2))-exp(2*Ln(D/2-F+(kx-1)*delY))));
        REPEAT
          Begin
            IF X=delY THEN
              Begin
                Xx[kx,m]:=DelY;
                m:=m+1;
              End
            ELSE
            IF X>delY THEN
              Begin
                X:=X-delY;
                Xx[kx,m]:=delY;
                m:=m+1;
              End
            ELSE
            IF X<delY THEN
              Begin
                m:=m;
                Xx[kx,m]:=X;
              End;
            Cx[kx]:=m;
            C:=Cx[kx];
          End;
        UNTIL
Abs((m-1)*delY+Xx[kx,m]-exp(0.5*Ln(exp(2*ln(D/2))-exp(2*Ln(D/2-F+(kx-1)*delY))
))))<1E-5;
      End;
```

```
UNTIL Abs((D/2-F+kx*delY)-(D/2))<1E-5;
Begin
 Y:=D/2-F;
 FOR m:=1 TO num-1 DO
  Begin
   Yy[m,1]:=DelY;
  End;
 Cy[1]:=num;
 Yy[num,1]:=0;
End;
ky:=1;
REPEAT
Begin
na:=1;
ky:=ky+1;
Y:=exp(0.5*Ln(exp(2*Ln(D/2))-exp(2*Ln((ky-1)*DelY))));
Y:=Y-(D/2-F);
 REPEAT
  Begin
   IF Y=delY THEN
    Begin
     Yy[na,ky]:=DelY;
     na:=na+1;
    End
   ELSE
   IF Y>delY THEN
    Begin
     Y:=Y-delY;
     Yy[na,ky]:=delY;
     na:=na+1;
    End;
```

```
        IF Y<delY THEN
          Begin
            na:=na;
            Yy[na,ky]:=Y;
          End;
        Cy[ky]:=na;
      End;
    UNTIL
Abs((na-1)*delY+Yy[na,ky]+D/2-F-exp(0.5*Ln(exp(2*Ln(D/2))-exp(2*Ln((ky-1)*Del
Y)))))<1E-5;
    X:=exp(0.5*Ln(exp(2*ln(D/2))-exp(2*Ln(D/2-F))));
  End;
  UNTIL (ky)*DelY > X;
End;



Procedure Store;
 Begin
  Assign(C_x,'C:\Cx. 'at');
  Rewrite(C_x);
  i:=0;
  REPEAT
   Begin
    i:=i+1;
    write(C_x,Cx[i]);
   End;
  UNTIL i=(num-1);
  Close(C_x);
  Assign(C_y,'C:\Cy.dat');
  Rewrite(C_y);
```

```
 i:=0;
 REPEAT
   Begin
     i:=i+1;
     write(C_y,Cy[i]);
   End;
 UNTIL i=Cx[1],
 Close(C_y);
 Assign(XY_x,'C:\XGrid.dat');
 Rewrite(XY_x);
 FOR kan:=1 to num-1 DO
   Begin
     FOR j:=1 to Cx[kan] DO
       Begin
         write(XY_x,Xx[kan,j]);
       End;
   End;
 Close(XY_x);
 Assign(XY_y,'C:\YGrid.dat');
 Rewrite(XY_y);
 FOR kan:=1 to num-1 DO
   Begin
     FOR j:=1 to Cx[kan] DO
       Begin
         write(XY_y,Yy[kan,j]);
       End;
   End;
 Close(XY_y);
End;
```

```
 Procedure NodalLength;
  Begin
   clrscr;
   Initial;
   CalcLength;
   Doen;
   readln;
   clrscr;
   Store;
  End;
END.
```

G.7 UNIT "QSolid.TPU"

This is the unit for calculating the radiative heat transfer rate to the solids.

```
Unit QSolid;

{$R+}

InterFace
        Procedure EInS( Var
TpS,Tpwi,TGLm,TG2Lm,TG3Lm,Fwwss,Fssww,Fwwww,
                AreaS,AreaEx,EmmG,TGAc,mG,Dm,Tpg,one :real;flow:integer );
        Procedure EtoS( Var Eners : real);
        Procedure SolidQs;

Implementation
```

```
Uses Crt;

Const

  Ro=8.314;   {[kJ/kmol.K]}
  sigma=5.67E-8;

Var

  OutGasYN : File of char;
  plug:integer;
  Emw,EmS,Ts,Qss,AlfaS,TauGLm,TauG2Lm,TauG3Lm,Fws,Fsw,Fww  : real;
  some,AlfaW,Eww,Egg,Ess,Twi,Row,Ros,As,AwExp,EmG,TauAcLm,MassG,D,Tg :
real;
  name : char;


Procedure EInS;
 Begin
  EmS:=0.87;
  EmW:=0.4;
  Ts:=TpS;
  Twi:=Tpwi;
  AlfaS:=0.8;
  AlfaW:=0.2;
  TauGLm:=TGLm;
  TauG2Lm:=TG2Lm;
  TauG3Lm:=TG3Lm;
  Fws:=Fwwss;
  Fsw:=Fssww;
  Fww:=Fwwww;
```

```
    As:=AreaS;
    AwExp:=AreaEx;
    EmG:=EmmG;
    TauAcLm:=TGAc;
    MassG:=mG;
    D:=Dm;
    Tg:=Tpg;
    plug:=flow;
    sone:=one;
  End;


Procedure EnergyToSolids;
  Begin
    Ros:=1-AlfaS;
    Row:=1-AlfaW;
    Ess:=sigma*EmS*Ts*Ts*Ts*Ts;
    Qss:=EmS*As*Ess;
    Qss:=Qss - AlfaS*TauG2Lm*Fws*Fsw*Row*EmS*As*Ess;
    Qss:=Qss - AlfaS*TauG3Lm*Fws*Fww*Fsw*Row*Row*EmS*As*Ess;
    Qss:=Qss - Fws*TauG3Lm*Fww*Fww*Fsw*Row*Row*Row*EmS*As*Ess;
    Qss:=Qss - Fws*TauG3Lm*Fws*Fsw*Fsw*Ros*Row*Row*EmS*As*Ess;
    Eww:=sigma*EmW*Twi*Twi*Twi*Twi;
    Qss:=Qss - AlfaS*TauGLm*Fws*EmW*AwExp*Eww;
    Qss:=Qss - AlfaS*TauG2Lm*Fws*Fww*Row*EmW*AwExp*Eww;
    Qss:=Qss - AlfaS*TauG3Lm*Fws*Fww*Fww*Row*Row*EmW*AwExp*Eww;
    Qss:=Qss - AlfaS*TauG3Lm*Fws*Fws*Fsw*Ros*Row*Emw*AwExp*Eww;
    Qss:=Qss -
Fws*TauG3Lm*Fww*Fww*Fww*Row*Row*Row*EmW*AwExp*Eww;
    Qss:=Qss -
2*Fws*TauG3Lm*Fws*Fww*Fsw*Ros*Row*Row*EmW*AwExp*Eww;
```

```
    Egg:=sigma*EmG*Tg*Tg*Tg*Tg;
    Qss:=Qss - AlfaS*EmG*As*Egg;
    Qss:=Qss - AlfaS*Fws*Row*TauAcLm*EmG*AwExp*Egg;
    Assign(OutGasYN,'KilnYN.dat');
    Reset(OutGasYN);
    Read(OutGasYN,name);
    Close(OutGasYN);
    CASE name OF
    'n','N':
          Begin
            Qss:=Qss;
          End;
    'y','Y':
          Begin
            Qss:=Qss+0.4*exp(0.62*Ln(MassG*3600/(pi/4*sqr(D))))*As*(Tg-Ts);
          End;
        End;
  End;

Procedure EtoS;
  Begin
    Eners:=Qss;
  End;


Procedure SolidQs;
  Begin
    EnergyToSolids;
  End;
End.
```

G.8 UNIT "QGas.TPU"

This is the unit for calculating radiative heat transfer rate to the gas.

```
Unit QGas;

{$R+}

interFace
        Procedure EInG( Var
TpS,Tpwi,TGLm,TG2Lm,TG3Lm,Fwwss,Fssww,Fwwww,
                AreaS,AreaEx,EmmG,TGAc,mG,Dm,Tpg,AreaG,AlGAc,cne
:real;flow:integer );
        Procedure EtoG( Var Eners : real);
        Procedure GasQg;

Implementation

Uses Crt;

Const

 Ro=8.314;   {[kJ/kmol.K]}
 sigma=5.67E-8;

Var

 OutGasYN : File of char;
 plug:integer;
```

```
AlfaW,Emw,EmS,Ts,Qgg,AlfaS,TauGLm,TauG2Lm,TauG3Lm,Fws,Fsw,Fww,Ag    :
real;
  sone,Eww,Egg,Ess,Twi,Row,Ros,As,AwExp,EmG,TauAcLm,MassG,D,Tg,AlfaGAc :
real;
  name : char;


Procedure EInG;
  Begin
    EmS:=0.87;
    EmW:=0.4;
    Ts:=TpS;
    Twi:=Tpwi;
    AlfaS:=0.8;
    AlfaW:=0.2;
    TauGLm:=TGLm;
    TauG2Lm:=TG2Lm;
    TauG3Lm:=TG3Lm;
    Fws:=Fwwss;
    Fsw:=Fssww;
    Fww:=Fwwww;
    As:=AreaS;
    AwExp:=AreaEx;
    EmG:=EmmG;
    TauAcLm:=TGAc;
    MassG:=mG;
    D:=Dm;
    Tg:=Tpg;
    Ag:=AreaG;
    AlfaGAc:=AlGAc;
    plug:=flow;
```

```
    sone:=one;
  End;


Procedure EnergyToGas;
  Begin
    Assign(OutGasYN,'KilnYN.dat');
    Reset(OutGasYN);
    Read(OutGasYN,name);
    Close(OutGasYN);
    CASE name OF
    'n','N':
          Begin
          End;
   'y','Y':
          Begin
            Ag:=Ag+(Ag*plug/sone);
          End;
       End;
   Ros:=1-AlfaS;
   Row:=1-AlfaW;
   Egg:=sigma*EmG*Tg*Tg*Tg*Tg;
   Qgg:=EmG*Ag*Egg;                    {Kyk na hierdie Ag}
   Ess:=sigma*EmS*Ts*Ts*Ts*Ts;
   Qgg:=Qgg - (1-TauGLm)*Fsw*EmS*As*Ess;
   Qgg:=Qgg - (TauGLm-TauG2Lm)*Fsw*Row*EmS*As*Ess;
   Qgg:=Qgg - (TauG2Lm-TauG3Lm)*Fww*Fsw*Row*Row*EmS*As*Ess;
   Qgg:=Qgg - (TauG2Lm-TauG3Lm)*Fws*Fsw*Fsw*Ros*Row*EmS*As*Ess;
   Eww:=sigma*EmW*Twi*Twi*Twi*Twi;
   Qgg:=Qgg - (1-TauGLm)*EmW*AwExp*Eww;
   Qgg:=Qgg - (TauGLm-TauG2Lm)*Fww*Row*EmW*AwExp*Eww;
```

```
    Qgg:=Qgg - (TauG2Lm-TauG3Lm)*Fww*Fww*Row*Row*EmW*AwExp*Eww;
    Qgg:=Qgg - (TauG2Lm-TauG3Lm)*Fws*Fsw*Ros*Row*EmW*AwExp*Eww;
    Qgg:=Qgg -
(TauG2Lm-TauG3Lm)*Fws*Fww*Fsw*Ros*Row*EmW*AwExp*Eww;
    Qgg:=Qgg - (TauGLm-TauG2Lm)*Fws*Fsw*Ros*EmW*AwExp*Eww;
    Qgg:=Qgg - AlfaGAc*Row*EmG*AwExp*Egg;
    Qgg:=Qgg - (Row*Fww+Ros*Fws)*Row*TauAcLm*EmG*AwExp*Egg;
    Qgg:=Qgg - (AlfaGAc+Row*TauAcLm)*Fsw*Ros*EmG*As*Egg;
  End;


 Procedure EtoG;
  Begin
    Eners:=Qgg;
  End;


 Procedure GasQg;
  Begin
    EnergyToGas;
  End;
End.
```

```
    Qgg:=Qgg - (TauG2Lm-TauG3Lm)*Fww*Fww*Row*Row*EmW*AwExp*Eww;
    Qgg:=Qgg - (TauG2Lm-TauG3Lm)*Fws*Fsw*Ros*Row*EmW*AwExp*Eww;
    Qgg:=Qgg -
(TauG2Lm-TauG3Lm)*Fws*Fww*Fsw*Ros*Row*EmW*AwExp*Eww;
    Qgg:=Qgg - (TauGLm-TauG2Lm)*Fws*Fsw*Ros*EmW*AwExp*Eww;
    Qgg:=Qgg - AlfaGAc*Row*EmG*AwExp*Egg;
    Qgg:=Qgg - (Row*Fww+Ros*Fws)*Row*TauAcLm*EmG*AwExp*Egg;
    Qgg:=Qgg - (AlfaGAc+Row*TauAcLm)*Fsw*Ros*EmG*As*Egg;
  End;


Procedure EtoG;
  Begin
    Eners:=Qgg;
  End;


Procedure GasQg;
  Begin
    EnergyToGas;
  End;
End.
```